STATIC AND DYNAMIC BEHAVIOR OF AXIALLY FUNCTIONALLY GRADED STRUCTURAL ELEMENTS WITH DIFFERENT BOUNDARY CONDITIONS

Thesis submitted by

HARERAM LOHAR

Doctor of Philosophy

(Engineering)

DEPARTMENT OF MECHANICAL ENGINEERING

FACULTY COUNCIL OF ENGINEERING & TECHNOLOGY

JADAVPUR UNIVERSITY

KOLKATA, INDIA

2019

JADAVPUR UNIVERSITY

KOLKATA-700032, INDIA

INDEX NO. 111/15/E

1. Title of Thesis:

Static and Dynamic Behavior of Axially Functionally Graded Structural Elements with Different Boundary Conditions

2. Name, Designation & Institution of the Supervisor:

Prof. Anirban Mitra

Assistant Professor, Department of Mechanical Engineering,

Jadavpur University, Kolkata-700032

Prof. Sarmila Sahoo

Associate Professor, Department of Civil Engineering,

Heritage Institute of Technology, Kolkata-700107,

3. List of Publications (Referred Journals):

I. **Lohar, H., Mitra, A. and Sahoo, S.,** 2016, Geometric Nonlinear Free Vibration of Axially Functionally Graded Non-Uniform Beams Supported on Elastic Foundation. Curved and Layered Structures, 3, 223–239.

II. **Lohar, H., Mitra, A. and Sahoo, S.,** 2016, Natural Frequency and Mode Shapes 0f Exponential Tapered AFG Beams on Elastic Foundation. International Frontier Science Letters, 9, 9-25.

III. **Lohar, H., Mitra, A. and Sahoo, S.,** 2016, Free Vibration Analysis of Axially Functionally Graded Linearly Taper Beam on Elastic Foundation. IOP Conference Series: Materials Science and Engineering, 149, 012130-1-10.

IV. **Lohar, H., Mitra, A. and Sahoo, S.,** 2018, Large Amplitude Forced Vibration Analysis of an Axially Functionally Graded Tapered Beam Resting on Elastic Foundation. Materials Today: Proceedings, 5, 5303–5312.

V**. Lohar, H., Mitra, A. and Sahoo, S.,** 2018, Geometrically Non-Linear Frequency Response of Axially Functionally Graded Beams Resting on Elastic Foundation under Harmonic Excitation. International Journal of Manufacturing, Materials, and Mechanical Engineering, 8(3), 23-43.

VI. **Lohar, H., Mitra, A. and Sahoo, S.,** 2018, Mode Switching Phenomenon in Geometrically Nonlinear Free Vibration Analysis of In-Plane Inhomogeneous Plates on Elastic Foundation. Curved and Layered Structures, 5, 156–179.

VII. **Lohar, H., Mitra, A. and Sahoo, S.,** 2018, Free Vibration of Initially Deflected Axially Functionally Graded Non-Uniform Timoshenko Beams on Elastic Foundation. Romanian Journal of Acoustics and Vibration, 15(2), 75-89.

VIII. **Lohar, H., Mitra, A. and Sahoo, S.,** 2018, Nonlinear Response of Axially Functionally Graded Timoshenko Beams on Elastic Foundation under Harmonic Excitation. Curved and Layered Structures (Accepted).

4. List of Patents: Nil

5. List of Presentations in National/International Conferences:

I. **Lohar, H., Mitra, A. and Sahoo, S.,** 2016, Free Vibration Analysis of Axially Functionally Graded Linearly Taper Beam on Elastic Foundation. International Conference on Advances in Materials & Manufacture Applications (IConAmma 2016), Amrita University, Bangalore.

II. **Lohar, H., Mitra, A. and Sahoo, S.,** 2017, Large Amplitude Forced Vibration Analysis of an Axially Functionally Graded Tapered Beam Resting on Elastic Foundation. International Conference on Materials Processing and Characterization (ICMPC-2017), GRIET, Hyderabad.

III. **Lohar, H., Mitra, A. and Sahoo, S.,** 2018, Large Amplitude Static Deflection of Axially Functionally Graded Plates on Elastic Foundation. 1st International Conference on Mechanical Engineering (INCOM 2018), Jadavpur University, Kolkata.

CERTIFICATE FROM THE SUPERVISOR/S

This is to certify that the thesis entitled ***"Static and Dynamic Behavior of Axially Functionally Graded Structural Elements with Different Boundary Conditions"*** *submitted by Mr. HARERAM LOHAR who got his name registered on 15.06.2015 for the award of Ph.D. (Engineering) degree of Jadavpur University is absolutely based upon his own work under the supervision of Dr. Anirban Mitra (Mechanical Engg. Dept., J.U.) and Dr. Sarmila Sahoo (Dept. of Civil Engg., Heritage Institute of Technology, Kolkata) and that neither his thesis nor any part of the thesis has been submitted for any degree/ diploma or any other academic award anywhere before.*

_____ _____

(Dr. Anirban Mitra) **(Dr. Sarmila Sahoo)**

Signature of the Supervisor and date with Office Seal

Signature of the Supervisor and date with Office Seal

Acknowledgement

The completion of this PhD thesis represents quite a pleasant journey of four years of my life learning, gaining knowledge and gathering experiences in the research field. It, of course, gives me an opportunity to thank all those people with whom I have had interaction and their contribution in many ways in the final form of this work. Without their collective efforts and cooperation, this thesis could not have been completed as it stands. I would like to convey my regards and express my gratitude to all of them. This acknowledgement is just a mere reminder that they will never be forgotten and my apology to anyone whom I fail to mention.

I would like to convey my sincere thanks to my thesis supervisors, Dr. Anirban Mitra and Dr. Sarmila Sahoo, for their generous assistance, inspired ideas and unrelenting support from the very early stage of this research as well as giving me extraordinary experiences throughout the work. Their continuous support, stimulation to guide and critical discussion led me to develop a critical sense of thinking and to evolve myself as a keen research student. I shall always remain indebted to them.

I am extremely grateful to Prof. Kashinath Saha for teaching the basics of structural analysis that proved to be very useful to carry out this research work.

I also wish to acknowledge kind and active support, cooperation and encouragement of Dr. Prasanta Sahoo and Dr. Sukanta Sarkar (Head of the Department, Heritage Institute of Technology, Kolkata).

I am also thankful to all the past and present members of the Machine Element Laboratory, who have been with me throughout the completion of this thesis. I would like to acknowledge Priyambada Nayak, Brajesh Panigrahi and Santanu Duari who supported me from their respective positions and stood by me in time of need. I can never forget the long-lasting memories of spending time with these people. My special thanks to Tamonash Jana for his involvement and support during the presented work. My heartfelt thanks to my fellow labmates, Amit Banerjee, Milan Das, Bikash Panja, Ajay Waghmare, Prasanna Gadhari, Sanjib Kundu, Abhijit Biswas, Arkadeb Mukhopadhyay, Smrutiranjan Pradhan, Sushanta Ghuku, for their support and generous attitude, whenever needed. I

would like to thank to my colleagues Shouvik Ghosh, Tanmoy Bandhopadhya and Sourav Sarkar for their wonderful time.

I would like to convey my thanks to the Head of the Department, Laboratory-in-Charge, Machine Elements Laboratory and all academic and technical staffs of Mechanical Engineering Department, Jadavpur University.

In this respect, I would also like to grab this opportunity to express my heart-felt gratitude to my family members and friends whose support, suggestions and helping attitude helped my way out to the completion of the thesis. I am always grateful to the Almighty for his mercy and kindness shown upon me. I dedicate this thesis to my beloved parents.

Hareram Lohar

Table of Contents

List of Notations

A_0	Cross-sectional area of the plate at root side
a	Length of the plate
b	Breadth of the beam/plate
c_i	Unknown coefficients for static analysis
d_i	Unknown coefficients for dynamic analysis
E_0	Elastic modulus of the beam/plate material at root side
$\{f\}$	Load vector
I_0	Moment of inertia of the beam/plate at root side
$[K]$	Stiffness matrix
$[K_s]$	Stiffness matrix corresponding to static analysis
K_f	Foundation stiffness for beam/plate
L	Length of the beam
$[M]$	Mass matrix
n	Number of iteration
ng	Number of Gauss points
nw, nu	Number of constituent functions for w and u displacement for beam/plate
nv	Number of constituent functions for w displacement for plate
P	Magnitude of uniformly distributed load on beam
$q(x,y)$	External uniformly distributed load on plate
T	Kinetic energy of the system
t_0	Thickness of the beam/plate at root side
U	Strain energy stored in the system
U_b	Strain energy stored due to bending
U_m	Strain energy stored due to stretching
U_f	Strain energy stored in the foundation
u	Displacement field in x-axis

V	Potential energy of the external forces
v	Displacement field in y-axis
w	Displacement field in z-axis
$w_{\max}$	Maximum deflection of the beam/plate
α	Taper parameter
β	Material gradient parameter
α_i, β_i *and* ϕ_i	Set of orthogonal functions for u, v and w displacement for plate
ϕ_i *and* ψ_i	Set of orthogonal functions for u and v displacement for beam
Ω	Dimensionless natural frequency of the system
ω	Natural frequency of the system
ω_1	Fundamental linear frequency
ω_{nl}	Non-linear frequency
δ	Variational operator
μ	Poisson's ratio
ρ_0	Density of the beam/plate material at (ξ=0)
τ	Time coordinate
ξ, η	Normalized coordinates along x and y direction
ε	Allowable error limit
ε_x^b	Axial strain due to bending
ε_x^s	Axial strain due to stretching
λ	Relaxation parameter

List of Figures

List of Tables

Abstract

The present thesis investigates static and dynamic behaviour of axially functionally graded structural elements (beams and plates) on elastic foundation with different boundary conditions. For beams, Euler-Bernoulli and Timoshenko beam model are separately considered, whereas, the plate is taken as thin plate. The material of structural elements is considered to be functionally graded continuously along longitudinal direction. To incorporate the material gradation, different material models are selected depending on the gradation of the elastic modulus and density in the axial direction. Non-uniform structural geometry has also been taken into account in the present thesis considering variation in thickness along the axial direction. For that purpose, linear, parabolic and exponential taper patterns are chosen for thickness. The structural elements are considered to be resting on elastic foundation with different classical boundary conditions and subjected under externally applied uniformly distributed load. The foundation has been mathematically incorporated into the analysis as a set of linear springs attached uniformly at the bottom surface of the structure. A displacement based semi-analytical method associated with the whole physical domain of the system is utilized for formulation of the problems throughout the thesis. Geometric nonlinearity is also included in the present thesis considering nonlinear strain-displacement relations. The governing set of nonlinear equations of the system are derived adopting suitable energy methods and solved by numerical application of suitable iterative methods. For beam (thin & thick), study of free vibration and forced vibration characteristics are performed, whereas, in case of plate, static and free vibration analysis are taken up.

The main concern of the static analysis is to represent the load versus deflection plot and deflected shape plot under the application of steady state loading considering the effect of various parameters viz. material model, taper pattern, system geometry and elastic foundation. The governing set of nonlinear equation in static analysis is derived utilizing principle of minimum total potential energy and unknown co-efficient of the governing equations are solved using an iterative method (direct substitution with relaxation).

The main focus of the free vibration analysis is to represent backbone curves and corresponding mode shapes. In order to generate these, it is necessary to find out the natural

frequencies of the system under undeformed and deformed conditions. The problem is divided in two distinct parts. Firstly, the static problem is carried out through an iterative scheme using a relaxation parameter and later on the subsequent dynamic problem is solved as a standard eigen value problem. The obtained results are validated from previously published results and are found to be in good agreement. The free vibrational frequencies are tabulated for different taper profile, taper parameter and foundation stiffness. The dynamic behaviour of the system is presented in the form of backbone curves in dimensionless frequency-amplitude plane. Investigation of mode switching for AFG plate on elastic foundation is also a vital consideration and leads to identification of particular conditions for which the above mentioned phenomenon is observed. Linear and nonlinear mode shape plots are also presented to compare the free vibration behaviour.

Forced vibration analysis is conducted with an objective to find out the response of the system, in terms of displacement amplitude, under externally applied time varying excitations. The derivation of governing equations is accomplished following Hamilton's principle. In the present work, only steady-state response is presented and frequency of response of the undamped system is assumed to be equal to that of the external excitation. An indirect approach is adopted for solving the problem, where it is reduced to a static scenario by assuming that under maximum amplitude of excitation, i.e., when the system suffers maximum deformation, the dynamic system fulfils force equilibrium conditions. Broyden method, which is a multidimensional secant method used for numerically solving a system of nonlinear equations. A convergence study is performed to determine the values for various parameters related to the numerical scheme. Established result from existing literature is used to provide validation for the adopted method and solution procedure. The geometric nonlinear forced vibration characteristic of the system is represented through frequency response curves in non-dimensional excitation frequency-maximum response amplitude diagrams. the effects of excitation frequency on the ODS (Operational Deflection Shape) is also investigated. New results, capable of acting as benchmark results, are provided for a ombination of different flexural boundary conditions, various material models and foundation stiffness values.

Chapter 1

INTRODUCTION

1.1 Introduction:

As far as structures are concerned, beams and plates can be considered as fundamental elements of a variety of engineering structure. These basic elements find their use in wide range of structural applications. It is well known that a beam is an element with considerably large longitudinal dimension compared to the cross-sectional dimensions and is primarily capable of carrying loads perpendicular to its longitudinal axis. Structures such as helicopter rotor blades, spacecraft antennae, robot arms, air-plane wings and many more subsystems of complex structures can be modelled as beams for the purpose of performing a variety of mathematical analysis. Most engineering analyses are based on the classical Euler-Bernoulli theory, in which straight lines or planes normal to the neutral beam axis remain straight and normal after deformation. This theory thus neglects the effect of transverse shear deformations, a condition that holds only in the case of slender beams. It is well-known that variation in shear force and moment distribution can become significant in the case of foundation beams with small length-to-depth ratio subjected to closely spaced discrete column loads, as well as in the case of flanged beams and beams with sandwich-like cross-section. To confront this problem, the well-known Timoshenko beam model, in which the effect of transverse shear deflections is considered, can be used.

On the other hand, a plate is a structural element which is characterized by small thickness in comparison with the other two dimensions (length and width). Generally, such structural elements are capable of withstanding transverse as well as axial loads. Building floors and walls, dams, bridge decks, ship hulls etc. are examples of structures that can be idealised as plates. Similar to the case of beams, there exist thin and thick plate theories to analyses such structures and the difference between them is on the basis of consideration of the shear deformation in the transverse direction. In case of both structural elements,

linear as well as nonlinear analysis are necessary depending on the situation under consideration and there are many theories catering to these aspects.

1.1.1 Functionally Graded Material (FGM):

Materials have played a significant role in the development of society throughout human history. Advancement in the field of materials has seen development of new and improved materials and their utilisation in engineering applications. One such category of materials is composites. Multi-layered composite materials are useful in aerospace, civil, mechanical engineering, automotive and nuclear industries due to their outstanding behaviour such as high ratio of stiffness and strength to weight and low maintenance cost. But contemporary laminated composite materials exhibit a mismatch of mechanical properties at an interface due to bonding of two discrete materials. As a result stress concentration usually occurs at the interface (Nguyen et al. 2013). This can lead to damage in the form of delamination, matrix cracking and adhesive bond separation.

One way to overcome the limitations of laminar composites is to combine materials with continuous variation in composition from one surface to another along any orthogonal direction. The materials created in such a way are called functionally graded materials (FGMs). The material properties such as elastic modulus, shear modulus, material density and Poisson's ratio vary continuously and smoothly along desired spatial directions. The advantage of FGMs over traditional composites is that, they retain most of the properties of their constituent materials. The continuous transition of materials also reduces residual and thermal stresses, stress concentration and provides high strength to weight ratio (Suresh and Mortensen 1998). With these characteristics, FGMs naturally attract the attention of various structural engineers and researchers and are gaining widespread applications in the various engineering industries including aerospace, mechanical, civil and nuclear domains. The FGMs were first developed by Japanese researchers in 1984 during a space-plane project when they came across the problem of thermal shielding due to high temperature during re-entry to atmosphere. The detailed information regarding FGMs such as its history, applications, fabrication process, modelling etc. are provided in reviews conducted by Markworth (1995), Suresh and Mortensen (1998), Berman and Byrd (2007), Liew et al. (2011), Jha et al. (2013), Thai and Kim (2015) and Swaminathan (2015) and. Apart from

man-made FGMs, there are some natural FGMs as well such as bamboo tree, bone, human skin etc.

Functionally graded materials can be broadly classified into two types on the basis of the direction of material gradation. One type is where the material properties vary along a single direction, either depth or any one of the longitudinal directions. If material properties vary along the thickness direction, the class of materials is called transversely functionally graded materials (TFG). This type of FGMs are the most popular and are presently used in many engineering applications such as spacecraft heat shields, heat exchanger tubes, biomedical implants, flywheels, and plasma facings for fusion reactors, etc. If the material is graded along the axial direction, it is classified under the axially functionally graded material (AFG). Structures made of AFG material may be advantageous over TFG structures in cases where cantilever and rotating structure is involved such as turbo-machine and turbine blades, helicopter rotor blades, and spacecraft with flexible appendages etc. The other type of graded material has property variations along multiple directions, i.e., properties vary along both transverse and axial directions simultaneously.

Although most of the engineering applications may be taken care of using unidirectional FGMs, there are practical occasions which require tailored grading of macroscopic properties in two or three directions (Nemat-Alla, 2003; Lu et al., 2008; Zhao et al., 2012; Simsek, 2015; Nejad and Hadi, 2016; Hao and Wei, 2016; Pydah and Sabale, 2017; Nguyen et al., 2017; Nemat-Alla, 2003; Shafiei et al., 2017). The temperature distributions in machine elements that are used in several applications such as space shuttles, nuclear reactors, aircrafts, ovens, combustion chambers, etc., change in two or three directions. Thus, proper and efficient operation of such elements necessities the use of effective high-temperature resistant materials. Steinberg (1986) showed the variations of the temperature at various places on the outer surface of a new aerospace craft during sustained flight at a speed of Mach 8 and altitude of 29 km. The temperature on the outer surface of such a plane ranges from 1033 K along the top of the fuselage to 2066 K degrees at the nose. Furthermore, this temperature level has to decay severely, through the thickness of the craft body, to the room temperature inside the craft. Such kind of aerospace craft added a new challenge to introduce and develop more effective high-temperature resistant

materials that can withstand high-external temperatures that have variations in two or three directions.

1.1.2 Elastic foundation:

In practice, boundary conditions of the structural elements are seldom classical. Under externally applied loads (axial or transverse) these elements rarely behave as ideal simply supported or ideal clamped structures. On the basis of practical considerations, an effective way to model the boundaries of structural elements is to incorporate elastic restraints or introducing elastic foundation. Specifically, various critical and frequently used load bearing components (very often encountered in analysis of building, geotechnical, highway, and railroad applications) can be idealised as a structure resting on elastic foundation. Its solution demands the modelling of the mechanical behaviour of the structure, the mechanical behaviour of the foundation and the form of interaction between the structure and the foundation.

While fairly realistic and efficient models of the material properties and the mechanical behaviour of the structure can be established by using beam (Timoshenko and Bernoulli–Euler theory) or even plate theory, the characteristics that represent the mechanical behaviour of the foundation and its interaction with the structure resting on it are difficult to model. Assuming a linear elastic, homogeneous and isotropic behaviour of the foundation, two major classes of foundation models can be identified in the literature:

(i) Continuous medium models: It can be surmised that these models, which are based upon the fundamental hypothesis of an elastic semi-infinite space, are more accurate. But, obtaining an exact analytical solution, even with the introduction of simplifying assumptions, turns out to be quite difficult (Selvadurai, 1979) in certain cases. However, numerical solutions for most situations are attainable via finite element simulations. Such finite element models guarantee precise calculation of stresses and deformations, but, are often associated with significant resources in terms of computer capacity and processing time. To reduce the computational burden, symmetries in the existing system can be utilized to reduce the initial three dimensional problem to a two dimensional one. Still, thorough knowledge and sound judgment is a pre-requisite on the part of the engineer to ensure satisfactory results.

(ii) Mechanical models: On the other hand, mechanical models are clearly less precise, but conceptually simple and easier to use. Winkler (1867) devised the oldest, yet most famous and most frequently used, mechanical model, where the foundation is replaced by a series of closely spaced linear elastic vertical springs that offer resistive forces proportional to the deflection of the beam. It was assumed that the springs were mutually independent of one another. In the Winkler model, the properties of the foundation are described only by the stiffness of the vertical spring (k). Hence, it is often referred to as single- or one-parameter elastic foundation. Owing to the simplicity of mathematical formulation, this model can be easily employed in a variety of problems and practical situations (Hetenyi, 1946) with satisfactory results.

However, due to its inability to take into account the continuity or cohesion of the foundation, it is considered as a rather crude approximation of the true mechanical behaviour of the foundation. This limitation, i.e., the assumption that there is no interaction between adjacent springs, also results in neglecting the influence of the foundation on either side of the beam. To overcome this weakness, several two-parameter elastic foundation models have been suggested (Filonenko-Borodich, 1940; Pasternak, 1954; Vlasov and Leontiev, 1966). In these models, the first parameter represents the stiffness of the vertical spring, as in the Winkler model, whereas the second parameter is introduced to account for the coupling effect of the linear elastic springs. It is worth mentioning that the interaction enabled by this second parameter also allows the consideration of the influence of the foundation on either side of the beam. Despite the introduction of a second parameter, the mathematical formulation of the problem and the corresponding analytical solutions remain relatively simple (Selvadurai, 1979). Thus, two-parameter models are less restrictive than the Winkler model but not as complicated as the elastic continuum model.

Three-parameter models constitute a generalization of two-parameter models, the third parameter being used to make them more realistic and effective. This category includes the models developed by Kerr, Hetenyi and Reissner (Kerr, 1965). One of the basic features of the three-parameter models is the flexibility and convenience that they offer in the determination of the level of continuity of the vertical displacements at the boundaries between the loaded and the unloaded surfaces of the foundation (Hetenyi,

1950). This feature renders them capable of distributing stresses correctly. Among all three-parameter models, the Kerr model is of particular interest. It represents a generalization of the two-parameter Pasternak model for which a series of solutions and applications are already available.

1.1.3 Structural analysis:

Structural analysis of a particular system can be studied mainly in two direction depending on the nature of the external influence on the system. Situations, where, response is considered under time invariant loading, are known as static analysis. Here, the focus is to determine maximum deflection, deflected profile, load carrying capacity, stress generated etc. in the system. On the other hand, there is dynamic analyses, which can pose serious and fatal consequences for the structure. Dynamic behaviour of systems is often characterized by vibration, which can be defined as the repetitive motion in alternately opposite directions from a position of equilibrium when that equilibrium has been disturbed. It involves continuous to and fro motion with alternative transfer of potential energy to kinetic energy and vice-versa.

Vibration can be classified in various ways, for example, free and forced vibration, damped and undamped vibration, linear and nonlinear vibration etc. If a system is subjected to an initial disturbance and then left to vibrate without interference from any external sources, the ensuing vibration is called free vibration. Vibration of a system under continuous time dependent repetitive external influence is known as forced vibration. Undamped vibration is an idealised scenario where no energy is dissipated during oscillation whereas, in case of damped vibration some energy is lost to the surrounding in each cycle of oscillation (due to friction or any other resistance) and eventually the system comes to a stop. Linear and nonlinear vibrations are defined on the basis of the linear and nonlinear behaviour of the system or its components. It is worth stating that nonlinearities are inherent in mechanical systems and assumption of linear behaviour is an idealisation based on the necessity for simplification.

1.1.4 Nonlinearity in structure:

Nonlinearity in a structure may arise from different sources but the two most commonly manifested nonlinearities are geometric and material nonlinearity. Geometric

nonlinearity is induced due to large deformations or large rotations of elastic bodies. The large deformation causes mid-plane stretching which couples the transverse displacement to axial strain, resulting in nonlinear strain-displacement relations. There are also instances when the deformation may not overstrain the material or produce stretching, but the system may exhibit curvature-displacement nonlinearity. Another type of nonlinearity is material or physical nonlinearity arising out of nonlinear stress-strain behaviour. Usually the stress-strain curve is nonlinear, but can be linearized within a limit under certain assumptions (Hooke's Law). It should be mentioned here that the assumption of linear elasticity forms the basis of analysis for structural elements such as beams and plates. Nonlinear elasticity, generally exhibited by elastomers (rubber like materials), is an example of material nonlinearity. Post-elastic behaviour of materials also usually falls into this category. Depending on the nature of the problem any one or both of geometric and material nonlinearities can be included in the analysis. Nonlinearity may also be induced in the system through nonlinear boundary conditions. Linear viscous damping is an idealization but damping may also essentially be treated as a nonlinear phenomenon. Hysteretic damping, aerodynamic drag etc. are examples of nonlinear damping.

The above description of different type of nonlinearities is far from complete or exhaustive. In fact, such discussion can hardly be taken up within the confines of a few paragraphs. Evan-Ivanowsky (1976), Nayfeh and Mook (1979) and Moon (1987) have explained the various nonlinearities in great detail with examples. There are many other sources of nonlinearities and linear systems are only approximations to simplify the complexity of the problem. It is well known that the presence of nonlinearity in a system complicates the analytical investigations. This is mainly due to the fact that the problems governed by nonlinear differential equations do not have the advantages of uniqueness and superposition of solutions.

1.2 Layout of thesis:

The present thesis is organised into a series of correlated chapters for better clarity and representation. In the following lines a brief description about these chapters are provided to bring out the layout of the thesis.

Chapter 1: Introduction

It describes the nature of the general subject area with concise discussion on certain keywords relevant to the present thesis. Brief description of functionally graded materials is provided along with a separate discussion on the mechanical behaviour of the structure and elastic foundation and their interaction. An introduction to structural analysis ia also provided, while various types of nonlinearities are discussed keeping in mind the relevance to the present work.

Chapter 2: Literature review

This chapter presents detailed review of the available literature that has helped in identifying the most important issues and unexplored areas related to the current study. It is needless to say that a comprehensive review of research done in the domain would far exceed the confines of a single chapter. So, an effort is made to proffer only those papers that are most relevant and help in setting up the background and motivation behind the present work.

Chapter 3: Free Vibration: Axially Functionally Graded Thin Beams on Elastic Foundation

This chapter deals with large amplitude (geometric nonlinear) free vibration analysis of a Euler-Bernoulli axially functionally graded (AFG) non-uniform beam on elastic foundation under the transverse loading. The analysis looks into amplitude dependency of the loaded natural frequency. The free vibration frequencies are tabulated for non-uniform profile subject to various boundary conditions and foundation stiffness. The dynamic behaviour of the system is presented in the form of backbone curves in dimensionless frequency-amplitude plane to detect the effect of the elastic foundation, material models and taper patterns. In some particular case the mode shape results are furnished.

Chapter 4: Forced Vibration: Axially Functionally Graded Thin Beams on Elastic Foundation

This chapter discusses large amplitude forced vibration analysis of Euler Bernoulli AFG beams resting on elastic foundation subjected to transverse harmonic excitation with

an objective to find out the response of the system, in terms of displacement amplitude. Broyden method, which is a multidimensional secant method, is used for numerically solving a system of nonlinear equations. The large amplitude dynamic behaviour of the system in terms of non-dimensional frequency response curves is validated against established results and new results are furnished for tapered AFG beam on linear elastic foundation to represent the effect of the excitation amplitude, material model, taper pattern and foundation stiffness.

Chapter 5: Free and Forced Vibration Analysis: Axially Functionally Graded Timoshenko Beam on Elastic Foundation

This chapter deals with both free and forced vibration analyses of AFG Timoshenko beams on elatic foundation in two separate sections with different basic assumptions. The nonlinear free vibration problem is solved in two steps where the objective in the first part is to compute the stiffness matrix in deflected configuration through a static analysis. This equivalent stiffness matrix is directly used in dynamic analysis for obtaining eigenvalues and eigenvectors which form the natural frequency and mode shape of the system, respectively. The assumption in the nonlinear forced vibration analysis is that all the forces acting on the system attains equilibrium at the peak amplitude, which enables the dynamic problem to be solved as an equivalent static problem. The static analysis in the first part of free vibration is based on principle of minimum total potential energy whereas Hamilton's principle is used in dynamic analysis of both free and forced vibration. The results are presented in terms of backbone curves and mode shapes in free vibration analysis and frequency-response curves and operational deflection shapes in forced vibration scenario.

Chapter 6: Static and Free Vibration Analysis: Axially Functionally Graded Thin Plates on Elastic Foundation

This chapter presents the static and free vibration analyse of AFG thin plate on elastic foundation separately with different basic assumptions. Load vs amplitude plot, deflected shape plot are presented in static analysis, whereas in free vibration analysis backbone curve corresponding to different combinations of system parameters are presented in non-dimensional plane. Mode switching phenomenon are detected and linear and nonlinear mode shapes are furnished to support the presence of switching phenomenon.

The effects of the boundary conditions and non-uniformity of the plate shape are also highlighted.

Chapter 7: Conclusion and future scope of work

This chapter draws the conclusion for the present research work and provides the scope for future work for further investigation in this field.

Appendix

A section of subsidiary matters are provided here. The element details of the stiffness matrix, mass matrix and load vector are enlisted here separtely for beam (Euler bernoulli beam and Timoshenko beam) and plate.

Bibliography

A list of references used in the present thesis is provided here.

Chapter 2

LITERATURE REVIEW

2.1 Introduction:

Being the most commonly used structural elements, beams and plates have always been the centre of attention of structural engineers and scholars. After the introduction of functionally graded materials (FGMs) in structures, many researchers have concentrated their efforts in the area of modelling and analysis of such elements made up of graded materials. On the other hand, study of behaviour of beams and plates on elastic foundation is an interesting domain of research as several critical engineering structures which generally serve as the key load-bearing components, like rail track, rigid pavements, bridge decks, mat and raft foundations etc., can be idealized as structure on foundation. The sheer quantity of published literature related to these elements makes it impossible to list all of them within the confines of a single chapter. However, keeping within the space limitation, most of the relevant articles and books are referred in the following paragraphs to provide an idea about the background and current status of research in the corresponding area. The section is mainly categorised into three parts –

- Literatures on Euler-Bernoulli Beam
- Literatures on Timoshenko Beam
- Literatures on Plate

For better clarity to the readers, these three sections are further classified into two subsections to cite the related literatures on material gradation and elastic foundation.

2.2 Literatures on Euler-Bernoulli beam:

Euler Bernoulli beams are the most simplified class of all types of beams which follow some basic assumptions under deformation. The cross sections of such beam do not deform in a significant manner under the application of transverse or axial loads and can

be assumed as rigid. The cross section of the deformed beam is assumed to remain planar and normal to the deformed axis of the beam. These assumptions have been extensively confirmed for slender beams made of isotropic materials with solid cross-sections. The thickness-to-length ratio are approximately considered less than 1:100. By virtue of slenderness, shear deformation and rotary inertial effects are ignored. Still, simplicity of Euler Bernoulli beam theory makes it an important tool, especially for structural and mechanical engineering and attacts researchers to explore different aspects of it. Some recent and relevent literatures are reviewed in the following sections to set the background of the present work. These papers are further categorized into two sub-sections containing research on thin beams with material gradation and thin beams supported by foundation, respectively.

2.2.1 Literatures on material gradation:

The variation of material properties in functionally graded (FG) Euler-Bernoulli beams may be oriented in transverse (thickness) direction or longitudinal/axial (length) direction or both. An exhaustive literature review of the relevant domain reveals that majority of the studies are concentrated on free vibration analysis of FG Euler-Bernoulli beams with material property variation along the depth of the beam.

Li (2008) presented a unified approach for analysing static and dynamic behaviours of functionally graded beams (FGB), in which, all material properties were arbitrarily varied along the beam thickness. For the need of analysis, the author analytically reduced Euler–Bernoulli beam theories from the Timoshenko beam theory. Simsek and Kocatürk (2009) investigated free vibration characteristics and the dynamic behaviour of a functionally graded simply-supported beam under a concentrated moving harmonic load assuming continuous variation of material properties in the thickness direction according to exponential and power-law form. The system of equations of motion were derived by using Lagrange's equations under the assumptions of the Euler–Bernoulli beam theory. Simsek (2010) investigated vibration of a functionally graded (FG) simply-supported beam due to a moving mass by using Euler–Bernoulli, Timoshenko and the third order shear deformation beam theories considering thickness directional material properties variation. A mixed method was presented by Khalili et al. (2010) to study the dynamic behaviour of transversely functionally graded (TFG) beams subjected to moving loads. In the paper,

theoretical formulations were based on Euler–Bernoulli beam theory, and the governing equations of motion of the system were derived using the Lagrange equations. The Rayleigh–Ritz method was employed to discretize the spatial partial derivatives and a step-by-step differential quadrature method (DQM) was used for the discretization of temporal derivatives. Nonlinear vibration of beams made of transversely functionally graded (TFG) materials was studied by Ke et al. (2010) based on Euler-Bernoulli beam theory and von Kármán geometric nonlinearity. The authors assumed that material properties follow either exponential or power law distributions through thickness direction. Alshorbagy et al. (2011) presented the dynamic characteristics of functionally graded beam with material graduation in axial or transverse direction through the thickness based on the power law. In the paper, system of equations of motion was derived by using the principle of virtual work under the assumptions of the Euler–Bernoulli beam theory and finite element method was employed to discretize the model for numerical approximation. Eltaher et al. (2012) presented free vibration analysis of transversely functionally graded (TFG) size-dependent nanobeams using finite element method on the basis of Euler–Bernoulli beam theory and nonlocal continuum model. The authors (Eltaher et al., 2013) also investigated size-dependent static-buckling behaviour of functionally graded (FG) nanobeams on the basis of the nonlocal continuum model, where material properties were assumed to vary through the thickness according to the power law. In this paper as well, nanobeam was modelled according to the Euler–Bernoulli beam theory with small deformation. The finite element method was used to discretize the model and obtain a numerical approximation of equilibrium equations. They (Eltaher et al., 2013) also exploited a modified functionally graded beam theory to investigate natural frequencies of macro/nanobeams. The FG nanobeam, where, material properties were assumed to vary through the thickness according to a power law, was studied on the basis of the nonlocal Eringen continuum model. The authors considered Euler–Bernoulli beam theory for kinematic assumption and finite element method for numerical approximation. A size-dependent functionally graded Euler–Bernoulli beam model was developed by Kahrobaiyan et al. (2012) based on the strain gradient theory to capture the size-effect in micro-scaled structures. Here, the properties were assumed to vary through the thickness according to a power law. Pradhan and Chakraverty (2013) investigated free vibration of functionally graded Euler beams by Rayleigh–Ritz method, where Material properties of the beam varied continuously in the

thickness direction according to the power-law exponent form. Ebrahimi et al. (2016) analysed thermo-mechanical vibration of transversely functionally graded (TFG) Euler beams made of porous material subjected to various thermal loadings. The authors employed a semi analytical differential transform method (DTM) for the first time to obtain a Navier type solution.

On the other hand, investigation of axially functionally graded (AFG) structural elements is a relatively newer domain of study that has gained prominence in the present decade. Huang and Luo (2011) presented a simple approach to exactly calculate the critical buckling loads of beams with arbitrary axial inhomogeneity. Shahba and Rajasekaran (2012) investigated the free vibration and stability of axially functionally graded tapered Euler–Bernoulli beams through solving the governing differential equations of motion. Kien (2013) carried out large displacement analysis of tapered cantilever beams made of axially functionally graded material by the finite element method. Li et al. (2013) derived closed form characteristic equations for axially functionally graded (exponential gradation) beams with various end conditions, such as clamped, pinned, guided, free etc., in order to examine the influence of gradient on frequency spectrum. Euler Bernoulli theory alongside modified couple stress theory was utilised by Akgöz and Civalek (2013) to present free vibration behaviour of non-homogenous (along the axis) and non-uniform fixed-free microbeams. Zeighampour and Beni (2015) studied the vibration of axially functionally graded material (AFGM) nano-beam by using strain gradient theory. Kumar et al. (2015) carried out free vibration analysis on axially functionally graded (AFG) tapered slender beams under different boundary conditions.

Modern aerospace shuttles and craft are subjected to super high temperatures that have variation in two or three directions, which need to introduce new materials that can endure such applications. A few numbers of literatures are available in this perticular class of FGM for Euler-Bernoulli beam. Lu et al. (2008) presented elasticity solutions for bending and thermal deformations of functionally graded beams with various end conditions, using the state space-based differential quadrature method. Zhao et al. (2012) suggested a symplectic framework for the analysis of plane problems of bi-directional functionally graded materials (FGMs). The elastic modulus was assumed to vary exponentially along both longitudinal and transverse coordinates while the Poisson's ratio

remained constant. Lezgy-Nazargah (2015) studied fully coupled thermo-mechanical behaviour of bi-directional functionally graded material (FGM) beam structures using a computationally low cost isogeometric finite element model. Nejad and Hadi (2016) performed non-local bending, buckling and free vibration analysis of of bi-directional functionally graded euler–bernoulli nano-beams with small scale effects. Zhao et al. (2016) presented elasticity solutions for bi-directional functionally graded beams subjected to arbitrary lateral loads, with emphasis on the end effects. In this paper, the material was considered macroscopically isotropic, with Young's modulus varying exponentially in both axial and thickness directions, while Poisson's ratio remained as constant. Flexure of bi-directional functionally graded (FG) circular beams was analyzed using the kinematical assumptions of the Euler–Bernoulli theory by Pydah and Sabale (2017) by simultaneously varying the material properties along the axis (tangential direction) and thickness (radial direction) of the beam.

2.2.2 Literatures on elastic foundation:

Theory of Euler-Bernoulli beams on elastic foundation is one of the cornerstones of engineering mechanics and is applicable to a wide range of practical problem in both the civil and mechanical engineering fields. As it constitutes the best practical idealization for many real life problems, it has application in geotechnics, bio-mechanics, road, railroad and marine engineering. The importance of the problem is underscored by large number of research articles which are in existence in the literature. Its beginning can be traced back to 1867 classical textbook by Emil Winkler. However, throughout the years the interest in this particular research domain has remained strong and a survey of existing literature reveals a plethora of recent work related to this field. However, under the present circumstances of emphasizing reasearch related to graded materials, the following paragraphs cite work related to graded thin beams on foundation.

Huang and Luo (2011) presented a new and simple method to calculate the critical buckling loads of beams with axial inhomogeneity on elastic foundation. Simsek and Cansız (2012) studied the dynamic responses of an elastically connected double-functionally graded beam system (DFGBS) carrying a moving harmonic load at a constant speed by using Euler–Bernoulli beam theory. The equations of motion were derived with the aid of Lagrange's equations. Murin et al. (2013) presented a differential equation of the

homogenized functionally graded material (FGM) beam deflection. The solution was used in free vibration analysis of the beams with polynomial continuous longitudinal and transversal variation of material properties. The FGM beams were considered to be resting on longitudinal variable (Winkler) elastic foundation. Kanani et al. (2014) investigated large amplitude free and forced vibration behaviour of FG beam resting on nonlinear elastic foundation containing shearing layer and cubic nonlinearity. Niknam and Aghdam (2015) made an attempt to obtain a closed form solution for both natural frequency and buckling load of nonlocal FG beams resting on nonlinear elastic foundation. Akgöz and Civalek (2015, 2016) investigated the bending response of non-homogenous micro-beams (2015), as well as single-walled carbon nanotubes (SWCNTs) (2016) embedded in an elastic medium based on modified strain gradient elasticity theory in conjunctions with various beam theories.

2.3 Literatures on Timoshenko beam:

Timoshenko beam theory takes into account shear deformation and rotational bending effects, making it suitable for describing the behaviour of thick beams. The resulting equation is of higher order but, unlike Euler–Bernoulli beam theory, there is also a second-order partial derivative present. Physically, taking into account the added mechanisms of deformation effectively lowers the stiffness of the beam, while the result is larger deflection under a static load and lower predicted eigen-frequencies for a given set of boundary conditions. For this reason, the Euler–Bernoulli model always overestimates the analysis outcomes i.e. deflections in static analysis, natural frequencies in free vibration analysis and the frequency response in forced vibration analysis. Hence, the Timoshenko beam theory has to be employed to analyse structural problem effectively. Over the years, many researchers have done exactly that by utilising the said theory in various research scenarios. In the following sub-sections a few relevant papers in the domain of graded Timoshenko beams and graded thick beams on foundation are cited.

2.3.1 Literatures on material gradation:

Analysis of functionally graded Timoshenko beam provides many fronts in which research can be carried out and includes both unidirectional as well bidirectional variation of material properties, along with other complicating effects. Research work on FGM

beams involving depth/thickness-wise variation of material properties are abundant in literature. A brief overview of few of such researches is offered in the following paragraphs.

Analysis of thermal post-buckling of FGM (Functionally Graded Material) Timoshenko beams subjected to transversely non-uniform temperature rise was presented by Li et al. (2006) considering the axial extension and transverse shear deformation in the sense of theory of Timoshenko beam. Geometrical nonlinear governing equations were formulated including seven basic unknown functions for functionally graded beams subjected to mechanical and thermal loads. In the analysis, it was assumed that the material properties of the beam vary continuously as a power function of the thickness coordinate. Li (2008) presented a new unified approach for analysing the static and dynamic behaviours of functionally graded beams (FGB) with the rotary inertia and shear deformation included and analytically reduced the Euler–Bernoulli and Rayleigh beam theories from the Timoshenko beam theory. All material properties were considered arbitrary functions along the beam thickness. Nonlinear vibration of beams made of functionally graded materials (FGMs) containing an open edge crack was studied by Kitipornchai et al. (2009) and Ke et al. (2009) based on Timoshenko beam theory and von Karman geometric nonlinearity. The cracked section was modelled by a massless elastic rotational spring. It was assumed that material properties follow exponential distributions through beam thickness. For the same problem, the authors (Kitipornchai et al.,2009) studied the post buckling response of the beams. They (2010) also investigated the nonlinear free vibration of functionally graded nanocomposite beams reinforced by single-walled carbon nanotubes (SWCNTs) based on Timoshenko beam theory and von Kármán geometric nonlinearity. The material properties of functionally graded carbon nanotube-reinforced composites (FG-CNTRCs) were assumed to be graded in the thickness direction and estimated through the rule of mixture. Simsek (2010) performed non-linear dynamic analysis of a functionally graded (FG) beam with pinned–pinned supports due to a moving harmonic load by using Timoshenko beam theory with the von-Kármán's non-linear strain–displacement relationships. Material properties of the beam varied continuously in thickness direction according to a power-law form. The system of equations of motion was derived by using Lagrange's equations. A size-dependent formulation was presented by Asghari et al. (2011) for Timoshenko beams made of a functionally graded material (FGM). The formulation was developed on the basis

of the modified couple stress theory to capture the small-scale size effects in the mechanical behaviour of structures. The beam properties were assumed to vary through the thickness of the beam. Ansari et al. (2011) investigated the free vibration characteristics of microbeams made of functionally graded materials (FGMs) based on the strain gradient Timoshenko beam theory. The material properties of the functionally graded beams were assumed to be graded in the thickness direction according to the Mori–Tanaka scheme. Ke et al. (2012) investigated nonlinear free vibration of microbeams made of functionally graded materials (FGMs) based on the modified couple stress theory and von Kármán geometric nonlinearity. The non-classical beam model was developed within the framework of Timoshenko beam theory which contained a material length scale parameter related to the material microstructures. The material properties of FGMs were assumed to be graded in the thickness direction according to the power law function and were determined by Mori-Tanaka homogenization technique. Simsek and Yurtcu (2013) examined static bending and buckling of a functionally graded (FG) nanobeam based on the nonlocal Timoshenko and Euler–Bernoulli beam theory incorporating the length scale parameter (nonlocal parameter) which can capture the small scale effect. The material properties of the FG nanobeam were assumed to vary in the thickness direction. A microscale functionally graded Timoshenko beam model was developed by Simsek et al. (2013) for the static bending analysis based on the modified couple stress theory (MCST). The material property variation in the thickness direction of the FG microbeams were estimated through the Mori–Tanaka homogenization technique and the classical rule of mixture. In a paper that also considered graded Euler beams (previously cited in the section dealing with thin beams), Pradhan and Chakraverty (2013) investigated the free vibration analysis of functionally graded material (FGM) Timoshenko beams subjected to different sets of boundary conditions. The analysis was based on the classical and first order shear deformation beam theories, while, material properties varied continuously in the thickness direction according to the power-law exponent form. Li and Batra (2013) derived analytical relations between the critical buckling load of a functionally graded material (FGM) Timoshenko beam and that of the corresponding homogeneous Euler–Bernoulli beam subjected to axial compressive load. Ansari et al. (2013) studied bending, buckling and free vibration responses of Timoshenko microbeams made of functionally graded materials (FGMs). In the study, to take size effect into account, the most general strain gradient

elasticity theory was incorporated into the classical Timoshenko beam theory to develop a size-dependent beam model containing five additional material length scale parameters. Rahmani and Pedram (2014) discussed with Timoshenko beam theory that applied the size dependent effects in functionally graded material (FGM) beam. The material properties of FG nanobeams were considered to vary over the thickness based on the power law. The equations of motion were derived according to Eringen nonlocal theory, using Hamilton's principle and a closed-form solution was presented for vibration behaviour of the proposed model.

There are several articles devoted to explore static, dynamic and buckling behaviour of axially functionally graded (AFG) non-uniform thick beams based on Timoshenko beam theory. Due to the presence of variable coefficients and non-linear equations, exact solutions of the governing equations are generally unavailable. Therefore, several numerical methods have been used to obtain solutions to AFG beam problems. In the following paragraph, selected research works are highlighted in order to set the backdrop for the present thesis.

Shahba et al. (2011) introduced a new beam element and studied the free vibration and buckling behaviour on AFG tapered Timoshenko beams through FE approach. Huang et al. (2013, 2016) presented a unified approach to investigate free vibration and buckling behaviours of AFG Timoshenko non-uniform beams. Rajasekaran (2013) adopted differential transformation method and differential quadrature element method of lowest order to perform free vibration analysis of rotating AFG Timoshenko tapered beams considering four first order differential equations. Sarkar and Ganguli (2014) obtained closed form solution for free vibration of AFG Timoshenko beams with uniform cross-section, having clamped-clamped boundary condition. Calim (2016) used complementary functions method and modified Durbin's algorithm to study transient behaviour of AFG Timoshenko tapered beams. Shafiei et al. (2016) performed free vibration analysis on a rotary AFG micro-beam on the basis Euler–Bernoulli and Timoshenko beam theories using generalized differential quadrature method and compared the results of the two beam theories. Kiani (2016) studied the transverse vibration of AFG tapered nanobeams in a longitudinal temperature gradient. Based on the hypotheses of the Rayleigh, higher-order, and Timoshenko beam theory, the equations of motion of the nanobeam were displayed

using surface elasticity theory of Gurtin–Murdoch. El-Ashmawy et al. (2016) proposed a generalized non-conventional finite element (FE) model for beam following Timoshenko beam theory and performed static and dynamic analysis for AFG Beam. Wang and Wu (2016) investigated the dynamic response of an AFG beam under thermal environment and subjected to a moving harmonic load on the basis of classical beam theory as well as Timoshenko beam theory. Zhao et al. (2017) introduced a new approach based on Chebyshev polynomials theory to study free vibrational behaviours of AFG Timoshenko beams with tapered cross-sections. Lagrange's equation was applied to obtain the discrete governing equation. Sari et al. (2017) developed a model based on Timoshenko beam theory for AFG non-uniform nanobeams with Eringen's nonlocal residuals and studied the effects of the residuals on the natural frequencies and mode shapes. Chen et al. (2017) conducted free vibration analysis on a nanoparticle carrying AFG nano-cantilevers with an emphasis on the effect of mass and rotational inertia of the nanoparticle. Ghayesh (2018) performed nonlinear forced vibration study of AFG Timoshenko tapered beams. Recently, Huang et al. (2018) studied the free vibration a spinning AFG Timoshenko beam. A spectral-Tchebychev method was employed to solve the dynamic properties of the beam and finally, the effect of AFG material on critical speeds and whirling frequencies was obtained.

Special types of material, where, gradation of material properties is considered along two orthogonal directions simeltaneously, may have excellent thermal property to specifically deal with unevenly distributed thermal loads in two directions. However, literatures on such type of FGM on the basis of Timoshenko beam theory are not abundant. Simsek (2015) investigated free and forced vibration of bi-directional functionally graded (BDFG) Timoshenko beam under the action of a moving load by varying the material properties of the beam exponentially in both axial and thickness directions. The author (2016) also presented two-dimensional functionally graded materials (2D-FGMs) for the first time to investigate buckling of beams with different boundary conditions. Hao and Wei (2016) established the motion differential equations of the bi-directional functionally graded Timoshenko beam using Hamilton's principle to analyse the free and forced vibration behaviours. Nguyen et al. (2017) studied the vibration of bi-dimensional functionally graded Timoshenko beams excited by a moving concentrated load assuming

the volume fraction of constituent materials to vary in both the thickness and longitudinal directions by power-law functions. A shear deformation theory including a logarithmic function in the postulated expression for the circumferential displacement was developed by Pydah and Batra (2017) for thick circular beams and was used to analytically solve static deformations of bi-directional functionally graded circular beams. Shafiei et al. (2017) presented an analysis on the vibration behaviour of the two-dimensional functionally graded (2D-FG) nano and microbeams based on Timoshenko beam theory. In this paper, the beams, made of two kinds of porous materials, were modelled as 2D-FGMs according to the power law.

2.3.2 Literatures on elastic foundation:

Study of behaviour of Timoshenko beams on elastic foundation is an interesting domain of research as several critical engineering structures can be idealized as beams on foundation. Issues related to such structures are taken up for investigation because they belong to a class of frequently used structural elements which generally serve as the key load-bearing components, like rail track, rigid pavements, bridge decks, mat and raft foundations etc. Literature review reveals that there exist a number of papers related to FG Timoshenko beam on elastic foundation.

Mohanty et al. (2011) investigated the dynamic stability of FG Timoshenko beam and FG sandwich (FGSW) beam on Winkler elastic foundation through FE method. Yan et al. (2011) studied the dynamic response of FG beams with an open edge crack supported on elastic foundation and subjected to a moving transverse load. Timoshenko beam theory was used in theoretical formulations to account for the transverse shear deformation. Yas and Samadi (2012) studied free vibration and buckling behaviour of nanocomposite Timoshenko beams reinforced by single-walled carbon nanotubes on an elastic foundation. The governing equations were derived through employing Hamilton's principle and solved by utilizing the generalized differential quadrature method. Esfahani et al. (2013) examined thermal buckling and post-buckling analysis of FGM Timoshenko beams on a non-linear elastic foundation. Timoshenko beam theory and von-Karman's strain–displacement relations were employed to obtain the non-linear equations. Generalized Differential Quadrature Method was applied to solve the non-linear equations in space domain. Komijani et al. (2014) investigated buckling, post-buckling behaviour and vibrations of FG

Timoshenko beams rested on nonlinear elastic foundation and subjected to in-plane thermal loads. The von Kármán nonlinearity and modified couple stress theory were employed to derive the governing nonlinear equations. Generalized differential quadrature method was used to discretize the motion equation and Newton's method was used to solve the nonlinear algebraic equations. Tossapanon and Wattanasakulpong (2016) utilized Chebyshev collocation method to solve buckling and vibration problems of FG sandwich beams resting on two-parameter elastic foundation on the basis of Timoshenko beam theory in order to incorporate the significant effects of shear deformation and rotary inertia. Deng et al. (2017) proposed an exact solutions of double-FG Timoshenko beams on Winkler-Pasternk elastic foundation. Hamilton's principle was used to derive the differential equations of motion. Arefi and Zenkour (2017) studied wave propagation analysis of a FG nanobeam made of magneto-electro-elastic materials and rested on Visco-Pasternak foundation using Timoshenko beam model. Surface elasticity was applied for modelling the behaviour of nanobeam. Hamilton principle was used to derive the equations of motion. Arefi and Zenkour (2017) studied wave propagation analysis for a FG nanobeam with rectangular cross-section on visco-Pasternak's foundation using Timoshenko's beam model and nonlocal elasticity theory. The equations of motion were derived using Hamilton's principle.

The research papers described in the above paragraph dealt with transversely graded Timoshenko beams on elastic foundation. On the other hand, AFG Timoshenko beam on elastic foundation is a more recent domain of research and till now, only a few articles are available in literature in this field. Calim (2016) analysed free and forced vibrations of AFG Timoshenko beams on two-parameter viscoelastic foundation. Complementary functions method was utilized to solve the differential equations in Laplace domain and modified Durbin's algorithm was applied to transform the results into the time domain. However, there are a few research works relating to elastic foundation supported AFG thin beams (previously highlighted in Section 2.2.2), where Euler-Bernoulli theory is utilised for mathematical formulation of the problem.

2.4 Literatures on plate:

Applications involving uneven distribution of mechanical, thermal or chemical loading are relevant to graded plates. As a classic example of such an application the outer

skin of a space re-entry vehicle may be cited, where the material has to withstand elevated temperatures on one side along with high structural strength. The applications FGM plate can also be found in various other engineering scenarios, such as, reinforced slabs, highways bridge decks, flight wings, ship hulls, aerospace structures and automobile components. Defence industries, electronics and bio-medical sectors also find extensive applications for these types of materials (Tornabene and Viola, 2009).

2.4.1 Literatures on material gradation:

Analysis of FGM plate is an interesting and important subject of research, which has attracted and continues to attract the focus of researchers over the last few decades. In a FGM plate inhomogeneity can be present in single or multiple orthogonal directions, namely, transverse and/or in-plane directions. Investigations involving material inhomogeneity in the thickness direction are abundant in literature. Birman and Byrd (2007) presented a review on most recent development of structures made of FG materials since 2000. Various theoretical aspects and applications of FGM were reflected upon in this paper. A critical review on the recent research activity on the functionally graded plates was presented by Jha et al. (2013). An attempt was made in this article to identify and highlight the most relevant topics to FGM and review the corresponding publications. In the following paragraphs a few research papers relating to thickness-wise gradation are described in brief in order to set the framework of the present work.

Buckling analysis of FGM plate was studied by Feldman and Aboudi (1997) under uniaxial compression loading using classical plate theory. Static deflection and stress analysis of FGM plates was studied in details using third order shear deformation theory by Reddy (2000). Chi and Chung (2006) investigated the mechanical behaviour of a simply supported FGM plate of moderate thickness loaded under transverse loading. The solution was based on the classical plate theory (CPT) and Fourier series expansion. Abrate (2008) proposed a new approach to analyse FG plate by using no special tools as he postulated that FG plates behaved same as homogeneous plates. In the model the variation in material properties of the plate was performed by introducing a coupling between the in-plane and transverse deformations. An edge-based smoothed finite element method was proposed by Nguyen-Xuan et al. (2011) with stabilized discrete shear gap technique to analyse static bending, free vibration and buckling behaviours of FGM plate. Von Karman type of

geometric nonlinearity was also considered. Singha et al. (2011) utilized high precision FE method to study the nonlinear behaviours of FGM plates. The formulation was based on First Order Shear Deformation Theory (FSDT) and solution was obtained through Newton–Raphson iteration technique. Akbarzadeh et al. (2011) represented an analytical solution to investigate the behaviour of FGM rectangular plates based on FSDT and 3rd order Shear Deformation Theory (SDT). The mathematical formulation was displacement based and derived governing sets of equations were solved by the Fourier series expansion to obtain the natural frequencies. Ramu and Mohanty (2014) performed same type of analysis on FGM plate but under uniaxial and biaxial compression load. The kinematics of plates was based on S-FSDT, which was four-variable refined plate theory. Static and free vibration analysis was performed on FGM plate by Bernardo et al. (2016). Bending and free vibrations analysis of FGM annular and circular micro-plates was conducted by Eshraghi et al. (2016) under thermal loading condition. Modified couple stress theory was used for formulation and governing set of equations was derived using Hamilton's principle. Kennedy et al. (2016) equivalently modelled a FG plate as a plate of sequentially stacked multiple isotropic layers. Classical Plate theory (CPT), First Order Shear Deformation Theory (FSDT) and Higher Order Shear Deformation Theory (HSDT) were used to obtain the governing equations for separate models to study buckling and dynamic behaviour. Sharma and Parashar (2016) employed Generalized Differential Quadrature method to study the free vibration of FG piezoelectric annular plate on the basis of modified Mindlin plate theory. An efficient mesh-free numerical approach was studied to analyse bending and free vibration of FG plates by Vu et al. (2017). The methodology was based on a meshless method and a FEM approach. Liu et al. (2017) performed static bending, free vibration and buckling behaviour study of FGM plates. The formulation of the plate was based on isogeometric analysis and a simple quasi-3D hyperbolic shear deformation theory. Mantari and Monge (2017) studied the buckling, free vibration and bending analysis based on an optimized hyperbolic unified formulation of FGM sandwich plates. Mohammadzadeh-Keleshteri et al. (2017) utilized generalized differential quadrature method to study non-linear vibration of FG carbon nanotube reinforced composite annular sector plates with piezoelectric layers on the basis of FSDT. Von Karman type of geometrical nonlinearity was considered. The governing set of equations were derived

through Hamilton principle, while solution was achieved using direct iterative method and GDQM to highlight the variation of frequency vs amplitude plot.

On the other hand, research work involving material inhomogeneity in the in-plane/axial direction are comparatively less in literature, although they have potential for applications in civil, mechanical, aerospace and marine engineering. Liu et al. (2010) presented free vibration of a FG rectangular plate with in-plane material imperfection. The edge condition was considered as simply supported and a Levy-type solution was formulated. The differential equations were solved considering a particular integration method. Uymaz et al. (2012) carried out vibration analysis of FG plates with in-plane material gradation with different boundary conditions. Formulation was on the basis of shear deformable plate theory and assumed displacement field. Xiang et al. (2014) used scaled boundary FE approach to study free vibration and buckling of FG plates with in-plane material imperfection. Two-dimensional higher order spectral element was considered to model the in-plane dimensions of the plate. The stiffness matrix was derived directly from spectral element. Chu et al. (2014) proposed a mesh-free free vibration analysis on in-plane inhomogeneous FGM plate using Hermite-type collocation method. Effect of material inhomogeneity on the natural frequencies and mode shapes were investigated. The authors (Chu et al., 2016) also used the same type of methodology on same type of inhomogeneous material to investigate the buckling behaviour of FGM plate. Yin et al. (2016) investigated buckling and free vibration analysis of FGM plates considering in-plane material inhomogeneity using an effective approach which was based on higher-order shear deformation theory and isogeometric analysis. The effects of material inhomogeneity, boundary conditions and length to thickness ratio on critical buckling loads and natural frequencies were studied. The authors (Yin et al., 2017) also formulated a rotation free isogeometric analysis on the basis of Kirchhoff-Love theory to investigate free vibration analysis and buckling behaviours of thin FGM plate with in-plane material inhomogeneity. Recently, Kumar et al. (2014, 2015, 2016, 2017) made an effort to explore the static and dynamic behaviour of in-plane/axial inhomogeneous FG plate by using energy principle based on displacement field. The authors (Kumar et al., 2015; Kumar et al., 2017) performed nonlinear forced vibration on non-uniform AFG plates. For the formulation purpose Hamilton's principle was used to obtain the set of governing equations

and the solution of equations were performed through Broyden method and direct iterative method. The influences of taper parameter and excitation amplitude on forced vibration frequency response of the plates were observed. The authors (Kumar et al., 2014; Kumar et al., 2016) also studied free vibration of axial inhomogeneous plate through backbone curves to show the geometric nonlinearity effects. Hussein and Mulani (2018) dealt with the optimization of in-plane FG nano-reinforced panels for buckling load. For that purpose different types of panels with or without stiffner and cutouts were considered. The main objective was to minimize the nano inforcement to satisfy the desired buckling constraints.

Few researcher have stuided the case of FGM plate in which multiple direction material gradation is considered simalteniously. Nemat-Alla (2003) introduced a two-dimensional functionally graded materials to withstand super high temperatures and to give more reduction in thermal stresses. The author (Nemat-Alla, 2009) carried out an investigation on composition optimization for ZrO_2/6061-T6/Ti-6Al-4V 2D-FGM, under a severe thermal loading cycle (consisting of heating followed by cooling) based on the minimization of temperatures and thermal and residual stresses. Nemat-Alla et al. (2009) proposed a 3D finite element model of two dimensional functionally graded plates made of ZrO_2, 6061-T6 and Ti-6Al-4V with temperature dependent material properties to perform elastic–plastic analysis under thermal loading. Lu et al. (2009) presented semi-analytical 3-D elasticity solutions for orthotropic multi-directional functionally graded plates using the differential quadrature method (DQM) based on the state-space formalism. Material properties were varied not only through the thickness but also in the in-plane directions following an exponential law. Nie and Zhong (2010) presented dynamic analysis of multi-directional functionally graded annular plates using a semi-analytical numerical method known as the state space-based differential quadrature method. The formulation was based on the three-dimensional elastic theory, while, it was assumed that the material properties (exponent-law variation) varied along the thickness, radial or both directions. Kermani et al. (2012) addressed the free vibration of multi-directional functionally graded circular and annular plates using a semi-analytical/numerical method, called state space-based differential quadrature method. Shariyat and Jafari (2013) performed low-velocity impact analysis of the functionally graded plates using commercial finite element softwares and discrete models for variations of the material properties. Shariyat and Alipour (2013)

developed a power series solution for free vibration and damping analyses of viscoelastic functionally graded plates with variable thickness on elastic foundations. The material properties of the functionally graded plate were assumed to vary in the transverse and radial directions, simultaneously. Tahouneh and Naei (2014) performed three dimensional vibration analysis of bi-directional FG rectangular plates resting on two-parameter elastic foundations. Yas and Moloudi (2015) investigated the three-dimensional free vibration analysis of a multi-directional functionally graded piezoelectric (FGP) annular plate resting on two parameter (Pasternak) elastic foundations under different boundary conditions. In this paper, the material properties were assumed to vary continuously along the radial and thickness directions and considered exponent-law distribution. Do et al. (2017) analysed buckling and bending behaviours of 2D-FGM plates numerically by using a finite element model.

2.4.2 Literatures on elastic foundation:

Plates are widely known structural elements with variety of engineering and industrial applications. Beside the classical end conditions, plate structures are often connected to other members, supported by elastic restraints or supported by elastic foundation. So, studies should not be always limited to classical edges which are ideal clamped, simply supported and free edges. In reality, such type of structures are modelled by a number of distributed linear spring at the boundaries. Specifically, plates on elastic foundation can be considered as idealisation of various critical and frequently used load bearing components. Application of such type of supported structure can be found in rail road, bio-mechanics, road, marine, geo-technics and engineering. Hence, static, dynamic and buckling behaviour of these components under external loading thus becomes vital significance, and has received overwhelming attention for many years. Even now research in this field continues as some critical issues involving foundation type, methodology, involvement of various parameters and their corresponding influences are still worthy of investigation. A brief description of various research works dealing with plates resting on elastic foundation is provided in the following paragraph. However, it should be mentioned that in most cases the plates are graded in the transverse direction.

Yas and Aragh (2010) worked on a continuous grading fiber-reinforced plate on elastic foundation and studied the free vibration characteristics based on the three-

dimensional, linear and small strain elasticity theory. Kiani et al. (2012) considered a doubly curved FGM plate on Pasternak-type elastic foundation to investigate its static and dynamic behaviour. The equations of motion were derived by using modified Sanders shell theory and first order shear deformation theory. Yang et al. (2012) obtained the theoretical solution of a plate with free edges rested on elastic foundation. The reciprocal theory was used to derive the solution of the taken problem. The foundation was considered here as Pasternak or two parameter type. Kägo and Lellep (2013) considered a stepped anisotropic plate which was resting on elastic foundation and studied the free vibration characteristics. The dependency of geometric parameters and physical properties on natural frequencies were also analysed. Li et al. (2013) obtained analytical bending solutions of thin plates with free edges on elastic foundation. Foundation model was considered as Winkler type and a new sympletic superposition method was used to obtain the results. Akavci (2016) studied buckling, dynamic and static analysis of a sandwich plate with simply supported edges on elastic foundation. The analysis was carried out by representing a new hyperbolic shear and normal deformation plate theory. The foundation model was considered to be Pasternak type. Hamilton's principle was utilized to derive the equations of motion and Navier technique was used to obtain closed form solutions. Taczała et al. (2015) performed a post-buckling study of FG plates on elastic foundation. FSDT was used for the mathematical formulation and the results were obtained numerically by FE method. Wattanasakulpong and Chaikittiratana (2015) investigated static and dynamic behaviour of CNR composite plates resting on elastic foundation. The elastic foundation was considered to be Pasternak type which also included shear layer and springs. The formulation was on the basis of generalized shear deformation theory. Panyatong et al. (2016) used 2^{nd} order shear deformation theory (SDT) to determine the natural frequencies of Functionally Graded nanoplate which was embedded in elastic medium. The formulation was on the basis of nonlocal elasticity and the derivation of governing equations were performed through Hamilton's principle to investigate the influences of the medium stiffness and temperature on natural frequencies. Benferhat et al. (2016) performed free vibration study on graded plate supported on Winkler–Pasternak type of elastic foundation on the basis of the neutral surface concept. Barati et al. (2016) examined the buckling behaviour of FG piezoelectric porous plates on basis of a refined four-variable plate theory. Derivation of the governing set of equations were performed through Hamilton's principle and implementing an

analytical approach the equations were solved. Gupta et al. (2016) performed dynamic analysis of FG simply supported plates on elastic foundation, which was considered as two parameter Pasternak type. The formulation was displacement based and HSDT was used for derivation purpose. Adineh and Kadkhodayan (2017) conducted 3D thermo-elastic analysis for the first time of a FGM skew plate rested on elastic foundation and loaded under thermo-mechanical loading. Here, differential quadrature method was used to obtain the numerical results. Mukherjee and Dillard (2017) analytically studied the cylindrical buckling behaviour of a plate subjected to uniaxial compression. The plate was also considered to be rested on incompressible, elastomeric foundation. Gao et al. (2017) utilized an analytical computational scheme to study stability and dynamic characteristics of composite plate resting on Winkler-Pasternak elastic foundation and subjected to axial velocity. The compatibility equations were derived by using classical plate theory and Von-Kármán strain-displacement relation. The dynamic buckling equations were obtained by incorporating Galerkin method and Airy's stress function. To solve the non-linear equations numerically, fourth-order Runge-Kutta method was implemented. Ebrahimi et al. (2017) proposed a four-variable refined shear deformation theory to perform free vibration study of porous magneto-electro-elastic FG plates. The set of differential equations were obtained with the help of Hamilton's principle. Kutlu et al. (2017) presented a mixed FE method and utilised a boundary element approach to study the dynamics of thick plates on elastic foundation. The plate was considered to be interacting with a quiescent fluid on the other side. To represent the plate-foundation system, a two field mixed FE formulation, on the basis of Hellinger-Reissner variational principle, was used. A boundary element solution was incorporated for the fluid-structure interaction. Mohammadzadeh and Noh (2017) presented an analytical approach for obtaining nonlinear frequency response of sandwich plates. The equations of motion were obtained by using the HSDT along with Hamilton's principle. The Navier's solution and Runge-Kutta neumerical scheme was used to solve the problem. Zamani et al. (2017) investigated free vibration of laminated viscoelastic composite plate with simply supported edge resting on Pasternak viscoelastic foundation. Based on 3rd order SDT, the partial differential equations were attained by Hamilton principle and Laplace transformation. The equations were solved by iterative methods which were weighted residual method and Fourier transform. Najafi et al. (2017) presented the impact analysis of FGM plates which were resting on

elastic support with simply supported edge condition. The elastic foundation was considered as a nonlinear three-parameter one. The governing equations were derived based on a Reddy's HSDT and were solved by using an analytical procedure. Shahsavari et al. (2018) analyed the free vibration behaviour of FG porous plates which were supported on elastic foundations. Formulation was carried out on the basis of quasi-3D hyperbolic plate model and solution was performed using Galerkin method.

2.5 Closure:

A detailed literature survey in the proposed area of research has been carried out and presented in the preceding sections. In the present section, a gist about the research works on this regard is provided to outline the scope of further studies. This offers justification for the choice of the problems taken up in the present thesis work.

Literature is abundant with studies on structural analysis in the field of transversely functionally graded (TFG) beam/plate subjected to transverse loading. In most of the cases, material properties of the beam vary continuously in thickness direction according to a power-law form considering the Mori–Tanaka scheme. Geometric nonlinearity and corresponding large displacement is dealt with in quite a few of the works reviewed. In some of the cases non-uniform geometry is considered while dealing with the static and dynamic analysis. To some extent this particular field of study is saturated with innumerable research works dealing with various aspects.

Works on AFG Euler-Bernoulli beam are also available in the literature. In few cases, nonlinear analysis is cited. Non-uniform geometry is also considered in some cases. On the other hand, studies on AFG Timoshenko beam are limited. Only a few numbers of published works is available in standard literature acknowledging AFG Timoshenko beam for nonlinear analysis. Literatures on AFG plates are also rare. Only a few literature considered the case of in-plane inhomogeneity of the plate structure to analyse the static and dynamic aspects.

Review of existing literature reveals that studies are primarily focused on free vibration analysis, where the natural frequencies are computed and their corresponding mode shapes are determined. Quite a few different techniques, such as, finite difference method, finite element method, variational formulation etc. have been utilized to obtain the

above mentioned results for different classes of FG structure. It is also noted that emphasis is mainly on developing these methodologies or tools to obtain the natural frequencies compared to studying the variations in the dynamic behaviour corresponding to changes in system geometry and boundary conditions.

Literature review exposes the fact that only a few numbers of published works is available in standard literature presenting nonlinear forced vibration analysis on AFG beam/plate. In majority of the research works the gradation is assumed in the thickness direction. Thorough documentation of frequency response curves in the excitation frequency response amplitude plane subjected to harmonic excitation is not available in literature. The influence of different flexural conditions on the response of such plates is also an unexplored domain.

Regarding boundary conditions, it is found that majority of the studies are confined to classical boundary conditions which are ideally clamped, simply supported or free. However, real physical systems often are not governed by ideal end conditions and elastic restraints in terms of linear and torsional springs may be incorporated in the system to cater to these conditions. Similarly, structures may also be supported by linear or non-linear elastic foundations. Literature survey reveals that in few cases FG structures on elastic foundation are considered. To analyse those cases various types of linear and nonlinear foundation are cited considering Winkler, Pasternak, Kerr foundation models. Most of the studies deal with the TFG structure on elastic foundation but the cases of AFG structure on such foundation are rare. The case of elastic foundation along with classical boundary is also hardly found in literature. So, there is no doubt scope for exploring the effects of elastic foundation on AFG beam/plate adding the complexity of geometric nonlinearity and non-uniformity in the system.

Chapter 3

FREE VIBRATION: AXIALLY FUNCTIONALLY GRADED THIN BEAMS ON ELASTIC FOUNDATION

3.1 Introduction:

Beams are one of the basic structural elements that can be used to idealise various kinds of engineering structures. In their working environment such structural elements are expected to successfully carry different types and magnitudes of static and dynamic loads. So, understanding and analysis of static and dynamic behaviour of beams under loaded as well as unloaded conditions are critical towards design of these structural elements and subsequently, complicated engineering systems as a whole. There are multiple theories that that deal with the structural mechanics of beams and one of the simplest models utilised is the Euler Bernoulli theory. It is applicable for thin beams with sufficiently large length to thickness ratio. As one of the lateral dimensions of the beam is considered to be comparatively small in relation to its length, the effect of shear deformation and rotary inertia can be ignored. Simplicity of Euler Bernoulli beam theory makes it an important tool, especially in the field of structural and mechanical engineering.

Depending on loading, the response of the thin beam is categorized into two categories, linear and nonlinear. Many a times the deflection caused by the external loads is sufficiently large (of the order of its thickness) to cause the system to exhibit nonlinear behaviour. This type of nonlinearity originates due to large deflection and is known as geometric nonlinearity. In such a situation a straight-forward linear analysis is unable to capture the true system behaviour. Hence, incorporation of the stretching effect into the formulation is necessary and it constitutes a geometric nonlinear analysis of the system. In the present chapter, large amplitude (geometric nonlinear) free vibration analysis of a Euler-Bernoulli (thin) AFG non-uniform beam on elastic foundation is taken up under transverse loading. The analysis is carried out under the following basic assumptions:

- The beam is considered to be slender enough to neglect rotary inertia and shear deformation effects.
- Geometric nonlinearity induced through large displacement is taken care of by nonlinear strain-displacement relations.

The main focus of the current chapter is to establish the free vibration characteristics of the system by providing backbone curves and corresponding mode shapes. In order to generate these, it is necessary to find out the natural frequencies of the system under undeformed and deformed conditions. The free vibration problem is solved in two steps where the objective of the first part is to compute the stiffness matrix in deflected configuration through a static analysis. This equivalent stiffness matrix is directly used in dynamic analysis (second part) for obtaining eigenvalues and eigenvectors which provide the natural frequencies and mode shape of the system, respectively. The static analysis is based on principle of minimum total potential energy whereas, Hamilton's principle is used for formulation of the dynamic problem. The nonlinear governing equation of the static problem is solved through an iterative scheme using a relaxation parameter and the subsequent dynamic analysis is carried out as a standard Eigen value problem.

The present methodology is an approximate one and it is displacement field based. The approximate displacement fields are assumed on the basis of the boundary conditions at certain reference points (called Gauss points) distributed over the whole domain. It should be mentioned here that the domain is not discretised (as in finite element methods); instead the analysis is carried out over the whole domain. The displacement fields are expressed as linear combinations of orthogonal kinematically admissible functions and unknown parameters. These functions are completely known for a particular boundary condition, so the only variables are the unknown parameters. Computation of these unknown parameters leads to the displacement fields of the system. Validation of current study is done by comparing the results with those already available in the literature. The free vibration frequencies are tabulated for non-uniform profile subject to various boundary conditions and foundation stiffness. The dynamic behaviour of the system is presented in the form of backbone curves to detect the effect of the elastic foundation, material models and taper patterns.

3.2 Geometric parameter:

For the present analysis an axially functionally graded non-uniform beam of length L, variable width $b(x)$ and variable thickness $t(x)$ is considered, as shown in Figure 3.1(a). The beam is considered to be supported on elastic foundation which is idealized as a series of linear springs of stiffness K, attached to the bottom surface of the beam (Figure 3.1(b)). As already mentioned, the cross-sectional dimensions are considered to be considerably smaller than the length of the beam and the effects of shear deformation and rotary inertia are neglected. For the mathematical formulation, normalized coordinate ($\xi = x/L$) is utilized.

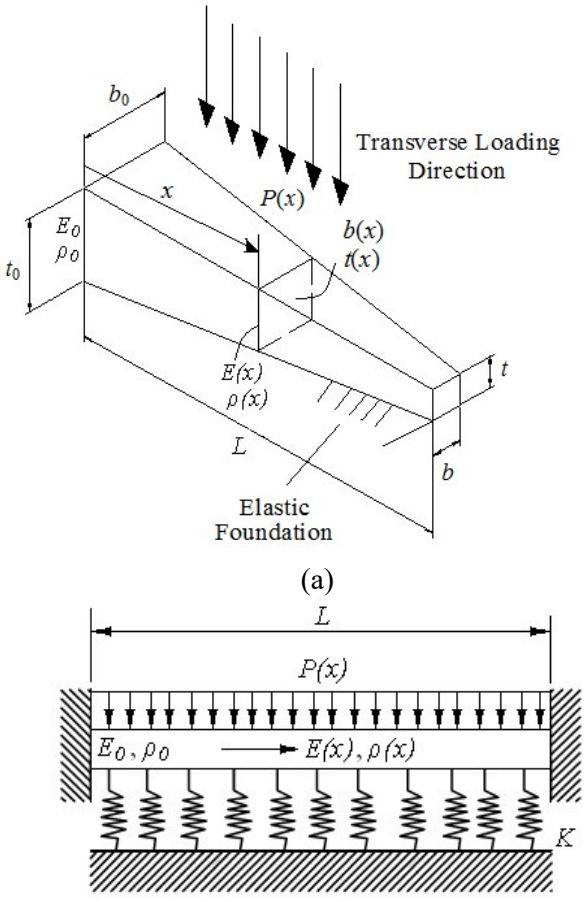

Figure 3.1: (a) Schematic representation of an AFG beam on elastic foundation, (b) idealization of elastic foundation by a series of linear springs.

Table 3.1: Different types of taper pattern

Taper Pattern	$t(\xi)$
Linear taper	$t(\xi) = t_0(1-\alpha\xi)$
Parabolic taper	$t(\xi) = t_0(1-\alpha\xi^2)$
Exponential taper:	$t(\xi) = t_0 \exp(-\alpha\xi^{1/2})$

Table 3.2: Values of taper parameter for different taper patterns

Linear Taper	$\alpha = 0$	$\alpha = 0.2$	$\alpha = 0.4$	$\alpha = 0.6$
Parabolic Taper	$\alpha = 0$	$\alpha = 0.2$	$\alpha = 0.4$	$\alpha = 0.6$
Exponential Taper	$\alpha = 0$	$\alpha = 0.223144$	$\alpha = 0.510826$	$\alpha = 0.916291$

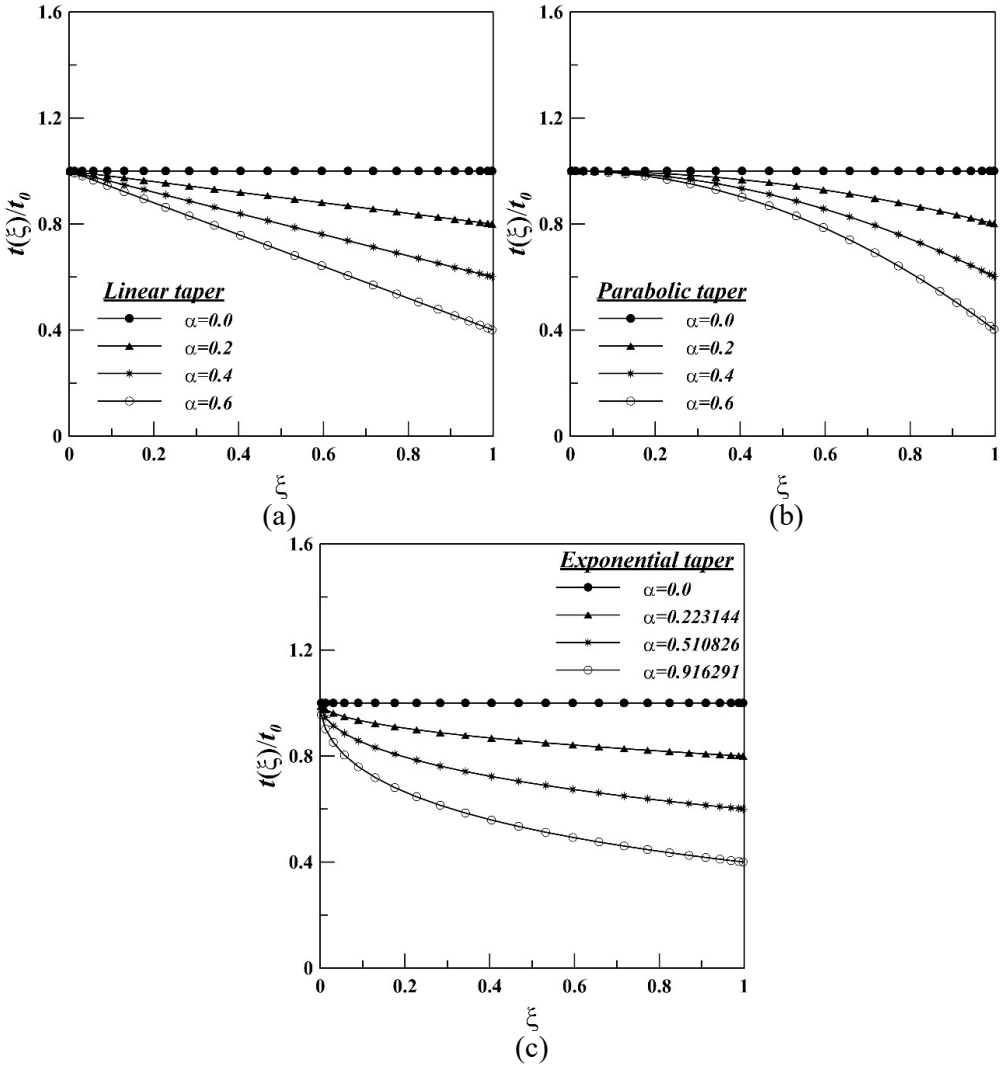

Figure 3.2: Variation of thickness for (a) linear taper (b) parabolic taper and (c) exponential taper for different taper parameters

Non-uniform beam geometry has also been taken into account in the present considering variation in thickness along the axial direction. For that purpose, three different taper patterns, linear, parabolic and exponential, are chosen for thickness and the variations of thickness are mentioned in the Table 3.1. Here, a beam with uniform width is considered for the analysis. Here t_0 is the thickness of the beam at the root of the beam, *i.e.*, at the left hand end of the beam as shown in Figure 3.1 and α is the taper parameter. Four different values of the taper parameter (α) are considered for each of the profile and these values are shown in Table 3.2. The values of α have been so selected that the thickness at the other end remains same for all the taper patterns to provide a better understanding on the effects of taper pattern on the results. It should be mentioned here that the case $\alpha = 0$ corresponds to a uniform beam. For four different taper parameter, the variation of the normalized thickness along the normalized axial coordinate are shown in Figures 3.2 for three different taper pattern. Figure 3.2(a), 3.2(b) and 3.2(c) are plotted respectively for linear, parabolic and exponential taper pattern. Here, the thickness is normalized using the root side constant thickness value (t_0). From the Figure 3.2, it is observed that at $\alpha = 0$, no variation in the thickness can be found. The normalized thickness value will be fixed at constant value 1. Whereas, at $\alpha = 0.6$ the variation will be maximum for linear and parabolic taper and for the case of exponential taper pattern maximum variation of the thickness can be found at $\alpha = 0.916291$.

3.3 Material parameter:

The material of beam is considered to be functionally graded continuously along spatial directions. The modulus of elasticity, $E(x)$, and the mass density, $\rho(x)$, of the beam vary along the axial direction as shown in Figure 3.3. To incorporate this material gradation in the analysis, three different material models are selected depending on the gradation of the elastic modulus and density in the axial direction. They are mentioned in the Table 3.3 as a function of normalized axial co-ordinate (ξ). It is apparent that the first model corresponds to a homogeneous material and it is included for comparison purpose. The variation of the normalized material properties along the along the normalized axial coordinate as shown in Figures 3.3 for three different material models. Figure 3.3(a) and 3.3(b) are plotted respectively to show the variation for elastic modulus and density. It should the mentioned that the poission's ratio (μ) in the present study is kept as constant.

Here, the elastic modulus and density is normalized by using the root side constant value elastic modulus (E_0) and density (ρ_0). From the Figures 3.3, it is observed that for material 1, no variation in the elastic modulus and density can be found. The normalized material property value will be fixed at constant value 1. Whereas, for material model 3 the variation will be maximum for elastic modulus as well as for material density.

Table 3.3: Three different material model used for gradation

Material	$E(\xi)$	$\rho(\xi)$
Material 1	E_0	ρ_0
Material 2	$E_0(1+\xi)$	$\rho_0(1+\xi+\xi^2)$
Material 3	$E_0 e^{\xi}$	$\rho_0 e^{\xi}$

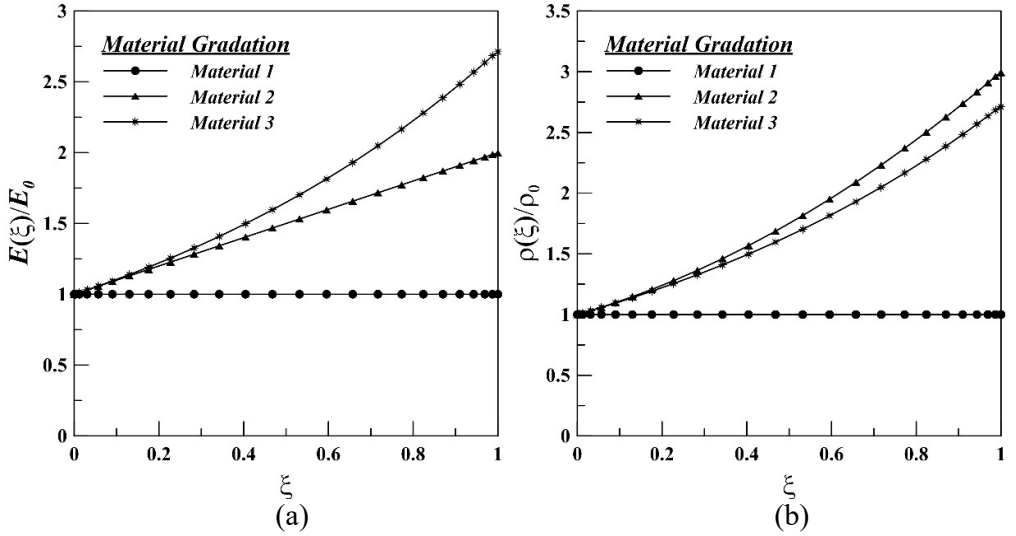

Figure 3.3: Gradation of (a) elastic modulus ($E(\xi)/E_0$) and (b) density ($\rho(\xi)/\rho_0$) in the axial direction (ξ) for different material model.

3.4 Mathematical formulation:

A displacement field based semi-analytical method that employs appropriate energy methods is used for deriving the governing equations of the system. It should be mentioned here that prediction of the large amplitude vibration frequencies or loaded natural frequencies is carried out by performing a static analysis under external transverse loading, followed by an Eigen value problem corresponding to the deformed system stiffness. The static analysis yields the initial deflection profile, which is used in the subsequent free vibration analysis. For both static and dynamic analysis, the formulation is carried out on

the basis of variational form of appropriate energy principles. Geometric nonlinearity is incorporated into the system by consideration of non-linear strain-displacement relations.

3.4.1 Static analysis:

The governing set of equations for the static analysis is derived through application of principle of minimum total potential energy, which states that,

$$\delta(U+V)=0 \tag{3.1}$$

where, U represents strain energy of the system and V denotes potential energy due to externally applied transverse load.

In the case of large displacement analysis of beam both bending and stretching effects are considered. Therefore, total strain energy in the beam is given by,

$$U=U_b+U_m+U_f$$

Here, U_b and Um are strain energy stored due to bending and strain energy stored due to stretching, respectively, while, U_f is strain energy stored in the foundation, *i.e.*, total strain energy stored in the series of linear springs under transverse loading on the beam. The strain energies due to bending (U_b) and stretching (U_m) of beam are dependent on the axial strain due to bending (ε_x^b) and stretching (ε_x^s), respectively, and these strains are expressed as,

$$\varepsilon_x^b = -z\left(\frac{d^2w}{dx^2}\right) \tag{3.2a}$$

$$\varepsilon_x^s = \left(\frac{du}{dx}\right)+\frac{1}{2}\left(\frac{dw}{dx}\right)^2 \tag{3.2b}$$

Quite clearly the strain-displacement relation for stretching (Equation 3.2b) is nonlinear in nature and hence, the governing equations derived subsequently would also contain nonlinear terms.

The expressions of the strain energies are given below,

$$U_b = \frac{1}{2}\int_{vol} E(x)\left(\varepsilon_x^b\right)^2 dv \tag{3.3a}$$

$$U_m = \frac{1}{2}\int_{vol} E(x)\left(\varepsilon_x^s\right)^2 dv \tag{3.3b}$$

$$U_f = \frac{1}{2}\int_0^L Kw^2 dx \tag{3.3c}$$

So, the total strain energy of the system is given as follows,

$$U = \frac{1}{2}\int_{vol} E(x)\left(\varepsilon_x^b\right)^2 dv + \frac{1}{2}\int_{vol} E(x)\left(\varepsilon_x^s\right)^2 dv + \frac{1}{2}\int_0^L Kw^2 dx$$

Substituting the relevant expressions, total strain energy of the system can be expressed as follows,

$$U = \frac{1}{2}\int_0^L \left(\frac{d^2w}{dx^2}\right)^2 E(x) I(x) dx + \frac{1}{2}\int_0^L \left[\left(\frac{du}{dx}\right)^2 + \frac{1}{4}\left(\frac{dw}{dx}\right)^4 + \left(\frac{dw}{dx}\right)^2\left(\frac{du}{dx}\right)\right] E(x) A(x) dx + \frac{1}{2}\int_0^L Kw^2 dx \tag{3.4}$$

The total potential energy (V) due to externally applied transverse load $P(x)$ is given by,

$$V = \int_0^L P(x) w dx \tag{3.5}$$

Figure 3.1 shows the AFG beam subjected to a uniformly distributed load spanning the length of the beam. However, as indicated by Equation (3.5), total potential energy corresponding to other type of transverse loading pattern $P(x)$, expressible mathematically by analytical or numerical functions, can be determined from the above expression. Hence, the present formulation is certainly not limited to only uniformly distributed loading.

Applying the principle of minimum total potential energy and using normalized coordinate ($\xi = x/L$) following intermediate expression is obtained.

$$\delta\left[\begin{array}{l}\frac{1}{2}\int_0^1\frac{1}{L^3}\left(\frac{d^2w}{d\xi^2}\right)^2E(\xi)I(\xi)d\xi\\+\frac{1}{2}\int_0^1\left\{\frac{1}{L}\left(\frac{du}{d\xi}\right)^2+\frac{1}{4L^3}\left(\frac{dw}{d\xi}\right)^4+\frac{1}{L^2}\left(\frac{dw}{d\xi}\right)^2\left(\frac{du}{d\xi}\right)\right\}E(\xi)A(\xi)d\xi\\+\frac{1}{2}\int_0^1 Kw^2Ld\xi+\int_0^1 P(\xi)wLd\xi\end{array}\right]=0 \qquad (3.6)$$

Performing the variational operation Equation (3.6) reduces to the form as shown in Equation (3.7),

$$\begin{array}{l}\frac{1}{L^3}\int_0^1\left(\frac{d^2w}{d\xi^2}\right)\delta\left(\frac{d^2w}{d\xi^2}\right)E(\xi)I(\xi)d\xi\\+\left[\begin{array}{l}\frac{1}{L}\int_0^L\left(\frac{du}{d\xi}\right)\delta\left(\frac{du}{d\xi}\right)+\frac{1}{2L^3}\int_0^1\left(\frac{dw}{d\xi}\right)^3\delta\left(\frac{dw}{d\xi}\right)+\frac{1}{L^2}\int_0^1\left(\frac{du}{d\xi}\right)\left(\frac{dw}{d\xi}\right)\delta\left(\frac{dw}{d\xi}\right)+\\\frac{1}{2L^2}\int_0^1\left(\frac{dw}{d\xi}\right)^2\delta\left(\frac{du}{d\xi}\right)\end{array}\right]E(\xi)A(\xi)d\xi\\+KL\int_0^1 w\delta wd\xi+\int_0^1 P(\xi)\delta wLd\xi=0\end{array} \qquad (3.7)$$

The approximate displacement fields (w and u) of the above expression are assumed as linear combination of unknown coefficients (c_i) and orthogonal admissible functions (ϕ and ψ). In the present method,

$$w(\xi)=\sum_{i=1}^{nw}c_i\phi_i(\xi) \qquad (3.8a)$$

$$u(\xi)=\sum_{i=1+nw}^{nw+nu}c_i\psi_{i-nw}(\xi) \qquad (3.8b)$$

Here, ϕ_i and ψ_i are sets of nw and nu numbers of orthogonal functions for w and u, respectively. The functions ϕ_i are associated with displacements due to bending, whereas ψ_i describe stretching of the mid-plane of the beam. These displacement fields are assumed to be kinematically admissible, which implies that they are continuous and differentiable within the domain and also satisfy the boundary conditions of the beam. It is also important

that these functions come from an orthogonal set in order to obtain satisfactory results. Appropriate start functions for these orthogonal sets are selected in such a way that they satisfy the flexural and membrane boundary conditions of the beam. The higher-order functions are generated from the selected start functions following Gram-Schmidt orthogonalization scheme. Substituting the approximate displacement fields into Equation (3.8) provides the governing set of equations of the static problem in matrix form.

$$[K_s][c] = \{f\} \tag{3.9}$$

where, $[K_s]$ is the stiffness matrix corresponding to static analysis, $\{f\}$ is the force vector for transverse static external load and $\{c\}$ is a vector of unknown coefficients. The details of the stiffness matrix and load vector elements are provided in Appendix. The present formulation being displacement based, the two basic unknowns are the two displacement fields (w and u). But once the assumed approximate displacement fields are substituted, the problem is reduced to finding a set of unknown coefficients (c_i).

The present analysis is based on a methodology where the solution of the static displacement field of the AFG beam on elastic foundation under uniformly distributed transverse loading is obtained. The solution methodology of the static problem involves an iterative numerical scheme using successive relaxation due to presence of nonlinearity in the stiffness matrix.

3.4.2 Dynamic analysis:

To formulate the dynamic problem Hamilton's principle is utilized, which is represented as,

$$\delta\left(\int_{\tau_1}^{\tau_2}(T-U)\,d\tau\right) = 0 \tag{3.10}$$

In the above expression T denotes the kinetic energy of the system and τ is time. U is the total strain energy stored in the system and has the same expression as presented in Equation (3.4) of static analysis segment. Expression for the kinetic energy of the system is as follows. The spring being massless do not contribute towards total kinetic energy and hence are ignored in Equation (3.11).

$$T = \frac{1}{2}\int_0^L \left\{ \left(\frac{dw}{d\tau}\right)^2 + \left(\frac{du}{d\tau}\right)^2 \right\} \rho(x) A(x)\, dx \tag{3.11}$$

Assuming approximate dynamic displacement fields w and u to be separable in time and space and the spatial part being represented by linear combination of unknown coefficients (d_i) and orthogonal admissible functions (ϕ and ψ), they can be written as,

$$w(\xi,\tau) = \sum_{i=1}^{nw} d_i \varphi_i(\xi) e^{i\omega\tau} \tag{3.12a}$$

$$u(\xi,\tau) = \sum_{i=nw+1}^{nw+nu} d_i \psi_i(\xi) e^{i\omega\tau} \tag{3.12b}$$

where, ω is the natural frequency of the system and d_i represents a new set of unknown coefficients that denote the eigenvector in the matrix form. The spatial functions are identical to those for the static analysis in Equation (3.6). Substitution of the kinetic (T) and strain energy (U) expressions along with the dynamic displacement fields gives the governing equation of the free vibration problem in the following matrix form.

$$-\omega^2 [M]\{d\} + [K]\{d\} = 0 \tag{3.13}$$

Here, [M] is mass matrix, the elements of which are provided in Appendix.

Equation (3.13) is a standard eigenvalue problem, whose solution is obtained using Matlab subroutine ‘eig’.

3.5 Solution procedure:

From the mathematical formulation for the static analysis it is clear that the elements of the stiffness matrix [K_s] are functions of the unknown parameter, c_i. Hence the governing equation (Equation (3.9)) is nonlinear in nature and cannot be solved directly. To solve the set of equations an iterative numerical technique is introduced and a direct substitution technique with successive relaxation scheme is utilized. The solution steps are given below,

Step 1: The input parameters i.e. appropriate load, allowable error limit and the relaxation parameter are defined. It is assumed that the unknown coefficients have zero value at the initial stage.

Step 2: Utilizing the input parameter the stiffness matrix for bending and stretching (and thus the total stiffness matrix) are generated, along with the load vector. As the initial values for c_i are zero the initial stiffness matrix corresponds to a linear situation.

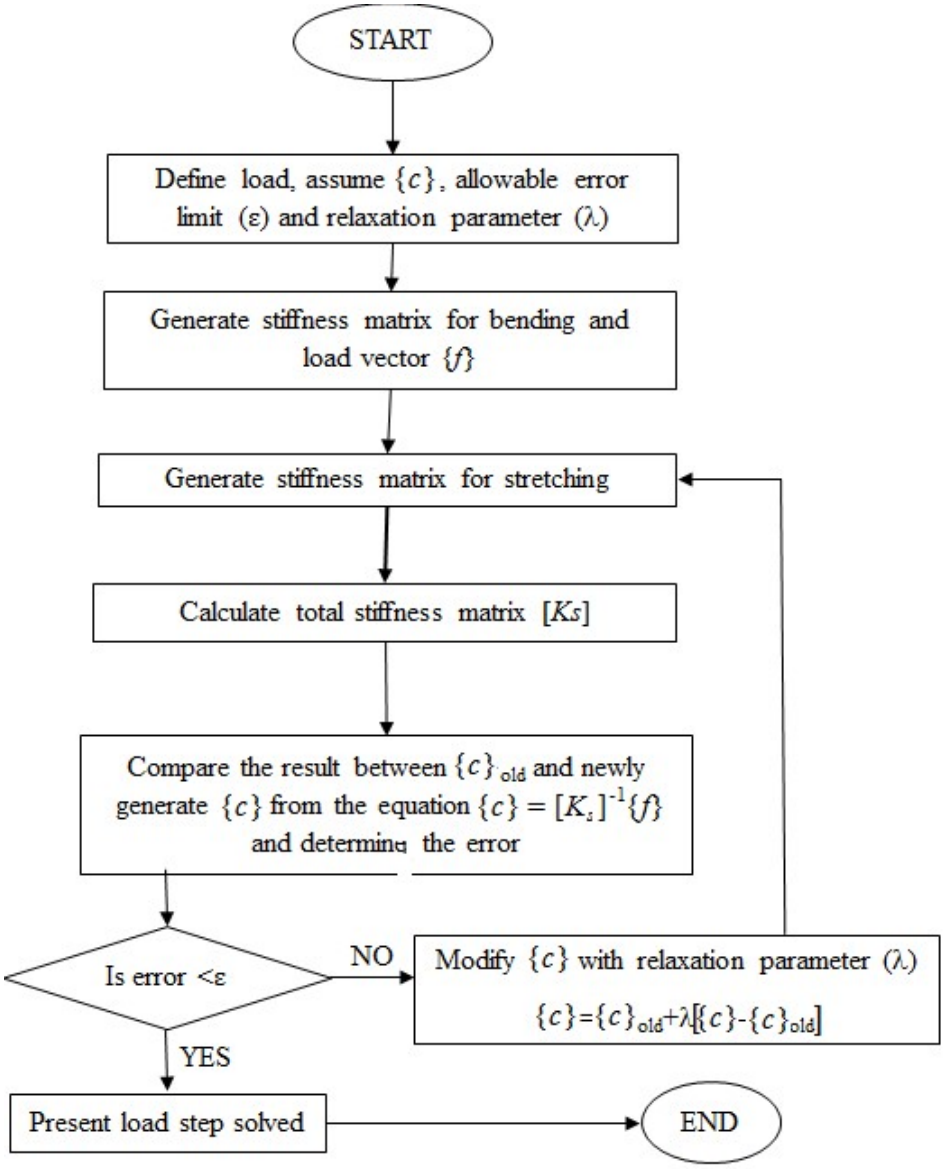

Figure 3.4: Flowchart of the solution procedure

Step 3: A new set of unknown coefficients are evaluated by inversion of the stiffness matrix and subsequent pre-multiplication with the load vector. $\{c\}(n + 1) = [K_s(\{c\}(n))]\text{-}1\{f\}$, where n represents the iteration counter.

Step 4: The calculated set of unknown coefficients is compared with the ones from previous iteration and if the error is above the predefined allowable error limit, the next iteration is performed with modified values of unknown coefficients. The modification takes into account a relaxation parameter to predict the guess for the next iteration.

Step 5: The modified coefficient values are used to generate the modified stiffness matrix and the process is repeated till convergence is achieved, i.e., the error value falls below the predefined limit. The corresponding flowchart for the solution procedure is given in Figure 3.4. The converged stiffness matrix from the static analysis is carried into the dynamic analysis, which is a standard eigenvalue problem. The solution to Equation (3.13) is obtained by developing a Matlab code that utilizes the subroutine 'eig'. The square root of the eigenvalues gives the natural frequency of the system at the deflected configuration, whereas the eigenvectors associated with these eigenvalues can be processed to plot the mode shapes of the vibrating system.

Table 3.4: Base functions for assume displacement field (*w*, *u*)

Flexural Boundary Condition	$\phi_1(\xi)$
CC	$\{\xi(1-\xi)\}^2$
CF	$\xi^2(\xi^2-4\xi+6)$
SS	$\sin(\pi\xi)$
CS	$\xi^2(2\xi^2-5\xi+3)$
In-plane Boundary Condition	$\psi_1(\xi)$
Immovable	$\xi(1-\xi)$

3.6 Result and discussion:

The main objective of the present study is to investigate the large amplitude dynamic behavior of axially functionally graded non uniform beams supported on elastic foundation and the variation of the loaded natural frequencies with the change in the taper profile, material model and stiffness of the foundation. In the present analysis, it is considered that the AFG taper beam on elastic foundation is subjected to uniformly distributed transverse load for different flexural boundary condition. The present paper also investigates the effect of different boundary conditions on the large amplitude free vibration behavior of the system. Four different boundary condition, namely, CC, CS, SS, CF, are

considered arising out of combinations of Clamped (C), Simply supported (S) and Free (F) ends. The same formulation can be utilized to handle non-classical boundary conditions such as elastically restrained ends. The different boundary conditions are used for selecting the base functions for the transverse displacement (w) where as for the axial displacement (u) the membrane boundary conditions are used. The in-plane displacement at the boundaries are assumed as zero. These functions are tabulated in Table 3.4. Gram-Schmidt orthogonalization scheme is used to generate the higher order functions.

The other aspect of complexity of the current system is the elastic foundation upon which the system rests. As already mentioned, the foundation has been incorporated into the mathematical formulation by a series of parallel massless linear springs with equivalent spring stiffness (K).Four different values of dimensionless stiffness (K_f) are taken for the present study which are varied from 0 to 30 in the interval of 10. The foundation stiffness (K) is normalized using the expression, as given as $K_f = K\ \{(L/t_0)^3/E_0 b\}$. Here, the situation with 0 spring stiffness corresponds to a case where the foundation is absent, i.e., the beam is not supported by the foundation at all. This case has also been included to provide a better comparison for the response with and without the foundation. Following geometrical dimensions and material properties are used to generate the results: L = 1.0 m, b = 0.02 m, t_0 = 0.005 m, E_0 = 210 GPa, ρ_0 = 7850 kg/m^3.

3.6.1 Convergence study:

The solution methodology, specially adopted in the present study for the nonlinear system, employs an iterative numerical scheme using the technique of successive relaxation, as described in the previous section. It is surmised that the outcome of the numerical scheme is dependent on several parameters – number of orthogonal functions, number of Gauss points, tolerance value of the error limit etc. So, it is important to carry out extensive convergence studies involving the above mentioned parameters, in order to determine the correct values of these parameters to be used while generating results. The studies are performed on a clamped (CC) AFG beam which following material model 2 and linear taper pattern with taper parameter 0.4. The normalized foundation stiffness value is taken as 10.

Results of the various convergence studies are presented in Figure 3.5. Number of functions corresponding to two orthogonal directions, transverse and in-plane, are denoted by *nw* and *nu* respectively. Figure 3.5(a) presents the convergence results for variation in number of orthogonal functions keeping all the other parameter as unchanged and the change in dimensionless first natural frequency $\left(\Omega = \omega L^2 \sqrt{\rho_0 A_0 / E_0 I_0}\right)$ of the system is indicated. The figure shows that the values of dimensionless first natural frequency decreases with the increase of number of orthogonal function and the difference of the values for *nw/nu* = 7 and 8 are minimal. It is also expected from the figure that for the next value (*nw/nu* = 9) the difference will be negligible but the computational time will increase due to involvement of more number of orthogonal functions. So, the number of functions along each coordinate direction is chosen as 8.

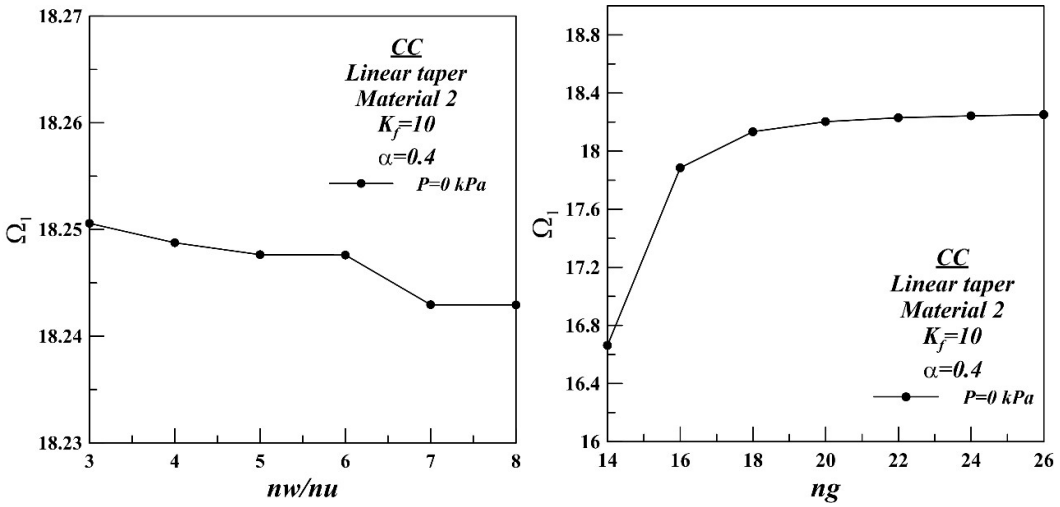

(a) (b)

Figure 3.5: Convergence studies for (a) no of orthogonal functions (*nw=nu*) and (b) no of gauss point (*ng*)

Similar way the convergence study on number of gauss point (*ng*) is also conducted where the dimensionless first natural frequency $\left(\Omega = \omega L^2 \sqrt{\rho_0 A_0 / E_0 I_0}\right)$ of the system is plotted against the number of gauss point as shown in Figure 3.5 (b). A choice of 24 Gauss points for the present work is made from this study and the posion of the number of gauss points in the normalized coordinate (ξ) is tabulated in the Table3.5. The tolerance value of the error limit (ε) for the numerical iterative scheme is fixed at 0.50% and the relaxation

parameter (λ) is taken as 0.50. The solution of the dynamic problem is obtained using MATLAB routines.

Table 3.5: Position of Gauss points within computational domain

Gauss Point Number	Position in normalised coordinate (ξ)
1	0.0024
2	0.0126
3	0.0309
4	0.0568
5	0.0900
6	0.1299
7	0.1760
8	0.2273
9	0.2831
10	0.3425
11	0.4044
12	0.4680
13	0.5320
14	0.5956
15	0.6575
16	0.7169
17	0.7727
18	0.8240
19	0.8701
20	0.9100
21	0.9432
22	0.9691
23	0.9874
24	0.9976

3.6.2 Validation study:

Validation for the present formulation and solution technique is done by comparison with established results already available in literature. The backbone curve for fundamental mode of a clamped-clamped homogeneous uniform beam is validated with the results published by Gupta et al. (2009) as shown in Figure 3.6. The two sets of results show similar trends and the values show satisfactory matching, hence, establishing the validity of the present method.

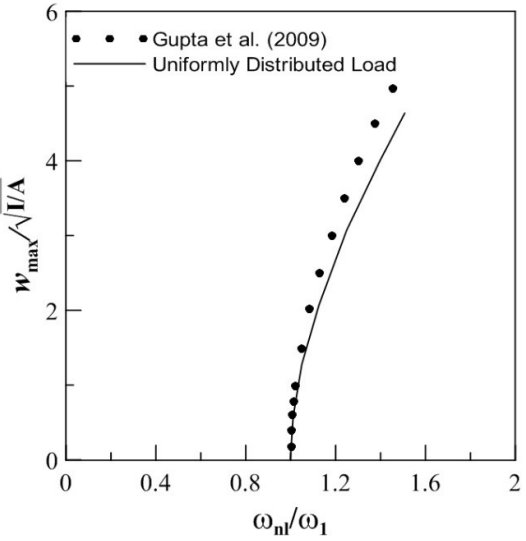

Figure 3.6: Comparison of backbone curves for fundamental mode of a clamped-clamped homogeneous uniform beam.

3.6.3 Natural frequencies:

Dimensionless natural frequencies $\left(\Omega = \omega L^2 \sqrt{\rho_0 A_0 / E_0 I_0}\right)$ for the first two modes (Ω_1 and Ω_2) for four different boundary conditions (CC, CS, SS, CF) of AFG beams are provided in Tables 3.6-3.17 for different combination of material models, taper patterns, taper parameters and foundation stiffness values. For each boundary condition, separate three tables are furnished to accommodate linear, parabolic and exponential taper pattern accordingly. The taper parameter (α) is varied from 0.0 to 0.6 for each linear and parabolic taper pattern whereas for the case of exponential taper pattern the variation is considered from 0 to 0.916291 and under each taper pattern four different foundation stiffness values are considered, which is varied from 0 to 30 in the fixed interval of 10. The values of α have been so selected that the thickness at the other end remains same for all the taper patterns to provide a better understanding on the effects of taper pattern on the results. Under three different material model four boundary separate boundary conditions are chosen to tabulate first two non-dimensional natural frequency of the system. These are to be noted that taper parameter 0.0 indicates the case of uniform beam, foundation stiffness 0 implies the case of beam without foundation and material 1 indicates the case of homogeneous beam (without material gradation).

Table 3.6: Values of dimensionless natural frequencies $\left(\Omega = \omega L^2\sqrt{\rho_0 A_0/E_0 I_0}\right)$ for 1st and 2nd mode (Ω_1 and Ω_2) corresponding to linearly tapered CC AFG beam for different combinations of taper parameter, spring stiffness and material properties

Taper Pattern	Taper Parameter	Stiffness	Material 1		Material 2		Material 3	
			CC		CC		CC	
			Ω_1	Ω_2	Ω_1	Ω_2	Ω_1	Ω_2
Linear	0	0	22.28	61.42	20.30	56.31	22.43	61.61
		10	24.84	62.39	22.01	56.94	24.01	62.21
		20	27.14	63.34	23.52	57.55	25.50	62.81
		30	29.27	64.28	24.93	58.16	26.90	63.40
	0.2	0	20.00	55.11	18.15	50.27	19.96	55.06
		10	23.11	56.31	20.11	51.03	21.89	55.79
		20	25.84	57.49	21.90	51.77	23.66	56.52
		30	28.31	58.65	23.55	52.51	25.309	57.24
	0.4	0	17.57	48.38	15.77	43.84	17.35	48.08
		10	21.49	49.95	18.24	44.81	19.78	49.02
		20	24.79	51.47	20.42	45.75	21.94	49.94
		30	27.70	52.95	22.38	46.68	23.90	50.84
	0.6	0	14.90	40.99	13.18	36.81	14.51	40.45
		10	20.11	43.21	16.47	38.13	17.74	41.73
		20	24.20	45.32	19.20	39.41	20.47	42.92
		30	27.68	47.34	21.59	40.65	22.87	44.35

Table 3.7: Values of dimensionless natural frequencies $\left(\Omega = \omega L^2\sqrt{\rho_0 A_0/E_0 I_0}\right)$ for 1st and 2nd mode (Ω_1 and Ω_2) corresponding to parabolic tapered CC AFG beam for different combinations of taper parameter, spring stiffness and material properties

Taper Pattern	Taper Parameter	Stiffness	Material 1		Material 2		Material 3	
			CC		CC		CC	
			Ω_1	Ω_2	Ω_1	Ω_2	Ω_1	Ω_2
Parabolic	0.2	0	20.36	56.63	18.47	51.66	20.32	56.57
		10	23.28	57.75	20.32	52.36	22.13	57.26
		20	25.87	58.85	22.01	53.06	23.80	57.94
		30	28.23	59.93	23.58	53.73	25.35	58.61
	0.4	0	18.28	51.39	16.42	46.58	18.07	51.08
		10	21.71	51.73	18.58	47.41	20.18	51.89
		20	24.67	54.05	20.51	48.23	22.09	52.68
		30	27.30	55.33	22.28	49.03	23.85	53.46
	0.6	0	15.96	45.45	14.16	40.85	15.59	44.88
		10	20.15	47.16	16.78	41.87	18.16	45.87
		20	23.60	48.81	19.46	42.88	20.41	46.84
		30	26.59	50.41	21.07	43.85	22.44	47.80

In Table 3.6 for CC boundary condition results pertaining to $\alpha = 0$, *i.e.*, a uniform beam, has also been presented. However, in the subsequent tables (Table 3.7 and 3.8)

Table 3.8: Values of dimensionless natural frequencies $\left(\Omega = \omega L^2\sqrt{\rho_0 A_0 / E_0 I_0}\right)$ for 1st and 2nd mode (Ω_1 and Ω_2) corresponding to exponential tapered CC AFG beam for different combinations of taper parameter, spring stiffness and material properties

Taper Pattern	Taper Parameter	Stiffness	Material 1		Material 2		Material 3	
			CC		CC		CC	
			Ω_1	Ω_2	Ω_1	Ω_2	Ω_1	Ω_2
Exponential	0.223144	0	19.47	53.33	17.69	48.68	19.45	53.31
		10	22.80	54.62	19.80	49.50	21.53	54.11
		20	25.70	55.89	21.70	50.31	23.41	54.89
		30	28.30	57.13	23.45	51.11	25.16	55.67
	0.510826	0	16.39	44.45	14.75	40.36	16.23	44.25
		10	21.02	46.35	17.70	41.54	19.14	45.40
		20	24.80	48.17	20.22	42.69	21.65	46.52
		30	28.08	49.93	22.46	43.81	23.90	47.62
	0.916291	0	12.89	34.38	11.46	30.98	12.62	34.03
		10	20.04	37.63	16.07	32.97	17.18	35.96
		20	25.22	40.63	19.62	34.85	20.77	37.80
		30	29.50	43.42	22.61	36.63	23.81	39.55

Table 3.9: Values of dimensionless natural frequencies $\left(\Omega = \omega L^2\sqrt{\rho_0 A_0 / E_0 I_0}\right)$ for 1st and 2nd mode (Ω_1 and Ω_2) corresponding to linear tapered CS AFG beam for different combinations of taper parameter, spring stiffness and material properties

Taper Pattern	Taper Parameter	Stiffness	Material 1		Material 2		Material 3	
			CS		CS		CS	
			Ω_1	Ω_2	Ω_1	Ω_2	Ω_1	Ω_2
Linear	0	0	15.39	49.87	13.23	45.00	14.35	49.01
		10	18.89	51.06	15.43	45.76	16.56	49.76
		20	21.84	52.22	17.36	46.51	18.50	50.49
		30	24.43	53.35	19.08	47.25	20.25	51.22
	0.2	0	14.23	45.16	12.20	40.55	13.27	44.25
		10	18.39	46.63	14.82	41.48	15.89	45.15
		20	21.77	48.05	17.04	42.38	18.13	46.03
		30	24.70	49.43	18.99	43.27	20.12	46.90
	0.4	0	12.97	40.14	11.07	35.83	12.08	39.17
		10	18.05	42.04	14.27	36.99	15.27	40.31
		20	21.99	43.85	16.87	38.12	17.91	41.42
		30	25.32	45.60	19.12	39.22	20.20	42.50
	0.6	0	11.54	34.63	09.79	30.66	10.71	36.63
		10	18.01	37.29	13.87	32.24	14.79	35.16
		20	22.68	39.78	17.01	33.74	17.97	36.64
		30	26.51	42.14	19.64	35.18	20.66	38.05

results for $\alpha = 0$ condition has been omitted to avoid repetition. It should be mentioned here that the mathematical expressions for the different taper profiles are such that in each case

$\alpha = 0$ corresponds to a uniform beam and hence, same natural frequency values are obtained in these cases. For CS, SS and CF boundary conditions as well such type pattern in the table of natural frequencies can be found.

Table 3.10: Values of dimensionless natural frequencies $\left(\Omega = \omega L^2\sqrt{\rho_0 A_0 / E_0 I_0}\right)$ for 1st and 2nd mode (Ω_1 and Ω_2) corresponding to parabolic tapered CS AFG beam for different combinations of taper parameter, spring stiffness and material properties

Taper Pattern	Taper Parameter	Stiffness	Material 1		Material 2		Material 3	
			CS		CS		CS	
			Ω_1	Ω_2	Ω_1	Ω_2	Ω_1	Ω_2
Parabolic	0.2	0	14.64	46.62	12.58	41.88	13.68	45.71
		10	18.54	47.99	15.03	42.74	16.13	46.54
		20	21.75	49.32	17.13	43.58	18.25	47.37
		30	24.54	50.61	18.99	44.41	20.14	48.18
	0.4	0	13.77	43.06	11.82	38.47	12.90	42.09
		10	18.19	44.69	14.59	39.47	15.66	43.06
		20	21.73	46.25	16.91	40.44	18.00	44.01
		30	24.77	47.77	18.94	41.39	20.06	44.93
	0.6	0	12.70	39.03	10.89	34.63	11.93	37.98
		10	17.88	41.07	14.11	35.84	15.13	39.16
		20	21.84	43.02	16.73	37.01	17.77	40.30
		30	25.17	44.89	18.99	38.14	20.06	41.41

Table 3.11: Values of dimensionless natural frequencies $\left(\Omega = \omega L^2\sqrt{\rho_0 A_0 / E_0 I_0}\right)$ for 1st and 2nd mode (Ω_1 and Ω_2) corresponding to exponential tapered CS AFG beam for different combinations of taper parameter, spring stiffness and material properties

Taper Pattern	Taper Parameter	Stiffness	Material 1		Material 2		Material 3	
			CS		CS		CS	
			Ω_1	Ω_2	Ω_1	Ω_2	Ω_1	Ω_2
Exponential	0.223144	0	13.70	43.54	11.74	39.13	12.76	42.68
		10	18.16	45.13	14.55	40.13	15.57	43.66
		20	21.72	46.66	16.90	41.11	17.95	44.62
		30	24.77	48.14	18.95	42.07	20.04	45.56
	0.510826	0	11.79	36.54	10.05	32.67	10.95	35.69
		10	17.78	38.85	13.86	34.11	14.77	37.09
		20	22.21	41.02	16.81	35.48	17.78	38.45
		30	25.88	43.09	19.32	36.81	20.34	39.75
	0.916291	0	09.53	28.52	08.64	25.32	08.81	27.72
		10	18.29	32.41	13.71	27.70	14.50	30.05
		20	24.02	35.89	17.62	29.90	18.51	32.22
		30	28.60	39.08	20.80	31.95	21.79	34.25

For the tables 3.6-3.17, it is prominent that in all cases with the increase of stiffness of the foundation the natural frequencies in all cases increase. This is due to the fact that

Table 3.12: Values of dimensionless natural frequencies $\left(\Omega = \omega L^2 \sqrt{\rho_0 A_0 / E_0 I_0}\right)$ for 1st and 2nd mode (Ω_1 and Ω_2) corresponding to linear tapered SS AFG beam for different combinations of taper parameter, spring stiffness and material properties

Taper Pattern	Taper Parameter	Stiffness	Material 1		Material 2		Material 3	
			SS		SS		SS	
			Ω_1	Ω_2	Ω_1	Ω_2	Ω_1	Ω_2
Linear	0	0	09.87	39.47	09.28	36.37	09.73	39.56
		10	14.74	40.96	12.21	37.34	12.96	40.51
		20	18.37	42.40	14.72	38.29	15.50	41.44
		30	21.39	43.80	16.84	39.22	17.67	42.35
	0.2	0	08.85	35.44	08.13	32.52	08.84	35.45
		10	14.56	37.28	11.88	33.69	12.58	36.59
		20	18.59	39.04	14.69	34.83	15.44	37.70
		30	21.89	40.73	17.04	35.96	17.83	38.78
	0.4	0	07.73	31.19	07.15	28.47	07.81	31.11
		10	14.54	33.58	11.65	29.95	12.30	32.55
		20	19.04	35.82	14.84	31.36	15.55	33.93
		30	22.66	37.93	17.45	32.71	18.22	35.26
	0.6	0	06.47	26.60	06.36	24.11	06.63	26.43
		10	14.78	29.96	11.61	26.10	12.20	28.38
		20	19.82	33.00	15.27	27.96	15.93	30.19
		30	23.77	35.81	18.21	29.70	18.94	31.91

Table 3.13: Values of dimensionless natural frequencies $\left(\Omega = \omega L^2 \sqrt{\rho_0 A_0 / E_0 I_0}\right)$ for 1st and 2nd mode (Ω_1 and Ω_2) corresponding to parabolic tapered SS AFG beam for different combinations of taper parameter, spring stiffness and material properties

Taper Pattern	Taper Parameter	Stiffness	Material 1		Material 2		Material 3	
			SS		SS		SS	
			Ω_1	Ω_2	Ω_1	Ω_2	Ω_1	Ω_2
Parabolic	0.2	0	09.27	36.85	08.53	33.80	09.26	36.86
		10	14.61	38.56	12.01	34.89	12.74	37.92
		20	18.46	40.20	14.68	35.95	15.45	38.95
		30	21.64	41.77	16.93	37.98	17.74	39.96
	0.4	0	08.58	33.98	7.93	31.01	08.66	33.90
		10	14.50	36.00	11.80	32.27	12.51	35.12
		20	18.62	37.93	14.68	33.48	15.42	36.30
		30	21.98	39.76	17.07	34.64	17.87	37.44
	0.6	0	07.72	30.73	07.20	27.86	07.91	30.55
		10	14.44	33.26	11.59	29.37	12.27	32.02
		20	18.87	35.62	14.72	30.81	15.44	33.42
		30	22.42	37.85	17.29	32.19	18.06	34.77

natural frequency is the function of mass and stiffness. While stiffness of the foundation is increased, overall stiffness of the system increases but the mass of the overall system

Table 3.14: Values of dimensionless natural frequencies $\left(\Omega = \omega L^2\sqrt{\rho_0 A_0/E_0 I_0}\right)$ for 1st and 2nd mode (Ω_1 and Ω_2) corresponding to exponential tapered SS AFG beam for different combinations of taper parameter, spring stiffness and material properties

Taper Pattern	Taper Parameter	Stiffness	Material 1		Material 2		Material 3	
			SS		SS		SS	
			Ω_1	Ω_2	Ω_1	Ω_2	Ω_1	Ω_2
Exponential	0.223144	0	08.44	33.91	07.75	31.16	08.41	33.95
		10	14.54	35.92	11.78	32.44	12.45	35.20
		20	18.75	37.82	14.73	33.68	15.46	36.41
		30	22.17	39.62	17.18	34.88	17.96	37.59
	0.510826	0	06.86	27.84	06.33	25.49	06.89	27.82
		10	14.97	30.77	11.66	27.33	12.25	29.62
		20	19.75	33.46	15.21	29.07	15.88	31.32
		30	23.68	35.94	18.06	30.72	18.82	32.94
	0.916291	0	05.07	21.01	04.71	19.14	05.15	20.95
		10	15.92	25.99	12.24	22.21	12.76	23.95
		20	21.86	30.20	16.63	24.92	17.28	26.62
		30	26.44	33.93	20.07	27.37	20.84	29.05

Table 3.15: Values of dimensionless natural frequencies $\left(\Omega = \omega L^2\sqrt{\rho_0 A_0/E_0 I_0}\right)$ for 1st and 2nd mode (Ω_1 and Ω_2) corresponding to linear tapered CF AFG beam for different combinations of taper parameter, spring stiffness and material properties

Taper Pattern	Taper Parameter	Stiffness	Material 1		Material 2		Material 3	
			CF		CF		CF	
			Ω_1	Ω_2	Ω_1	Ω_2	Ω_1	Ω_2
Linear	0	0	03.52	22.03	02.43	18.60	02.56	20.03
		10	11.50	24.60	07.37	20.24	07.73	21.67
		20	15.89	26.93	10.12	21.75	10.61	23.19
		30	19.30	29.08	12.25	23.18	12.84	24.63
	0.2	0	03.61	20.62	02.51	17.38	02.65	18.77
		10	12.50	23.71	08.01	19.31	08.40	20.69
		20	17.30	26.44	11.03	21.07	11.56	22.46
		30	21.03	28.92	13.37	22.70	14.02	24.10
	0.4	0	03.74	19.12	02.62	16.07	2.78	17.41
		10	13.84	22.98	08.89	18.43	09.31	19.76
		20	19.17	26.30	12.28	20.52	12.87	21.86
		30	23.29	29.27	14.92	22.42	15.63	23.78
	0.6	0	03.94	17.49	02.78	14.66	02.96	15.94
		10	15.74	22.72	10.20	17.70	10.69	18.97
		20	21.65	27.13	14.16	20.29	14.82	21.58
		30	26.03	31.07	17.23	22.59	18.03	23.91

remain same. It is also can be seen that It is also observed that for particular taper parameter, foundation stiffness value and material model, the natural frequency is the lowest for CF boundary condition as the system is less stiff under CF boundary condition and highest for CC boundary condition. For fixed non-zero taper parameter it can be observed that in

Table 3.16: Values of dimensionless natural frequencies $\left(\Omega = \omega L^2 \sqrt{\rho_0 A_0 / E_0 I_0}\right)$ for 1st and 2nd mode (Ω_1 and Ω_2) corresponding to parabolic tapered CF AFG beam for different combinations of taper parameter, spring stiffness and material properties

Taper Pattern	Taper Parameter	Stiffness	Material 1		Material 2		Material 3	
			CF		CF		CF	
			Ω_1	Ω_2	Ω_1	Ω_2	Ω_1	Ω_2
Parabolic	0.2	0	03.71	21.44	02.57	18.09	02.72	19.53
		10	12.35	24.33	07.94	19.88	08.32	21.31
		20	17.06	26.91	10.91	21.53	11.43	22.97
		30	20.71	29.26	13.23	23.06	13.86	24.51
	0.4	0	03.95	20.85	02.76	17.56	02.92	19.01
		10	13.40	24.19	08.67	19.57	09.08	21.01
		20	18.49	27.15	11.94	21.39	12.50	22.84
		30	22.41	29.85	14.49	23.07	15.17	24.53
	0.6	0	04.28	20.29	03.02	17.05	03.19	18.53
		10	14.75	24.44	09.66	19.41	10.11	20.87
		20	20.17	28.13	13.32	21.51	13.92	22.98
		30	24.23	31.50	16.16	23.43	16.89	24.91

Table 3.17: Values of dimensionless natural frequencies $\left(\Omega = \omega L^2 \sqrt{\rho_0 A_0 / E_0 I_0}\right)$ for 1st and 2nd mode (Ω_1 and Ω_2) corresponding to exponential tapered CF AFG beam for different combinations of taper parameter, spring stiffness and material properties

Taper Pattern	Taper Parameter	Stiffness	Material 1		Material 2		Material 3	
			CF		CF		CF	
			Ω_1	Ω_2	Ω_1	Ω_2	Ω_1	Ω_2
Exponential	0.223144	0	03.39	19.69	02.35	16.59	02.49	17.91
		10	12.57	23.02	08.03	18.69	08.42	20.00
		20	17.49	25.93	11.09	20.59	11.63	21.91
		30	21.23	28.54	13.45	22.32	14.11	23.67
	0.510826	0	03.19	17.00	02.23	14.29	02.37	15.46
		10	14.14	21.62	09.00	17.17	09.44	18.34
		20	19.72	25.42	12.51	19.65	13.12	20.84
		30	24.03	28.73	15.20	21.86	15.94	23.08
	0.916291	0	02.87	13.76	02.04	11.52	02.17	12.51
		10	16.74	20.94	10.65	15.97	11.17	16.97
		20	23.36	26.33	14.89	19.45	15.62	20.50
		30	28.32	30.90	18.15	22.40	19.05	23.51

between linear and parabolic taper pattern, the system with parabolic taper pattern has the higher natural frequency. It is also observed that for all the cases with increase in taper parameter the natural frequency decreases. Reduction in cross-sectional area and moment of inertia causes a softening effect, which is manifested in this decrement of frequencies. Comparing the values, it is observed that softening effect is severe in exponentially tapered beam and least in parabolic tapered beam. It is also observed that for particular taper parameter, boundary condition and foundation stiffness value, the natural frequency is the highest for Material 1 and lowest for Material 2.

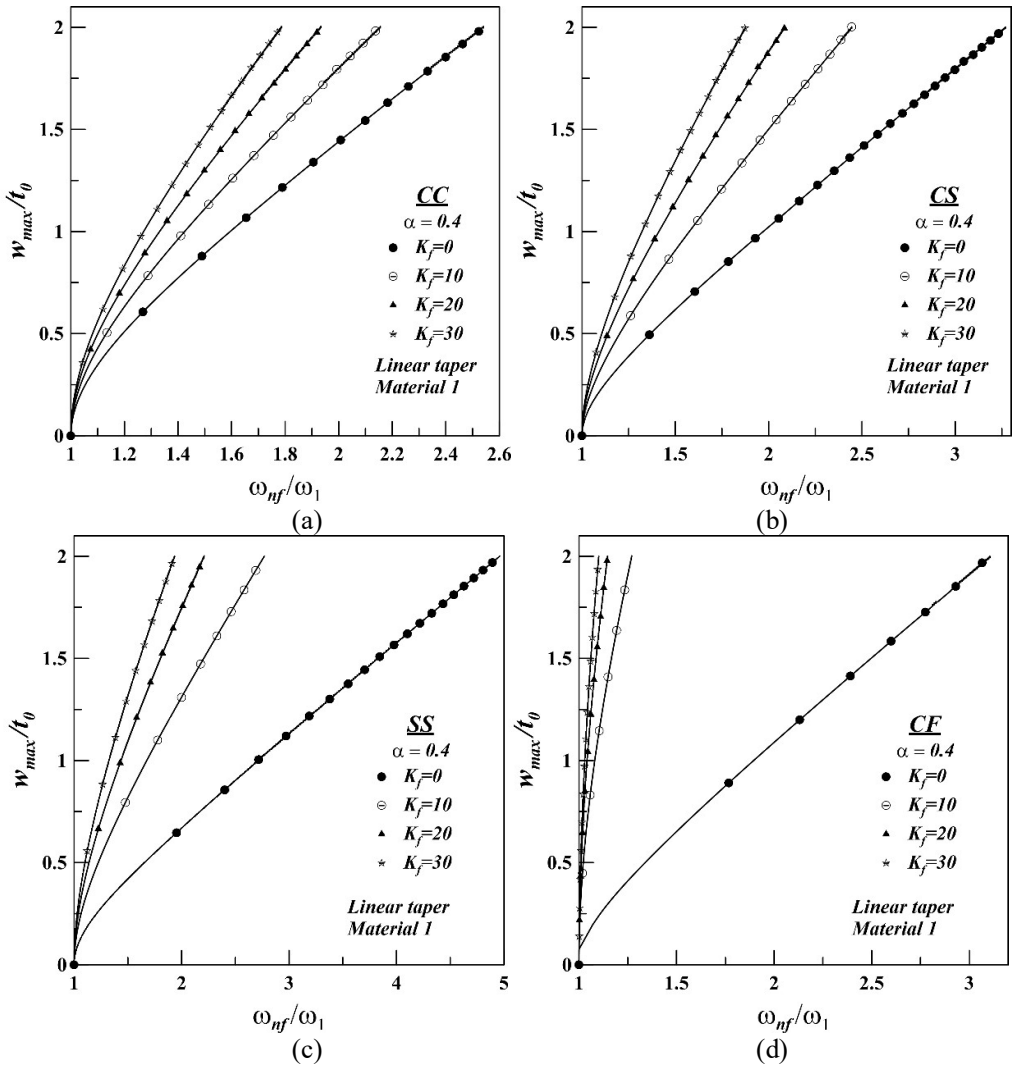

Figure 3.7: Backbone curves of AFG linear taper beam (Material 1) for different boundary conditions: (a) CC (b) CS (c) SS and (d) CF

3.6.4 Backbone curves:

Backbone curves of a vibratory system provide information about the measure of amplitude dependence of natural frequencies of the system. The dynamic behavior of the system is shown in Figures 3.7-3.14 as backbone curves for the first modes in non-dimensional frequency amplitude plane, where the ordinate is dimensionless amplitude (w_{max}/t_0) and abscissa is normalized frequency (ω_{nf}/ω_1). In the present study (w_{max}/t_0) is taken as 2.0 for all cases. The fundamental frequency (ω_1) is used to normalize the nonlinear frequencies are taken from Tables 3.6-3.17.

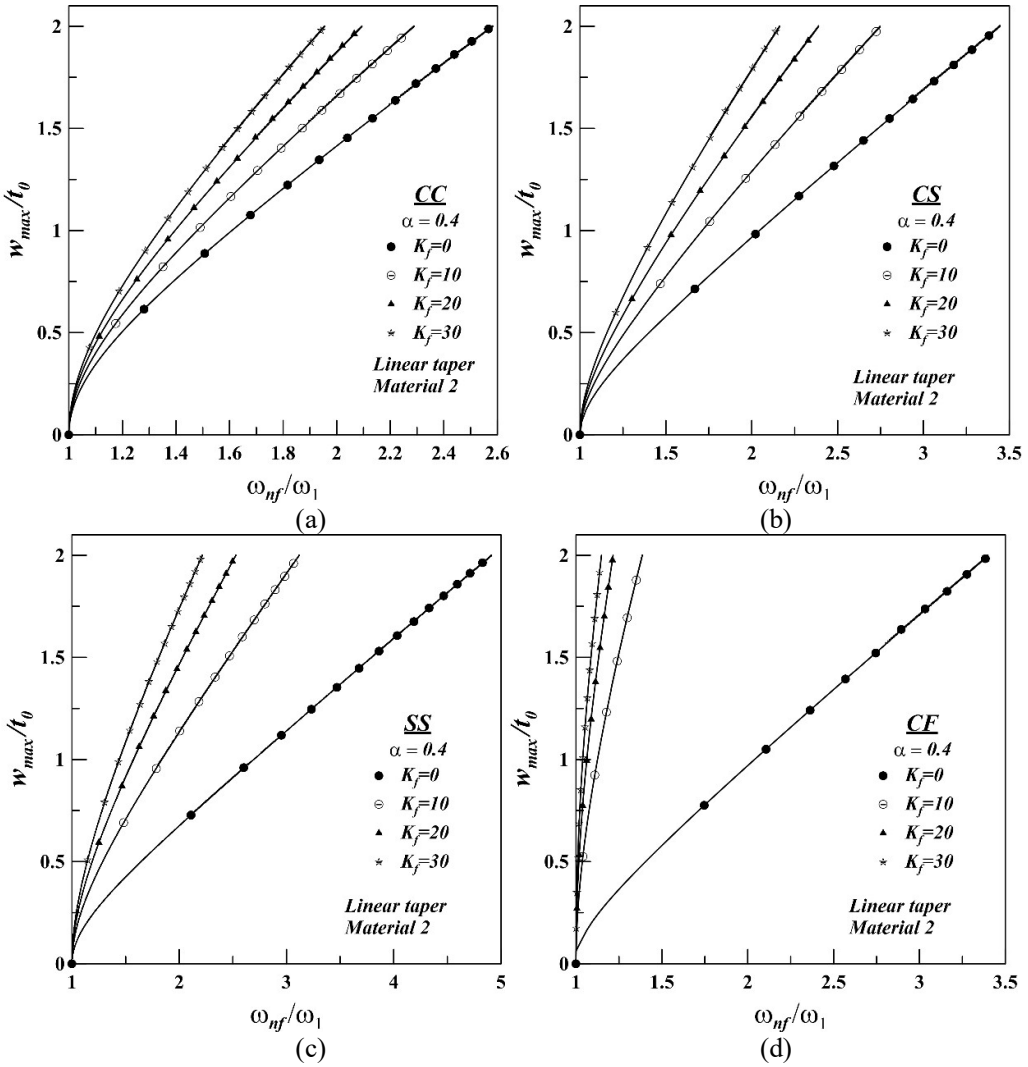

Figure 3.8: Backbone curves of AFG linear taper beam (Material 2) for different boundary conditions: (a) CC (b) CS (c) SS and (d) CF

For all the cases, stiffness of the beam increases with increasing load due to geometric nonlinearity present in the system. This increased stiffness causes the increase in free vibration frequencies with increase in the deflection of the beam, as can be observed from any of the figures. So, hardening type nonlinear behaviour is exhibited by the system for all combinations of taper profile, stiffness values and boundary conditions.

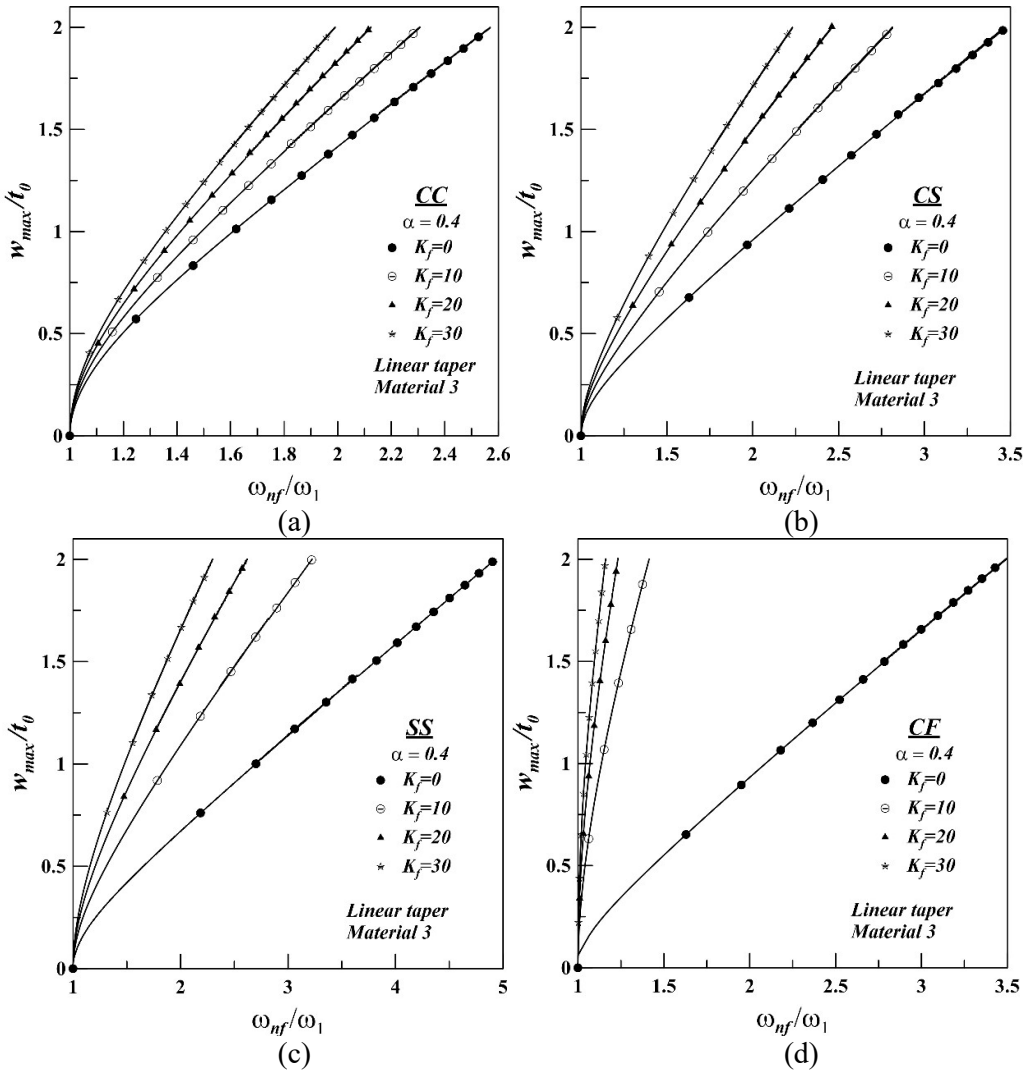

Figure 3.9: Backbone curves of AFG linear taper beam (Material 3) for different boundary conditions: (a) CC (b) CS (c) SS and (d) CF

3.6.4.1 Effects of foundation stiffness:

Figures 3.7-3.9 represent the backbone curve for fundamental mode of linearly tapered beam with three different material models (Material 1, Material 2 and Material 3).In

each figure, there are four sets of plots for four different boundary condition (CC, CS, SS, CF) and in each plot four backbone curves are depicted corresponding to various spring stiffness values which varies from 0 to 30. The taper parameter is kept as constant, at 0.4 to plot the results with an objective to study the influences of the foundation stiffness. Similar plots for parabolic tapered beams are provided in Figures 3.10-3.11, whereas backbone curves for exponential AFG beams are shown in Figures 3.12-3.13. However, in these figures results corresponding to material 1 is only furnished for linear taper pattern. As material 1 is fully homogeneous for the comparison purpose the results are generated and are shown at Figure 3.7. It should also be mentioned that the taper parameter values in Figures 3.12-3.13 are α = 0.223144, 0.510826 and 0.916291 (as shown in Table 3.3).

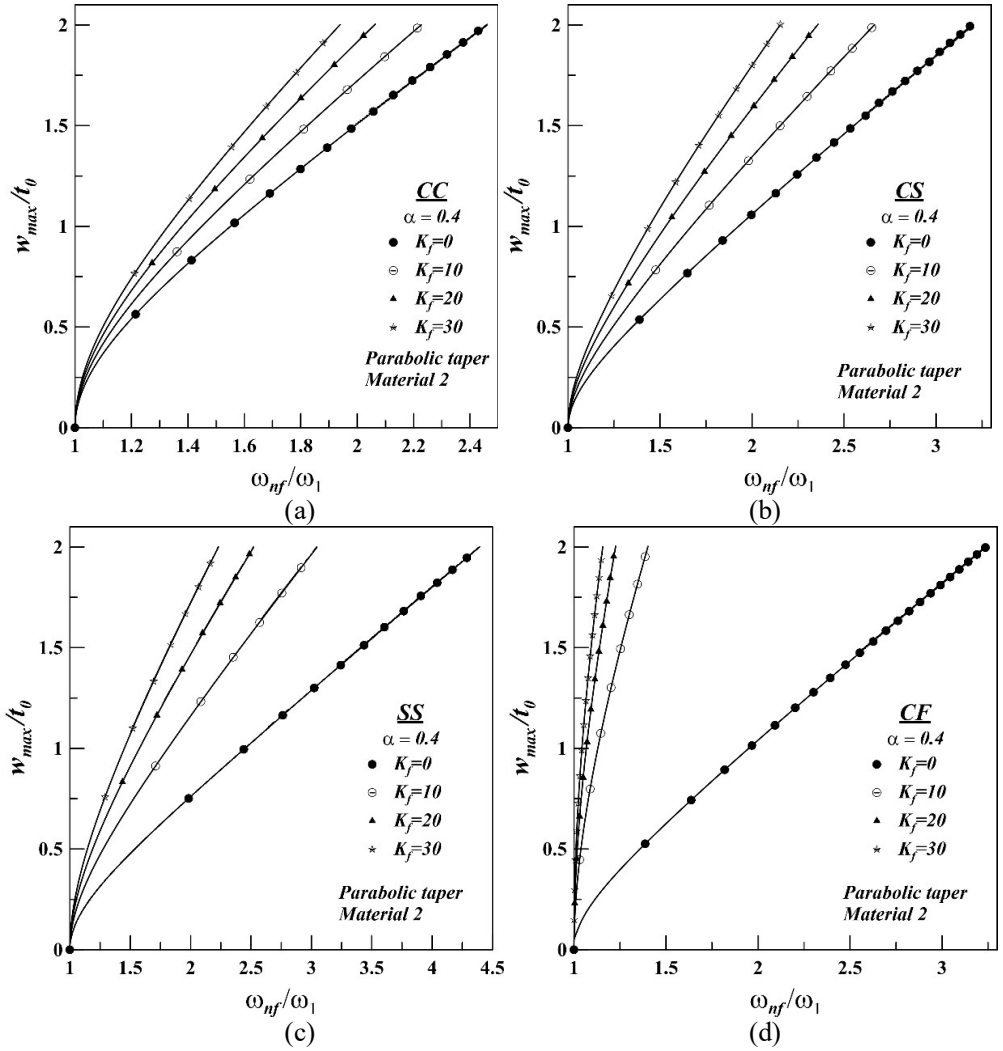

Figure 3.10: Backbone curves of AFG parabolic taper beam (Material 2) for different boundary conditions: (a) CC (b) CS (c) SS and (d) CF

It is observed from Figure 3.7-3.14, in all the cases, with the increase of the foundation stiffness the slope of the backbone curve is increasing in nature. This effect is severe for CF boundary condition whereas for CC beam backbone curves are closely clustered. From the above discussion it can be concluded that nonlinearity involved in case of CF beam is higher than the other two taper patterns. For CC and CS beam profile the difference between the backbone curves is found to be small.

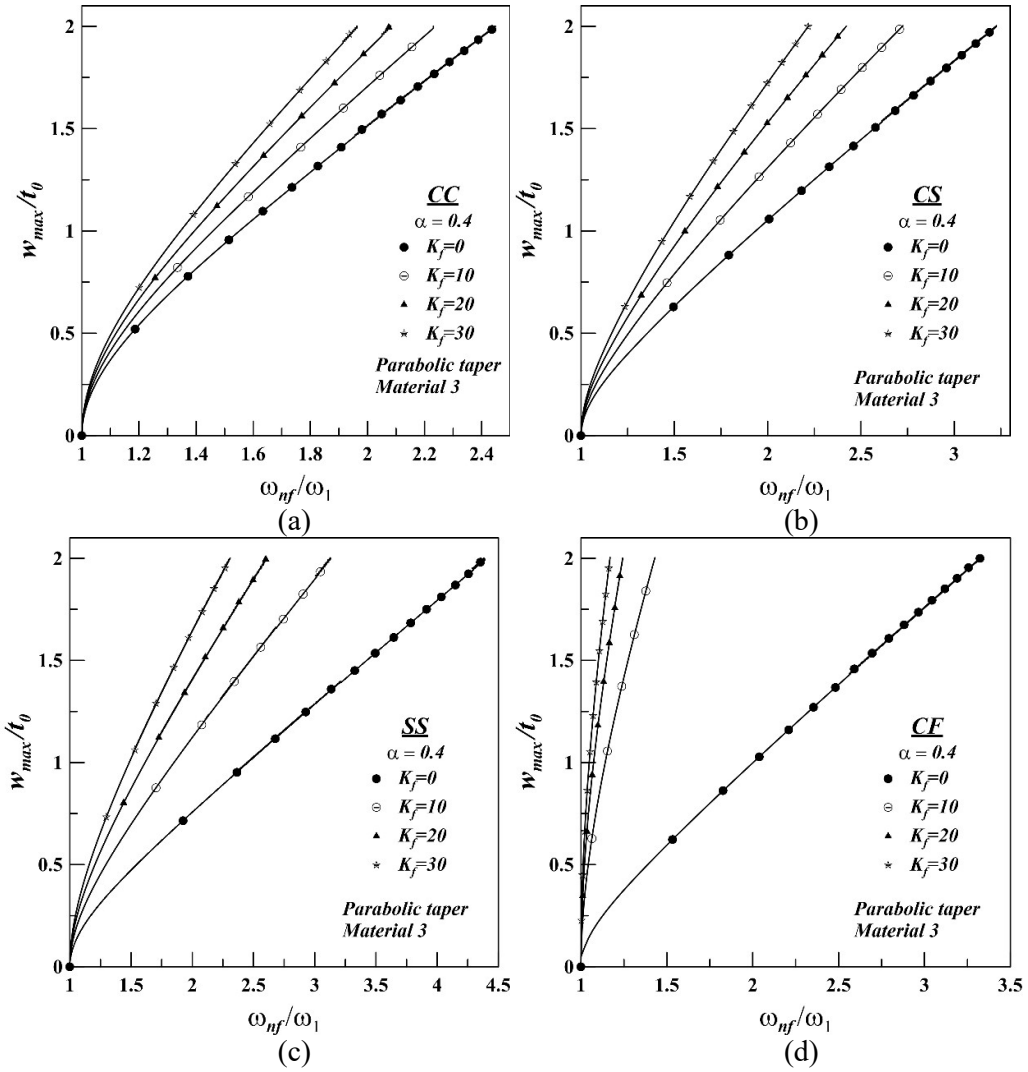

Figure 3.11: Backbone curves of AFG parabolic taper beam (Material 2) for different boundary conditions: (a) CC (b) CS (c) SS and (d) CF

For linear taper pattern, it is quite cleared that the change in backbone curve for different material model is hardly found for a particular case of boundary condition, as shown in Figures 3.7 -3.9. For other type of taper pattern i.e. parabolic and exponential taper same

trend can be found. It is also observed from the figures that for particular boundary condition and material model, in exponential taper the backbone curves are more openly clustered than the other two (linear and parabolic) for different foundation stiffness values.

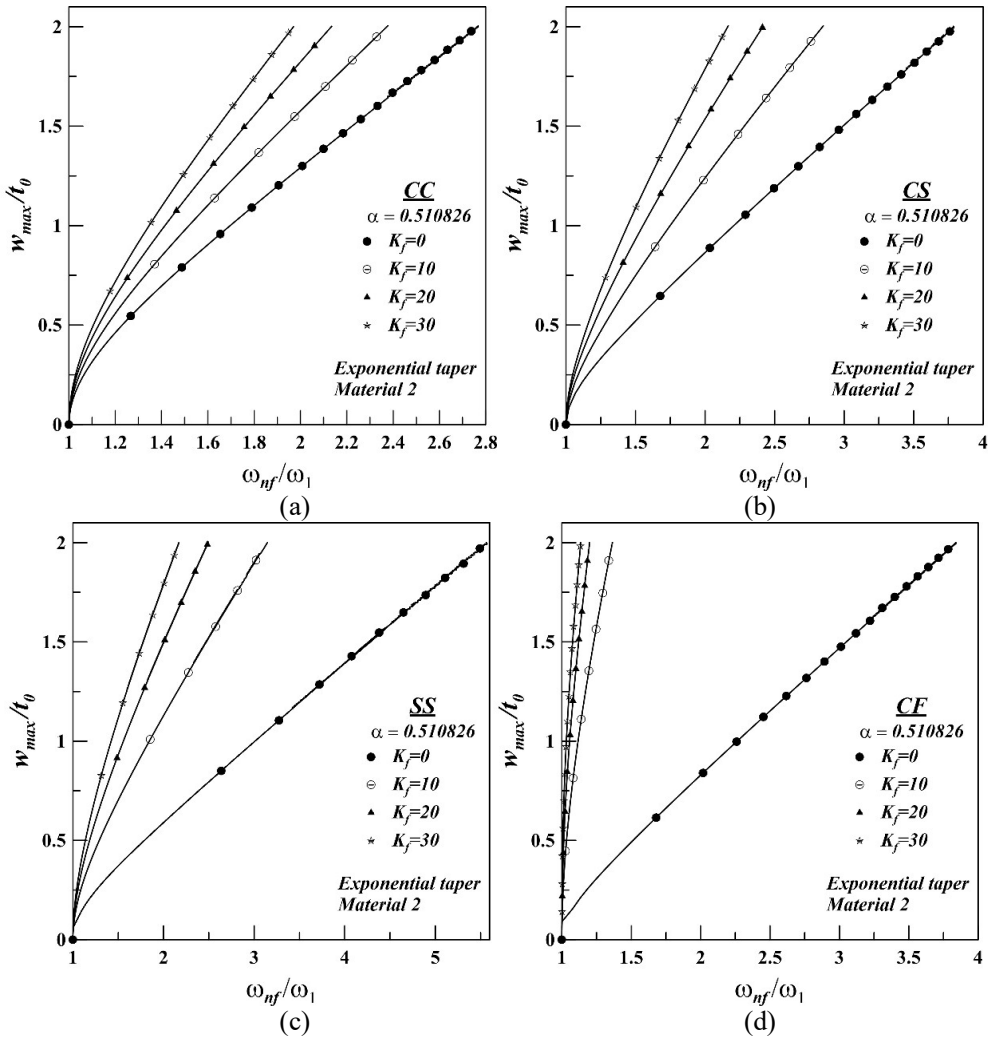

Figure 3.12: Backbone curves of AFG exponential taper beam (Material 2) for different boundary conditions: (a) CC (b) CS (c) SS and (d) CF

3.6.4.2 Effect of taper parameter:

Figure 3.14 shows the effect of taper parameters on backbone curve for CC AFG beam. Curves are depicted for three different taper pattern in which taper parameter varied from 0 to 0.6 for linear and parabolic taper whereas, in case of exponential taper variation of taper parameter is taken from 0 to 0.916291. Material 2 is selected for all the cases whereas foundation stiffness is fixed at 10. It is to be noted that taper parameter 0 represents

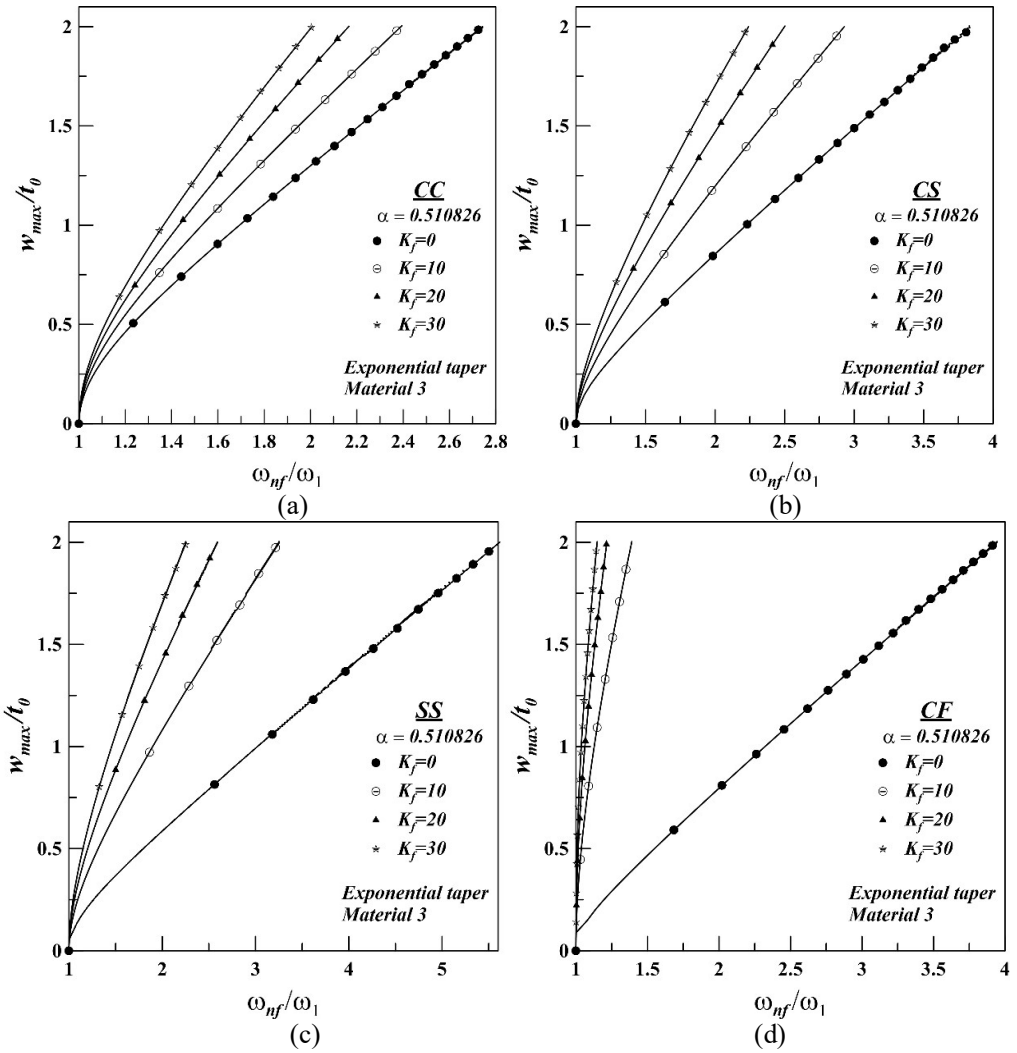

Figure 3.13: Backbone curves of AFG exponential taper beam (Material 3) for different boundary conditions: (a) CC (b) CS (c) SS and (d) CF

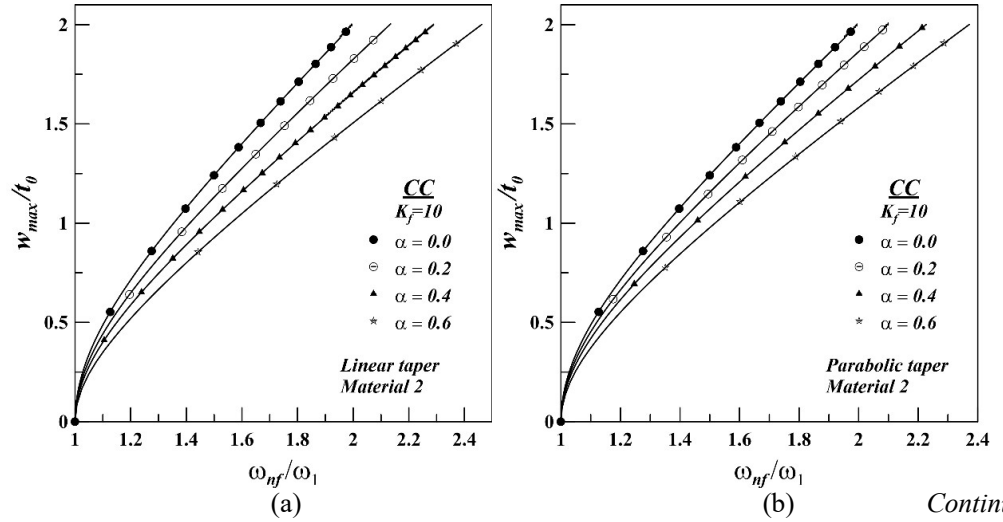

Continued

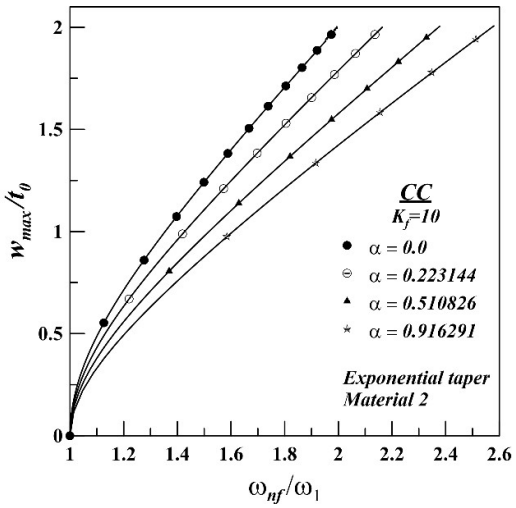

(c)

Figure 3.14: Effect of taper parameters on backbone curves of CC AFG beam for different taper pattern: (a) linear taper (b) parabolic taper and (c) exponential taper

the case of uniform beam and used for comparison purpose only. From the figure, it is observed that for all the cases with the increase of taper parameter values, the slope of the backbone curve is decreasing in nature.

3.6.4.3 Backbone curves at higher modes:

Backbone curves at higher modes (modes 2-5) of the linear taper AFG beam corresponding to four boundary conditions are presented in Figure 3.15. Results are plotted starting from modes 2 and continued upto mode 5. Results beyond mode 5 are also possible but it will create difficulty to accommodate all those into a single figure. For better clarity results are not shown beyond mode 5. Each of these figures consists of two different sub-plots for two different material models i.e. material 2 and material 3. In this regard, plot for the material 1 is not furnished as it is the case of homogeneous material. For all the cases the taper parameter is considered as 0.4, whereas, foundation stiffness is fixed at 10.

3.6.5 Mode shapes:

First three mode shape of the linear taper AFG beam corresponding to four boundary conditions are provided in Figure 3.16. Each of these figures consists of two different sub- plots for two different material models i.e. material 2 and material 3. Mode shape plot for the material 1 is not furnished as it is the case of homogeneous material. For all the cases the taper parameter is considered as 0.4, whereas, foundation stiffness is fixed

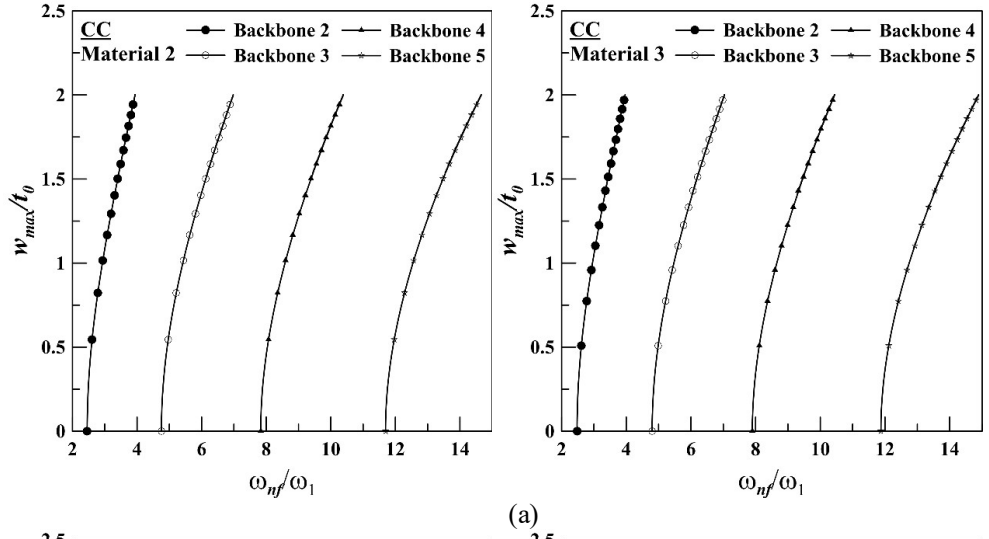

(a)

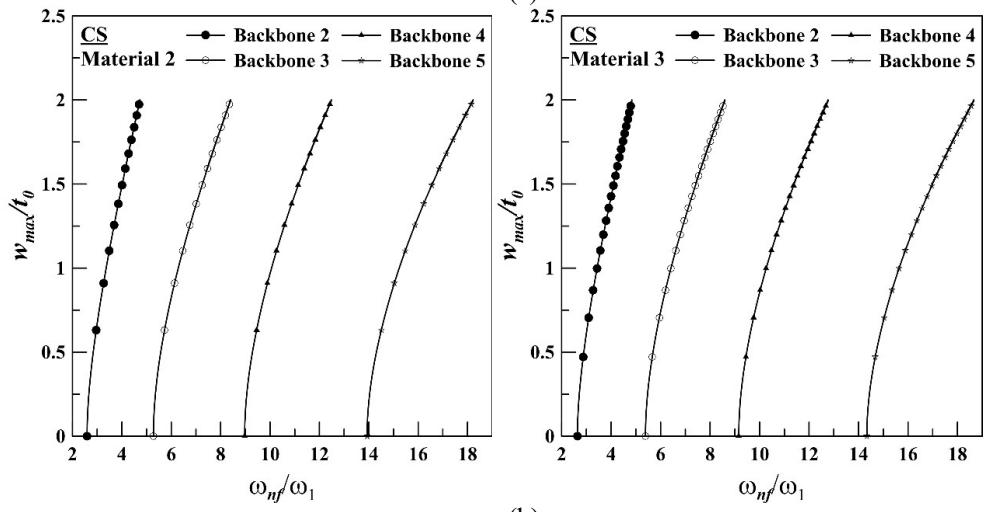

(b)

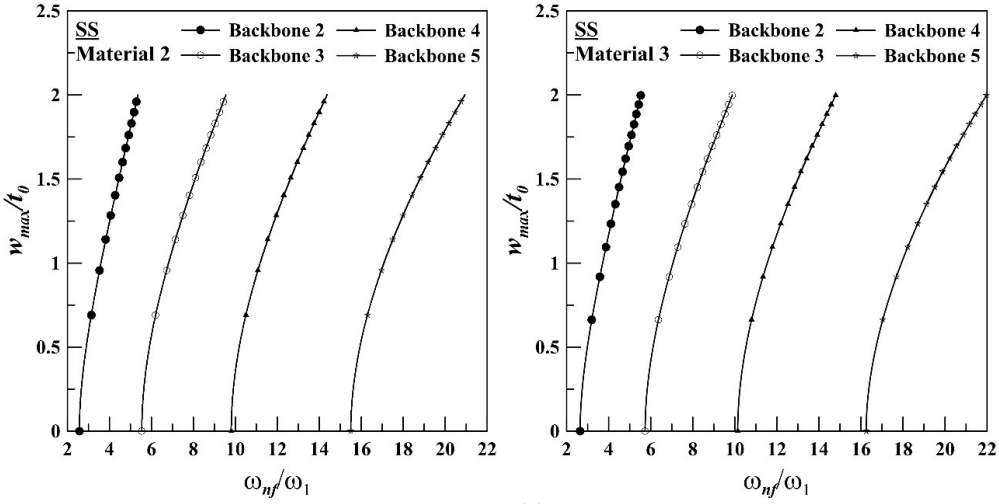

(c)

Continued

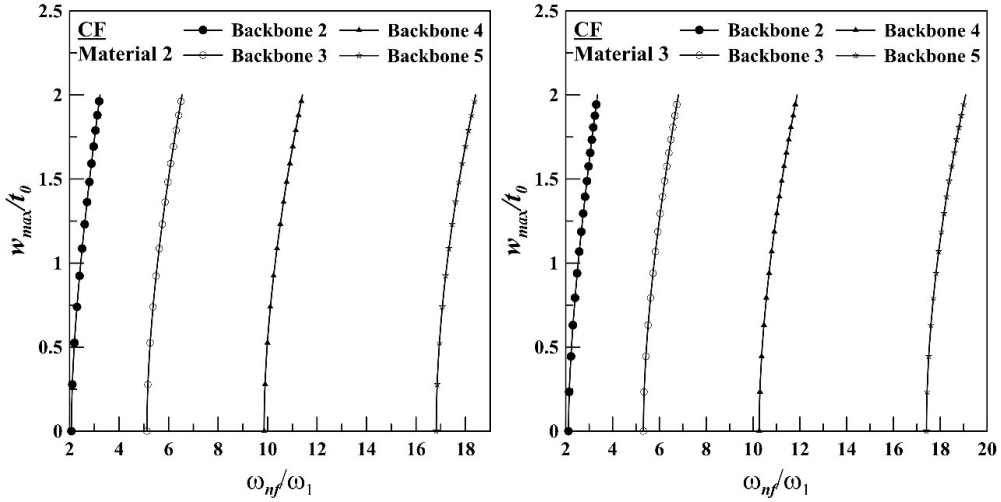

(d)

Figure 3.15: Backbone curves at higher modes of linear taper AFG beam corresponding to different boundary conditions: (a) CC (b) CS (c) SS (d) CF.

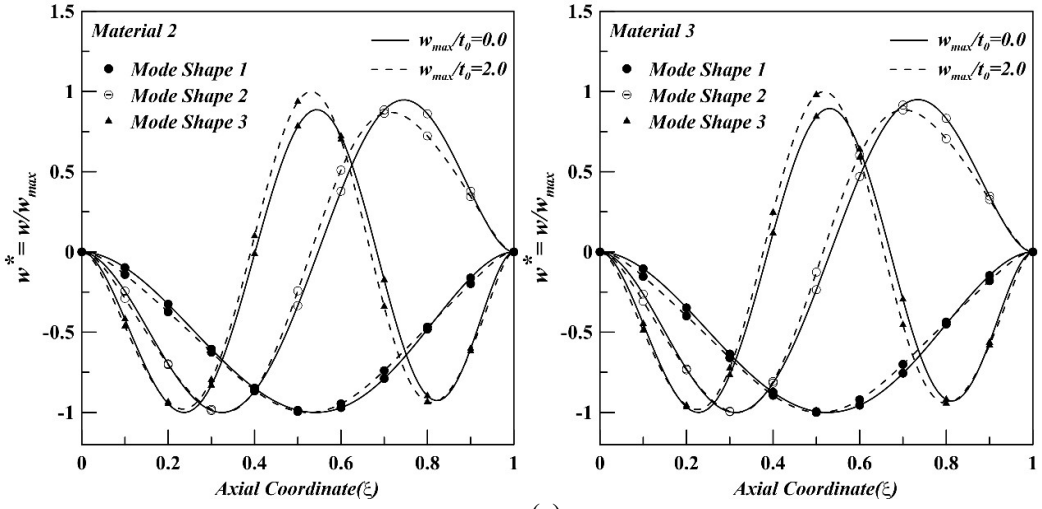

(a)

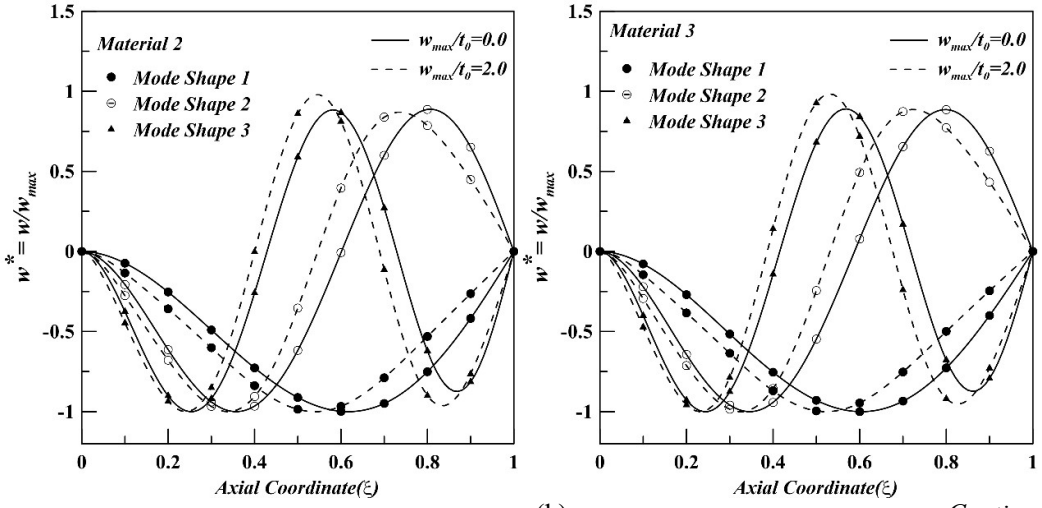

(b)

Continued

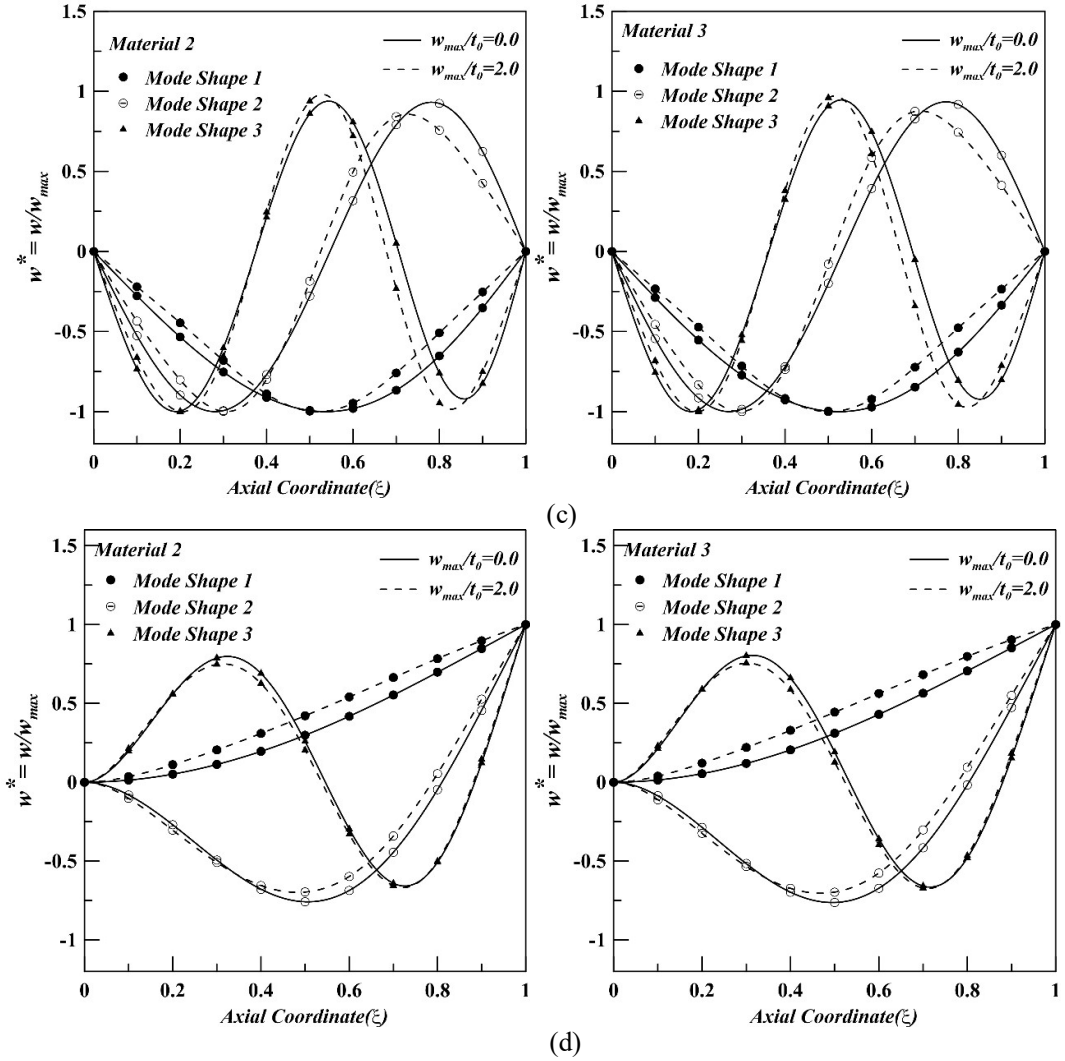

Figure 3.16: Mode shape of linear taper AFG beam corresponding to different boundary conditions: (a) CC (b) CS (c) SS (d) CF.

at 10. It is also worth pointing out that amplitude of vibration has an effect on the mode shape of the system. To study this aspect in more detail, two mode shape plots corresponding to linear ($w_{max}/t_0 = 0$) and nonlinear ($w_{max}/t_0 = 2$) frequencies are given for each of the vibration modes. It should also be noted that the amplitude of vibration for all the plots is normalized by the corresponding maximum deflection. It was observed that difference in linear and nonlinear mode shapes increase when the boundary condition changes from CC to CF, CS and SS due to the decreasing rigidity at the boundary. However, no considerable change in the mode shapes could be identified for the different material models perhaps due to normalization of the maximum displacement.

3.7 Closure:

In the present analysis, large amplitude free vibration behaviour of axially functionally graded thin taper beam with various taper profile and material gradation is investigated. The beam is further assumed to be on elastic foundation and subjected to uniformly distributed load. Different flexural boundary conditions are considered. However, the present methodology can be applied for other type of classical and non-classical boundary as well. Energy principle is applied for the mathematical formulation and the problem can be solved in two part, static and dynamic respectively. For the static problem minimum total potential energy principle is utilized whereas for dynamic analysis the formulation is based on Hamilton's principle. The methodology is general in nature as it can be applied for other type of material gradation and taper pattern. The obtained results are validated from previously published results and were found to be in good agreement. Results pertaining to various taper parameter and spring stiffness for different flexural boundary condition are furnished as backbone curve for the fundamental mode. Backbone curves of taper AFG beam for CC, CS, SS and CF boundary condition are supplied at different taper pattern, taper parameter and spring stiffness. For all combinations of the system parameters hardening type of nonlinearity is observed. Mode shape plots are also presented to show comparison between the linear and nonlinear mode shapes.

Chapter 4

FORCED VIBRATION: AXIALLY FUNCTIONALLY GRADED THIN BEAMS ON ELASTIC FOUNDATION

4.1 Introduction:

Analysis of dynamic behaviour of structural elements under time varying external force or excitation can be termed as forced vibration analysis. In engineering applications such dynamic loading conditions are generally produced by unbalance in rotating machinery, forces produced by the reciprocating machines, or the motion of machine itself. Harmonic excitation, i.e., forces varying harmonically with time is a very common example of dynamic loading condition. Pure harmonic excitation is less likely to occur in working environment than periodic or other types of excitation, but understanding the behaviour of a system under harmonic excitation is essential in order to comprehend how the system will respond to more general types of excitation. It is also understood that the response of a system under harmonic excitation may be periodic but non-harmonic. However, in the present scenario such conditions are not taken into account as it is assumed that harmonic excitation is going to produce harmonic response of the same frequency.

Forced vibration analysis is conducted with an objective to find out the response of the system, in terms of displacement amplitude, under externally applied time varying excitations. Presently, large amplitude forced vibration analysis of AFG beams resting on elastic foundation subjected to transverse harmonic excitation is performed. The foundation has been mathematically incorporated into the analysis as a set of linear springs attached uniformly at the bottom surface of the beam. The mathematical formulation is displacement based and derivation of governing equations is accomplished following Hamilton's principle. In the current study, only steady-state response is presented and frequency of response of the undamped system is assumed to be equal to that of the external excitation. Broyden method, which is a multidimensional secant method used for numerically solving the system of nonlinear equations. The large amplitude dynamic behaviour of the system

in terms of non-dimensional frequency response curves is validated against established results and new results are furnished for tapered AFG beam on linear elastic foundation.

4.2 System Geometry and Material Property Variation:

The present system under consideration is same as that described in Chapter 3. A different view of the system (from those presented in the previous chapter) is shown in Figure 4.1, which also details the geometric and material parameterms associated with the system. The figure depicts the deflected configuration of the beam under transverse external excitation along with the undeformed state. The tapered AFG beam, resting on linear elastic foundation, has a length L, while the cross-sectional dimensions are represented as variable width $b(x)$ and variable thickness $t(x)$. Gradation of material properties i.e. modulus of elasticity, $E(x)$, and mass density, $\rho(x)$ is along the longitudinal axis. The foundation stiffness is taken as K and the effect of the foundation on the system is incorporated in terms of series of linear springs with stiffness coefficient, K (Figure 4.1) same as that of the foundation. In this representative figure the thickness variation has not been depicted, although the formulation is certainly able to handle taper in either thickness or width individually or in conjunction.

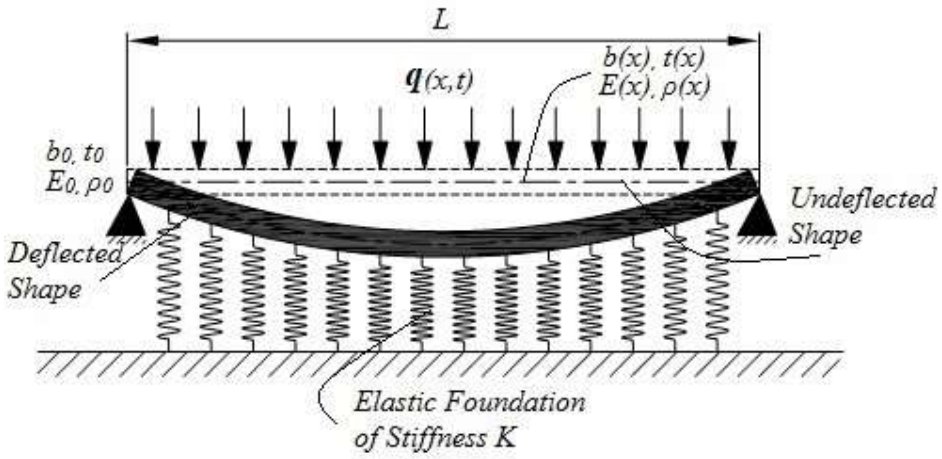

Figure 4.1: AFG beam supported on elastic foundation represented as series of linear

4.3 Mathematical formulation:

An indirect approach is adopted for formulation and corresponding solution to the problem. Here it is reduced to a static scenario by assuming that under maximum amplitude of excitation, i.e., when the system suffers maximum deformation, the dynamic system fulfils force equilibrium conditions. This supposition converts the problem of solving for the dynamic system into an equivalent static situation, where the excitation frequency and amplitude of the harmonic excitation are the parameters that control system response.

In the present chapter, the mathematical formulation is carried out taking the beam to follow Euler – Bernoulli hypothesis, as a result of which the effect of rotary inertia and shear deformation is neglected. It should be mentioned here that according to the above hypothesis plane cross-section of the beam remains plane and normal to the deformed axis once deformation has taken place. To introduce geometric nonlinearity into the formulation, Von Karman type nonlinear strain-displacement relations are considered along with Euler-Bernoulli theory.

$$\varepsilon_x^b = -z\frac{d^2w}{dx^2} \tag{4.1a}$$

$$\varepsilon_x^s = \frac{du}{dx} + \frac{1}{2}\left(\frac{dw}{dx}\right)^2 \tag{4.1b}$$

In the overall expression of axial strain due to bending (ε_x^b) and stretching (ε_x^s), terms corresponding to linear bending strain as well as linear in-plane strain and non-linear in-plane strains are present. The nonlinear in-plane term is associated with large deformation. The present analysis is a semi-analytical displacement based method that employs appropriate energy method to derive the governing equations. Hence the strain-displacement expressions provided in Equation (4.1) helps derive the energy expressions in terms of assumed displacement fields. In the present formulation of geometrically nonlinear forced vibration, Hamilton's principle (mathematically expressed in Equation (4.2)) is applied to obtain the governing set of equation.

$$\delta\left(\int_{\tau_1}^{\tau_2}\left(T-U-V\right)d\tau\right)=0 \tag{4.2}$$

Here, T is kinetic energy of the system, while, U and V designate total strain energy and work potential due to external excitation $q(x)$, respectively. The free vibration analysis presented in the previous chapter (Chapter 3) is also formulated on the basis of Hamilton's principle, but with a significant difference. Previously, in the mathematical expression of the principle the work potential of the external forces (V) was set to zero (Equation (3.10)), as it does not play any part in case of free vibration analysis. However, for forced vibration problem the potential of external excitation term must be retained.

As already mentioned with regards to strain-displacement relations (Equation (4.1)), both bending and stretching effect of the beam is considered to incorporate large displacement behaviour. Thus, strain energy components corresponding to both bending and stretching are present in the overall strain energy expression. Beside this, strain energy stored in the system due to deformation of elastic foundation (equivalently represented by deformation of cluster of springs) is also taken into consideration. Therefore, total strain energy of the system is presented as,

$$U=U_b+U_m+U_f \tag{4.3}$$

Here, U_b and U_m are total strain energies caused by bending deformation and stretching, respectively, while, U_f is the strain energy stored due to deformation of the elastic foundation i.e., in terms of formulation this part of the strain energy is taken care of by the deflection of the springs replacing the foundation. Substituting the relevant strain-displacement expressions, total strain energy of the system can be expressed as,

$$U=\frac{1}{2}\int_0^L\left(\frac{d^2w}{dx^2}\right)^2E\left(x\right)I\left(x\right)dx+\frac{1}{2}\int_0^L\left[\left(\frac{du}{dx}\right)^2+\frac{1}{4}\left(\frac{dw}{dx}\right)^4+\left(\frac{dw}{dx}\right)^2\left(\frac{du}{dx}\right)\right]E\left(x\right)A\left(x\right)dx$$
$$+\frac{1}{2}\int_0^L Kw^2dx \tag{4.4}$$

The total potential energy (V) due to externally applied transverse harmonic excitation can be given by,

$$V = \int_0^L q(x)\, w dx \tag{4.5}$$

where, q represents harmonic excitation for uniformly distributed type excitation, whose expression is given by $q = \bar{q}(\mathrm{x})e^{i\omega\tau}$, where ω is the frequency of excitation, $i = \sqrt{-1}$ and $\bar{q}$ represents the intensity of the harmonic excitation per unit length of the beam. The present formulation can be applied for other type of transverse excitations as well by changing the loading pattern in the Equation (4.5). Hence, the present study is certainly not limited to only uniformly distributed excitation.

The kinetic energy of the system can be given by,

$$T = \frac{1}{2}\int_0^L \left\{ (\dot{w})^2 + (\dot{u})^2 \right\} \rho(x) A(x)\, dx \tag{4.6}$$

Here, the overdots denote differentiation with respect to time (τ).

The above mentioned energy functionals are determined from the assumed dynamic displacement fields, which are given by,

$$w(\xi,\tau) = \sum_{i=1}^{nw} d_i \varphi_i(\xi) e^{i\omega\tau} \tag{4.7a}$$

$$u(\xi,\tau) = \sum_{i=nw+1}^{nw+nu} d_i \psi_i(\xi) e^{i\omega\tau} \tag{4.7b}$$

The transverse (w) and in-plane (u) displacement fields are defined at the neutral axis of the beam and are assumed to be separable in space and time. As shown in Equation (4.7), they are approximately represented by linear combinations of a set of unknown parameters (d_i) and orthogonal admissible functions (φ_i and ψ_i). It is quite clear that φ_i is associated with the transverse displacement (w), whereas ψ_i defines the in-plane displacements (u). Being admissible functions, φ_i and ψ_i possess certain properties such as, continuity and differentiability within the domain. Also satisfaction the flexural and membrane boundary conditions of the system is another major criterion. In order to generate a complete set of orthogonal admissible functions, first of all a start function

satisfying the boundary condition is chosen. For transverse displacement, beam deflection functions, derived from static deflection shape of the beam, corresponding to the boundary condition of the system are taken as the start function. The starting functions for stretching of the beam (u) come from the in-plane boundary conditions. For the present analysis, the in-plane boundary conditions are considered as immovable, i.e., no in-plane displacements are allowed at the boundaries. Once the start functions are selected, generation of higher order functions is accomplished by Gram-Schmidt orthogonalization scheme. The number of functions for w and u are denoted by nw and nu, respectively. For the present mathematical formulation, it is assumed that number of functions for w and u are equal i.e., $nw = nu$.

In expression (4.7), ω is the response frequency of the system and according to the basic assumption of current analysis response frequency is equal to the excitation frequency. It should be noted that the orthogonal functions are generated in a normalised computational domain that varies from 0 to 1. The physical domain in x coordinate is converted to the computational domain by dividing the coordinate by the beam length (L), i.e., $\xi = x/L$. In this computational domain ng number of Gausss points are generated that work as the reference points with respect to which all the numerical computations are performed.

Substitution of the Equation (4.4), (4.5) and (4.6), as well as the dynamic displacement fields, in Equation (4.2) the governing equation of the geometrically nonlinear forced vibration problem in the following matrix form.

$$-\omega^2 [M]\{d\} + [K]\{d\} = \{f\} \tag{4.8}$$

$[K]$, $[M]$ and $\{f\}$ are stiffness matrix, mass matrix and load vector, respectively. $\{d\}$ is the vector of unknown coefficient. It should be mentioned here that the governing equation of the presesent problem is quite similar to that derived for free vibration analysis (Equation (3.13)), with the exception that the right hand side here is not zero (due to presence of potential of the external excitation term). The form of the above mentioned matrices and vector are given in Appendix.

4.4 Solution procedure:

Equation (4.8) represents the governing set of nonlinear equations for the dynamic system. But the basic assumption of the present study reduces the problem to an equivalent static case. At the peak excitation amplitude value it is assumed that the system satisfies the force equilibrium condition and thus the problem can be considered as a static one where the system response is dependent on the excitation frequency and the amplitude of the harmonic excitation. So, at each excitation frequency for a given harmonic excitation amplitude the corresponding unknown coefficients are to be determined. However, determination of these unknown parameters is not straightforward and cannot be directly implemented through simple matrix inversion followed by pre-multiplication with the load vector as shown in Equation (4.9), as the stiffness matrix ([K]) itself is a function of the unknown parameters. A closer look at the stiffness matrix elements presented in the Appendix clearly shows that certain terms indeed contain the unknown coefficients (d_i). This coupling arises due to the consideration in-plane stretching term in the strain-displacement relation at the mathematical formulation stage.

$$\{d\} = \left[\left[K\right] - \omega^2 \left[M\right]\right]^{-1} \{f\} \tag{4.9}$$

To solve the set of nonlinear governing equations an iterative procedure with an initial guess value of the unknowns must be employed. In the present work, a multidimensional quasi-Newton method, known as Broyden's method that utilizes the Jacobian matrix and subsequent updation/correction of the initial Jacobian, is used for the numerical solution of the nonlinear system equations. Determination of the Jacobian matrix is usually an extensive and difficult computational task. Even for sufficiently simple functions, for which the partial derivatives can be analytically found out, the extent of computations necessary may well be excessive. In case of majority of practical problems, however, complicated functions are encountered and numerical determination of an approximation to the Jacobian matrix is inevitable. In the present scenario, an initial Jacobian of the system is computed based on the initial guess and subsequently, only updates, ensuring the minimum change to the Jacobian from the previous iteration, are effected, instead of determination of the whole Jacobian matrix in each step of iterations. So, in this case, the partial derivatives are not estimated or evaluated directly, but

corrections to the approximate Jacobian matrix are computed from the function values. The function is constituted by rearranging the terms of the governing Equation (4.8) as follows,

$$F(d)=\left[[K]-\omega^2[M]\right]\{d\}-\{f\} \tag{4.10}$$

So, the objective of the Broyden method is to solve for the roots of the set of equations, $F(d) = 0$. The codes for implementation of Broyden method is developed in Matlab following the algorithm provided by Press et al. (2005). Once the values of the unknown parameters are solved for a given excitation amplitude and frequency, the displacement fields can be computed following Equation (4.7). Finally, the maximum deflection (w_{max}) value corresponding to a frequency step is searched out from within the transverse displacement field (w).

4.5 Results and discussions:

The present work investigates the influence of various classical flexural boundary conditions as well as material property variations and stiffness of the elastic foundation on the large amplitude forced vibration behavior of axially functionally graded taper beams under harmonic excitation. For the current analysis only uniformly distributed excitation pattern, mathematically expressed as $q=\bar{q}(\mathrm{x})e^{i\omega\tau}$, has been considered. The intensity of the harmonic excitation, $\bar{q}$, is made dimensionless using the expression, $\bar{q}^*=\bar{q}(L^4/E_0I_0t_0)$ in the present study, $\bar{q}^*$ is varied from 30 to 60 in the interval of 10. But it is possible to replace the given expression with mathematical form of any other type of excitation pattern as well. Three different taper patterns are taken for the beam, which are linear taper, parabolic taper and exponential taper respectively and the variations of thickness are mentioned in the previous chapter (Chapter 3, Section 3.2) and tabulated in Table 3.1. Here four different taper parameter values are considered for each taper pattern and these values are shown in Table 3.2 as indicated in the Chapter 3 (Section 3.2). Variation of frequency response of the system with respect to taper pattern (such as linear, exponential etc.) and taper parameter value are also interesting avenues of study. Material property variations along the length of the beam are taken into account by considering gradation of elastic modulus and density. Three different models for variation of these two material parameters are presented in the present chapter. They are mentioned in the Table 3.3 in Chapter 3. It is

clear from the relations that material model 1 refers to a homogeneous beam, which has been included for comparison purpose. The other aspect of complexity of the current system is the elastic foundation upon which the system rests. As already mentioned, the foundation has been incorporated into the mathematical formulation by a series of parallel massless linear springs with equivalent spring stiffness (K). Four different values of non-dimensional stiffness (K_f) are taken for the present study and these values are 0, 10, 20 and 30 respectively. The conversion between dimensional (N/m) and non-dimensional stiffness follows the relationship, $K_f = K\ \{(L/t_0)^3/E_0 b\}$. Here, the situation with 0 spring stiffness corresponds to a case where the foundation is absent, i.e., the beam is not supported by the foundation at all. This case has also been included to provide a better comparison for the response with and without the foundation. Following geometrical dimensions and material properties are used to generate the results: L = 1.0 m, b = 0.02 m, t_0 = 0.005 m, E_0 = 210 GPa, ρ_0 = 7850 kg/m^3.

Three different classical flexural boundary conditions are considered (clamped-clamped (CC), clamped-simply supported (CS) and simply supported-simply supported (SS)), whereas the in-plane boundary is assumed to be immovable. The start functions for transverse displacement (w) and for axial displacement (u) are chosen fulfilling the conditions outlined in the Mathematical Formulation segment. It is imperative that these chosen functions satisfy the boundary conditions of the system. The start functions for transverse displacements corresponding to the boundary conditions are listed in tabular form in Table 3.4 in Chapter 3. The start function for in-plane boundary conditions (immovable i.e., no displacement at the two ends, $\xi = 0$ and $\xi = 1$) is taken as $\xi(1-\xi)$.

4.5.1 Convergence study:

These selected start functions are used to generate the higher order functions with the help of Gram-Schmidt orthogonalisation principle. One important aspect to decide is the number of higher order functions for w and u to be generated. Similarly, the number of Gauss points (ng) also has significant influence on the accuracy of the results obtained. Hence, necessary convergence tests must be performed to arrive at acceptable values for these parameters. The convergence study is carried out for a clamped beam resting on an elastic foundation of stiffness, $K = 10^3$ N/m and the profile of the beam is parabolic in

nature with taper parameter of 0.2. Material model for this particular study is considered as model 2. In order to conduct the test, the maximum normalised deflection of the system is tracked against the variation of relevant parameters at a given excitation amplitude (10 N/m) and excitation frequency value (31.85 Hertz). The results of the convergence study are presented in Figure 4.2. Normalized maximum deflection (w_{max}/t_0) of the system is plotted against number of Gauss points (*ng*) is plotted in Figure 4.2(a). A choice of 24 Gauss points for the present work is made from this study. The positions of these Gauss points within the computational domain are indicated in Table 3.5 in the chapter 3. It is evident that these points are equally spread out and they are densely spaced at the two extremities, while sparsely spaced towards the middle. The second part of the convergence study fixes the number of functions to be generated. The previously mentioned system is analyzed for variation in number of orthogonal functions assuming that the number of functions for *w* and *u* are equal (*nw* = *nu*). The convergence results are furnished in Figure 4.2(b) and a choice of 8 functions are made.

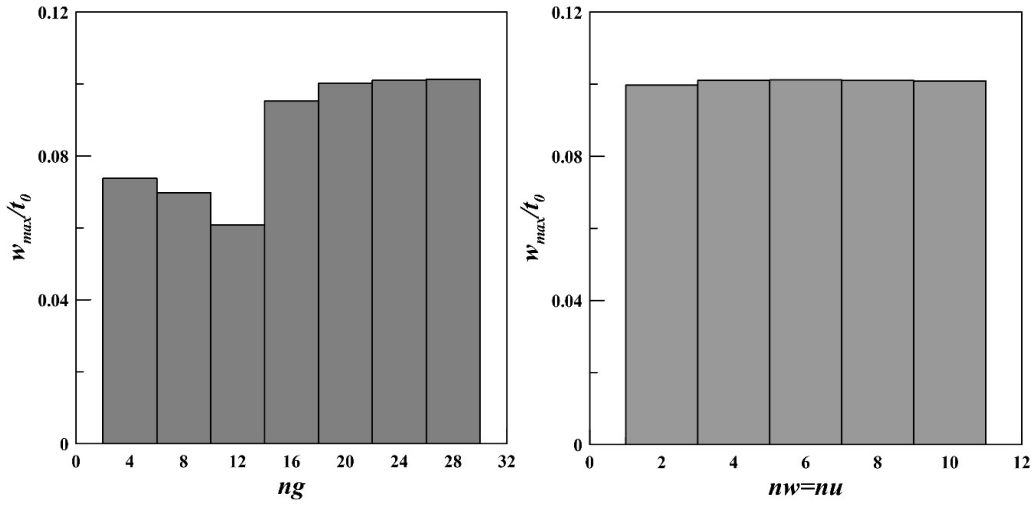

Figure 4.2: Convergence study for (a) number of gauss point and (b) number of orthogonal functions

4.5.2 Validation study:

Once the above-mentioned parameter values corresponding to the numerical scheme are ascertained, the next task is to establish the validity of the present methodology and solution technique. The validation of the current method is carried out through comparison with previously established results. However, the authors are not aware of any

benchmark results that provide frequency response curves for the system under consideration. So, comparison with a system having reduced complexity is undertaken. A simple clamped homogeneous uniform beam under a point harmonic excitation at the mid-span is considered (Ribeiro, 2004). In the present formulation the system is simulated by considering a foundation stiffness K = 0 N/m, while the taper parameter is reduced to 0. The generated results for frequency response curve as shown in Figure 4.3 exhibit good agreement with result published by Ribeiro (2004).

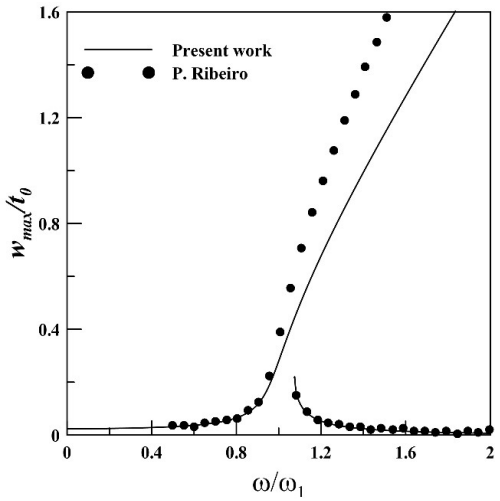

Figure 4.3: Validation plot for large amplitude forced vibration response of clamped uniform beam under point load (0.134 N) at mid-span of the beam following Broyden's method

4.5.3 Frequency response curves:

Numerical results for large amplitude forced vibration analysis are presented in terms of normalised frequency response plots, where the normalised excitation frequency (ω_f/ω_1) is the abscissa, while ordinate represents normalised maximum deflection. Maximum amplitude of vibration is normalized by root thickness (t_0) of the beam. On the other hand normalization of the forcing frequency is carried out by dividing with the fundamental frequency (ω_1) of the system. It should be mentioned here that the natural frequencies of the system are determined following a separate geometrically nonlinear free vibration analysis, whose details are provided in Chapter 3.

To determine the response curves frequency sweep is initiated at or near zero excitation frequency with a particular excitation amplitude and gradually increased beyond resonance.

Such a sweep is designated as sweep up, while, another frequency sweep, categorized as sweep down, is conducted by gradually reducing the excitation frequency from a finite high value towards zero.

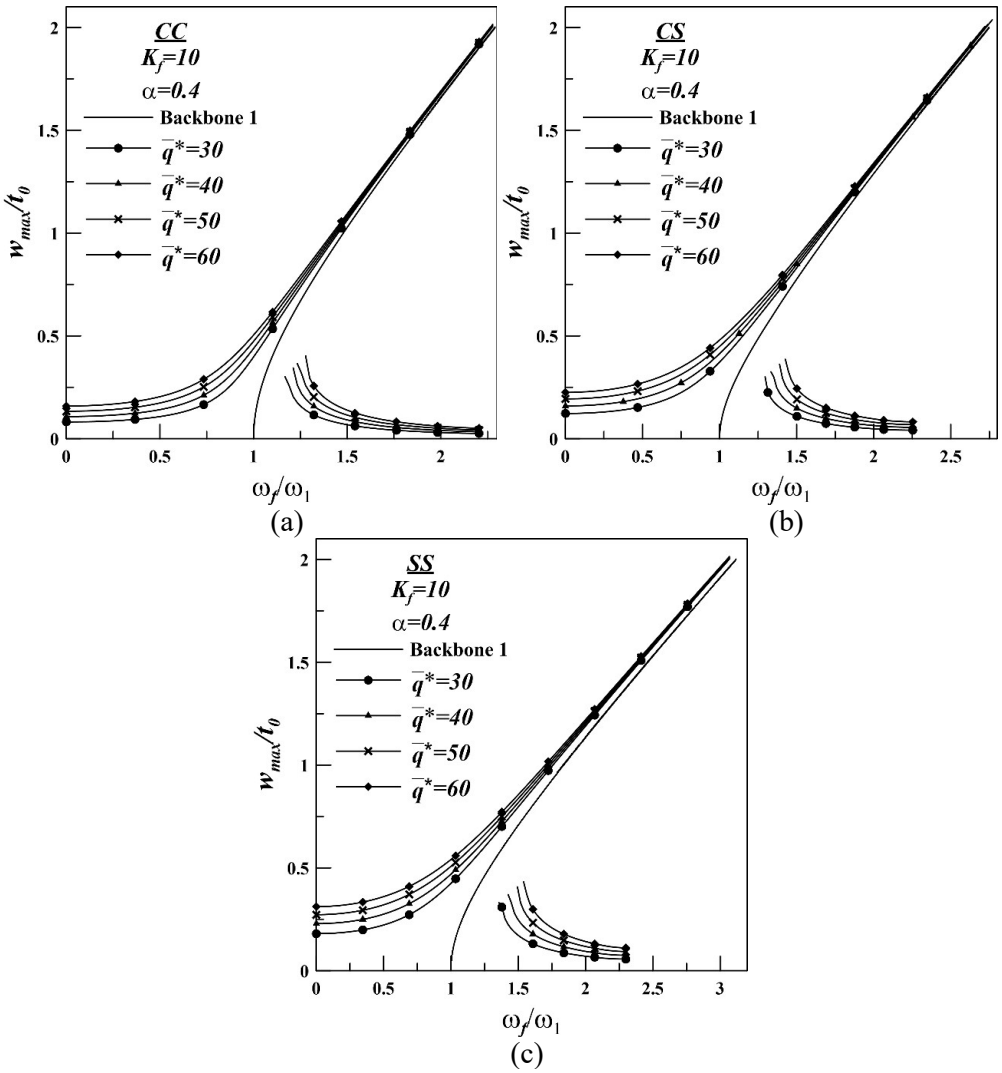

Figure 4.4: Effects of the excitation amplitude on frequency response for different boundary conditions: (a) CC (b) CS and (c) SS

The frequency response curves are categorized into two distinct zones. In the first zone, with the increase in excitation frequency, the response amplitude increases, while, in the other zone response amplitude reduces. Nonlinear behaviour of the system can be observed in the Multi response zone where two response amplitudes corresponding to the previously mentioned distinct zones are found. The branches of the response curve in these two zones are stable solutions. Theoretically, a third zone, where an unstable steady-state

solution is possible, exists but could not be captured through current methodology. The discontinuous appearance of the response curves is due to the fact that solutions in the unstable zone are not obtained.

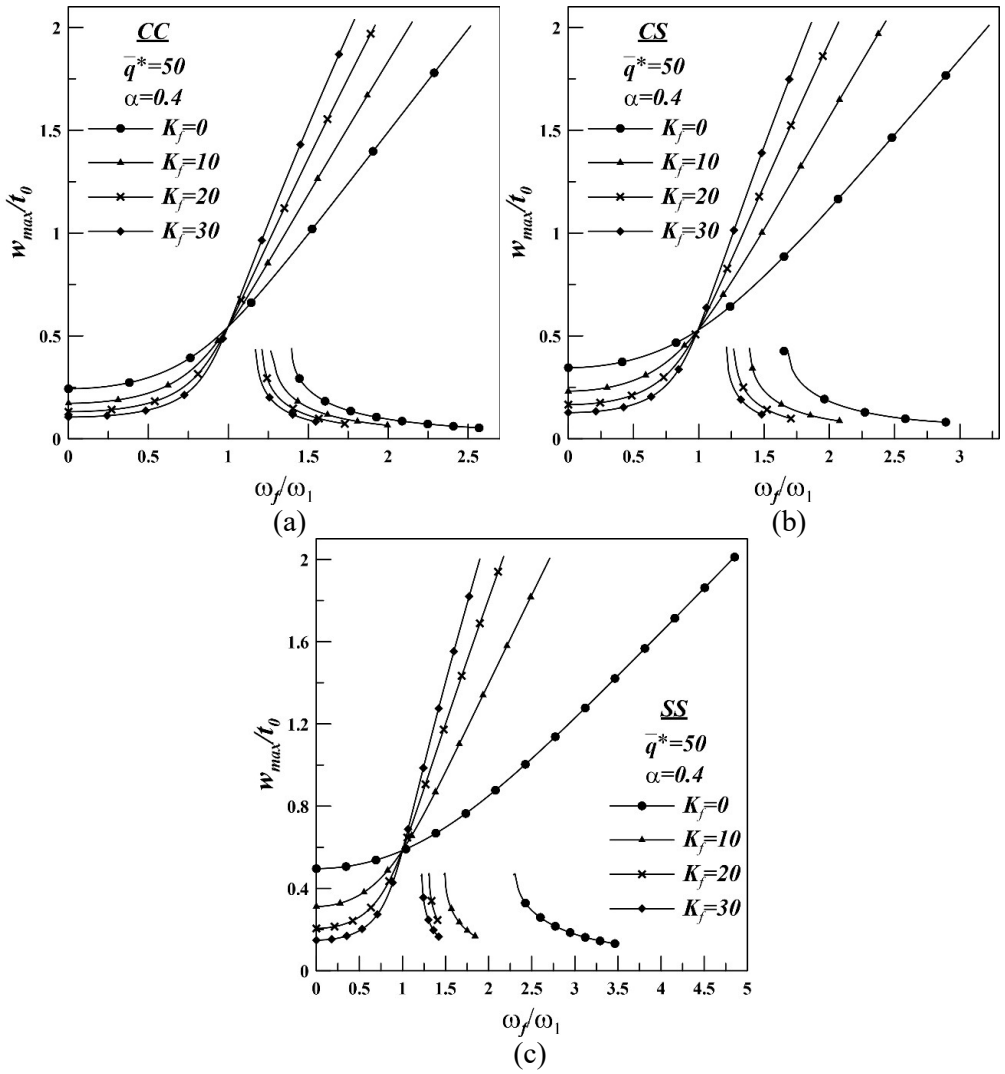

Figure 4.5: Frequency response of AFG linear taper beam (Material 1) for different boundary conditions: (a) CC (b) CS and (c) SS

4.5.3.1 Effect of exitation amplitude:

The effect of excitation amplitude on the frequency response of AFG beam is shown in Figure 4.4. Three plots for three different boundary conditions (CC, CS and SS) are presented corresponding to linear taper beam and material 2. Foundation stiffness and taper parameter have been fixed at 10 and 0.4, respectively, whereas the non-dimensional

excitation amplitude is varied from 30 to 60 in steps. The normalizing factor (fundamental frequency) for excitation frequency for the three boundary conditions are different and these values are furnished in Table 3.6, Table 3.9 and Table 3.12 for CC, CS and SS beam respectively in Chapter 3. Backbone curves corresponding to the system are also incorporated into the frequency response plots of Figure 4.4. These backbone curves are generated from the large amplitude free vibration analysis performed in the previous chapter. It is observed from Figure 4.4 that at a given excitation frequency, the response amplitude of beam with SS boundary conditions (Figure 4.4(c)) is the highest, whereas for beam with CC boundary conditions (Figure 4.4(a)) it is lowest.

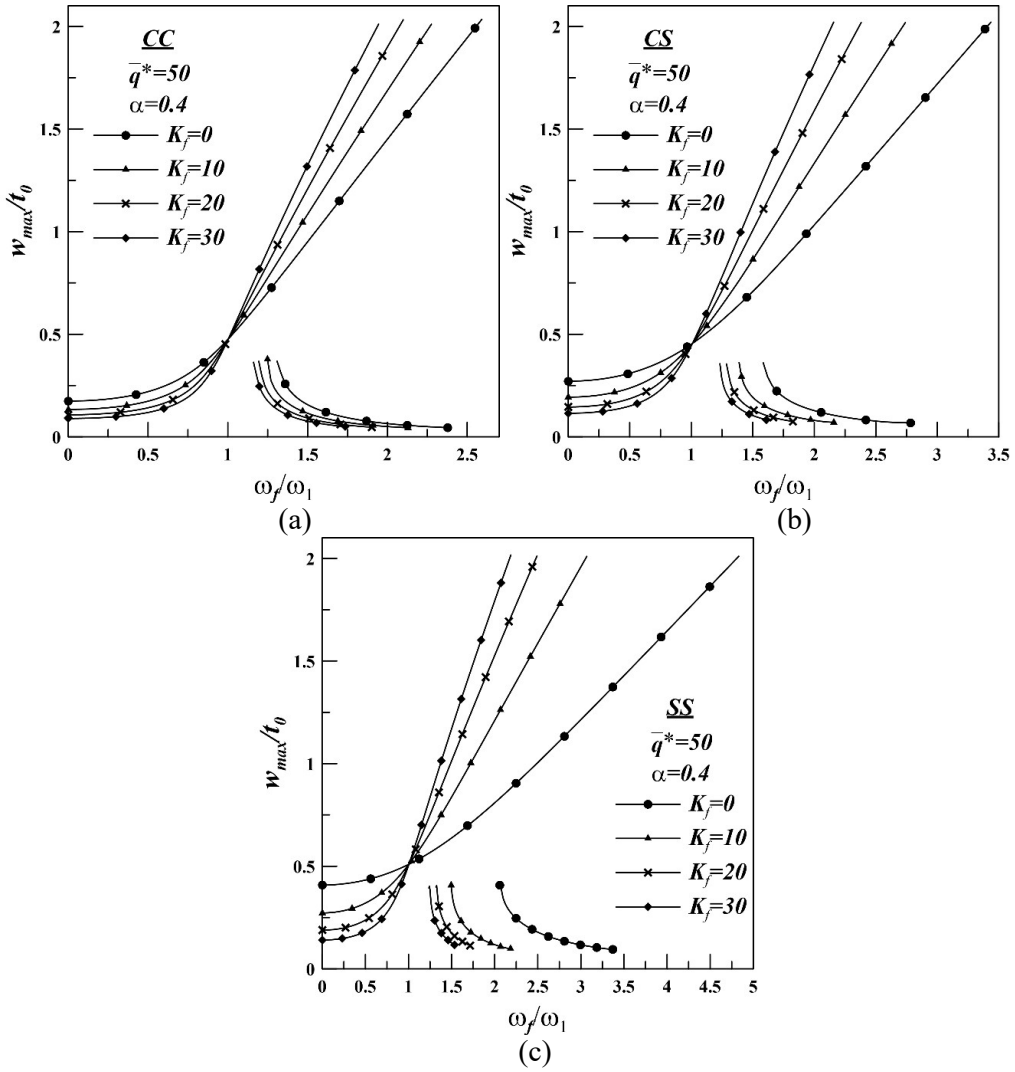

Figure 4.6: Frequency response of AFG linear taper beam (Material 2) for different boundary conditions: (a) CC (b) CS and (c) SS

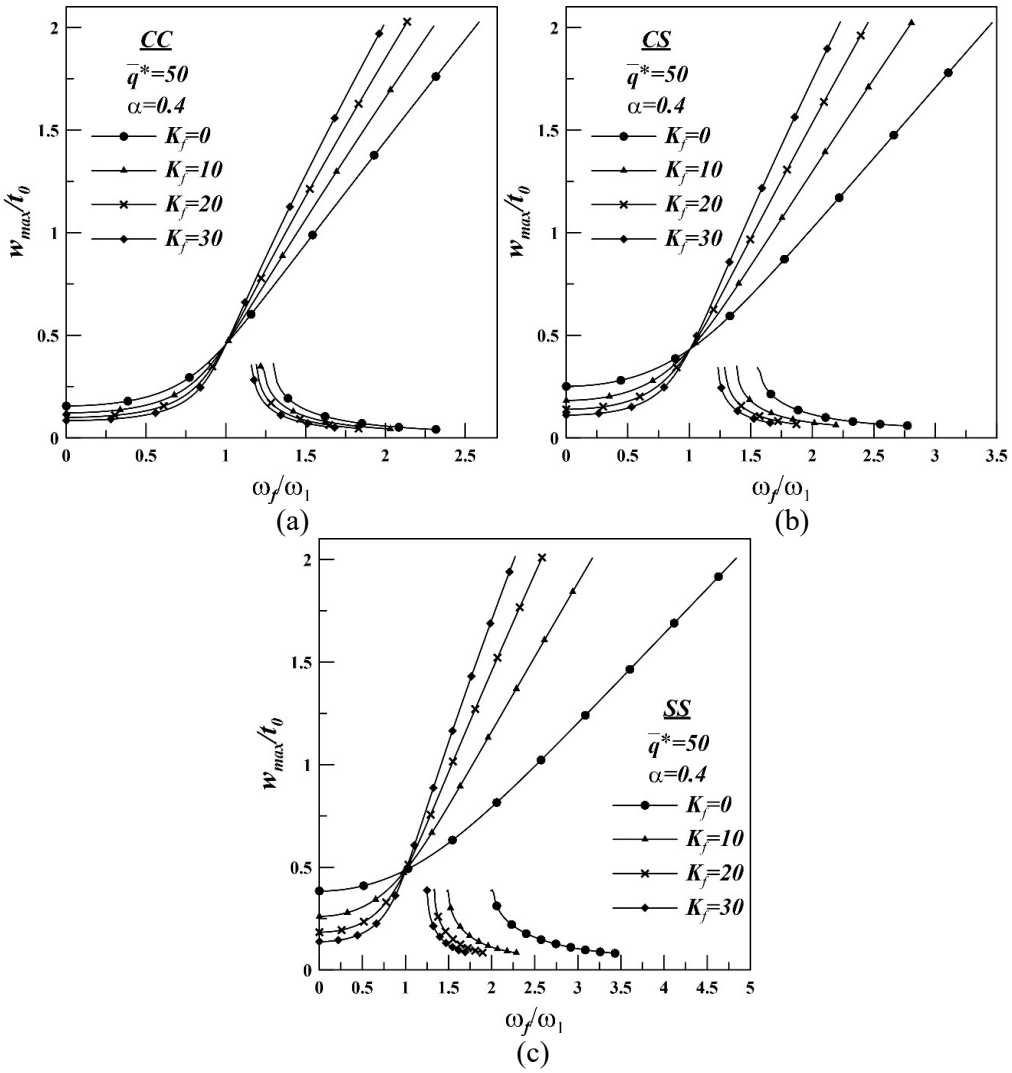

Figure 4.7: Frequency response of AFG linear taper beam (Material 3) for different boundary conditions: (a) CC (b) CS and (c) SS

It is evident from the figures that the general behaviour of the frequency response curves are similar. In all the cases two separate response branches are visible. In one branch, response amplitude monotonically increases with excitation frequency, while, in the other one it decreases with increase in forcing frequency. Interestingly, after a certain frequency value a multiple response zone is obtained, where, corresponding to one excitation frequency two responses are present. It is also observed that the plots are tilted towards the right of vertical in all three cases. This behaviour can be attributed to the stretching effect associated with large deflection resulting in additional stiffening of the system. It is also observed that the two segments of the frequency response envelop the backbone curve of

the system. As the excitation amplitude is continuously decreased the amplitude of the response also decreases and at very low excitation amplitude the response curve is likely to merge with the backbone curve. In fact, this behaviour corroborates the statement that the backbone curve is actually system response under zero amplitude excitation.

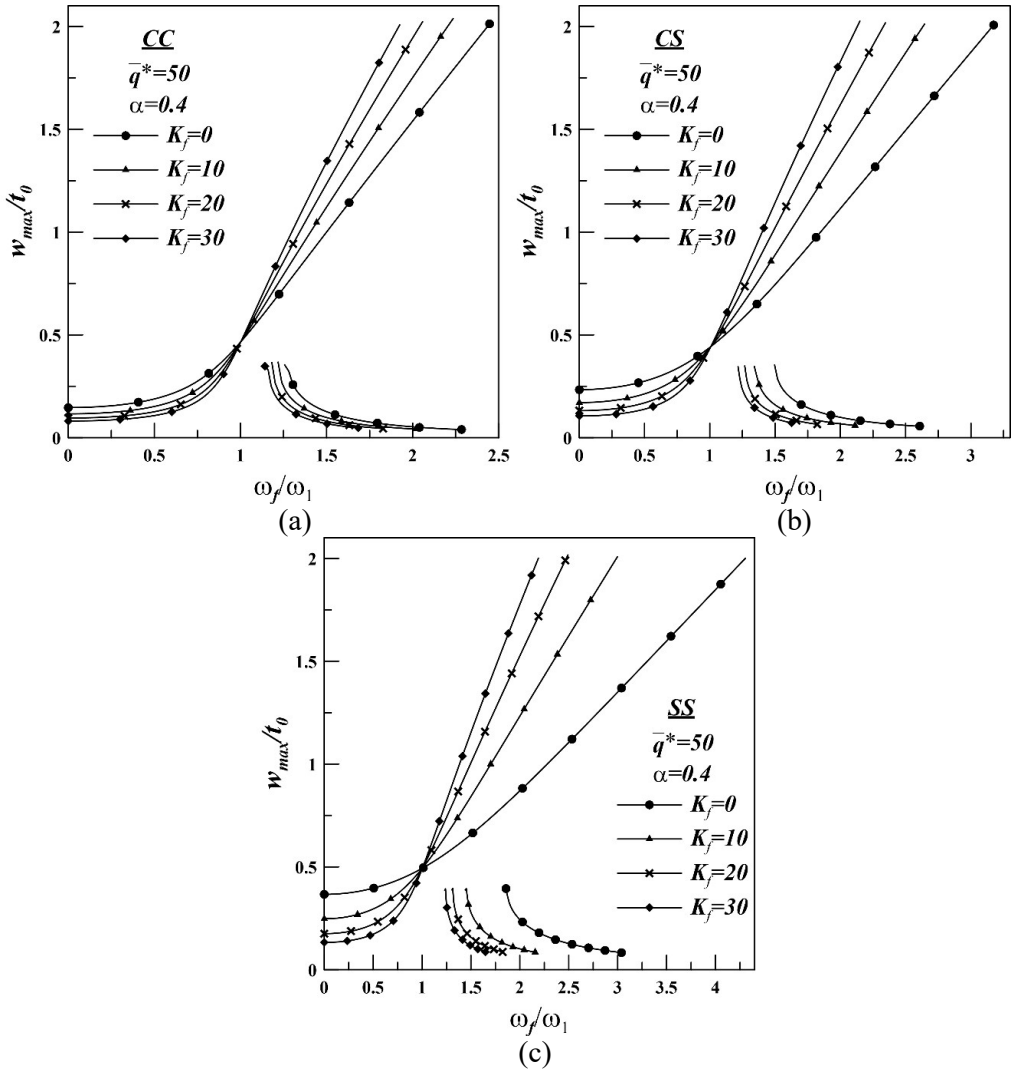

Figure 4.8: Frequency response of AFG parabolic taper beam (Material 2) for different boundary conditions: (a) CC (b) CS and (c) SS

4.5.3.2 Effect of foundation stiffness:

Figures 4.5-4.7 represent the frequency response in the vicinity of fundamental mode of vibration of linearly tapered beam on elastic foundation with three different material models (Material 1, Material 2 and Material 3). In each figure, there are three sets of plots

for three different boundary condition (CC, CS and SS) and in each plot four response curves are depicted corresponding to various spring stiffness values which varies from 0 to 30. The taper parameter is kept as constant, at 0.4 to plot the results with an objective to study the influences of the foundation stiffness. Similar plots for parabolic tapered beams are provided in Figures 4.8-4.9, whereas response curves for exponential AFG beams are shown in Figures 4.10-4.11. Results corresponding to Material 1, which corresponds to a homogeneous material, is included for linearly tapered beams only. For the other two taper patterns (parabolic and exponential), results are provided only for Materials 2 and 3.

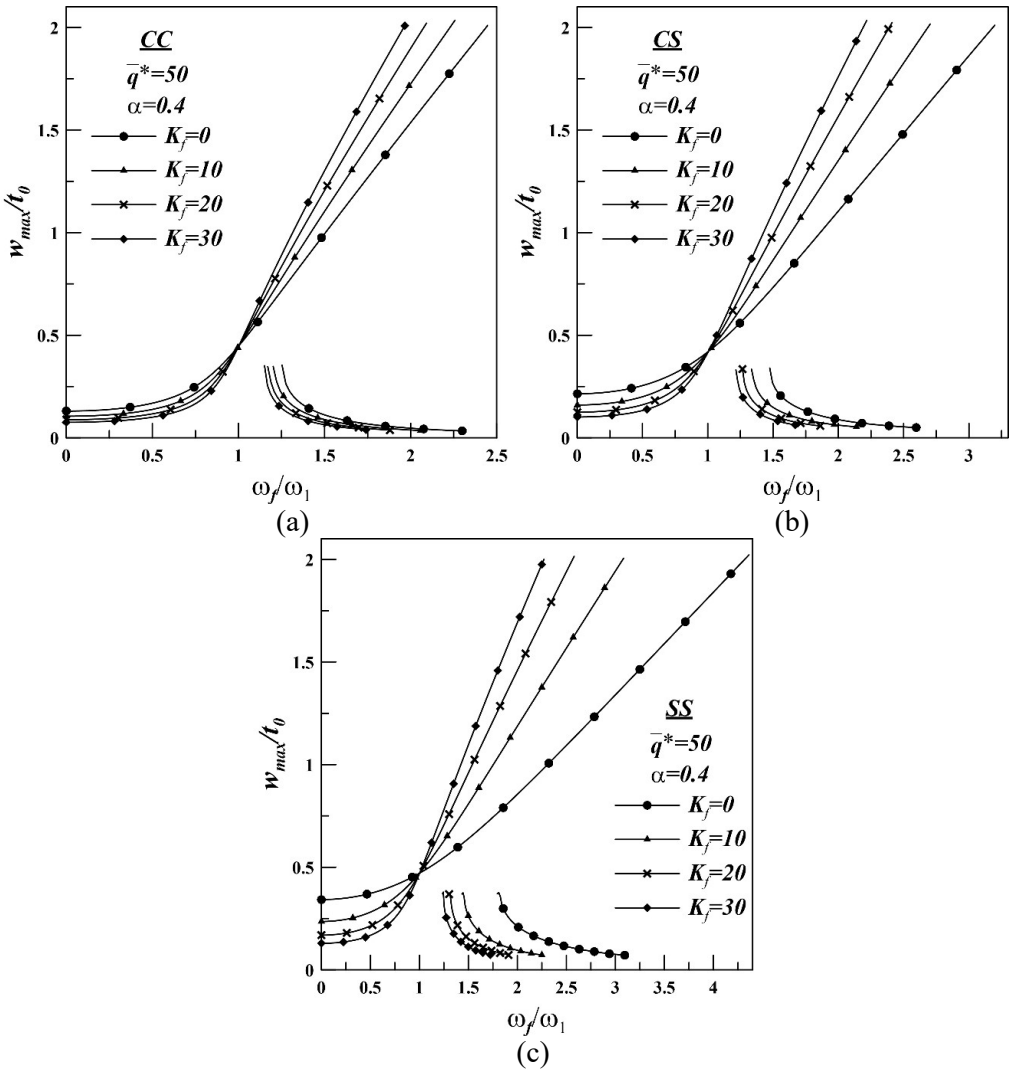

Figure 4.9: Frequency response of AFG parabolic taper beam (Material 3) for different boundary conditions: (a) CC (b) CS and (c) SS

In these sets of plots, with change in the foundation stiffness, four different backbone curves would have been obtained and putting them all together in the same figure would have made it cluttered. Hence, a conscious decision not to incorporate these system backbones is taken in order to maintain the clarity of the figures.

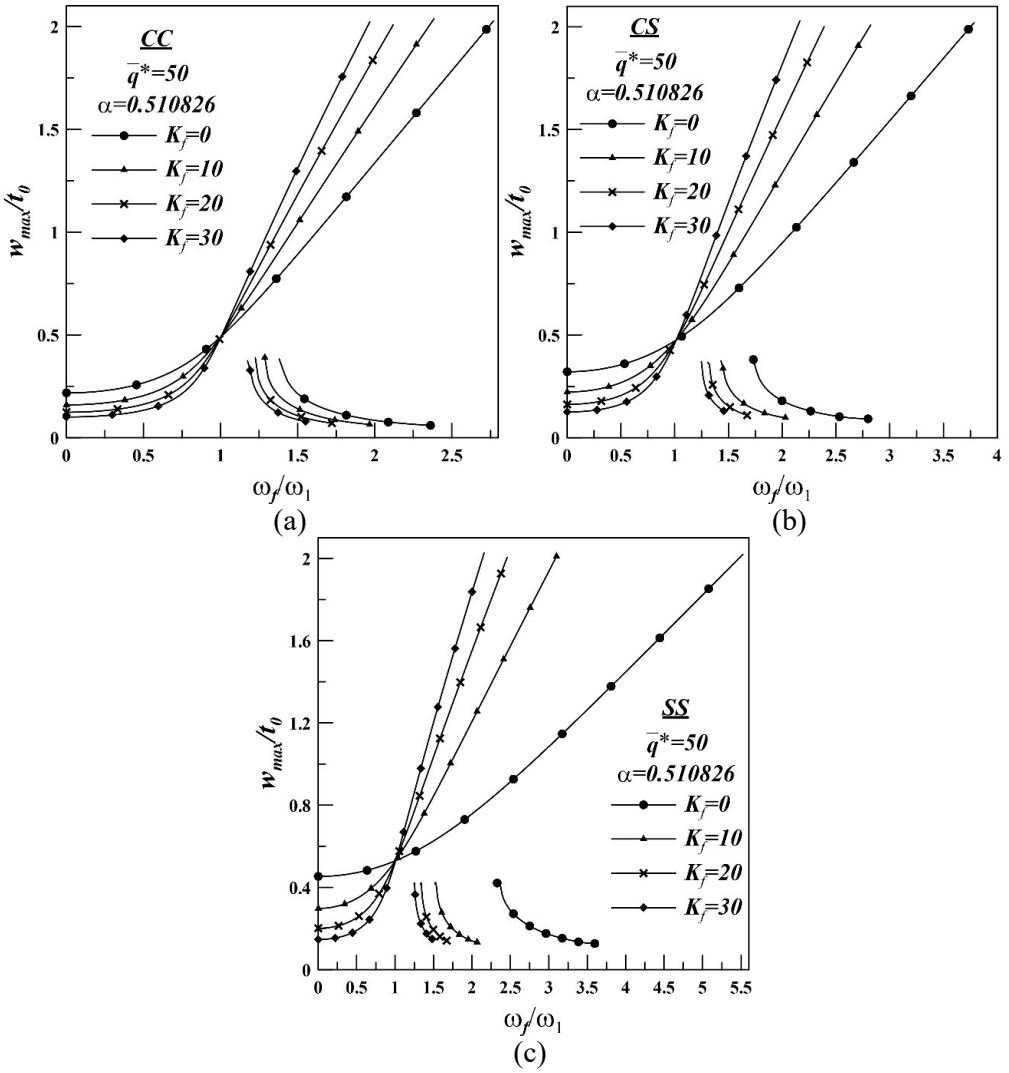

Figure 4.10: Frequency response of AFG exponential taper beam (Material 2) for different boundary conditions: (a) CC (b) CS and (c) SS

It is observed from Figures 4.5-4.11, in all the cases, with increase of foundation stiffness the response amplitude decreases in the low excitation frequency zone. But the trend is completely opposite in the higher frequency zone. There appears to be cross-over point in the response behaviour around ω_f/ω_1 = 1.00 in each case. Another important observation is that the response curves in forward sweep of SS beam are more diverging in

the non-dimensional plane from each other than the other two boundaries. From the above discussion it may be concluded that nonlinearity involved in case of SS beam is higher than the other two taper patterns. For CC and CS beam, the difference between the response curves are found to be small.

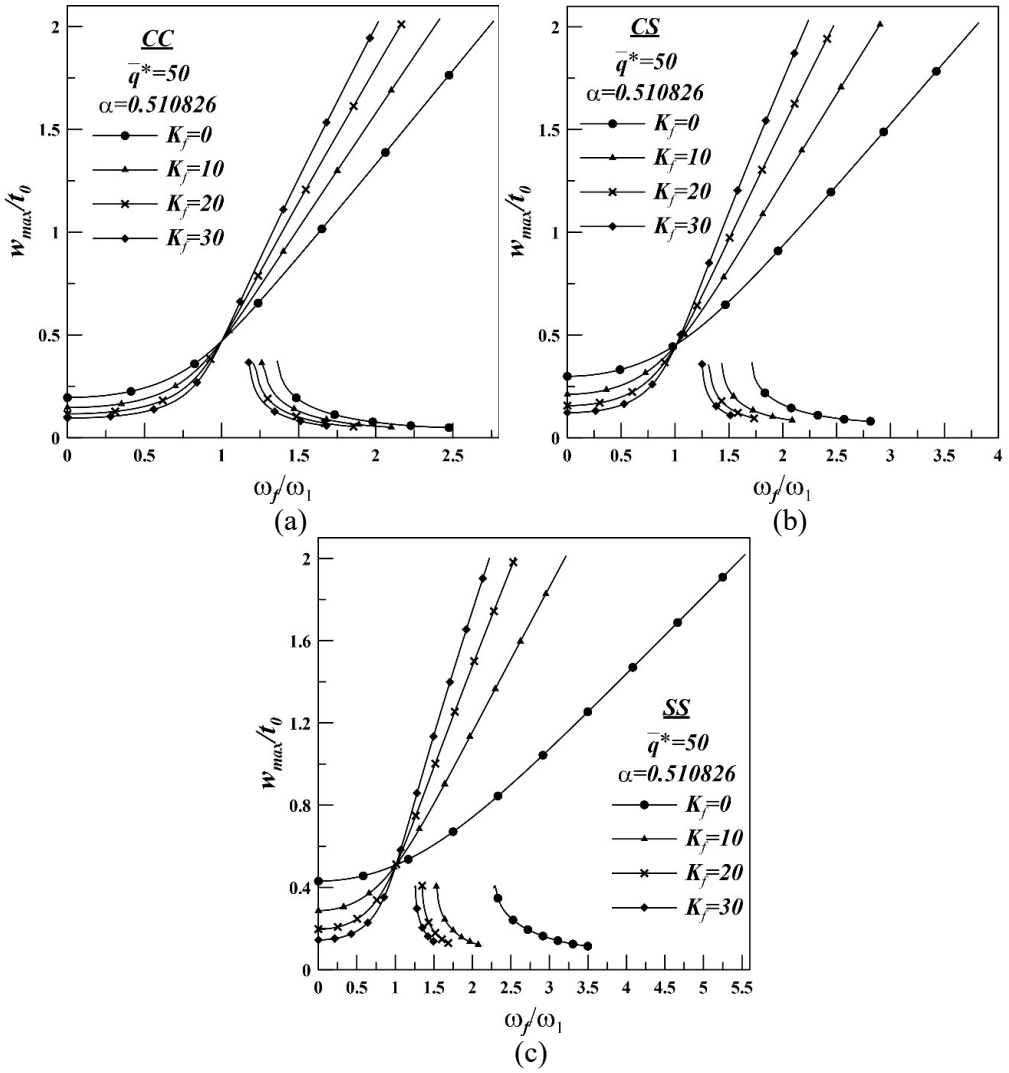

Figure 4.11: Frequency response of AFG exponential taper beam (Material 3) for different boundary conditions: (a) CC (b) CS and (c) SS

For linear taper pattern, it is quite clear that the change in response curves for different material model is hardly found for a particular case of boundary condition, as shown in Figures 4.5-4.7. For other type of taper pattern i.e. parabolic and exponential taper same trend can be found. It is also observed from the figures that for particular boundary

condition and material model, in exponential taper the response curves are more openly clustered than the other two (linear and parabolic) for different foundation stiffness values.

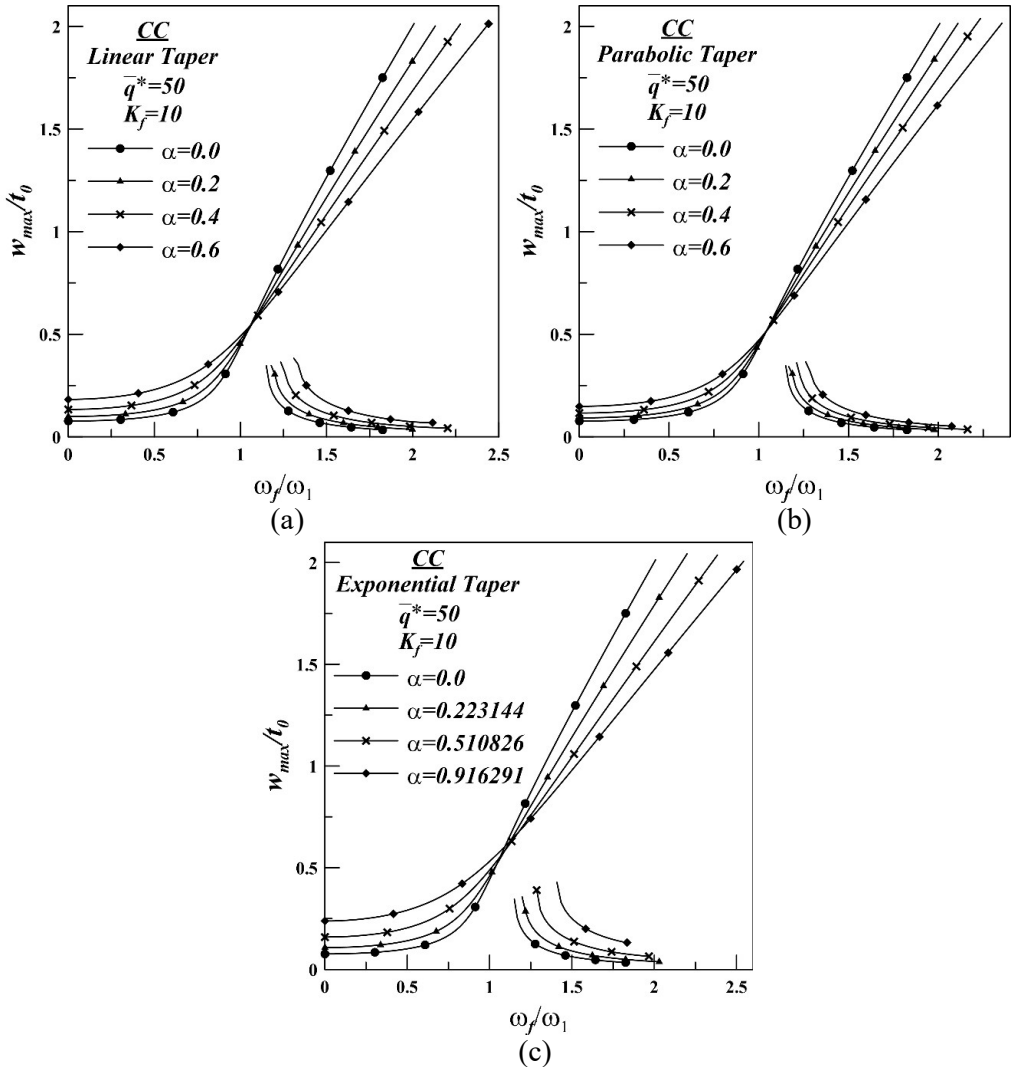

Figure 4.12: Effects of the taper parameter on frequency response for CC beam for (a) linear taper (b) parabolic taper and (c) exponential taper

4.5.3.3 Effect of tapering:

Figure 4.12 shows the effect of taper parameter on forced vibration response of AFG Timoshenko beam for different boundaries. Three different taper patterns are considered in which CC boundary condition is taken. For linear and parabolic taper pattern the taper parameter values are varied from 0 to 0.6, whereas, in the case of exponential taper pattern value are varied from 0 to 0.912691. It is to be noted that taper parameter 0.0 represents the case of uniform beam. The excitation amplitude and foundation stiffness

have been fixed at 50 and 10, respectively. From the Figure 4.12, it is observed that with the increase of taper parameter values, the amplitude of the response is increasing in nature in the low frequency domain, whereas, the trend is reversed at higher frequency range. This type of trend is found due to removal of material with increasing taper which further contributes to the reduction of beam stiffness. In these sets of figures, the backbone curves for the four individual cases are not incorporated for the sake of better clarity.

4.5.4 Operational deflected shape (ODS):

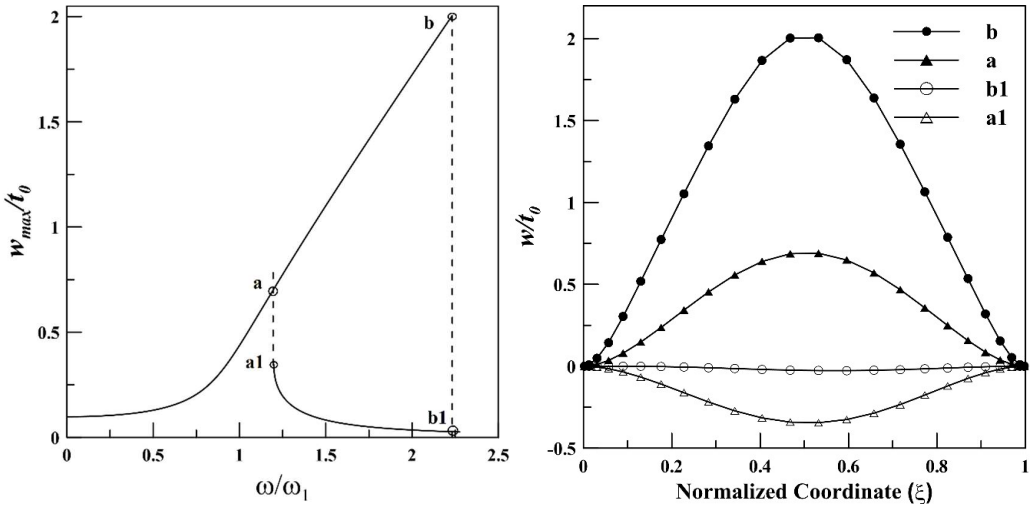

(a) (b)

Figure 4.13: Operational deflection shape (ODS) plots for non-uniform AFG beam with clamped boundary conditions under uniformly distributed excitation: (a) response curve showing representative points and (b) operational deflection shapes corresponding to the representative points.

The shape attained by the system while vibrating under the influence of external excitation is often referred to as operational deflection shape (ODS). For the present analysis, evolution of the ODS as one moves along the branches of the frequency response curves is studied carefully. In other words, the effects of excitation frequency on the ODS is investigated by analysing a clamped parabolic tapered AFG beam with taper parameter of 0.2 under the action uniformly distributed excitation with amplitude of 10 N/m. The beam is resting on a foundation with stiffness of 10^3 N/m and the Material model 2 is considered. Figure 4.13(a) shows the frequency-response curve along with some representative points. The ODS corresponding to these representative points are shown in Figure 4.13(b). The points on the response curve at which the ODS are shown correspond to different frequency-amplitude combinations. The start of the multi-response

zone is designated by point ‘a’ on the higher branch of the response. Point ‘a1’ is obtained by moving vertically down from point ‘a’ and it corresponds to the same excitation frequency level as ‘a’. Point ‘b’ represents the case when the system attains normalized response amplitude of 2.0. Point with the same frequency as point ‘b’ but on the lower branch is represented by point ‘b1’. The ODS of different representative points seems similar with different maximum response amplitude. However, one major difference that can be noted is that the response at the lower branch is out of phase with the response in the increasing branch.

4.6 Closure:

In the present chapter, large amplitude force vibration analysis is performed on a axially functionally graded tapered thin beam which is resting on elastic foundation with different end condition. A displacement based semi-analytical method along with energy principles is employed for the mathematical formulation and the governing differential equation of the system is developed through application of Hamilton’s principle. Due to consideration of nonlinear strain-displacement relations the set of governing equations also exhibits nonlinear features. To solve for the set of nonlinear equations Broyden’s method (quasi-Newton method) is applied and numerical solutions in terms of transverse and in-plane displacement fields are obtained. A convergence study is performed to determine the values for various parameters related to the numerical scheme. Established result from existing literature is used to provide validation for the present method and solution procedure. The geometric nonlinear forced vibration characteristic of the system is represented through frequency response curves in non-dimensional excitation frequency-maximum response amplitude diagrams. New results, capable of acting as benchmark results, are provided for a combination of four flexural boundary conditions, three material models and four foundation stiffness values. However, the general nature of the formulation and solution technique ensures that other type of taper pattern, material gradation as well as excitation pattern can be handled with minimum modifications.

Chapter 5

FREE AND FORCED VIBRATION ANALYSIS: AXIALLY FUNCTIONALLY GRADED TIMOSHENKO BEAM ON ELASTIC FOUNDATION

5.1 Introduction:

In case of beams with sufficient thickness, shear deformation and rotational bending effects across a section cannot be ignored without compromising the accuracy of the analysis. Hence, Timoshenko beam theory, which considers the shear deformation of a beam cross-section, is more suitable to describe the behaviour of thick beams. Governing equations in case of Timoshenko beam theory is of higher order and contains a second-order partial derivative, unlike Euler–Bernoulli beam theory. Physical significance of considering this theory is that the additional rotation of the cross-section with respect to the neutral axis lowers the stiffness of the beam. As a result there is larger deflection under static loading, while the predicted eigen-frequencies for a particular boundary condition is lower. For this reason, the Euler–Bernoulli model always overestimates the analysis outcomes i.e. deflections in static analysis, natural frequencies in free vibration analysis and the frequency response in forced vibration analysis. In the present chapter both free and forced vibration analysis has been carried out for an axially graded Timoshenko beam resting on elastic foundation.

The free and forced vibration analyses are carried out in two separate sections with different basic assumptions. The nonlinear free vibration problem is solved in two steps. The objective of the first part is to compute the stiffness matrix in deflected configuration through a static analysis. In the second step, this equivalent stiffness matrix is directly used in dynamic analysis for obtaining eigenvalues and eigenvectors which form the natural frequency and mode shape of the system, respectively. In this regard, it is important to note that separate static analysis in not performed and kept out of the present chapter to avoid

repetitiveness and maintain brevity, as it is an in-built part with the free vibration analysis. The assumption in the nonlinear forced vibration analysis is that all the forces acting on the system attains equilibrium at the peak amplitude. This unique assumption enables the dynamic problem to be solved as an equivalent static problem.

In the context of this chapter, it is important to note that the relations for material property variations and thickness variations, as well as the solution procedures used in free vibration problem of Timoshenko are similar to those presented in relation to analysis of Euler Bernoulli beams (Chapter 3). These are not repeated here to maintain conciseness. Similarly, the adopted solution techniques and procedures for forced vibration analysis are same as forced vibration problem of Euler Bernoulli beams which are presented in the previous chapter (Chapter 4). However, for forced vibration scenario a separate material model is considered along with linear taper pattern for thickness variation.

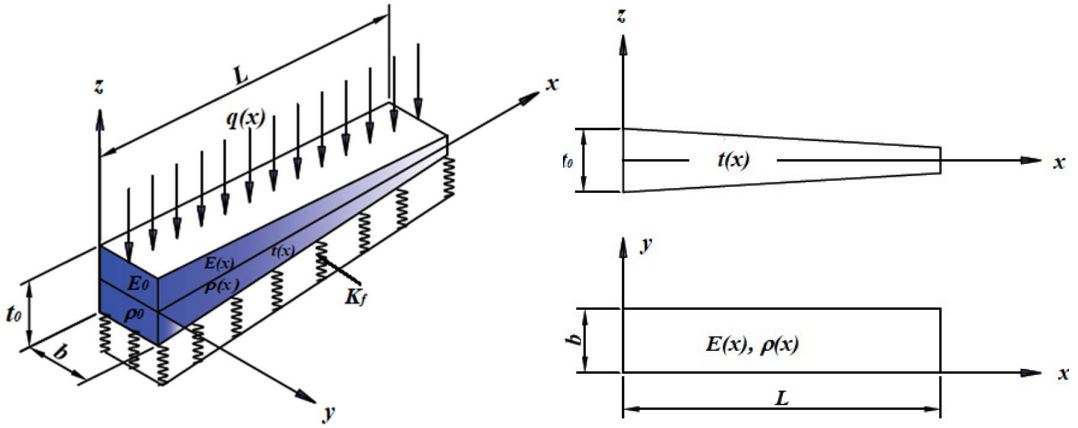

(a) (b)

Figure 5.1: (a) AFG beam on elastic foundation, (b) front and top view of the taper beam.

5.2 Geometric and material parameter:

A non-uniform AFG Timoshenko beam of length L, width b and variable thickness $t(x)$, subjected to uniformly distributed transverse loading is considered as shown in Figure 5.1. The variation of thickness of the beam, $t(x)$, is along the axial direction (Figure 5.1(b)). Similarly, the gradation of material properties i.e. modulus of elasticity, $E(x)$, and the mass density, $\rho(x)$, of the beam is considered along the longitudinal axis (x-axis) of the beam (Figure 5.1(b)). In the present formulation, the beam is considered to be supported on elastic foundation (Figure 5.1(a)). The foundation stiffness is quantified by the stiffness coefficient of the linear spring and it is denoted by k_f. The details about the thickness variation, material

property variation and characteristic of the elastic foundation are discussed in the Chapter 3 (Section 3.2 & 3.3).

5.3 Nonlinear free vibration analysis:

The effect of elastic foundation on free vibration of initially deflected non-uniform axially functionally graded (AFG) thick beam on elastic foundation on the basis of Timoshenko beam theory is studied. The elastic foundation is idealized as a set of parallel linear springs. Formulation is carried out through displacement based energy principle. First, the static problem is solved to find out the unknown displacement field by using minimum total potential energy principle. Solution methodology involves an iterative technique known as direct substitution with relaxation scheme. Secondly, subsequent dynamic problem is set up as an eigenvalue problem on the basis of the known displacement field. The governing set of equations in dynamic problem is obtained by using Hamilton's principle and solved with the help of Matlab's intrinsic solver. The results of the present method are validated with previously published articles. Frequency vs. displacement curve corresponding to different combinations of system parameters are presented in non-dimensional plane and are capable of serving as benchmark results.

5.3.1 Mathematical formulation:

Mathematical formulation of the problem is performed in such a way that it can be broken down into two distinct but interlinked problems - first, a static analysis and second, a free vibration analysis based on the static solution. The static analysis deals with the system under uniform transverse loading that imposes transverse deflection on the beam. This problem takes into account geometric nonlinearity and hence addresses the large deflection effect. Nonlinear strain-displacement relations are considered in order to incorporate geometric nonlinearity. Once the solution to the static problem is obtained pre-loaded static configuration of the beam under application of uniformly distributed load becomes known. Now, the system is assumed to execute a small amplitude vibration about the deflected configuration. Hence, the free vibration problem is formulated with the objective of finding out the loaded natural frequencies of the deformed system. The effect of the statically inflicted large deflection is incorporated into the dynamic system. Both the static and dynamic analyses are formulated based on variational form of appropriate energy

principles. Also, shear deformation and rotary inertia are incorporated by virtue of employing Timoshenko beam theory.

5.3.1.1 Static analysis:

The static analysis is based on the minimum total potential energy principle, which states that the total potential energy of the system is minimized by a kinematically admissible displacement field (out of all the kinematically admissible displacement fields) corresponding to the stable equilibrium. The principle is mathematically expressed as,

$$\delta\left(U+V\right)=0 \tag{5.1}$$

Here, δ designates variational operator, U is the total strain energy stored in the system (which includes the beam as well as the foundation) due to external loadings and V is the work done by the external loading. Total strain energy in the system is made up of strain energy stored in the beam and the foundation. Moreover, strain energy of the beam can again be split into two components, namely, strain energy due to axial strain (U_a) and strain energy due to shear strain (U_s). This implies that the total strain energy can be expressed as the summation of three distinct parts, as follows: $U = U_a + U_s + U_f$. Here, U_f is the strain energy stored in the system due to deformation of the elastic foundation.

The present formulation is a semi-analytical displacement based approximate method, which indicates that in the expression of strain energies, the strains (axial as well as shear) are to be replaced by appropriate displacement relations. In order to express the strain energies in terms of displacement fields, following strain-displacement expressions are invoked (Shames and Dym, 2009) for axial strain (ε_a) and shear strain (ε_s).

$$\varepsilon_a=\frac{1}{2}\left(\frac{dw}{dx}\right)^2+\frac{du}{dx}-z\frac{d\psi}{dx} \tag{5.2}$$

$$\varepsilon_s=\frac{1}{2}\left(\frac{dw}{dx}-\psi\right) \tag{5.3}$$

It is important to note that Equation (5.2) is nonlinear in nature and on neglecting the third term of the expression it resembles von Karman type nonlinear strain-displacement relation. The displacement fields associated with the above expressions are

as follow: transverse displacement field (w), in-plane displacement field (u) and rotational field (ψ) of beam section due to bending. All these displacement fields are dependent on the axial coordinate and they are defined at the mid-plane of the beam. Substituting the strain-displacement expressions, the strain energies, U_a, U_s and U_f, can be expressed as follows,

$$U_a = \frac{b}{2}\int_0^L \int_{-\frac{t}{2}}^{\frac{t}{2}} \left\{ \begin{array}{l} \frac{1}{4}\left(\frac{dw}{dx}\right)^4 + \left(\frac{du}{dx}\right)^2 + z^2\left(\frac{d\psi}{dx}\right)^2 \\ + \left(\frac{dw}{dx}\right)^2 \frac{du}{dx} - z\left(\frac{dw}{dx}\right)^2 \frac{d\psi}{dx} - 2z\frac{du}{dx}\frac{d\psi}{dx} \end{array} \right\} E(x)\,dxdz \tag{5.4}$$

$$U_s = \frac{bk_{sh}}{2}\int_0^L \int_{-\frac{t}{2}}^{\frac{t}{2}} \left\{ \left(\frac{dw}{dx}\right)^2 - 2\frac{dw}{dx}\psi + \psi^2 \right\} G(x)\,dxdz \tag{5.5}$$

$$U_f = \frac{1}{2}\int_0^L K_f w^2 dx \tag{5.6}$$

k_{sh} is termed as shear correction factor. It is well known that for rectangular cross-section the numerical value of k_{sh} is taken as 5/6. Here, $G(x)$ is shear modulus which is expressed by, $G(x) = E(x)/2(1+\mu)$. In order to implement the minimum total potential energy principle, expression for potential for external work need to be obtained and it is provided corresponding to uniformly distributed load $q(x)$ in Equation (5.7). It is noteworthy that in the present study, only uniformly distributed load has been taken into account. However, this is not a limitation on the present methodology. Any other form of transverse loading (such as concentrated load, triangular load, hat load etc.) can be accommodated in the analysis, as long as it can be expressed mathematically in terms of analytical or numerical functions.

$$V = \int_0^L qw dw \tag{5.7}$$

As the present method is an approximate one, the displacement fields need to be approximated through finite linear combinations of kinematically admissible functions and unknown coefficients, as shown

$$w = \sum_{i=1}^{nw} d_i \phi_i(x) \tag{5.8a}$$

$$u = \sum_{i=1}^{nu} d_{nw+i} \alpha_i(x) \tag{5.8b}$$

$$\psi = \sum_{i=1}^{nsi} d_{nw+nu+i} \beta_i(x) \tag{5.8c}$$

In the above expressions, φ_i, α_i and β_i represent the set of orthogonal admissible functions corresponding to the displacement fields w, u and ψ, respectively, whereas, d_i denotes the set of unknown coefficients. The number of functions in these sets are taken as *nw*, *nu* and *nsi* (corresponding to w, u and ψ) and from the point of view of the numerical scheme for solution, $nw = nu = nsi$. The choice of the admissible functions are solely based on the boundary conditions of the beam. In fact, the first function within the set (φ_1, α_1 and β_1) is known as the start function and it is selected carefully satisfying the requisite boundary conditions, i.e., flexural, in-plane and end rotation conditions. It should also be pointed out that these functions need to be continuous and differentiable within the domain. Consequently, the higher order functions (upto *nw*/*nu*/*nsi*) are generated following a numerical implementation of Gram–Schmidt orthogonalization scheme. Once the approximate displacement fields are substituted into the appropriate energy functionals, the problem reduces to finding out the unknown coefficients (d_i).

Substituting the expression of the energy functionals, given by Equations (5.4), (5.5), (5.6) and (5.7) into Equation (5.1) and considering the assumed displacement fields, given by Equation (5.8), the governing set of equations are obtained in matrix form, as follows,

$$[K]\{d\} = \{f\} \tag{5.9}$$

where, $[K]$ are the stiffness matrix and $\{f\}$ are the load vector. The dimensions of these each matrix will be ($nu + nw + nsi$). The form and elements of $[K]$ and $\{f\}$ are furnished in detail in the Appendix.

5.3.1.2 Dynamic analysis:

Starting point for the dynamic analysis is Hamilton's principle, which is utilized to derive the governing sets equations,

$$\delta\left(\int_{\tau_1}^{\tau_2}\left(T-U-V\right)d\tau\right)=0 \tag{5.10}$$

Here, T is the kinetic energy of the beam due to external excitation, U refers to the system strain energy with respect to deflected configuration and τ is the time. The expression of U remains unchanged from that described by Equations (5.4) – (5.6) in static analysis. Kinetic energy of the present system is expressed through the expression shown in Equation (5.11). It needs to be mentioned here that the present free vibration study is performed on a pre-stressed beam, whose static solution has already been obtained in the previous step. So, the potential energy of the external load (V) can be set to zero.

$$T=\frac{b}{2}\int_0^L\int_{-\frac{t}{2}}^{\frac{t}{2}}\left\{\left(\frac{dw}{dt}\right)^2+\left(\frac{du}{dt}\right)^2+z^2\left(\frac{d\psi}{dt}\right)^2\right\}\rho(x)\,dxdz \tag{5.11}$$

Here, $\rho(x)$ is the mass density of the beam. The displacement fields associated with the above expression are dynamic in nature with a time varying component. So, these fields contain a spatial and a temporal part and it is assumed that these two parts are completely separable. The assumed dynamic displacement fields are expressed as follows,

$$w(x,\tau)=\sum_{i=1}^{nw}c_i\phi_i(x)e^{j\omega\tau} \tag{5.12a}$$

$$u(x,\tau)=\sum_{i=1}^{nu}c_{nw+i}\alpha_i(x)e^{j\omega\tau} \tag{5.12a}$$

$$\psi(x,\tau)=\sum_{i=1}^{nsi}c_{nw+nu+i}\beta_i(x)e^{j\omega\tau} \tag{5.12c}$$

Here, the spatial part apparently seems same as that considered in the static analysis and c_is are a set of unknown coefficients different from the unknown parameters defined in the static analysis. However, φ_i, α_i and β_i are same as the static problem. ω denotes the natural

frequency of the vibratory system and $j=\sqrt{-1}$. Substituting the expressions of strain energy (Equations (5.4), (5.5) and (5.6)) and kinetic energy (Equation (5.11)), as well as the assumed dynamic displacements (Equation (5.12)) into Equation (5.10), the governing equation is obtained as follows:

$$[K]\{c\}-\omega^2[M]\{c\}=0 \tag{5.13}$$

Here, [*K*] is the stiffness matrix of the system at deflected configuration and [*M*] is mass matrix, respectively. The elements of [*M*] are provided in Appendix.

5.3.2 Solution procedure:

A glance at the elements of the stiffness matrix reveals that the unknown coefficients (d_i) appear in certain terms. It means that stiffness matrix is a function of the undetermined parameters by virtue of considering nonlinear strain-displacement relations and consequently large deformation. Hence, the set of governing equations represented by Equation (5.9) is nonlinear in nature. A direct solution involving inversion of the stiffness matrix, followed by pre-multiplication with the load vector is not an option. Approximate solution for the unknown coefficients (d_i) from the set of nonlinear equations is obtained following direct substitution method with successive relaxation. This is a numerical iterative technique dependent on an initial guess. All the stiffness matrix elements can be completely evaluated on the basis of the converged static solution, while the elements of the mass matrix are derived from the problem definition. It is to be noted that the system governing equations given by Equation (5.13) represent a standard eigenvalue problem, solution to which is obtained by using Matlab's intrinsic solver. Natural frequencies of the pre-stressed system are provided by the square root of the eigenvalues. Mode shapes of the vibrating system are obtained from the eigenvectors. The techniques and solution procedures used are similar to those presented in relation to analysis of beams described in Chapter 3 (Section 3.5).

5.3.3 Result and discussion:

In the present study, free vibration analysis of transversely loaded non-uniform AFG Timoshenko beam resting on elastic foundation is performed. The static analysis inflicting large deformation under transverse uniform loading is geometrically nonlinear in

nature, while an eigenvalue analysis is undertaken to determine the loaded natural frequencies of the system. The geometric dimensions of the beam for length (L) and width (b) are taken as 0.2 m and 0.02 m respectively, whereas, length-to-thickness ratio (L/t_0) is taken as 20. Three different types of taper pattern are considered, which are linear, parabolic and exponential taper, respectively, and the expressions are tabulated in Table 3.1 in Chapter 3. Four taper parameter (α) are considered as indicated in Table 3.2 in Chapter 3. Three different material models are selected for the AFG beam, where gradation of material properties (i.e. elastic modulus and density) are considered in the axial direction. The details of the property variations in terms of expressions are provided in Table 3.3 (Chapter 3). Elastic modulus and mass density of the root side of the beam and taken as 210 GPa and 7850 kg/m^3, respectively, which resemble the property of structural steel. It is important to note that Poisson ratio (μ) is taken as constant throughout the entire analysis which is 0.3.

Table 5.1: List of start functions for the displacement fields.

Displacement field	Boundary	Conditions	Function
w	CC	$w(0)= 0$, $w(L)= 0$	$\phi_1=(x/L)\{1-(x/L)\}$
	CS		
	SS		
u	CC	$u(0) = 0$, $u(L)= 0$	$\alpha_1= (x/L)\{1-(x/L)\}$
	CS		
	SS		
ψ	CC	$\psi(0)= 0$, $\psi(L)= 0$	$\beta_1=sin(\pi x/L)$
	CS	$\psi(0)= 0$, $\psi(L) \neq 0$	$\beta_1=sin(\pi x/2L)$
	SS	$\psi(0)\neq 0$, $\psi(L) \neq 0$	$\beta_1=cos(\pi x/L)$

Three different flexural boundary conditions, namely, CC, CS and SS, of the beam are selected, while for in-plane boundary conditions it is assumed that all the ends are immovable. At the clamped (C) end the rotational field has a zero value, whereas it has a non-zero value at the simply supported (S) end. The selected start functions for each of the displacement fields are given in Table 5.1 for all the three boundary conditions under consideration. Higher order functions to complete the orthogonal set are generated by implementing a numerical scheme for Gram–Schmidt orthogonalization principle, where the start function and the number of functions to be generated serve as inputs. The appropriate number of functions to be used is decided after a careful convergence study and these results are discussed in the next paragraph. In practical applications beams are seldom supported by classical boundary conditions. Either they are supported by elastic restrain at

the ends or rested on elastic foundation. To make the problem more realistic, the beam under consideration is taken to be resting on elastic foundation. Four different value of the non-dimensional foundation stiffness, $K_f = k_f[(L/t_0)^3/E_0b]$ is consider here. These values are 0, 10, 20 and 30 respectively. Here, k_f is the dimensional value of stiffness.

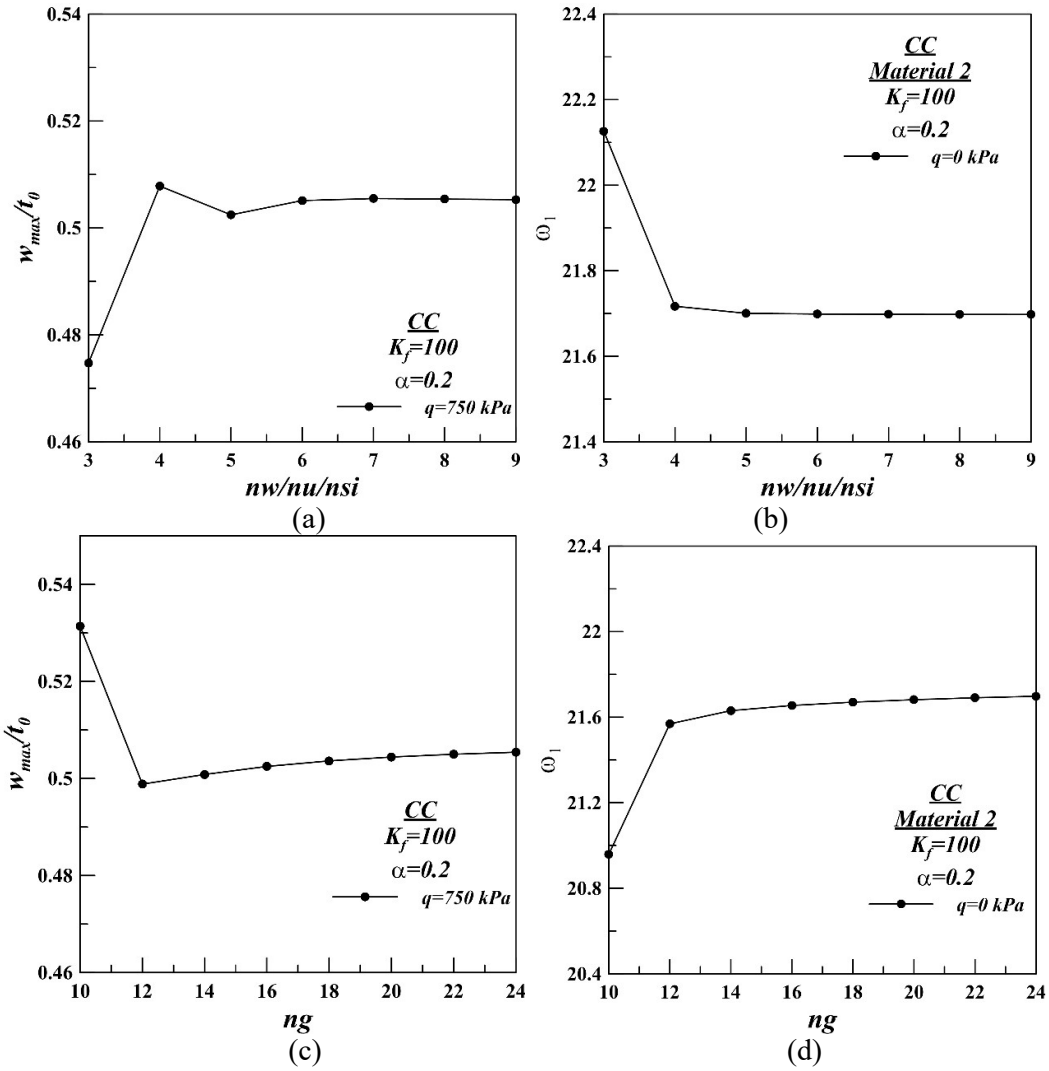

Figure 5.2: (a)-(b) Convergence studies for no. of orthogonal functions (*nw = nu = nsi*) corresponding to static and free vibration analysis and (c)-(d) Convergence studies for gauss points (*ng*) corresponding to static and free vibration analysis.

5.3.3.1 Convergence study:

In order to create the reference points for numerical evaluation within the computational domain, number of gauss points are generated along the length of the beam.

Choice of number of gauss points (*ng*) is an important issue, as it influences the outcome of the numerical scheme. Hence, detailed convergence study is necessary for selection of proper number of gauss points. This convergence study, along with the one carried out for determining the number of functions, is carried out on a linear tapered (α = 0.2) AFG (Material 2) beam with clamped ends and supported on an elastic foundation having K_f = 100. There are two aspects to these studies, first, comparison of normalised maximum static deflection and second, comparison of dimensional fundamental frequency with respect to the relevant parameters. For the static scenario, intensity of the distributed load is taken as 750 kPa, while, for the dynamic case, no load condition is assumed. The results of the study are presented in Figure 5.2 and from these figures, number of gauss points (*ng*) and number of orthogonal functions (*nw* = *nu* = *nsi*) are selected as 24 and 8, respectively.

Table 5.2: Comparisons of first four dimensionless $\left(\Omega = \omega L^2\sqrt{\rho_0 A_0/E_0 I_0}\right)$ natural frequencies of graded and non-uniform Timoshenko CC beam for different *n* value.

Literatures	**Ω**	***n*=1**	***n*=2**	***n*=3**	***n*=4**
Shahba et al. (2011)		-	12.4689	-	-
Huang et al. (2013)		12.6816	12.4633	12.3753	12.3622
Present study	1	12.6487	12.4292	12.3405	12.3267
Shahba et al. (2011)		-	26.4153	-	-
Huang et al. (2013)		26.4910	26.3804	26.3188	26.3116
Present study	2	26.4306	26.3181	26.2551	26.2465
Shahba et al.(2011)		-	43.0904	-	-
Huang et al. (2013)		42.642	42.9611	43.0839	43.135
Present study	3	42.5356	42.8552	42.9763	43.0256
Shahba et al. (2011)		-	59.6829	-	-
Huang et al. (2013)		58.6685	59.4023	59.6994	59.8150
Present study	4	58.5090	59.2332	59.5247	59.6382

5.3.3.2 Validation study:

The present methodology and analysis is validated with the results of previously published articles of Shahba et al. (2011) and Huang et al. (2013) for fully axial graded (ZrO_2 - Al) and non-uniform Timoshenko beam without elastic foundation. The comparison of linear dimensionless natural frequencies $\left(\Omega = \omega L^2\sqrt{\rho_0 A_0/E_0 I_0}\right)$ for first four mode are tabulated in Table 5.2 for CC end conditions. For this purpose, the length (*L*) and moment

of inertia to cross-section ratio (I_0/A_0) at root side of the beam are used as 1.0 m and 0.01, respectively. The material gradation along the axial direction follows the expressions, $E(\xi)= E_0+(E_1-E_0)(\xi^n)$ and $\rho(\xi)= \rho_0+(\rho_1-\rho_0)(\xi^n)$. The material properties used for comparison are as follows, E_0 = 200 GPa, ρ_0= 5700 kg/m^3, E_1 = 70 GPa and ρ_1 = 2702 kg/m^3. The non-uniform pattern of the beam is considered according to the expression, $t(\xi)= t_0(1-\alpha\xi)$ with taper parameter, α = 0.1. From the above comparison, it can be observed that the current results match satisfactorily with the established results.

5.3.3.3 Natural frequencies:

Table 5.3: Values of dimensionless natural frequencies $\left(\Omega = \omega L^2\sqrt{\rho_0 A_0/E_0 I_0}\right)$ for 1st and 2nd mode (Ω_1 and Ω_2) corresponding to linearly tapered CC AFG beam for different combinations of taper parameter, spring stiffness and material properties

Taper Pattern	Taper Parameter	Stiffness	Material 1		Material 2		Material 3	
			CC		CC		CC	
			Ω_1	Ω_2	Ω_1	Ω_2	Ω_1	Ω_2
Linear	0	0	21.92	59.16	20.06	54.23	22.06	59.33
		10	22.46	59.36	20.40	54.35	22.39	59.46
		20	22.99	59.56	20.73	54.48	22.71	59.58
		30	23.50	59.76	21.06	54.61	23.03	59.70
	0.2	0	19.74	53.47	17.91	48.77	19.70	53.41
		10	20.40	53.71	18.32	48.92	20.10	53.56
		20	21.05	53.96	18.73	49.08	20.50	53.71
		30	21.67	54.21	19.12	49.24	20.89	53.86
	0.4	0	17.39	47.26	15.61	42.82	17.17	46.96
		10	18.25	47.59	16.14	43.03	17.69	47.16
		20	19.07	47.91	16.65	43.23	18.19	47.35
		30	19.85	48.22	17.15	43.43	18.68	47.54
	0.6	0	14.80	40.31	13.08	36.21	14.40	39.77
		10	15.98	40.77	13.81	36.48	15.11	40.04
		20	17.08	41.22	14.50	36.75	15.78	40.30
		30	18.12	41.67	15.15	37.02	16.43	40.56

Dimensionless natural frequencies $\left(\Omega = \omega L^2\sqrt{\rho_0 A_0/E_0 I_0}\right)$ for the first two modes (Ω_1 and Ω_2) for three different boundary conditions (CC, CS and SS) of AFG Timoshenko beams are provided in Tables 5.3-5.11 for different combination of material models, taper patterns, taper parameters and foundation stiffness values. For each boundary condition, three tables are furnished to accommodate linear, parabolic and exponential taper pattern accordingly. The taper parameter (α) is varied from 0.0 to 0.6 for each linear and

parabolic taper pattern whereas for the case of exponential taper pattern the variation is considered from 0 to 0.916291. The values of α have been so selected that the thickness at the other end remains same for all the taper patterns to provide a better understanding on the effects of taper pattern on the results. Under each taper pattern four different foundation stiffness values are considered, as it is varied from 0 to 30 in the fixed interval of 10.

Table 5.4: Values of dimensionless natural frequencies $\left(\Omega = \omega L^2\sqrt{\rho_0 A_0 / E_0 I_0}\right)$ for 1st and 2nd mode (Ω_1 and Ω_2) corresponding to parabolic tapered CC AFG beam for different combinations of taper parameter, spring stiffness and material properties

Taper Pattern	Taper Parameter	Stiffness	Material 1		Material 2		Material 3	
			CC		CC		CC	
			Ω_1	Ω_2	Ω_1	Ω_2	Ω_1	Ω_2
Parabolic	0.2	0	20.08	54.83	18.22	50.02	20.03	54.77
		10	20.70	55.06	18.60	50.16	20.41	54.91
		20	21.30	55.29	18.99	50.31	20.78	55.03
		30	21.89	55.52	19.36	50.45	21.15	55.19
	0.4	0	18.07	50.03	16.24	45.35	17.86	49.72
		10	18.81	50.30	16.69	45.52	18.30	49.89
		20	19.53	50.58	17.14	45.69	18.74	50.05
		30	20.22	50.85	17.58	45.86	19.17	50.22
	0.6	0	15.83	44.51	14.04	40.02	15.45	43.94
		10	16.75	44.86	14.61	40.23	16.00	44.14
		20	17.63	45.21	15.15	40.44	16.54	44.35
		30	18.47	45.56	15.68	40.65	17.05	44.55

Table 5.5: Values of dimensionless natural frequencies $\left(\Omega = \omega L^2\sqrt{\rho_0 A_0 / E_0 I_0}\right)$ for 1st and 2nd mode (Ω_1 and Ω_2) corresponding to exponential tapered CC AFG beam for different combinations of taper parameter, spring stiffness and material properties

Taper Pattern	Taper Parameter	Stiffness	Material 1		Material 2		Material 3	
			CC		CC		CC	
			Ω_1	Ω_2	Ω_1	Ω_2	Ω_1	Ω_2
Exponential	0.223144	0	19.23	51.84	17.47	47.32	19.21	51.81
		10	19.95	52.10	17.91	47.49	19.65	51.98
		20	20.64	52.37	18.35	47.66	20.08	52.14
		30	21.31	52.64	18.78	47.83	20.49	52.30
	0.510826	0	16.25	43.59	14.62	39.58	16.09	43.38
		10	17.28	43.98	15.26	39.82	16.72	43.62
		20	18.25	44.37	15.88	40.06	17.32	43.85
		30	19.18	44.75	16.47	40.30	17.90	44.09
	0.916291	0	12.82	33.99	11.40	30.63	12.55	33.64
		10	14.55	34.67	12.46	31.05	13.59	34.04
		20	16.08	35.34	13.44	31.45	14.56	34.43
		30	17.48	35.99	14.35	31.85	15.46	34.82

Table 5.6: Values of dimensionless natural frequencies $\left(\Omega = \omega L^2\sqrt{\rho_0 A_0/E_0 I_0}\right)$ for 1st and 2nd mode (Ω_1 and Ω_2) corresponding to linear tapered CS AFG beam for different combinations of taper parameter, spring stiffness and material properties

Taper Pattern	Taper Parameter	Stiffness	Material 1 CS		Material 2 CS		Material 3 CS	
			Ω_1	Ω_2	Ω_1	Ω_2	Ω_1	Ω_2
Linear	0	0	15.24	48.56	13.10	43.83	14.21	47.73
		10	16.01	48.81	13.57	43.99	14.68	47.88
		20	16.74	49.05	14.03	44.15	15.14	48.03
		30	17.44	49.29	14.47	44.30	15.58	48.19
	0.2	0	14.12	44.18	12.10	39.69	13.16	43.28
		10	15.05	44.48	12.67	39.88	13.73	43.47
		20	15.92	44.78	13.22	40.06	14.27	43.65
		30	16.75	45.08	13.74	40.25	14.80	43.84
	0.4	0	12.88	39.44	11.00	35.22	12.00	38.49
		10	14.05	39.83	11.72	35.46	12.71	38.72
		20	15.13	40.42	12.39	35.69	13.38	38.95
		30	16.14	40.60	13.03	35.93	14.01	39.19
	0.6	0	11.48	34.17	9.74	30.27	10.66	33.18
		10	13.04	34.72	10.69	30.60	11.59	33.50
		20	14.43	35.27	11.56	30.92	12.46	33.81
		30	15.70	35.80	12.36	31.24	13.27	34.12

Table 5.7: Values of dimensionless natural frequencies $\left(\Omega = \omega L^2\sqrt{\rho_0 A_0/E_0 I_0}\right)$ for 1st and 2nd mode (Ω_1 and Ω_2) corresponding to parabolic tapered CS AFG beam for different combinations of taper parameter, spring stiffness and material properties

Taper Pattern	Taper Parameter	Stiffness	Material 1 CS		Material 2 CS		Material 3 CS	
			Ω_1	Ω_2	Ω_1	Ω_2	Ω_1	Ω_2
Parabolic	0.2	0	14.51	45.54	12.47	40.92	13.56	44.64
		10	15.38	45.82	13.00	41.10	14.09	44.81
		20	16.19	46.10	13.51	41.28	14.60	44.99
		30	16.97	46.37	14.00	41.45	15.09	45.16
	0.4	0	13.66	42.19	11.73	37.72	12.80	41.24
		10	14.66	42.53	12.34	37.92	13.40	41.44
		20	15.59	42.86	12.92	38.12	13.98	41.63
		30	16.48	43.19	13.47	38.33	14.53	41.83
	0.6	0	12.62	38.36	10.81	34.05	11.85	37.33
		10	13.82	38.78	11.54	34.30	12.56	37.57
		20	14.92	39.19	12.21	34.55	13.23	37.81
		30	15.94	39.61	12.86	34.79	13.87	38.05

In Table 5.3 for CC boundary condition results pertaining to $\alpha = 0$, *i.e.*, a uniform beam, has also been presented. However, in the subsequent tables (Table 5.4 and 5.5)

Table 5.8: Values of dimensionless natural frequencies $\left(\Omega = \omega L^2\sqrt{\rho_0 A_0 / E_0 I_0}\right)$ for 1st and 2nd mode (Ω_1 and Ω_2) corresponding to exponential tapered CS AFG beam for different combinations of taper parameter, spring stiffness and material properties

Taper Pattern	Taper Parameter	Stiffness	Material 1		Material 2		Material 3	
			CS		CS		CS	
			Ω_1	Ω_2	Ω_1	Ω_2	Ω_1	Ω_2
Exponential	0.223144	0	13.60	42.66	11.65	38.35	12.66	41.81
		10	14.60	42.99	12.27	38.55	13.28	42.01
		20	15.54	43.31	12.86	38.76	13.86	42.21
		30	16.43	43.63	13.42	38.96	14.43	42.81
	0.510826	0	11.73	36.02	10.00	32.21	10.89	35.17
		10	13.15	36.49	10.87	32.50	11.76	35.46
		20	14.43	36.96	11.68	32.80	12.56	35.75
		30	15.61	37.43	12.43	33.09	13.32	36.03
	0.916291	0	9.50	28.27	8.04	25.10	8.78	27.48
		10	11.79	29.09	9.44	25.60	10.18	27.96
		20	13.70	29.89	10.66	26.08	11.41	28.44
		30	15.38	30.67	11.76	26.56	12.51	28.90

Table 5.9: Values of dimensionless natural frequencies $\left(\Omega = \omega L^2\sqrt{\rho_0 A_0 / E_0 I_0}\right)$ for 1st and 2nd mode (Ω_1 and Ω_2) corresponding to linear tapered SS AFG beam for different combinations of taper parameter, spring stiffness and material properties

Taper Pattern	Taper Parameter	Stiffness	Material 1		Material 2		Material 3	
			SS		SS		SS	
			Ω_1	Ω_2	Ω_1	Ω_2	Ω_1	Ω_2
Linear	0	0	9.83	71.67	9.01	65.15	9.80	72.11
		10	10.98	71.84	9.73	65.25	10.51	72.21
		20	12.02	72.00	10.39	65.35	11.17	72.32
		30	12.98	72.17	11.02	65.44	11.79	72.42
	0.2	0	8.86	64.21	8.11	56.89	8.81	64.24
		10	10.25	64.43	8.99	57.01	9.67	64.35
		20	11.48	64.64	9.79	57.12	10.47	64.47
		30	12.58	64.85	10.53	57.24	11.21	64.59
	0.4	0	7.90	54.74	7.22	47.72	7.83	54.44
		10	9.61	55.04	8.32	47.88	8.91	54.59
		20	11.07	55.35	9.29	48.04	9.88	54.74
		30	12.35	55.66	10.07	48.20	10.76	54.90
	0.6	0	6.96	43.82	6.35	37.85	6.86	43.37
		10	9.11	44.33	7.76	38.10	8.25	43.62
		20	10.84	44.84	8.94	38.35	9.44	43.85
		30	12.33	45.34	9.99	38.60	10.49	44.09

results for $\alpha = 0$ condition has been omitted to avoid repetition. It should be mentioned here that the mathematical expressions for the different taper profiles are such that in each case

$\alpha = 0$ corresponds to a uniform beam and hence, same natural frequency values are obtained in these cases. For the other two boundary conditions, i.e., CS and SS, same approach in the table of natural frequencies has been taken to avoid duplication. It should also be pointed out that foundation stiffness '0' implies the case of beam without foundation support, while, Material 1 indicates the case of homogeneous beam (without gradation).

Table 5.10: Values of dimensionless natural frequencies $\left(\Omega = \omega L^2\sqrt{\rho_0 A_0 / E_0 I_0}\right)$ for 1st and 2nd mode (Ω_1 and Ω_2) corresponding to parabolic tapered SS AFG beam for different combinations of taper parameter, spring stiffness and material properties

Taper Pattern	Taper Parameter	Stiffness	Material 1		Material 2		Material 3	
			SS		SS		SS	
			Ω_1	Ω_2	Ω_1	Ω_2	Ω_1	Ω_2
Parabolic	0.2	0	9.28	66.40	8.50	58.88	9.23	66.43
		10	10.56	66.59	9.30	58.99	10.02	66.54
		20	11.70	66.79	10.04	59.10	10.76	66.64
		30	12.74	66.99	10.73	59.20	11.44	66.75
	0.4	0	8.73	59.32	7.99	51.81	8.66	59.04
		10	10.17	59.58	8.90	51.95	9.56	59.17
		20	11.42	59.84	9.72	52.08	10.38	59.30
		30	12.55	60.10	10.48	52.22	11.14	59.43
	0.6	0	8.19	50.83	7.47	44.01	8.08	50.41
		10	9.81	51.21	8.51	44.19	9.11	50.59
		20	11.19	51.58	9.44	44.38	10.03	50.77
		30	12.43	51.96	10.28	44.57	10.87	50.94

Table 5.11: Values of dimensionless natural frequencies $\left(\Omega = \omega L^2\sqrt{\rho_0 A_0 / E_0 I_0}\right)$ for 1st and 2nd mode (Ω_1 and Ω_2) corresponding to exponential tapered SS AFG beam for different combinations of taper parameter, spring stiffness and material properties

Taper Pattern	Taper Parameter	Stiffness	Material 1		Material 2		Material 3	
			SS		SS		SS	
			Ω_1	Ω_2	Ω_1	Ω_2	Ω_1	Ω_2
Exponential	0.223144	0	8.43	62.13	7.72	55.29	8.39	62.24
		10	9.95	62.35	8.69	55.41	9.34	62.37
		20	11.27	62.58	9.55	55.54	10.20	62.50
		30	12.45	62.80	10.34	55.66	10.99	62.62
	0.510826	0	6.93	50.43	6.35	44.16	6.88	50.28
		10	9.07	50.79	7.72	44.35	8.24	50.46
		20	10.79	51.15	8.89	44.53	9.41	50.64
		30	12.27	51.50	9.92	44.72	10.45	50.82
	0.916291	0	5.28	36.70	4.83	31.78	5.22	36.40
		10	8.54	37.41	7.01	32.14	7.39	36.74
		20	10.87	38.11	8.65	32.50	9.06	37.08
		30	12.78	38.79	10.03	32.85	10.46	37.44

From the tables 5.3-5.11, it is observed that for all the cases with the increase in stiffness of the foundation the natural frequency increases, which is quite an expected outcome. This increment of frequency is due to reason that stiffer foundation makes the system more rigid. It is also observed that the rigidity of the beam edges and consequently the boundary conditions significantly affect the free vibration response. That's why, the natural frequency in CC beam is the highest and in SS beam is the lowest for a fixed value of foundation stiffness. For fixed non-zero taper parameter it can be observed that in between linear and parabolic taper pattern, the system with parabolic taper pattern has the higher natural frequency. It is also observed that for all the cases with increase in taper parameter the natural frequency decreases. Reduction in cross-sectional area and moment of inertia causes a softening effect, which is manifested in this decrement of frequencies. Comparing the values, it is observed that softening effect is severe in exponentially tapered beam and least in parabolic tapered beam. It is also observed that for particular taper parameter, boundary condition and foundation stiffness value, the natural frequency is the highest for Material 1 and lowest for Material 2.

5.3.3.4 Backbone curves:

Variation of natural frequencies with respect to changes in transverse pre-load value is the main focus of the study. However, as the transverse load produces a given static deflection, the results are presented in the normalised frequency vs. normalised maximum deflection plane. The graphical representation, where the ordinate represents dimensionless amplitude (w_{max}/t_0) and abscissa represents the dimensionless frequency (ω_{nf}/ω_1), is akin to a backbone curve. Backbone curves of a vibratory system provide information about the measure of amplitude dependence of natural frequencies of the system. The dynamic behavior of the system is shown in Figures 5.3-5.11 as backbone curves for the first mode.

The formulation has been developed in such a way that the system can be equivalently assumed to represent a large amplitude vibration scenario. Such an approach is justified on the basis of the assumption that large amplitude vibration analysis of a nonlinear system may be considered equivalent to a case where the system undergoes small oscillations about the deflected configuration of same large amplitude. It is important to note that the fundamental frequencies (ω_1) at no load condition, which are already obtained

and tabulated in Tables 5.3-5.11, are used here to normalize nonlinear frequencies (ω_{nf}/ω_1). For all the cases, stiffness of the beam increases with increasing load. This type of occurrence is found due to the present of geometric nonlinearity in the system. This type of increased stiffness causes the increase in free vibration frequencies with increase in the deflection of the beam, which can be observed from any of the figures. So, hardening type nonlinear behaviour is exhibited by the system for all combinations of taper profile, stiffness values and boundary conditions.

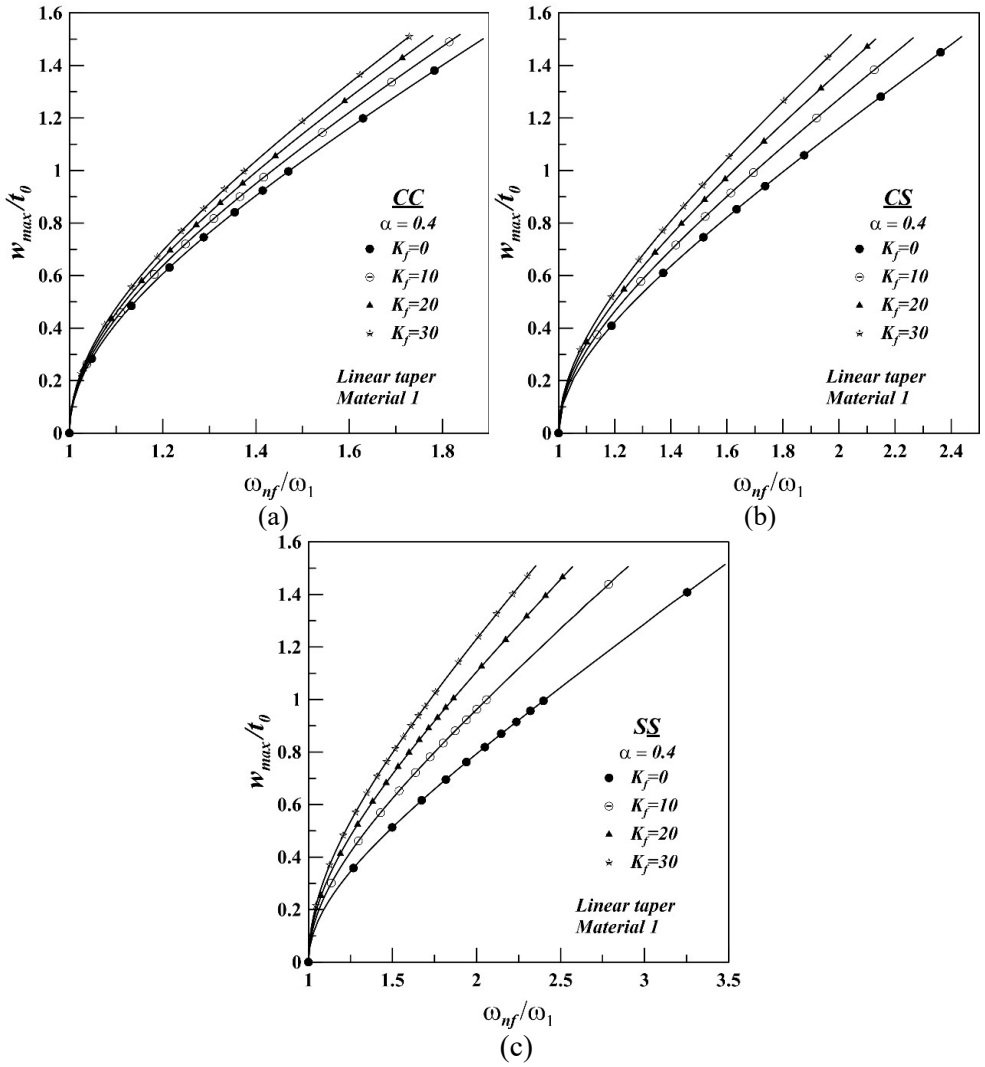

Figure 5.3: Backbone curves of AFG linear taper beam (Material 1) for different boundary conditions: (a) CC, (b) CS and (c) SS

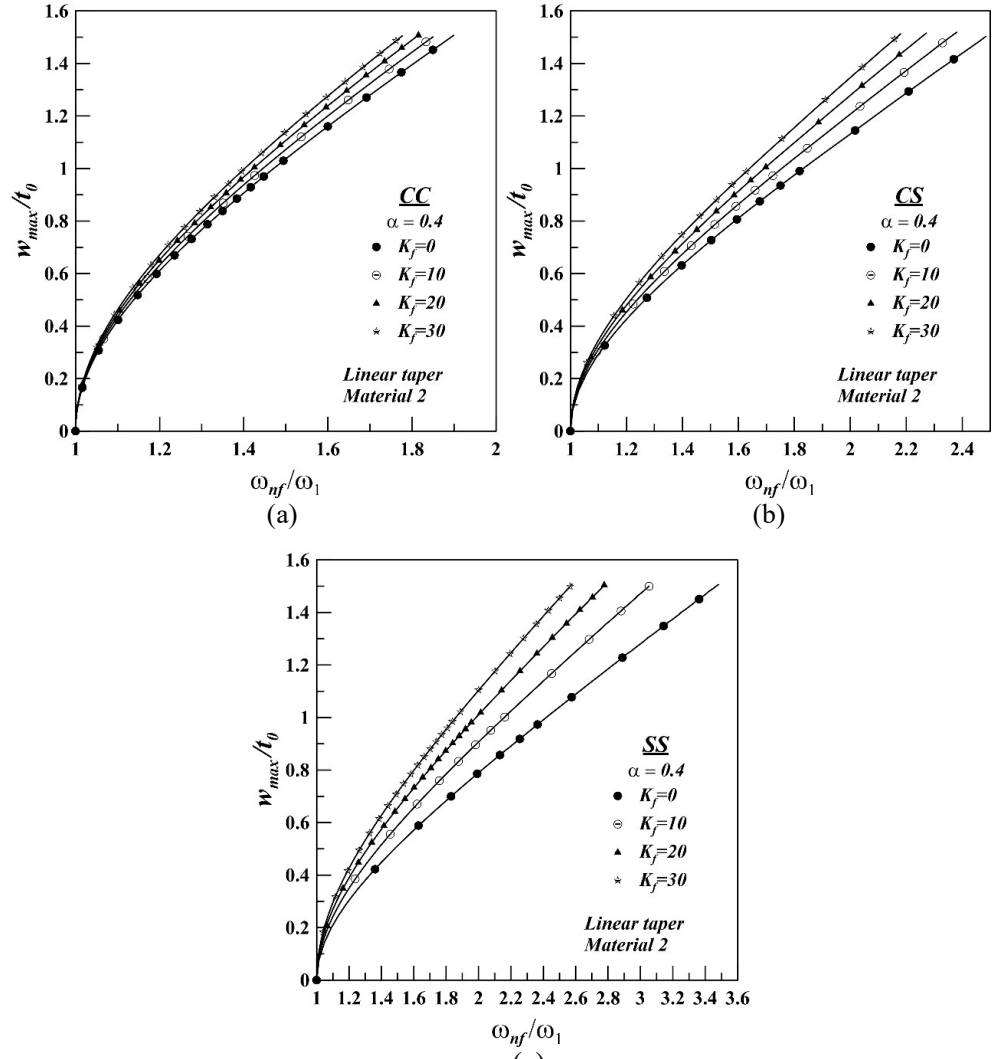

Figure 5.4: Backbone curves of AFG linear taper beam (Material 2) for different boundary conditions: (a) CC, (b) CS and (c) SS

5.3.3.4.1 Effects of foundation stiffness:

Figures 5.3-5.5 represent the 1st backbone curve for fundamental mode of linearly tapered beam with three different material models (Material 1, Material 2 and Material 3). In each figure, there are three sets of plots for three different boundary condition (CC, CS, SS) and in each plot four backbone curves are depicted corresponding to various spring stiffness values which varies from 0 to 30. The taper parameter is kept as constant, at 0.4 to plot the results with an objective to study the influences of the foundation stiffness. Similar plots for parabolic tapered beams are provided in Figures 5.6-5.7, whereas

backbone curves for exponential AFG beams are shown in Figures 5.8-5.9. However, for parabolic and exponential taper, results corresponding to Material 1 has been omitted, as it represents homogeneous material. It should also be mentioned that the taper parameter values in Figures 5.8-5.13 are α = 0.223144, 0.510826 and 0.916291 (as shown in Table 3.3) as these are the case of exponential taper pattern.

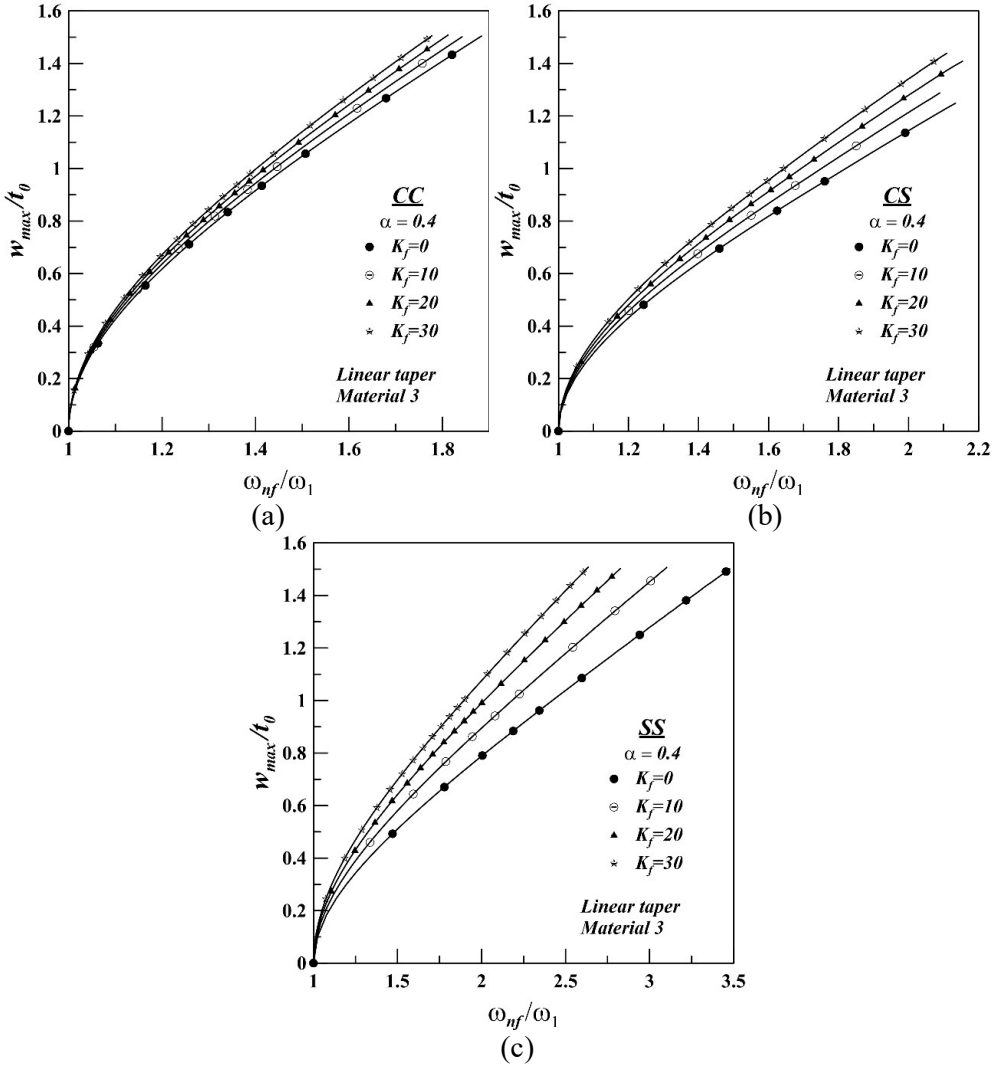

Figure 5.5: Backbone curves of AFG linear taper beam (Material 3) for different boundary conditions: (a) CC, (b) CS and (c) SS

It is observed from Figures 5.3-5.9, in all the cases, with the increase of the foundation stiffness the slope of the backbone curve is increasing in nature. This effect is severe for SS boundary condition whereas for CC beam backbone curves are closely clustered. From the above discussion it can be concluded that nonlinearity involved in case

of SS beam is higher than the other two taper patterns. For CC and CS beam profile the difference between the backbone curves is found to be small. For linear taper pattern, it is quite clear that the change in backbone curve for different material model is hardly noticeable for a particular case of boundary condition, as shown in Figures 5.3 - 5.5. For other type of taper patterns, i.e., parabolic and exponential taper, which are shown in Figures 5.6-5.7 and Figures 5.8-5.9 respectively, same trend can be found. It is also observed from the figures that for particular boundary condition and material model, in exponential taper the backbone curves are more openly clustered than the other two (linear and parabolic) for different foundation stiffness values.

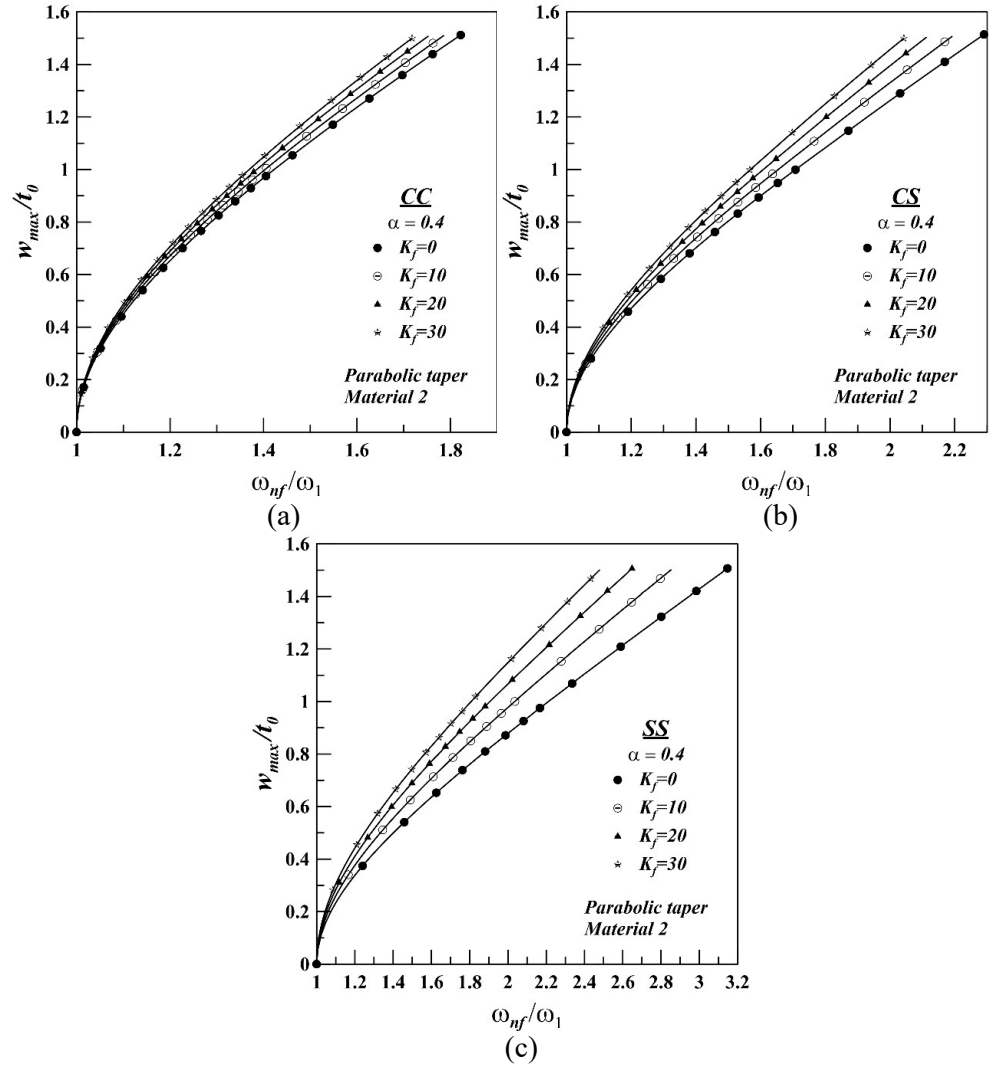

Figure 5.6: Backbone curves of AFG parabolic taper beam (Material 2) for different boundary conditions: (a) CC, (b) CS and (c) SS

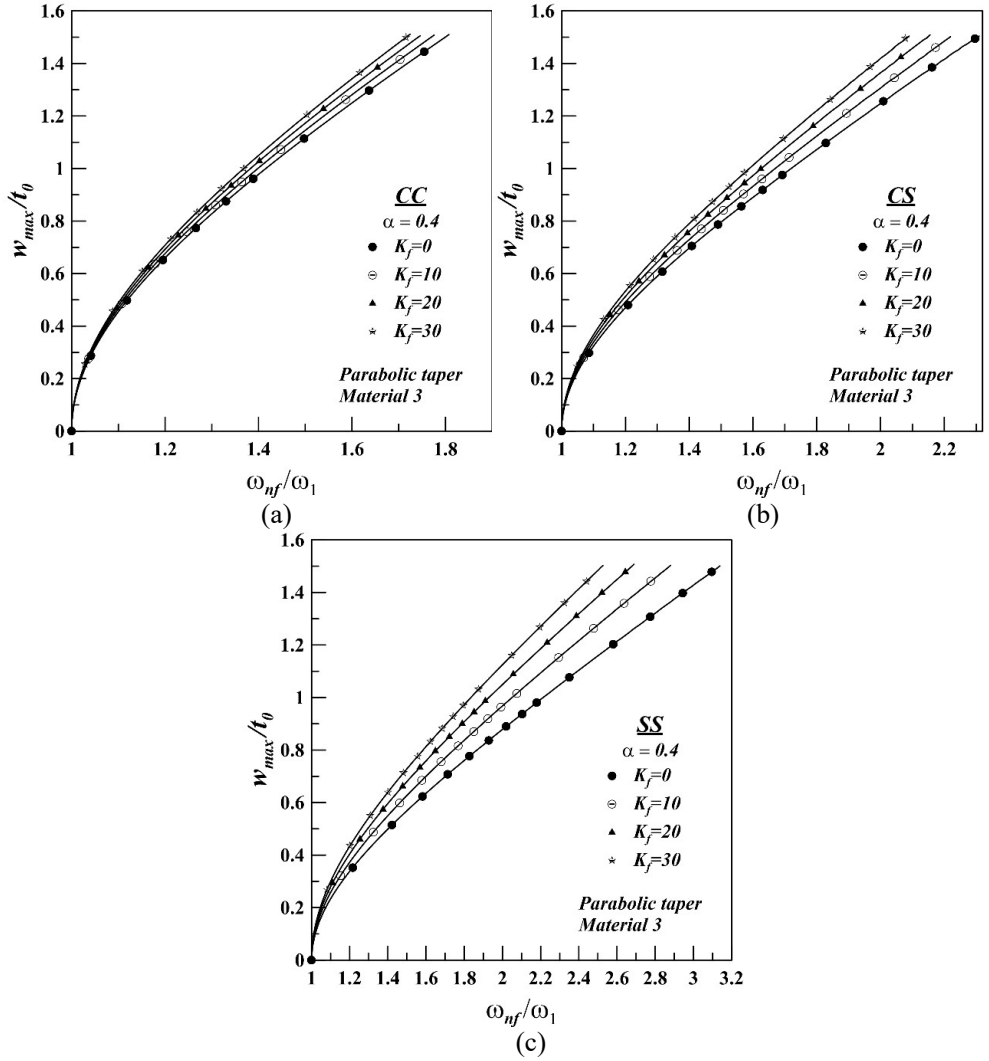

Figure 5.7: Backbone curves of AFG parabolic taper beam (Material 3) for different boundary conditions: (a) CC, (b) CS and (c) SS

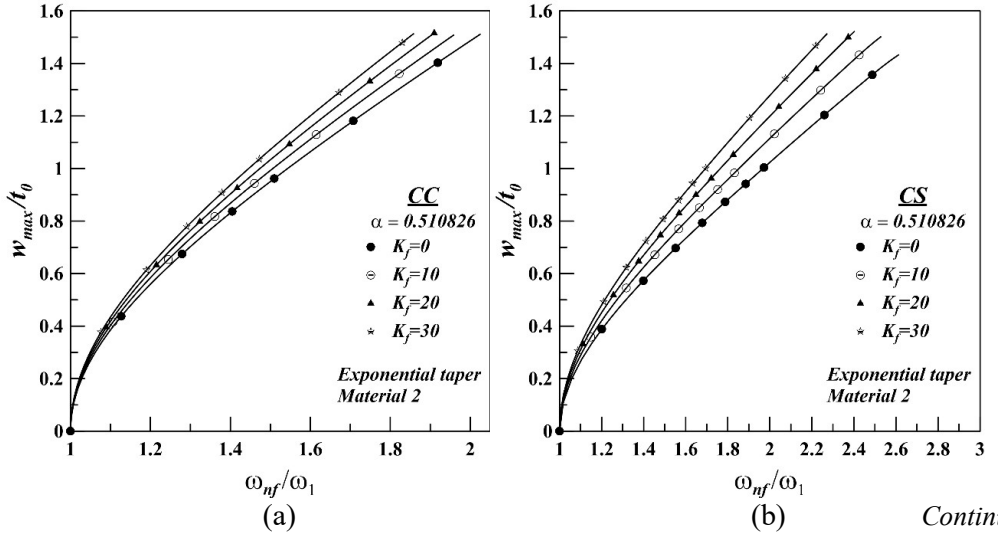

Continued

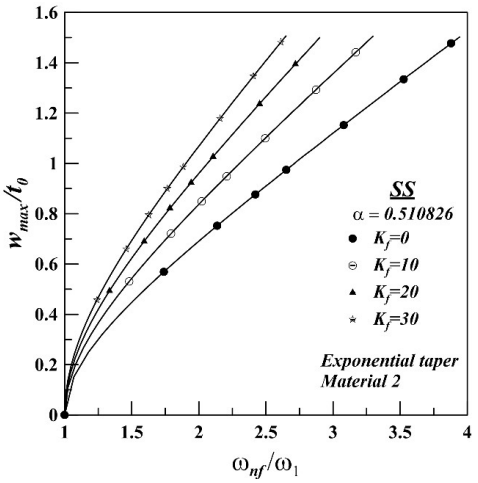

(c)

Figure 5.8: Backbone curves of AFG exponential taper beam (Material 2) for different boundary conditions: (a) CC, (b) CS and (c) SS

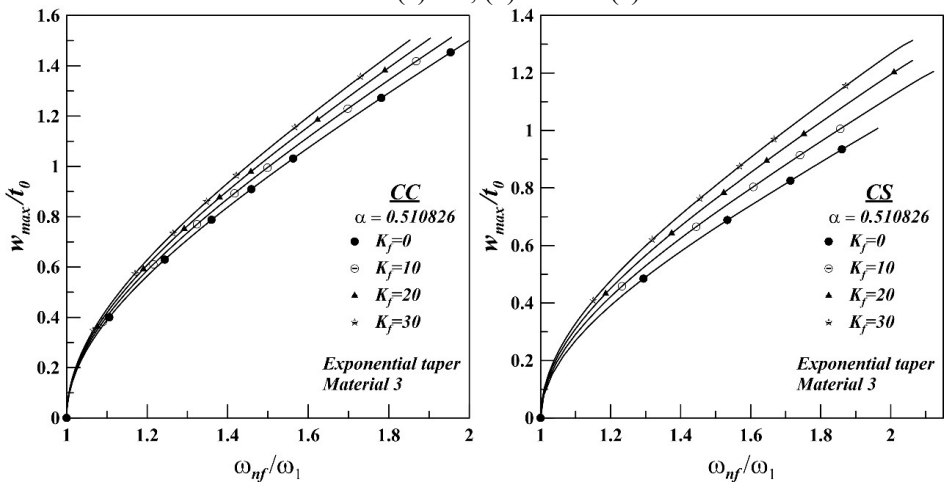

(a)

(b)

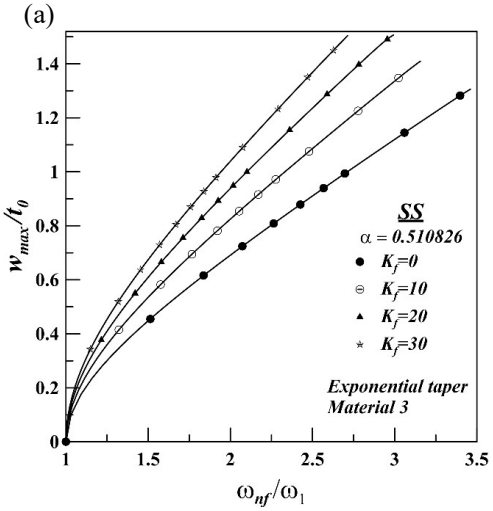

(c)

Figure 5.9: Backbone curves of AFG exponential taper beam (Material 3) for different boundary conditions: (a) CC, (b) CS and (c) SS

5.3.3.4.2 Effect of taper parameter:

Figure 5.10 shows the effect of taper parameters on backbone curve for CC AFG beam. Curves are depicted for three different taper pattern in which taper parameter varies from 0 to 0.6 for linear and parabolic taper whereas, in case of exponential taper variation of taper parameter is taken from 0 to 0.916291. Material 2 is selected for all the cases whereas foundation stiffness is fixed at 10. It is to be noted that taper parameter 0 represents the case of uniform beam and provides a basis for comparison. From the figure, it is observed that for all the cases with the increase of taper parameter values, the backbone curves progressively tilt towards the right side more and more.

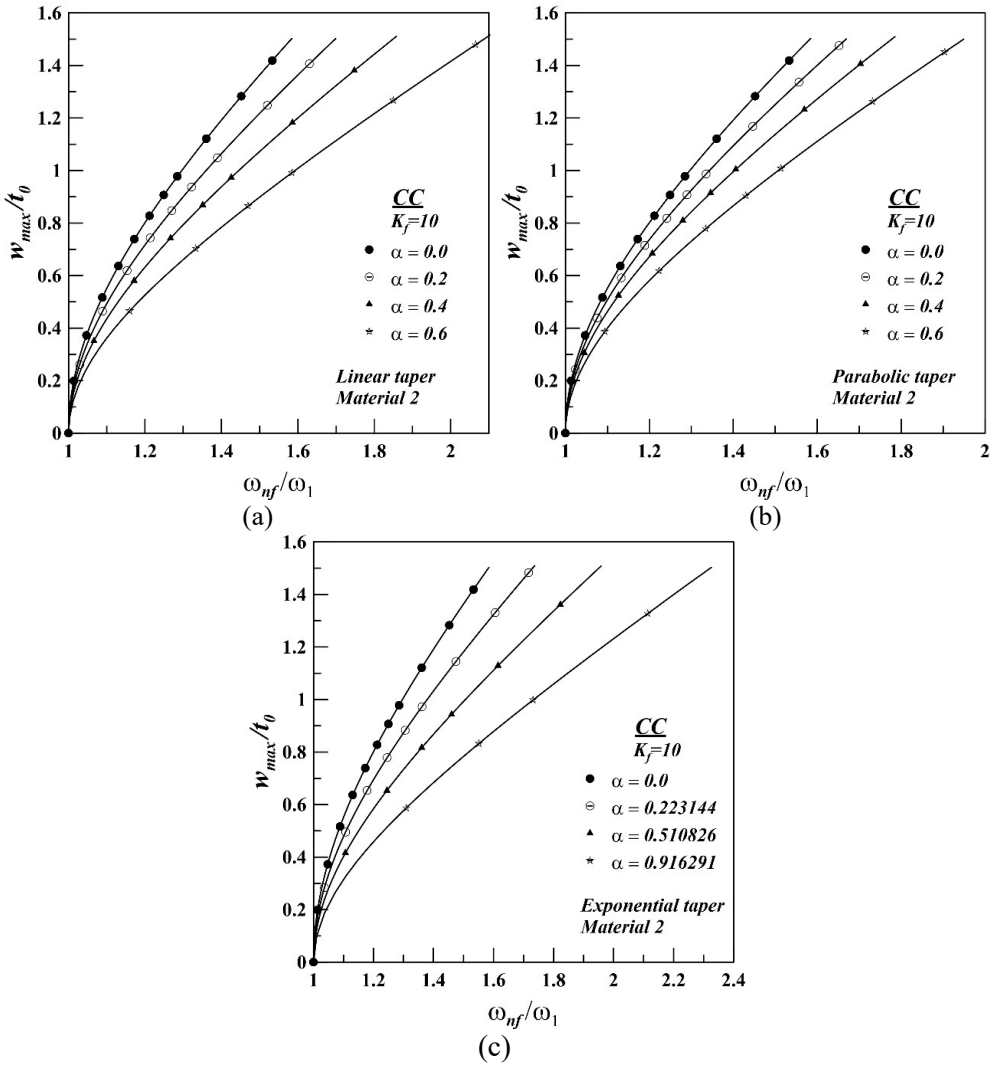

Figure 5.10: Effect of taper parameters on backbone curves of CC AFG beam for different taper pattern: (a) linear taper, (b) parabolic taper and (c) exponential taper

5.2.3.4.3 Higher mode backbone curves:

Backbone curves for higher modes (modes 2-5) of the linear taper AFG beam corresponding to three boundary conditions are presented in Figure 5.11. Each of these figures consist of two different sub-plots for two different material models i.e. Material 2 and Material 3. In this regard, plot for the material 1 is not furnished as it is the case of homogeneous material. For all the cases the taper parameter is considered as 0.4, whereas, foundation stiffness is fixed at 10.

5.3.3.5 Mode shapes:

The free vibration analysis as represented by Equation (5.13) is a standard eigenvalue problem and its solution provides not only information regarding the natural frequencies but also eigenvectors corresponding to the eigenvalues. In fact, the unknown parameters associated with Equation (5.13) denote the eigenvectors in matrix form and the contribution of individual spatial functions on the vibration modes. However, it is important to note that the stiffness matrix in this eigenvalue analysis corresponds to the converged large deflection static solution. So, equivalence may be drawn between large amplitude free vibration of a nonlinear system and its free vibration analysis, subjected to a static load producing same magnitude of large amplitude deflection. So, the evaluated mode shapes can be considered as corresponding to large amplitude vibration about the undeformed equilibrium position. First three mode shape of the linear taper AFG beam corresponding to three boundary conditions are provided in Figure 5.12. Each of these figures consists of two different sub-plots for two different material models i.e. Material 2 and Material 3. Mode shape plot for the Material 1 is not furnished as it is the case of homogeneous material. It is also worth pointing out that amplitude of vibration has an effect on the mode shape of the system. To study this aspect in more detail, two mode shape plots corresponding to linear ($w_{max}/t_0 = 0$) and nonlinear ($w_{max}/t_0 = 1.5$) frequencies are given for each of the vibration modes. It should also be noted that the amplitude of vibration for all the plots is normalized by the corresponding maximum deflection. It was observed that difference in linear and nonlinear mode shapes increase when the boundary condition changes from CC to SS due to the decreasing rigidity at the boundary. However, no considerable change in the mode shapes could be identified for the different material models perhaps due to normalization of the maximum displacement.

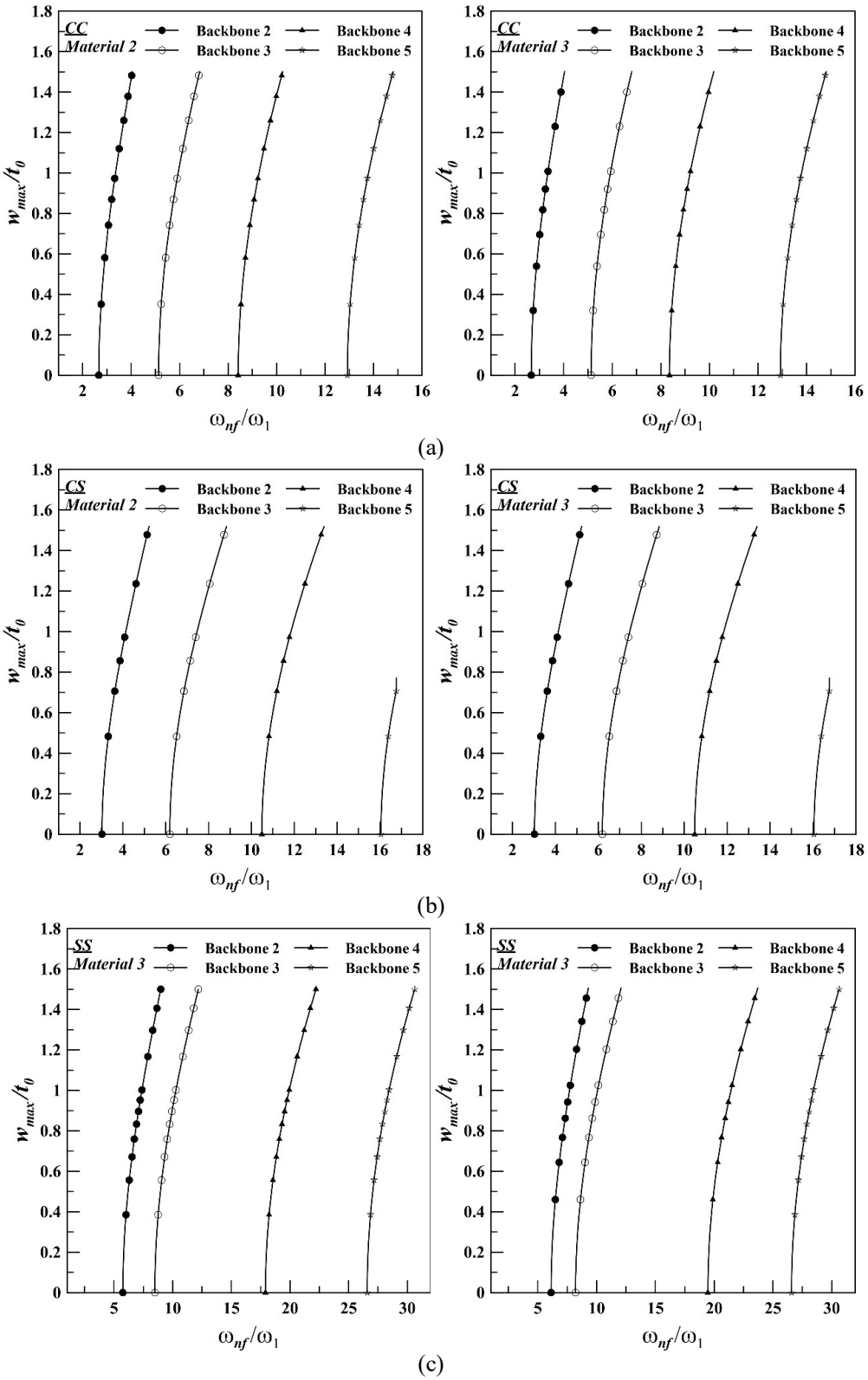

Figure 5.11: Backbone curves at higher modes of linear taper AFG beam corresponding to different boundary conditions: (a) CC (b) CS (c) SS.

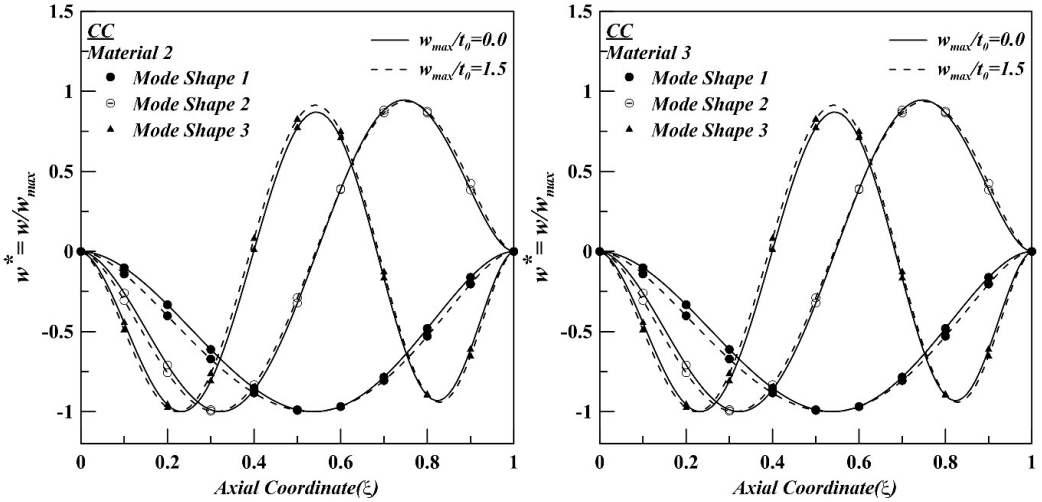

(a)

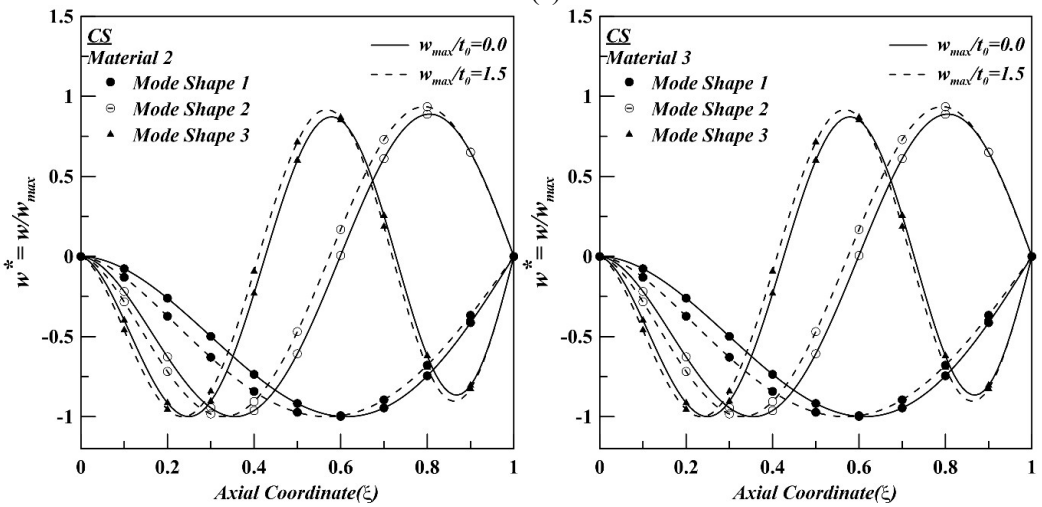

(b)

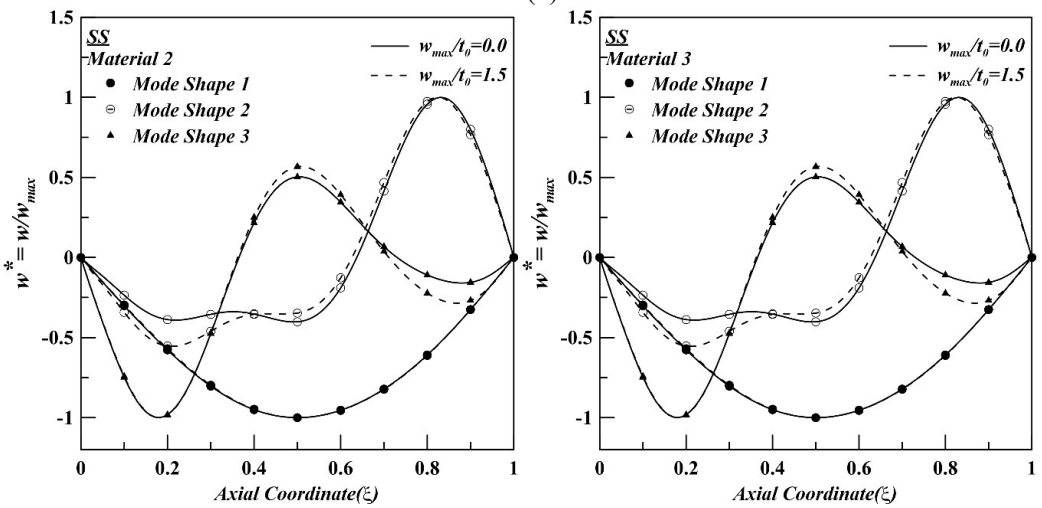

(c)

Figure 5.12: Mode shape of linear taper AFG beam corresponding to different boundary conditions: (a) CC (b) CS (c) SS.

5.4 Forced vibration analysis:

Forced vibration of non-uniform axially functionally graded (AFG) Timoshenko beam on elastic foundation is performed under harmonic excitation. A linear elastic foundation is considered with three different classical boundary conditions. The present approximate method is displacement based and Von-Karman type of geometric nonlinearity is considered with rotational component to incorporate transverse shear. The gradations of the martial properties are considered in the power law form along the axial direction. Hamilton's principle is used to derive nonlinear set of governing equation and Broyden method is implemented to solve the nonlinear equations numerically. The results are successfully validated with previously published article. Frequency vs. amplitude curve corresponding to different combinations of system parameters are presented and are capable of serving as benchmark results. A separate free vibration analysis is undertaken to include backbone curves with the frequency response curves in the non-dimensional plane.

5.4.1 Mathematical formulation:

The present formulation is carried out following energy method where Hamilton's principle has been adopted for deriving the governing differential equations of the system. The formulation is based on Timoshenko beam theory, where, shear deformation and rotary inertia effect is taken into account. In the present system geometric nonlinearity is incorporated by considering nonlinear strain-displacement relations. It is assumed that the system exhibits dynamic equilibrium at maximum amplitude of excitation which implies that at this point of time there exist no unbalanced forces in the dynamic system. This unique assumption converts the dynamic problem to static one.

Hamilton's principle, whose mathematical form (Shames and Dym, 2009) is provided below, is utilized to derive the governing set of equations.

$$\delta\left(\int_{\tau_1}^{\tau_2}\left(T-U-V\right)d\tau\right)=0 \tag{5.14}$$

Here, δ is the variational operator, T is the kinetic energy of the system, U is the total strain energy stored in the system, V is the work done by the external loading/excitation and τ is

the time. The expressions for these energy functionals (U, V and T) are furnished in the previous section 5.3.1 (Equations. (5.4), (5.5), (5.6), (5.7) and (5.11)). From the expressions it is noticeable that all the energy functionals are dependent on the displacement fields. In these expressions w, u and ψ are dynamic displacement fields which are completely separable by space and time. They are assumed as linear combinations of orthogonal admissible functions, φ_i, α_i and β_i and a set of unknown coefficients (d_i) as follows,

$$w(\xi,\tau)=\sum_{i=1}^{nw} d_i\phi_i(\xi)e^{j\omega\tau} \tag{5.15a}$$

$$u(\xi,\tau)=\sum_{i=1}^{nu} d_{nw+i}\alpha_i(\xi)e^{j\omega\tau} \tag{5.15b}$$

$$\psi(\xi,\tau)=\sum_{i=1}^{nsi} d_{nw+nu+i}\beta_i(\xi)e^{j\omega\tau} \tag{5.15c}$$

ω is the response frequency of the vibratory system, $j = \sqrt{-1}$ and τ is the time. nw, nu and nsi are the number of orthogonal functions for each of the displacement fields w, u and ψ, respectively. Appropriate start functions for these orthogonal set of functions (φ_1, α_1 and β_1) must be selected to satisfy the flexural, in-plane and rotational boundary conditions of the beam. These start functions must also be continuous and differentiable within the domain. In section 5.3.3, Table 5.1, the selected start functions for each of the displacement fields are shown for different boundary conditions. These start functions are used to generate the higher order functions (upto nw/nu/nsi) implementing Gram–Schmidt orthogonalization scheme (Kumar et al., 2015).

Substituting the appropriate energy expressions and displacement fields into Eq. (12), the governing equation is obtained as follows:

$$[K]\{d\}-\omega^2[M]\{d\}=\{f\} \tag{5.16}$$

Here, [K] is the stiffness matrix, [M] is mass matrix, {f} is load vector and {d} is the vector of unknown coefficient, respectively. The dimension of these matrices and vectors is (nu + nw + nsi). The elements of [K], [M] and {f} are same as that of free vibration analysis which are provided in Appendix.

5.4.2 Solution procedure:

It is noteworthy that the stiffness matrix contains terms with unknown coefficients, thus making it nonlinear. As a result, the governing set of equations as represented by Equation (5.16) is nonlinear in nature as well. An indirect method, in which the dynamic problem is reduced to an equivalent static problem, is adopted to solve nonlinear set of equations. The unknown coefficients are calculated for given amplitude of excitation and excitation frequency. The analysis assumes that at the peak excitation amplitude value the system satisfies the force equilibrium condition. The solution technique adopted in this analysis is one of the multidimensional quasi-Newton methods known as Broyden's method (Press et al*.,* 2005). In this method the Jacobian is calculated on the basis of an initial guess and its value is updated in the successive iterations. The detailed solution technique and solution procedure is discussed in Chapter 4.

5.4.3 Result and discussion:

Presently, large amplitude forced vibration analysis of AFG Timoshenko beams resting on elastic foundation subjected to transverse harmonic excitation is performed to find out the frequency response of the system in terms of displacement amplitude. In the current study, only steady-state response is presented and frequency of response of the undamped system is assumed to be equal to the forcing frequency. An indirect approach is adopted for solving the problem, where it is reduced to a static scenario by assuming that under maximum amplitude of excitation, i.e., when the system suffers maximum deformation, the dynamic system satisfies force equilibrium conditions. This assumption converts the dynamic problem into an equivalent static situation, in which the excitation frequency and amplitude of the harmonic excitation are the input parameters that control system response.

Linear tapering of thickness in the axial direction from the root (t_0) to the other end (t_1) is considered. The decrement in thickness takes place according to the expression, $t(x) = t_0(1-\alpha x/L)$, while width of the beam remains constant. Length (L) and width (b) of the beam are taken as 0.2 m, 0.02 m, respectively, while, Length-to-thickness ratio (L/t_0) values are varied from 5 to 100. The length of the beam is fixed throughout the analysis, whereas, the thickness is calculated for each value of Length-to-thickness ratio (L/t_0). It should be

noted that the higher values of (L/t_0) correspond to thin beams and are considered here for comparison purpose. For AFG beam, variation of elastic modulus and density are taken into account along the axial coordinate, according to the following power-law forms.

Elastic modulus, $E(x) = E_0 + (E_1 - E_0)(x/L)^n$

Density, $\rho(x) = \rho_0 + (\rho_1 - \rho_0)(x/L)^n$

Here, n is the gradient parameter describing volume fraction change of both constituents involved. Poisson ratio (μ) is taken as constant throughout the entire analysis. In order to have a better weight distribution, material properties are gradually increased from the root side (E_0 and ρ_0) to the other end of the beam (E_1 and ρ_1), considering opposite distribution to the thickness variation. In the present work, two materials are chosen as Aluminium and Zirconia, and their material properties are: Al: E_0 = 70 GPa, ρ_0 = 2702 kg/m^3; ZrO_2: E_1 = 200 GPa, ρ_1 = 5700 kg/m^3. It is also important to note that, for the present AFG beam model, the root side of the beam (ξ = 0) is purely Aluminium and continuous gradation is performed along the length to obtain the material property at the other end (ξ = 1), which is purely Zirconia. The gradation of the material properties for different gradient parameter (n) are shown in Figure 5.13. From the figures, it is observed that for n = 1 linear gradation of the material properties can be obtained, where 50% of each material (Aluminium/Zirconia) property contribution is observed. Due to this reason, for the best practice gradient parameter (n) beyond 3 and below 1/3 is not considered (Nakamura et al., 2000). Poisson ratio (μ) with a value of 0.3 is taken as constant throughout the entire analysis.

Three different classical boundary conditions i.e. clamped-clamped (CC), clamped-simply supported (CS) and simply supported-simply supported (SS) are selected. In-plane boundary conditions are assumed as immovable. The beam is subjected to uniformly distributed transverse time varying excitation, $q(x,t)$ as shown in Fig. 1(a). The expression of the external excitation is given by, $q = \bar{q}(x)e^{j\omega\tau}$, where ω is the frequency of excitation, $j = \sqrt{-1}$, $\bar{q}$ represents the intensity of the harmonic excitation per unit length of the beam and τ is the time. Four non-dimensional externally applied time varying excitations [$\bar{q}^* = \bar{q}(L^4/E_0I_0t_0)$] are considered which are varied from 20 to 60 in equal steps of 10. Four

different value of the non-dimensional foundation stiffness parameter [$K_f = k_f \{(L/t_0)^3/E_0 b\}$] is consider here. These values are 0, 20, 40 and 60 respectively. Here, k_f is the dimensional value of stiffness.

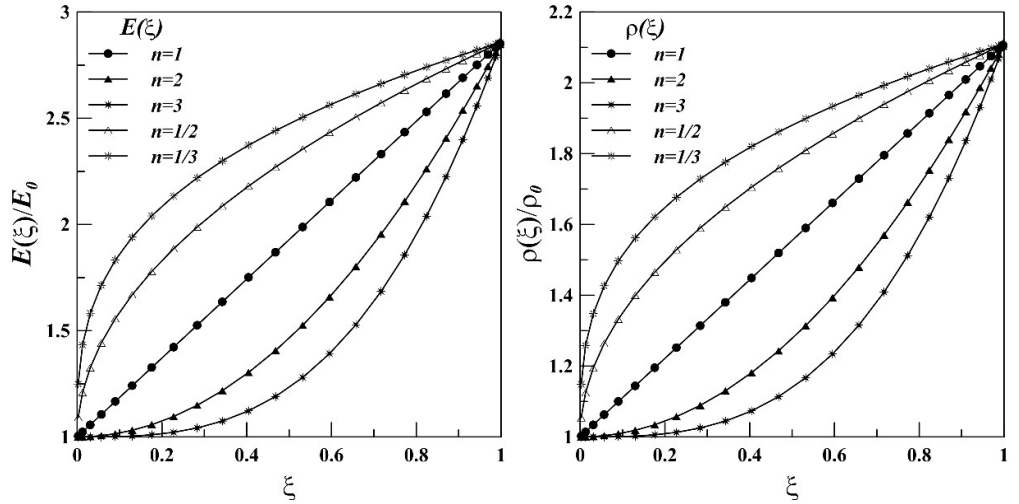

Figure 5.13: Axial gradation of material properties (a) elastic modulus (b) density

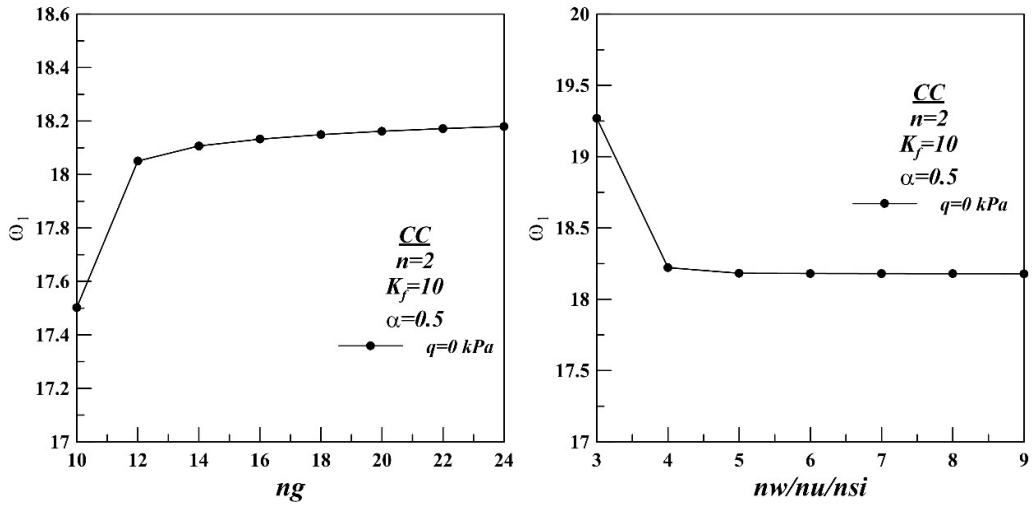

Figure 5.14: Convergence study (a) number of gauss points (*ng*) (b) number of orthogonal functions (*nw=nu=nsi*)

5.4.3.1 Convergence study:

In the present study, computation is conducted in a normalized domain ($\xi = x/L$). For generating the computation points for numerical solution within the normalized domain, gauss points (*ng*) are created along the length of the beam. A detailed convergence

study is required for the choice of number of gauss points. Similar study is also applicable for the selection of the number of functions in the assumed displacement field as well. Such a study is necessary as these selections greatly influence the results of the numerical scheme. This convergence study is carried out on CC AFG non-uniform ($\alpha = 0.5$) beam with gradient parameter, $n = 2$ on an elastic foundation having $K_f = 10$. The comparison of non-dimensional fundamental frequency is conducted with respect to the relevant parameters considering no load condition. The results of the study are presented in Figures 5.14 and from these figures, number of gauss points (*ng*) and number of orthogonal functions (*nw=nu=nsi*) are selected as 24 and 8, respectively.

Table 5.12 Comparisons of dimensionless natural frequencies $\left(\Omega_1 = \omega_1 L^2 \sqrt{\rho_0 A_0 / E_0 I_0}\right)$ of homogeneous uniform beam

Literature	Ω_1	Ω_2	Ω_3	Ω_4	Ω_5
Ribeiro [2004]	22.0125	59.4594	113.6121	183.3579	217.6559
Present Study	21.9148	59.1112	112.7598	180.4668	217.2188
% Error	0.44	0.58	0.75	1.5	0.2

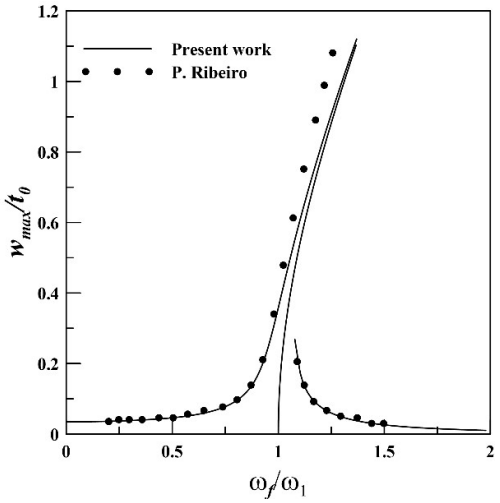

Figure 3.15: Comparison of nonlinear frequency response

5.4.3.2 Validation study:

The present methodology and solution procedure is validated with the results of previously published paper of Ribeiro (2004) for homogeneous and uniform thick beam without considering elastic foundation. The comparison of linear dimensionless natural frequencies for first five modes are tabulated in Table 5.12 for CC end conditions. Comparison of the nonlinear frequency response is also shown in Figure 5.15. For this

purpose, the length (L), width (b) and length to thickness ratio (L/t_0) of the beam are taken as 0.406 m, 0.02 and 20, respectively. Elastic modulus (E_0), Density (ρ_0) and Poisson ratio (μ) are considered as 71.72 GPa, 2800 kg/m^3 and 0.33 respectively. A 2 kN concentrated load is considered at the mid span of the beam. From the above comparison, it can be observed that the current results have satisfactory matching with the established results.

5.4.3.3 Frequency response plot:

The results are generated for different excitation amplitudes, foundation stiffness, gradation parameters, taper parameters and length to thickness ratio. These results are plotted in a non-dimensional frequency amplitude plane. The abscissa is represented by the non-dimensional frequency (ω_f/ω_1) and the ordinate represents the dimensionless response amplitude (w_{max}/t_0). Here, the excitation frequency (ω_f) is normalized using the fundamental natural frequency (ω_1), whereas the maximum deflection (w_{max}) is normalized using beam root thickness root (t_0). To detect the effect more accurately, results are plotted separately for three different boundary conditions (CC, CS and SS) which are shown in different sub-plots under the figure caption (a), (b) and (c).

To obtain the frequency response plots frequency sweep is initiated at zero excitation frequency with a particular value of excitation amplitude and increased gradually towards resonance. This type of sweep is termed as forward sweep. Conversely, a backward frequency sweep is carried out by gradually decreasing the excitation frequency from a finite high value.

From the Figures 5.16-5.20, the frequency response curves are categorized by two distinct zones. In the first zone, with the increase in excitation frequency, the response amplitude increases, while, in the other zone response amplitude reduces. Nonlinear behaviour of the system can be observed in the Multi response zone where two response amplitudes corresponding to the previously mentioned distinct zones are found. The branches of the response curve in these two zones are stable solutions. Theoretically, a third zone, where an unstable steady-state solution is possible, exists but cannot be captured through current methodology.

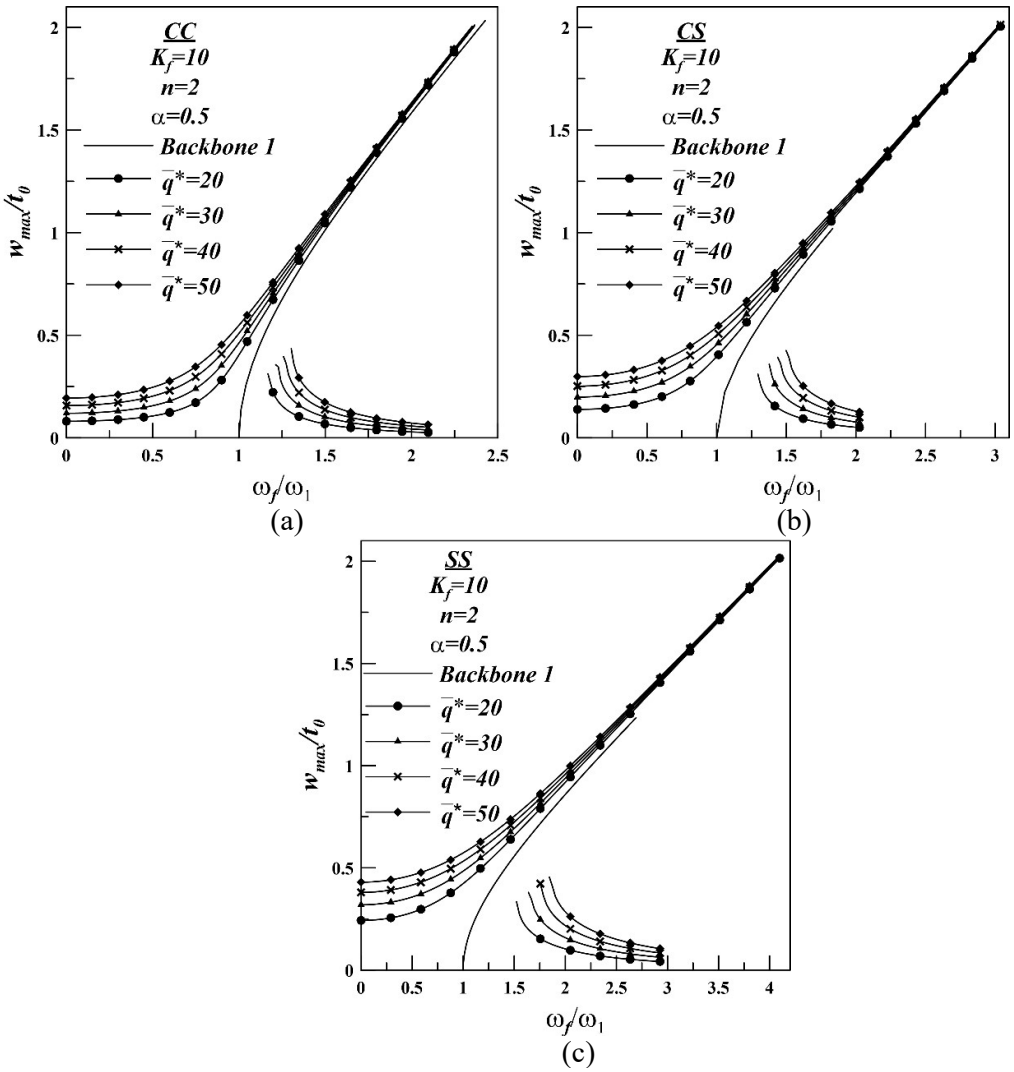

Figure 5.16: Effects of the force amplitude on frequency response for (a) CC beam (b) CS beam and (c) SS beam

5.4.3.3.1 Effect of excitation amplitude:

The effect of excitation amplitude on the frequency response of AFG beam is shown in Figure 5.16. Three plots for three different boundary conditions (CC, CS and SS) are presented. Foundation stiffness, gradient parameter, length-to-thickness ratio and taper parameter have been fixed at 10, 2, 20 and 0.5, respectively, whereas the non-dimensional excitation amplitude is varied from 20 to 50 in steps. It is noted that the normalizing factor for the three boundary conditions are different as shown in Table 5.14. As the clamped end conditions are replaced by simply supported ends, overall rigidity of the system reduces as evidenced by the lower natural frequencies. It is observed from Figure 5.16 that at a given

excitation frequency, the response amplitude of beam with SS boundary conditions (Figure 5.16(c)) are the highest, whereas for beam with CC boundary conditions (Figure 5.16(a)) it is lowest. The figures also show that increasing of the excitation amplitude increases the forced vibration response amplitude of the beam.

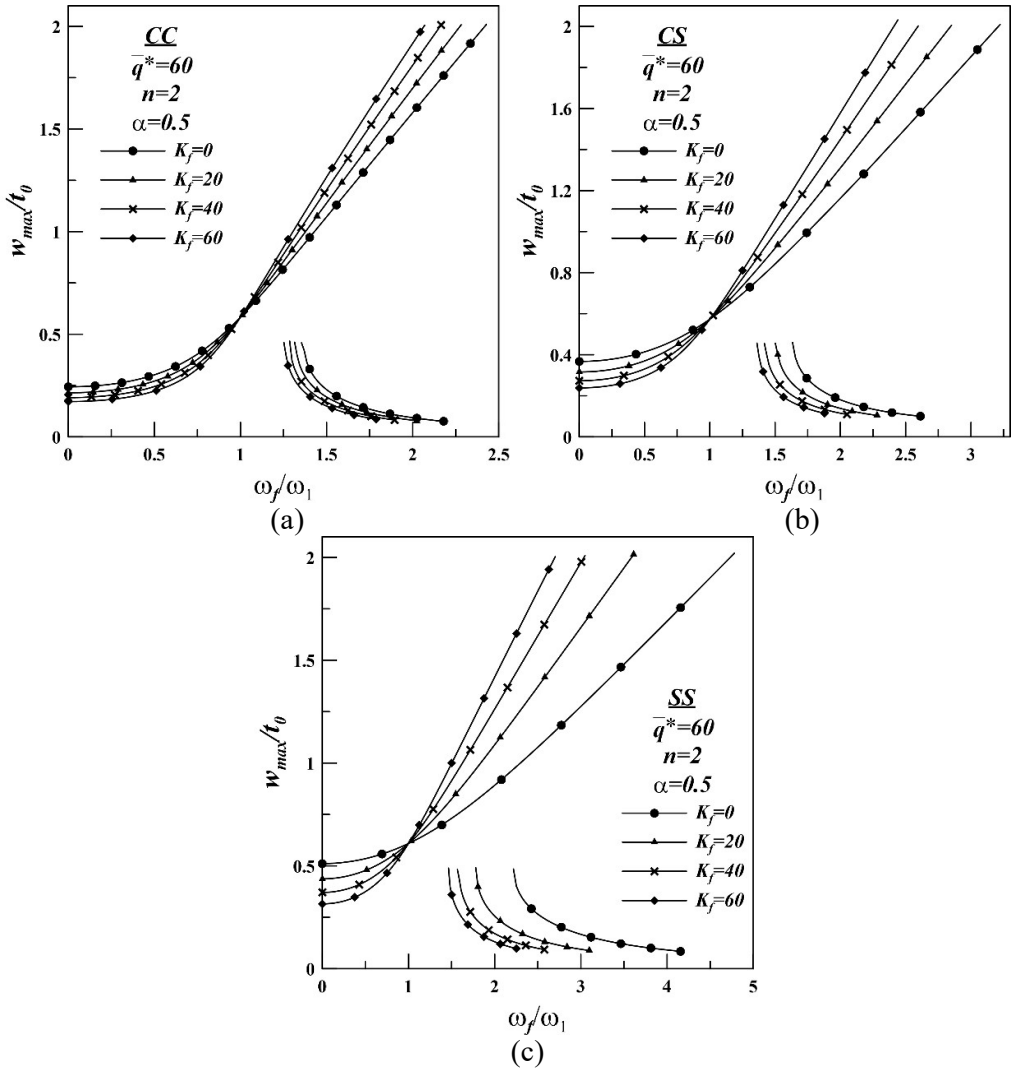

Figure 5.17: Effects of the foundation stiffness on frequency response for (a) CC beam (b) CS beam and (c) SS beam

It is evident from the figures that the general behaviour of the frequency response curves is similar. In all the cases two separate response branches are visible. In one branch, response amplitude monotonically increases with excitation frequency, while, in the other one it decreases with increase in forcing frequency. Interestingly, after a certain frequency

value a multiple response zone is obtained, where, corresponding to one excitation frequency two responses are present. It is also observed that the plots are tilted towards the right of vertical in all three cases. This behaviour can be attributed to the stretching effect associated with large deflection resulting in additional stiffening of the system. Another important observation that can be made from these figures is that, if the excitation amplitude is continuously decreased the amplitude of the response is also going to decrease and at very low excitation amplitude the response curve will tend to almost merge with the backbone curve.

Table 5.13: First dimensionless $\left(\Omega_1 = \omega_1 L^2 \sqrt{\rho_0 A_0 / E_0 I_0}\right)$ natural frequencies of axially graded and non-uniform thick beam on elastic foundation for different foundation stiffness (K_f) considering $L/t_0 = 20$, $n = 2$, $\alpha = 0.5$

	Foundation Stiffness (K_f)			
BC	0	20	40	60
CC	17.4861	18.8479	20.1176	21.3118
CS	12.4992	14.3216	15.9368	17.4027
SS	7.8575	10.5490	12.6815	14.5037

5.4.3.3.2 Effect of the foundation stiffness:

The effect of the foundation stiffness on frequency response is shown in Figure 5.17. The excitation amplitude, gradient parameter, length-to-thickness ratio and taper parameter have been fixed at 60, 2, 20 and 0.5, respectively. Plots are generated considering four dimensionless foundation stiffness values, which are varied from 0 to 60. It is to be noted that foundation stiffness value '0' represents the case where the beam is without any foundation. Table 5.13 shows that, with the increase in foundation stiffness values fundamental natural frequencies increase in magnitude. The trend can be intuitively attributed to overall increase in stiffness of the system. From the figures, it is clear that, for CC beam (Figure 5.17(a)) with the increase of the foundation stiffness the response amplitude decreases in the low excitation frequency zone. But the trend is completely opposite in the higher frequency zone. Similar trends can be seen for CS and SS beam (Figures 5.17(b)-5.17(c)) as well. There appears to be cross-over point in the response behaviour around $\omega_f/\omega_1 = 1.00$ in each case. Another important observation is that the response curves of SS beam are more diverging in the non-dimensional plane from each other than the other two boundaries. Here, with change in foundation stiffness, four

amplitude decreases in the low excitation frequency zone. But the trend is completely opposite in the higher frequency zone. Similar trends can be seen for CS and SS beam (Figures 5.17(b)-5.17(c)) as well. There appears to be cross-over point in the response behaviour around ω_f/ω_1 = 1.00 in each case. Another important observation is that the response curves of SS beam are more diverging in the non-dimensional plane from each other than the other two boundaries. Here, with change in foundation stiffness, four different backbone curves would be obtained. These backbone curves are not included in the figures in order to make them less cluttered.

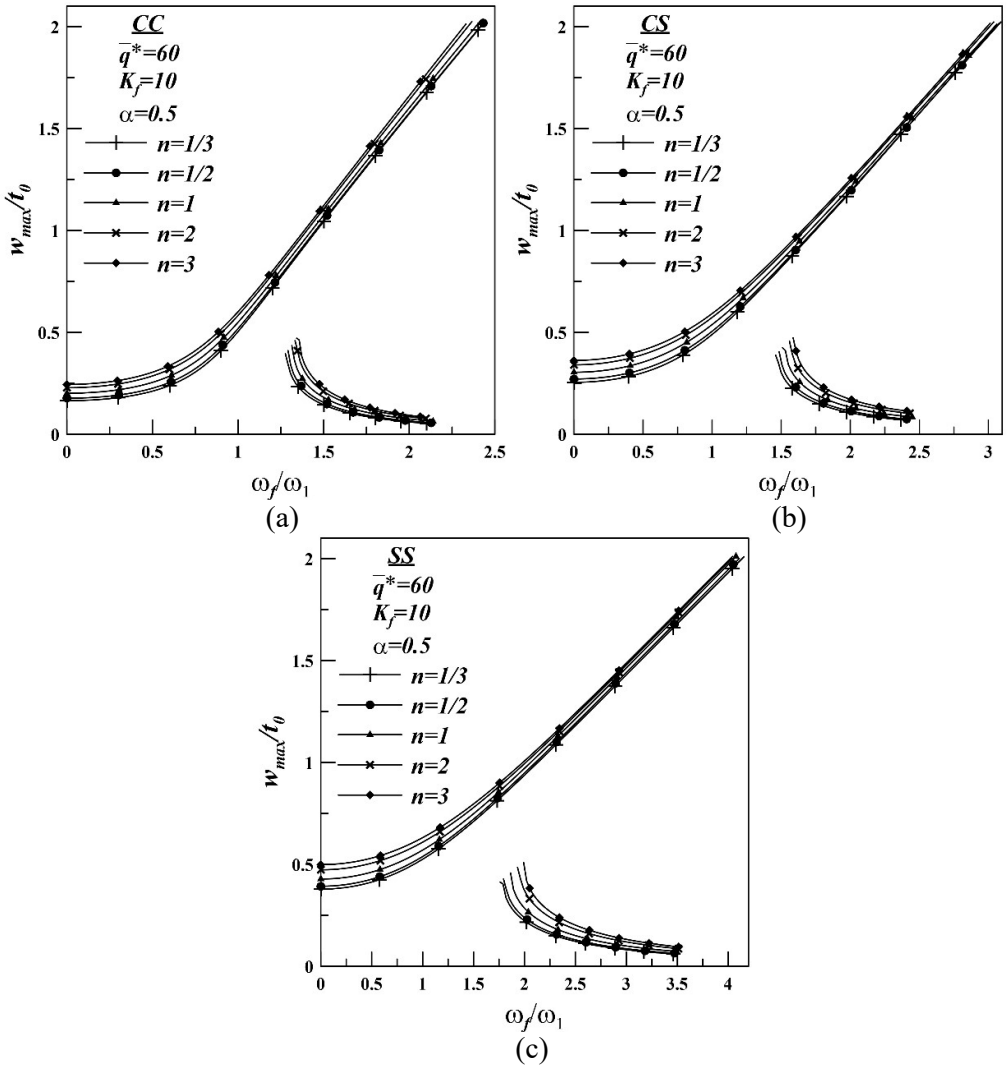

Figure 5.18: Effects of the gradation index on frequency response for (a) CC beam (b) CS beam and (c) SS beam

Table 5.14: First dimensionless $\left(\Omega_1 = \omega_1 L^2 \sqrt{\rho_0 A_0 / E_0 I_0}\right)$ natural frequencies of axially graded and non-uniform thick beam on elastic foundation for different gradient parameter (n) considering $L/t_0 = 20$, $K_f = 10$, $\alpha = 0.5$

	Gradient parameter (n)				
BC	**1/3**	**1/2**	**1**	**2**	**3**
CC	18.1331	17.9085	17.8151	18.1798	18.4563
CS	13.8023	13.5641	13.3417	13.4413	13.5562
SS	9.4313	9.4069	9.3503	9.3011	9.2918

5.4.3.3.3 Effects of the gradation index:

The effects of the gradation parameter on frequency response are shown in Figure 5.18. The excitation amplitude, foundation stiffness, length-to-thickness ratio and taper parameter have been fixed at 60, 10, 20 and 0.5 respectively. Plots are generated considering five gradation parameter, which are varied from 1/3 to 3. From the Figure, it is observed that in case of CC beam (Figure 5.18(a)), with the increase of gradation parameter the response amplitude is increasing in nature. Same trend can be found for the CS (Figure 5.18(b)) and SS beam (Figure 5.18(c)) as well.

Table 5.15: First dimensionless $\left(\Omega_1 = \omega_1 L^2 \sqrt{\rho_0 A_0 / E_0 I_0}\right)$ natural frequencies of axially graded and non-uniform thick beam on elastic foundation for different taper parameter (α) considering $L/t_0 = 20$, $K_f = 10$, $n = 2$

	Taper parameter (α)			
BC	0.0	0.2	0.4	0.6
CC	24.6796	22.1867	19.5582	16.7477
CS	16.0843	15.0841	14.0113	12.8443
SS	11.3748	10.4817	9.6674	8.9706

5.4.3.3.4 Effect of taper parameter:

Figure 5.19 shows the effect of taper parameter on forced vibration response of AFG Timoshenko beam for different boundaries. The excitation amplitude, foundation stiffness, length-to-thickness ratio and gradient parameter have been fixed at 60, 10, 20 and 2 respectively. The taper parameter is varied from 0.0 to 0.6 with intermediate values of 0.2 and 0.4. It is to be noted that taper parameter 0.0 represents the case of uniform beam. From Table 5.15 it is observed that the fundamental natural frequencies decrease with the increase of taper parameter values. This type of trend is found due to removal of material with increasing taper which further contributes to the reduction of beam stiffness. From the

figures, it is observed that with the increase of taper parameter values, the amplitude of the response is increasing in nature in the low frequency domain, whereas, the trend is reversed at higher frequency range. In these sets of figures, the backbone curves for the four individual cases are not incorporated for the sake of better clarity.

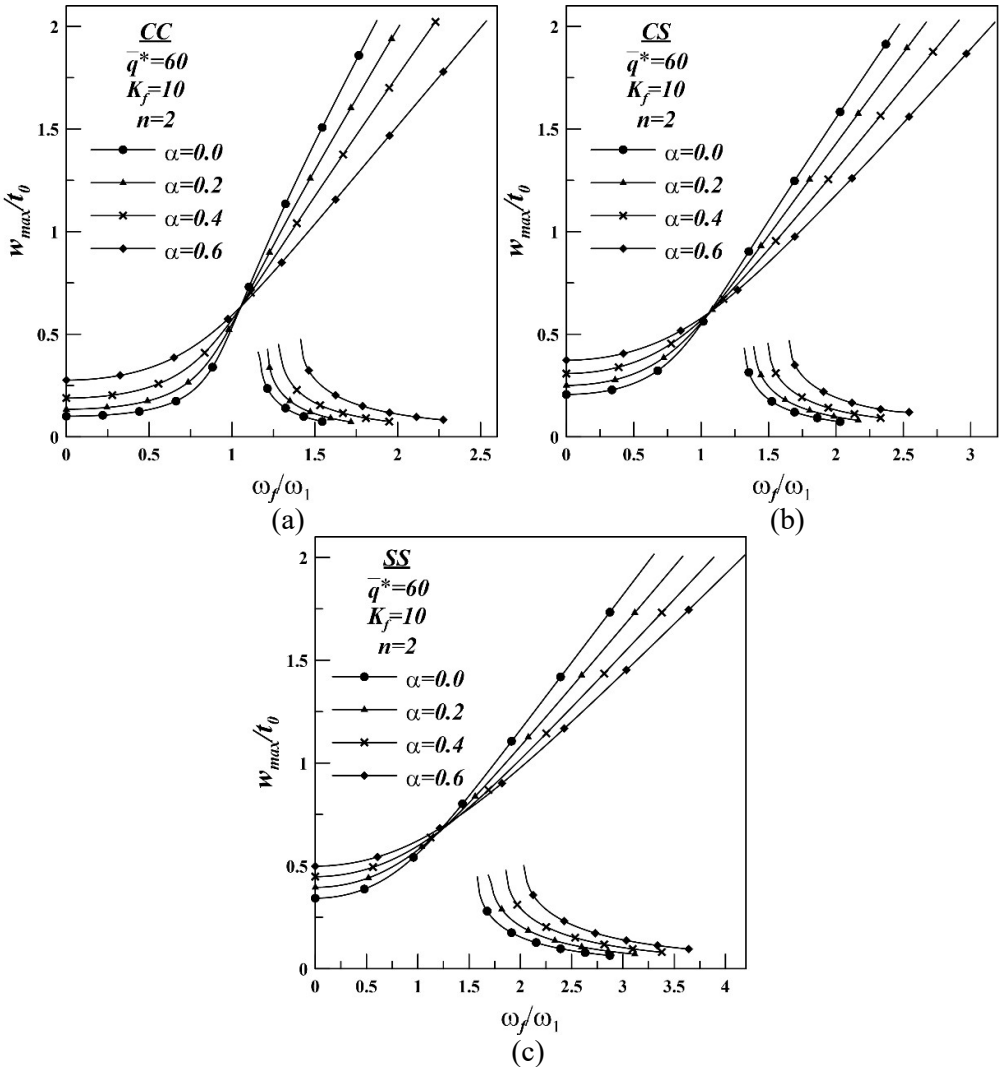

Figure 5.19: Effects of the taper parameter on frequency response for (a) CC beam (b) CS beam and (c) SS beam

5.4.3.3.5 Effects of the length-to-thickness ratio:

The effects of the length-to-thickness ratio on frequency response are shown in Figure 5.20. The excitation amplitude, foundation stiffness, gradation parameter and taper parameter has been fixed at 60, 10, 2 and 0.5, respectively. Plots are generated considering

four different length-to-thickness ratio values, which are 5, 20, 25 and 100. It is important to note that the beam with length-to-thickness ratio value 5 indicates that it is a very thick beam, whereas beam with length-to-thickness ratio value 100 resembles as a very thin beam. From Table 5.16, it is observed that the fundamental frequency increases with the increase of length-to-thickness ratio value. From Figure 5.20, it is noted that, with the increase of length-to-thickness ratio value, the response amplitude is decreasing in nature for all three boundary conditions. In case of CC beam (Figure 5.20(a)) the effect is more prominent than the other two. CS beam shows the moderate effect (Figure 5.20(b)), whereas this is negligible for SS beam, in which all the branches of curves for four different length-to-thickness ratio values are coinciding as a single curve (Figure 5.20(c)). However, it is important to keep in mind that these trends are obtained in the non-dimensional plane. In terms of dimensional values there is bound to be sufficient differences between the curves corresponding to different length to thickness ratios.

Table 5.16: First dimensionless $\left(\Omega_1 = \omega_1 L^2 \sqrt{\rho_0 A_0 / E_0 I_0}\right)$ natural frequencies of axially graded and non-uniform thick beam on elastic foundation for different Length-to-thickness ratio (L/t_0) considering $\alpha = 0.5$, $K_f = 10$, $n = 2$

	Length-to-thickness ratio (L/t_0)			
BC	5	10	25	100
CC	16.2471	17.7276	18.2368	18.3334
CS	12.5017	13.2315	13.4674	13.5112
SS	9.0525	9.2481	9.3077	9.3206

5.4.3.4 Operational Deflected Shape (ODS):

The effects of excitation frequency on the operational deflected shape (ODS) is studied and furnished in Figure 5.21. For that purpose, a CC beam is considered with taper parameter of 0.5. The excitation amplitude, foundation stiffness, length-to-thickness ratio and gradient parameter have been fixed at 60, 10, 20 and 2, respectively. Figure 5.21(a) shows the representative points on the frequency-response curve at different frequency-amplitude combinations. On the increasing curve, the start of the multi-response zone is denoted by point 'a' and point 'b' represents the point at $w_{max}/t_0 = 2$. Point 'a1' and 'b1' are obtained on the same excitation frequency level as 'a' and 'b' respectively but on lower curve. The operational deflected shape corresponding to these representative points are shown in Figure 5.21(b). The ODS corresponding to different representative points appear similar in nature but with different maximum response amplitude. However, one major

issue can be noted that the response at the lower branch is out of phase with the response in the upper branch.

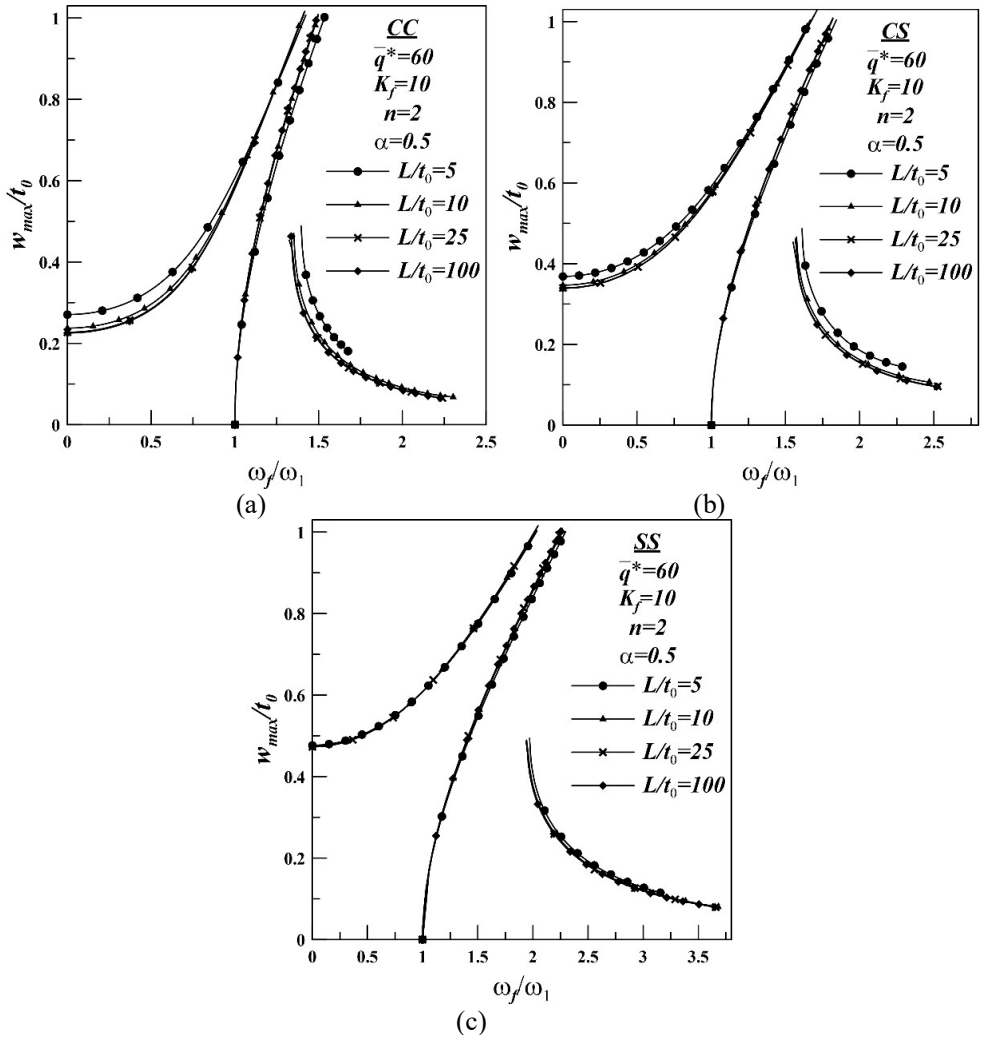

Figure 5.20: Effects of the length-to-thickness ratio on frequency response for (a) CC beam (b) CS beam and (c) SS beam

5.5 Closure:

A non-uniform AFG Timoshenko beam on elastic foundation under pre-loaded condition is analysed. Three different boundary conditions, which are combinations of clamped and simply supported edges, are selected. The elastic foundation, in the present study, is idealized as a set of parallel linear spring of constant stiffness and various values of the foundation stiffness are considered. The primary objective for free vibration study is to find out the effect of loading on the vibration frequencies of the system, whereas for

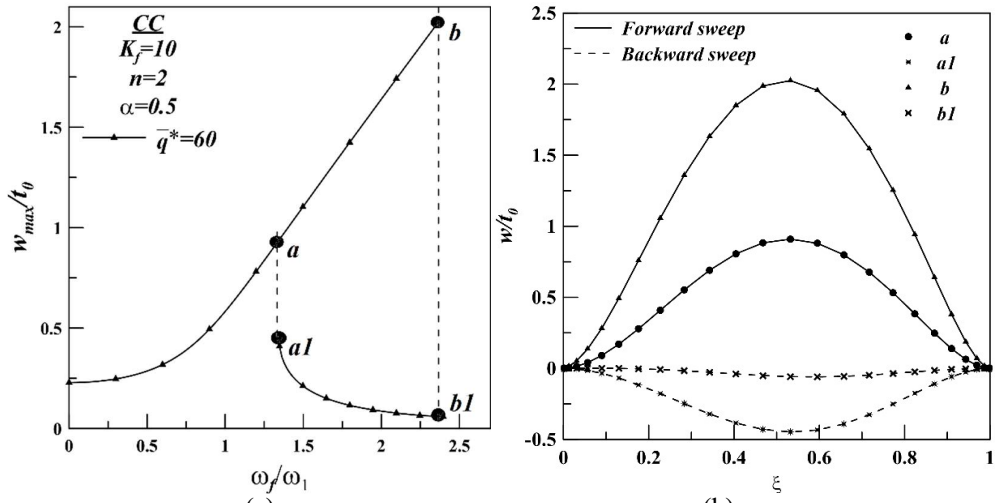

(a) (b)

Figure 5.21: Operational deflected shape (ODS) (a) nonlinear frequency response with representative points (b) deflected shape of the system at corresponding points

forced vibration analysis it is to represent the frequency response under harmonic excitation. The mathematical formulation for free vibration study is such that it sub-divides the problem into two distinct parts. At the initial stage the geometrically nonlinear static problem is solved through an iterative scheme with relaxation. Next, the free vibration problem is formulated as an eigenvalue analysis with statically converged stiffness matrix as an input. Subsequently, forced vibration is taken into account by considering dynamic displacement field and solved using a quasi-Newton method, known as Broyden's method. These problems are formulated using appropriate energy principles. The static analysis is based on total minimum potential energy principle, while the dynamic analyses are based on Hamilton's principle. The methodology of the mathematical formulation is general in nature. It has enough flexibility of solving with other different type of loading pattern, elastic foundation, gradation pattern, taper pattern and end conditions as well. Results generated from the proposed method are compared with previously published results and a certain degree of accuracy is observed in between the two sets of results. Overall, the present methodology and solution procedure are successfully validated, albeit for a system with reduced complexity (as the elastic foundation is not present in the validation problem). New results are furnished for an AFG Timoshenko beam in the normalised loaded natural frequency vs. normalised maximum deflection of the system for free vibration analysis and frequency response curve for forced vibration problem. These results are capable of serving as benchmark results.

Chapter 6

STATIC AND FREE VIBRATION ANALYSIS: AXIALLY FUNCTIONALLY GRADED THIN PLATES ON ELASTIC FOUNDATION

6.1 Introduction:

A plate is a structural element which is characterized by two key properties. First, its geometric configuration is a three-dimensional solid whose thickness is very small when compared with other dimensions. Second, the effects of the loads that are expected to be applied on it only generate stresses whose resultants are, in practical terms, exclusively normal to the element's thickness. Plates are widely utilised structural elements with variety of engineering and industrial applications. Specifically, plates on elastic foundation can be considered as idealisation of various critical and frequently used load bearing components (for example, rail track, bridge decks, rigid pavements, mat and raft foundations etc.). Arising out of its varied applications, both static and dynamic analyses are relevant in case of such structures. In the present chapter, a basic static analysis under transverse loading is performed, followed by a free vibration study.

The nonlinear static problem is solved in the first part to obtain the load-deflection characteristics and deflection shape under loading. The computed stiffness matrix of the system in deflected configuration is used in subsequent dynamic analysis for obtaining eigenvalues and eigenvectors, which provide the natural frequencies and mode shapes, respectively. The static analysis in the first part is based on principle of minimum total potential energy whereas Hamilton's principle is used in formulating the governing equations of free vibration. In static analysis, unknown co-efficient of the governing equations are solved using an iterative method, direct substitution with relaxation scheme, while the free vibration frequencies are solved with the help of intrinsic Matlab solver. The results of both the studies are validated with existing data, albeit for a system with reduced

complicacy. New results corresponding to different combinations of system parameters are furnished and, in absence of previously published results, are capable of serving as benchmark results.

6.2 Geometric and Material Parameters:

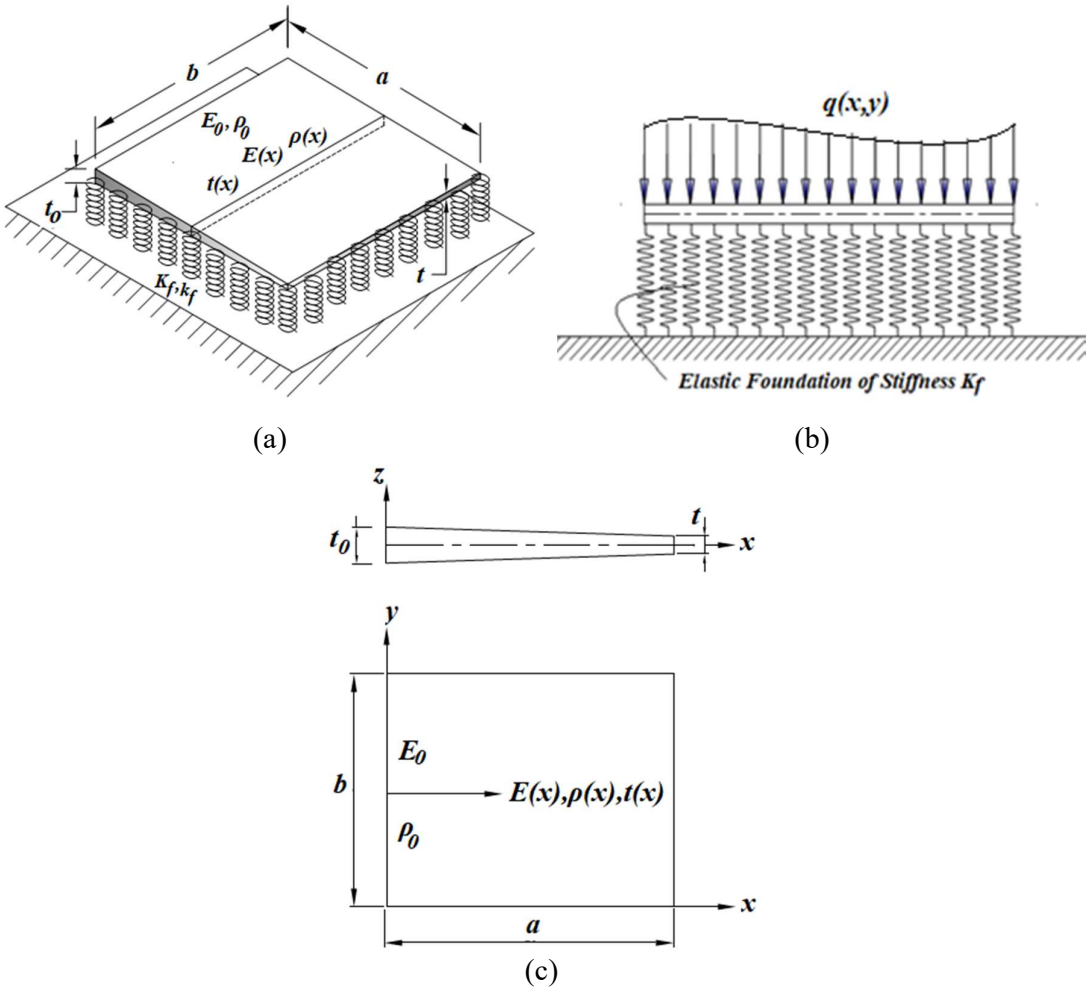

Fig. 6.1: (a) Plate on elastic foundation, (b) loading and elastic foundation and (c) front and top view of the tapered plate

A non-uniform plate with in-plane inhomogeneity is considered to be resting on an elastic foundation. The length and breadth of the plate are a and b, respectively. The stiffness of the elastic foundation is considered as k_f and the foundation is idealized as a set of parallel linear springs as shown in Figure 6.1. The stiffness parameter is normalised according to the following relation, $K_f = a^4 k_f / D$, where, K_f is the non-dimensional

stiffness and $D = E_0 t_0^3 / 12\left(1-\mu^2\right)$. The plate is loaded with uniformly distributed pressure type load of magnitude, $q(x,y)$ according to Figure 6.1(b). The thickness of the plate, $t(x)$, is varying along the axial direction. Similarly, the gradation of the elastic modulus, $E(x)$, and density, $\rho(x)$, are considered in axial direction as shown in Figure 6.1(c). It should be noted here that both tapering of the plate and material gradation is considered along only one coordinate (x) direction, while along the orthogonal direction (y) they are taken to be uniform or constant. However, the present formulation and solution technique are definitely capable of handling non-uniformity in thickness along either direction individually or in combination. Similarly, material gradation in two orthogonal directions can also be taken care of as long as they are expressible in terms of mathematical relations dependent on the coordinates.

One important aspect of the system under consideration is the boundary conditions. It is well known that there are three classical end conditions, i.e., clamped (C), simply supported (S) and free (F) ends and a total of 21 different boundary conditions can be derived for a plate, which, obviously, has four edges. The notations used to denote the boundary conditions are four letters representing the individual end conditions sequentially starting with the edge along y-axis and proceeding counter-clockwise.

6.3 Nonlinear static analysis:

A geometrical nonlinear static analysis is performed for an in-plane inhomogeneous (axially graded) tapered plate on elastic foundation under transverse loading. Governing set of equations of the system is obtained through appropriate energy principle and the derived nonlinear equations are handled through an iterative method known as direct substitution method. The geometric nonlinearity is introduced by considering nonlinear strain-displacement relations that incorporate stretching of mid-plane of the plate into the system. The effect of the elastic foundation is represented through load vs maximum deflection plot and deflected shape plots.

The successful formulation of static deflection problem and subsequent implementation of the solution methodology serves as a stepping stone to the large amplitude dynamic analysis axially graded tapered plates on elastic foundation. In the present thesis, computation of large amplitude vibration frequencies (or loaded natural

frequencies) is conducted by executing a static analysis under external transverse loading, followed by an eigen value problem corresponding to the deformed system stiffness. So, the significance of the work presented in this section is that it establishes the basic kernel which is extended to perform large amplitude free vibration analysis.

6.3.1 Mathematical formulation:

Formulation is performed entirely in normalized domain defined by normalized coordinate parameters, which are represented as $\xi = x/a$ and as $\eta = y/b$. Numerical values

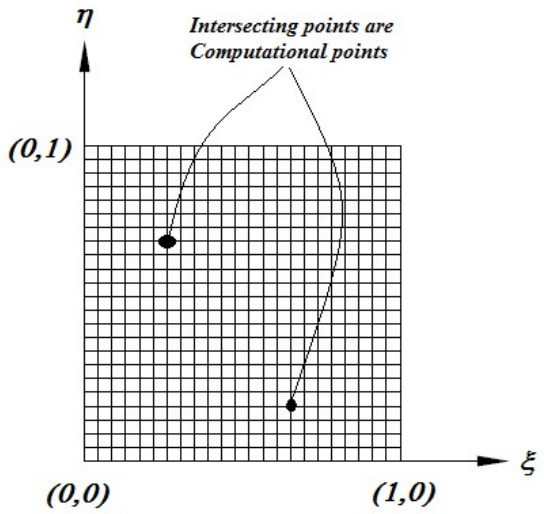

Figure 6.2: Computational points in the domain

of ξ and η vary from 0 to 1. The computational domain of the present study consists of a grid of computational points. In order to create this grid, points are generated along normalized ξ and η direction and constant ξ and constant η lines are drawn. Intersection points between these two sets of lines provide the computational reference points (as shown in Figure 6.2), where all displacement fields and their respective derivatives are evaluated.

The present formulation considers large deflection induced due to geometric nonlinearity (as already mentioned), which implies that effect of stretching of mid-plane of the plate must be incorporated besides the effect of pure bending. So, the total strain energy of the plate consists of strain energy of plate due to pure bending (U_b) and strain energy of plate due to stretching (U_s). These strain energies can be expressed in terms of axial strains corresponding to bending and stretching and for the present analysis Von Karman type

strain-displacements relations are considered. On the other hand, the foundation on which the plate rests gives rise to another component of strain energy (U_f). So, total strain energy *(U)* of the system is represented as,

$$U = U_b + U_s + U_f \tag{6.1}$$

The expression of U_b, U_s and U_f of the system can be written as,

$$U_b = \frac{a}{2\left(1-\mu^2\right)}\int_0^1\int_0^1\left[\left\{\frac{1}{a^2}\left(\frac{\partial^2 w}{\partial\xi^2}\right)+\frac{1}{b^2}\left(\frac{\partial^2 w}{\partial\eta^2}\right)\right\}^2+\frac{2(1-\mu)}{a^2b^2}\left\{\left(\frac{\partial^2 w}{\partial\xi\partial\eta}\right)^2-\left(\frac{\partial^2 w}{\partial\xi^2}\right)\left(\frac{\partial^2 w}{\partial\eta^2}\right)\right\}\right]E(\xi)I(\xi)\,d\xi d\eta \tag{6.2a}$$

$$U_s = \frac{a}{2\left(1-\mu^2\right)}\int_0^1\int_0^1\left[\begin{array}{l}\frac{1}{a^2}\left(\frac{\partial u}{\partial\xi}\right)^2+\frac{1}{a^3}\left(\frac{\partial u}{\partial\xi}\right)\left(\frac{\partial w}{\partial\xi}\right)^2+\frac{1}{b^2}\left(\frac{\partial v}{\partial\eta}\right)^2 \\ +\frac{1}{b^3}\left(\frac{\partial v}{\partial\eta}\right)\left(\frac{\partial w}{\partial\eta}\right)^2+\frac{1}{4}\left\{\frac{1}{a^2}\left(\frac{\partial w}{\partial\xi}\right)^2+\frac{1}{b^2}\left(\frac{\partial w}{\partial\eta}\right)^2\right\}^2+ \\ 2\mu\left\{\frac{1}{ab}\left(\frac{\partial u}{\partial\xi}\right)\left(\frac{\partial v}{\partial\eta}\right)+\frac{1}{2a^2b}\left(\frac{\partial v}{\partial\eta}\right)\left(\frac{\partial w}{\partial\xi}\right)^2+\frac{1}{2ab^2}\left(\frac{\partial u}{\partial\xi}\right)\left(\frac{\partial w}{\partial\eta}\right)^2\right\} \\ +\frac{1-\mu}{2}\left\{\begin{array}{l}\frac{1}{b^2}\left(\frac{\partial u}{\partial\eta}\right)^2+\frac{2}{ab}\left(\frac{\partial u}{\partial\eta}\right)\left(\frac{\partial v}{\partial\xi}\right)+\frac{1}{a^2}\left(\frac{\partial v}{\partial\xi}\right)^2 \\ +\frac{2}{ab^2}\left(\frac{\partial u}{\partial\eta}\right)\left(\frac{\partial w}{\partial\xi}\right)\left(\frac{\partial w}{\partial\eta}\right)+\frac{2}{a^2b}\left(\frac{\partial v}{\partial\xi}\right)\left(\frac{\partial w}{\partial\xi}\right)\left(\frac{\partial w}{\partial\eta}\right)\end{array}\right\}\end{array}\right]E(\xi)A(\xi)\,d\xi d\eta \tag{6.2b}$$

$$U_f = (ab)K_f\int_0^1\int_0^1(w\partial w)\,d\xi d\eta \tag{6.2c}$$

Potential energy due to external load *(V)* of the system can be expressed as,

$$V = (ab)\int_0^1\int_0^1(qw)\,d\xi d\eta \tag{6.3}$$

where, w, u and v are assumed displacement fields in the transverse (w) and in plane (u and v) directions. τ is the time co-ordinate. In equation (6.2) parameters such as elastic modulus,

density as well as cross-sectional area and moment of inertia appear within the integration sign to take care of the material gradation and tapering of the plate.

The static displacement fields (w, u and v) are assumed as linear combinations of orthogonal admissible functions (ϕ, α, β) and unknown coefficients (d_i) as shown,

$$w(\xi,\eta,\tau) = \sum_{i=1}^{nw} d_i \phi_i(\xi,\eta) \tag{6.4a}$$

$$u(\xi,\eta,\tau) = \sum_{i=nw+1}^{nw+nu} d_i \alpha_{i-nw}(\xi,\eta) \tag{6.4b}$$

$$v(\xi,\eta,\tau) = \sum_{i=nw+nu+1}^{nw+nu+nv} d_i \beta_{i-nw-nu}(\xi,\eta) \tag{6.4c}$$

where, nw, nu and nv are number of orthogonal functions of the displacement field w, u and v respectively. It is important to note that ϕ, α, β are kinematically admissible functions, i.e. they satisfy the following conditions: continuous and differentiable within the domain and satisfy the boundary conditions. So, appropriate start functions for these sets must be chosen in such a manner that they comply with the flexural and membrane boundary conditions of the plate. Equation (6.4) clearly indicates that these functions are dependent on the two coordinate directions and they are obtained through the process described in the following paragraph.

The first functions in these sets are known as the start function or basis and these 2D functions are derived dimensional (1D) functions corresponding to the two coordinate directions. For example, for a plate with SSSS end condition, the plate (2D) start function are generated from the ordered mortification of 1D start function of SS and SS in two normalized coordinate direction ξ and η, respectively. These 1-D start functions for transverse displacement are beam deflection functions derived from static deflection shape of the beam, corresponding to the boundary condition of the plate along the particular coordinate axis. The higher order functions are generated from the start functions numerically by following Gram-Schmidt orthogonalization procedure. Objective of the numerical implementation of Gram Schmidt orthogonalization scheme is to determine a set of orthogonal functions (admissible) in the interval $0 \le \xi, \eta \le 1$, provided the first function

of the set is known. Similarly, the functions for the in-plane boundary conditions are also obtained. In all the cases the start function is chosen to satisfy zero displacement condition at the edges of the plate. It should be pointed out that at the free end of the plate transverse displacements are unrestricted, but the in-plane boundary condition is immovable, i.e., in-plane displacements are restricted.

The starting point for the static formulation is the minimum total potential energy principle, mathematically expressed in equation (6.5). The governing set of equations is derived from the above-mentioned principle by substituting the appropriate energy functionals and approximate displacement fields.

$$\delta\left(U+V\right)=0 \tag{6.5}$$

The governing equation of the system in matrix form is represented in equation (6.6), where [K] is the stiffness matrix, {f} is the load vector, while {d} is the vector of unknown coefficients.

$$\left[K\right]\left\{d\right\}=\left\{f\right\} \tag{6.6}$$

Due to consideration of large deflection, along with the bending effect stretching effect is also present in the current formulation and the stiffness matrix can be broken up into three distinct parts. These parts are stiffness matrix due to bending [K^b], stretching [K^m] and elastic foundation [K^f] respectively. The form and individual elements of stiffness matrices and load vector are shown in Appendix.

6.3.2 Solution procedure:

It can be observed from the stiffness matrix elements that certain terms in the stretching part of the matrix contain the unknown coefficients (d). This implies that the stiffness matrix has become a function of the undetermined parameters and hence equation (6.6) is undoubtedly nonlinear in nature. Approximate solution for the unknown coefficients (d_i) is obtained with the help of an iterative technique, known as direct substitution with successive relaxation. As with most general approximate techniques the method is dependent on an initial guess. At the end of the static analysis the displacement field corresponding to transverse load is completely known along with the deformed system

stiffness. The techniques and solution procedures used are similar to those presented in relation to analysis of beams in Chapter 3 and are omitted here for the sake of conciseness.

6.3.3 Result and discussion:

In the static problem, non-linear structural behaviour of non-uniform AFG plate on elastic foundation is carried out considering clamped (CCCC) and simply supported (SSSS) end condition under pressure type of loading. This two boundary conditions are used for selecting the base functions for the transverse displacement (w) where as for the axial displacement (u) the membrane boundary conditions are used. The in-plane displacement at the boundaries are assumed as zero. The start functions for CCCC and SSSS boundary condition are tabulated in Table 6.1.

Table 6.1: Start functions for CCCC and SSSS boundary conditions

End conditions	Start functions
CCCC	$\{\xi(1-\xi)\}^2 \times \{\eta(1-\eta)\}^2$
SSSS	$\sin(\pi\xi) \times \sin(\pi\eta)$
Inmovable	$\xi(1-\xi) \times \eta(1-\eta)$

The thickness of the plate, $t(x)$, varying (parabolic) along the axial direction, is expressed as, $t(\xi) = t_0(1-\alpha\xi^2)$, where, t_0 and α are root thickness and taper parameter respectively. The geometric dimensions of the plate are taken as, $a = b = 0.4$ m and $t_0 = 0.0025$ m. The taper parameter for the parabolic taper pattern of the plate is considered as $\alpha = 0.2$. Similarly, the gradation of the elastic modulus, $E(x)$, and density, $\rho(x)$, are considered in axial direction, these are expressed mathematically by, $E(\xi) = E_0(1+\xi)$ and $\rho(\xi) = \rho_0(1+\xi+\xi^2)$. In this case, the corresponding root values are E_0 and ρ_0, respectively. The material properties at root side of the plate are considered as, $E_0 = 210$ GPa, $\rho_0 = 7850$ kg/m^3 and $\mu = 0.3$, which resemble the material properties of mild steel. The non-dimensional elastic foundation stiffness [$K_f = a^4 k_f / D$] values for each result are taken as, $K_f = 0$, 100, 1000 and 10000, respectively. Here, k_f is dimensional value of stiffness and $D = E_0 t_0^3 / 12(1-\mu^2)$. It is to be noted that in the present study results are

generated when dimensionless maximum amplitude (w_{max}/t_0) is less than 2.0 to minimize the computation time.

6.3.3.1 Convergence study:

Number of orthogonal functions along a coordinate direction is selected as 5. Hence total number of functions corresponding to a particular displacement is 25 (5×5). Number of Gauss points (*ng*) along a coordinate direction is taken as 24 and thus, total number of computational points within the domain comes out to be 24×24. The numbers quoted here are outcomes from the convergence study undertaken and the results of the study are depicted in Figure 6.3., An axially graded CCFF plate, in which linear material property

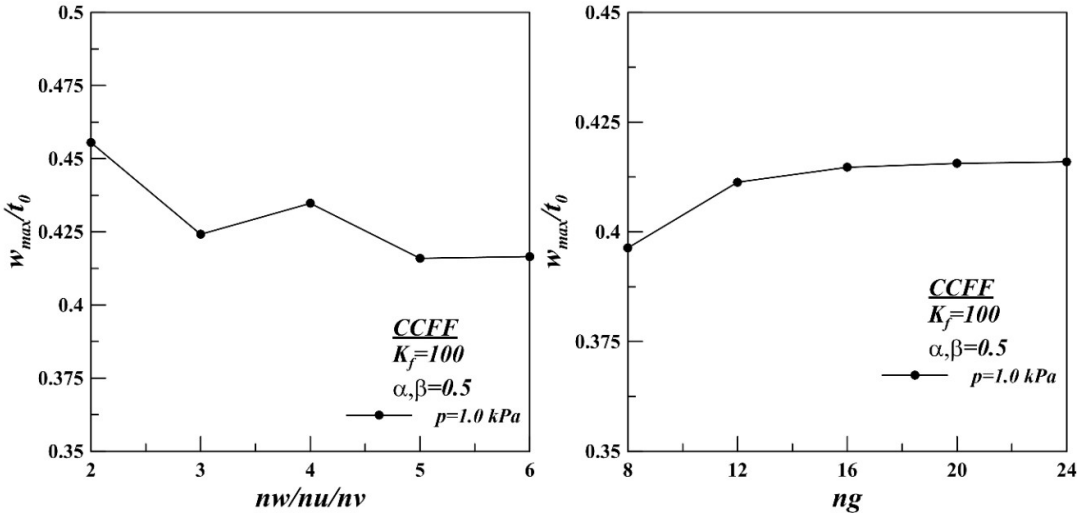

Figure 6.3: Convergence study for (a) no. of orthogonal functions (b) gauss point

(i.e. elastic modulus and density) gradation [$E(\xi) = E_0(1-\beta\xi)$ and $\rho(\xi) = \rho_0(1-\beta\xi)$] and linear tapering of the thickness, [$t(\xi) = t_0(1-\alpha\xi)$] in the axial direction (with taper parameter, α, and material gradation parameter, β, of 0.5) on foundation (K_f = 100) is analysed for maximum normalised deflection when subjected to uniformly distributed transverse load of 1 kPa. Figure 6.3(a) and 6.3(b) show the convergence results for variation in number of orthogonal functions (along a coordinate direction) and number of Gauss points by indicating the change in normalized maximum deflection (w_{max}/t_0) of the system, respectively. The figures sufficiently justify choice of 5 orthogonal functions and 24 gauss points for the present analysis. However, it should be mentioned here that difference in

w_{max}/t_0 values for *nw/nu/nv* = 5 and 6 is minimal, but there is considerable increase in computation time. Hence, number of functions along each coordinate direction is chosen as 5.

6.3.3.2 Validation study:

The present methodology and solution procedure is validated with the results of previously published articles of Timoshenko and Woinowsky-Krieger (1964). It must be mentioned here that the validation is carried out for a simplified system. To the best of author's knowledge there is no established results for the specific type of problem under consideration. Hence, the validation is carried out by comparison with an unsupported uniform homogeneous plate under transverse loading. In the present formulation, the parameters catering to tapering of the plate (α), material inhomogeneity (β) along with foundation stiffness (k_f) is set to zero in order to achieve equivalence. From Figure 6.4, it can be observed that the current results match satisfactorily with the established results.

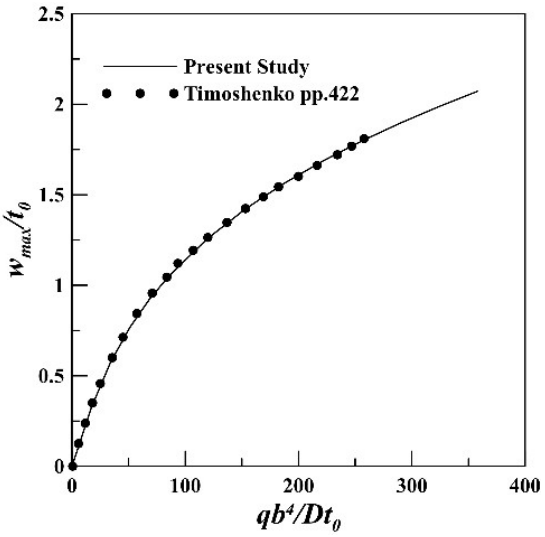

Figure 6.4: Comparison plot of load vs deflection curve

6.3.3.3 Load vs. amplitude plot:

In Figure 6.5**,** the load vs. deflection curves are shown in dimensionless load and deflection plane for CCCC and SSSS end conditions, respectively. The effects of the foundation stiffness on the deflection amplitude of the system can be found through this plot. Four curves are considered corresponding to different spring stiffness values (K_f = 0, 100, 1000 and 10000). It can be observed that with the increase of the foundation stiffness

value the curve gradually shifts towards the right side of the non-dimensional plane. Such type of results are found due to the reason that increase of foundation stiffness make the system more stiff to deflection under the application of same load. As a usual consequence of the increase in stiffness the load bearing capacity of the system also increases. It is also observed that for the same load application the deflection of the SSSS plate is more than the CCCC plate. This type of occurrence happen due to the reason that the CCCC plate is stiffer to deflect as compared to SSSS plate.

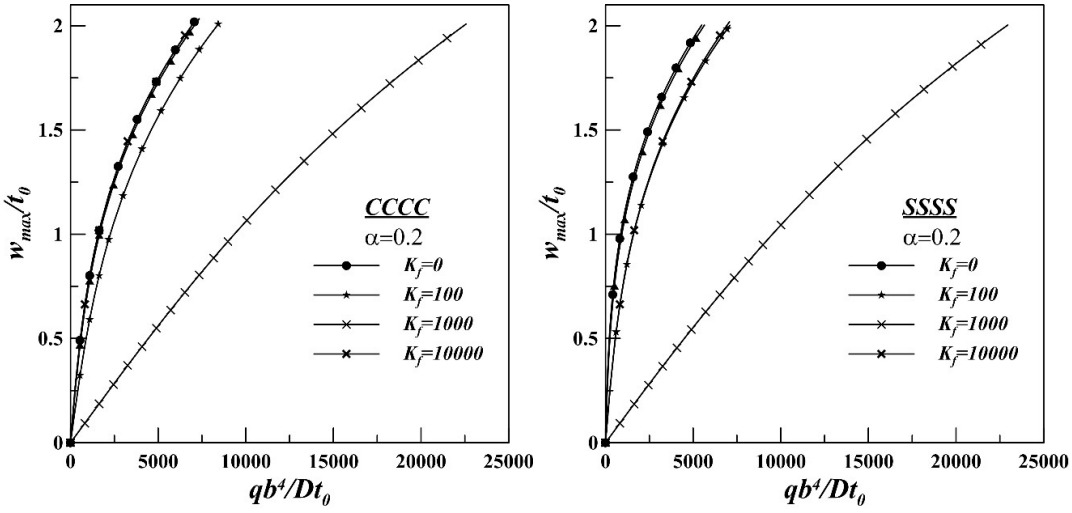

(a) (b)

Figure 6.5: Load vs deflection plot for different boundary conditions (a) CCCC and (b) SSSS

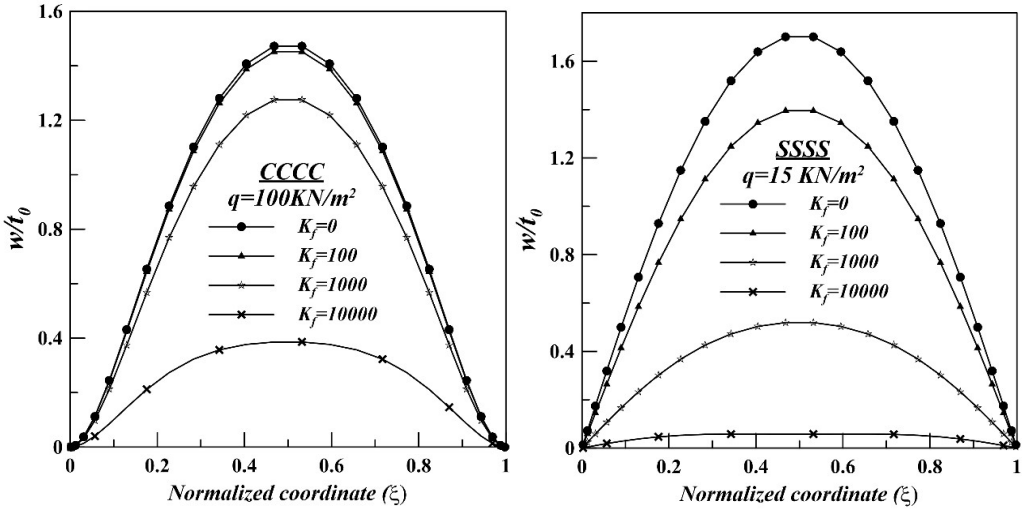

(a) (b)

Figure 6.6: Deflected shape of the plate at centreline along axial direction for different boundary conditions (a) CCCC and (b) SSSS.

6.3.3.4 Deflected shape plot:

Figure 6.6 represents the deflected shape of the plate centreline along axial (ξ) direction for four different foundation stiffness values. These plots are obtained taking a specific external load value of 100 KN/m^2 and 15 KN/m^2 for CCCC and SSSS plate, respectively. From the plot, it is seen that deflection is maximum near the middle of the plate. It is also observed that at zero value of stiffness the deflection is maximum and it is minimum when stiffness is maximum. Again it is also clear from the plots that SSSS plate deflect more than the CCCC plate under same load application.

6.4 Nonlinear free vibration analysis:

Effect of geometric nonlinearity on free vibration behaviour of a non-uniform in-plane inhomogeneous plate on elastic foundation is studied in the present section. The formulation is semi-analytical displacement based and it is carried out in two distinct steps. First, the static problem is solved to find out the unknown displacement field by using minimum total potential energy principle. Secondly, subsequent dynamic problem is set up as an eigenvalue problem on the basis of the known displacement field. The governing set of equations of the dynamic problem is obtained by using Hamilton's principle. The converged stiffness matrix from the static analysis is utilised at this step to set up the dynamic problem governing equations. Solution to this set of equations is obtained with the help of intrinsic Matlab solver. The results of the present method are validated with existing data.

It is well known that large amplitude free vibration behaviour, represented through backbone curves, is different from linear free vibration. Amplitude dependency of vibration frequencies is an important nonlinear feature, which is not exhibited in the linear case. Hence, backbone curve, which is the nonlinear frequency-vibration amplitude plot, should be studied in detail in order to understand the large amplitude behaviour of the system. A typical phenomenon that is sometimes observed in relation to backbone curves is mode switching, where backbone curves corresponding to two different modes intersect. The linear and nonlinear mode shapes are also furnished to support the presence of switching phenomenon. The effects of the boundary conditions and non-uniformity of the plate shape are also highlighted.

6.4.1 Mathematical formulation:

To derive the governing set of equations in the dynamic analysis, Hamilton's principle is utilized, which is expressed as,

$$\delta\left(\int_{\tau_1}^{\tau_2}\left(T-U-V\right)d\tau\right)=0 \tag{6.7}$$

Here, T is the kinetic energy of the system and U represents the strain energy of the system with respect to deflected configuration. U has the same expression as equations (6.1) and (6.2), while, kinetic energy (T) expression for the present system is furnished in equation (6.8). In expression (6.3) potential of external forces *(V)* has been reduced to zero as a free vibration scenario is under consideration.

$$T=\frac{a}{2}\int_0^1\int_0^1\left\{\left(\frac{\partial w}{\partial\tau}\right)^2+\left(\frac{\partial u}{\partial\tau}\right)^2+\left(\frac{\partial v}{\partial\tau}\right)^2\right\}\rho(\xi)A(\xi)d\xi d\eta \tag{6.8}$$

The assumed dynamic displacement fields, which are considered to be separable in space and time, are expressed by,

$$w(\xi,\eta,\tau)=\sum_{i=1}^{nw}d_i\phi_i(\xi,\eta)e^{j\omega\tau} \tag{6.9a}$$

$$u(\xi,\eta,\tau)=\sum_{i=nw+1}^{nw+nu}d_i\alpha_{i-nw}(\xi,\eta)e^{j\omega\tau} \tag{6.9b}$$

$$v(\xi,\eta,\tau)=\sum_{i=nw+nu+1}^{nw+nu+nv}d_i\beta_{i-nw-nu}(\xi,\eta)e^{j\omega\tau} \tag{6.9c}$$

Here, the displacement field is made up of a spatial part, where, the kinematically admissible orthogonal functions are identical to those considered in the static analysis at Section 6.2.2, and a temporal part. However, in this expression, $\{d\}$ represents a set of unknown parameters which are different from those considered in the static analysis. These unknown parameters denote the eigenvectors in matrix form and they represent the contribution of individual spatial functions on different vibration modes. Here, ω is the natural frequency of the system and τ is the time co-ordinate. Substituting the strain energy

(U) and kinetic energy (T) expressions from equations (6.2) and (6.8) along with the approximate dynamic displacement fields from equations (6.9) into equation (6.7), set of the governing equations are found as,

$$-\omega^2 [M]\{d\} + [K]\{d\} = 0 \tag{6.10}$$

Here, [K] and [M] are stiffness matrix of the system at the deflected configuration and mass matrix, respectively. The details of the elements of the mass matrix are furnished in Appendix.

6.4.2 Solution procedure:

These matrices are completely known as [K] is already solved in the static analysis in Section 6.3.2 and [M] is known from the problem definition. Equation (6.10) represents a standard eigenvalue problem and can be solved through usage of Matlab's intrinsic solver. Square root of the evaluated eigenvalues corresponds to the natural frequencies of the system, whereas, eigenvectors corresponding to the eigenvalues are exploited to obtain mode shapes of the vibrating system.

6.4.3 Result and discussion:

The plate in the present analysis is considered to be tapered one due to wide application of similar structures in the industry. The geometric dimensions of the plate for length and width are taken as, $a = b = 0.4$ m. Linear tapering of the thickness is considered in the axial direction as expressed as, $t(\xi) = t_0(1-\alpha\xi)$, in which t_0 and taper parameter (α) are taken as 0.0025 m and 0.5 respectively. Effect of variation in taper parameter on the large amplitude vibration behaviour is kept outside the purview of the present study. The plate in the present analysis has in-plane inhomogeneity as linear material property (i.e. elastic modulus and density) gradation is considered in the axial direction and these are expressed mathematically by, $E(\xi) = E_0(1-\beta\xi)$ and $\rho(\xi) = \rho_0(1-\beta\xi)$, where, E_0, ρ_0 and gradation parameter (β) are considered as 210 GPa, 7850 kg/m^3 and 0.5, respectively. It is to be pointed out that variation of gradation parameter is not included as part of the present study. Constant value of 0.3 for Poisson ratio (μ) is taken throughout the entire analysis.

The end conditions of the plate are selected in such a manner that at least two opposite edges of the plate are clamped (C) and free (F) end condition. So, herein the obtained end conditions are CCCF, CCFF, CCSF and SCSF respectively. These four different end conditions which are combinations among clamped (C), free (F) and simply supported (S), are selected for the present study. The start functions for these boundary conditions are generated following the similar procedure which is discussed in the Section 6.3.1 and are mentioned in Table 6.2. From these start functions higher order functions are generated following a numerical scheme.

Table 6.2: Start functions for different boundary conditions

End conditions	Start functions
CCCF	$\left\{\xi\left(1-\xi\right)\right\}^2\times\eta^2\left(\eta^2-4\eta+6\right)$
CCFF	$\xi^2\left(\xi^2-4\xi+6\right)\times\eta^2\left(\eta^2-4\eta+6\right)$
CCSF	$\xi^2\left(2\xi^2-5\xi+3\right)\times\eta^2\left(\eta^2-4\eta+6\right)$
SCSF	$\sin\left(\pi\xi\right)\times\eta^2\left(\eta^2-4\eta+6\right)$
Immovable	$\xi\left(1-\xi\right)\times\eta\left(1-\eta\right)$

Table 6.3: Comparison of Linear dimensionless Frequencies $\left(\Omega a^2/\sqrt{\rho_0 t_0/D}\right)$ for different Boundary Conditions

Boundary Condition	Literature	Linear dimensionless Frequencies					
		ω_1	ω_2	ω_3	ω_4	ω_5	ω_6
CCCF	Leissa (1973)	24.012	40.029	63.471	76.745	80.704	116.799
	Saha et al. (2004)	23.934	40.029	63.290	78.065	80.678	118.067
	Present Study	23.869	39.972	63.115	78.000	80.519	117.985
CCFF	Leissa (1973)	6.935	24.038	26.677	47.765	63.031	65.826
	Saha et al. (2004)	6.935	23.934	26.599	47.739	63.885	67.042
	Present Study	6.927	23.944	26.614	47.761	63.866	67.019
CCSF	Leissa (1973)	17.621	36.044	52.060	71.182	74.339	106.294
	Saha et al. (2004)	17.543	36.044	51.853	71.182	75.684	106.398
	Present Study	17.517	36.013	51.780	71.091	75.650	106.181
SCSF	Leissa	12.679	33.068	41.685	63.005	72.398	90.614
	Saha et al	12.679	33.068	41.736	63.083	73.769	91.261
	Present Study	12.680	33.061	41.709	63.051	73.744	91.106

In practical applications plates are seldom supported by classical boundary conditions. Either they are supported by elastic restrain at the end or rested on elastic foundation. To make the problem more realistic, the plate under consideration is assumed

to be resting on an elastic foundation. Five different value of the non-dimensional foundation stiffness ($K_f = a^4 k_f / D$) is consider here. They are 0, 10, 100, 1000 and 10000 respectively. Here, k_f is dimensional value of stiffness and $D = E_0 t_0^3 / 12(1-\mu^2)$ with t_0 = 0.0025 m.

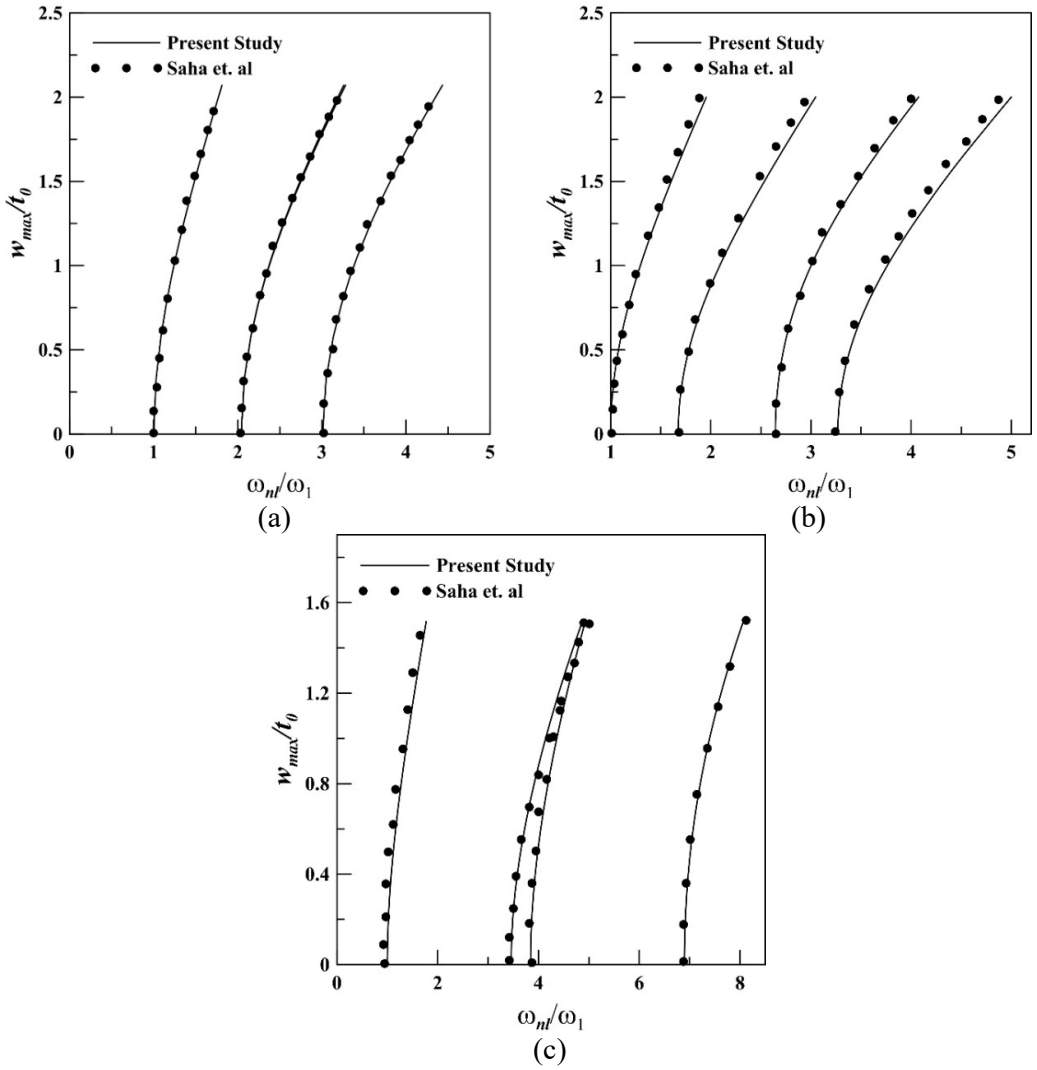

Figure 6.7: Comparison of first four backbone Curves for uniform homogeneous plate corresponding to (a) CCCC, (b) CCCF and (c) CCFF boundary conditions

6.4.3.1 Validation study:

Validation of the present analysis and solution methodology is carried out in the form of comparisons with established results. In this respect results corresponding to inhomogeneous plates with in-plane gradation and elastic foundation are not available in

published literature. Hence, comparative studies are performed for systems with reduced complicacy. First of all, the linear dimensionless frequency parameters $\left(\Omega a^2 / \sqrt{\rho_0 t_0 / D}\right)$ for various boundary conditions are compared with the results of previously published articles of Saha et al. (2004) and Leissa (1973). Here, Ω is dimensional frequency. The system under consideration is homogeneous and uniform plate without elastic foundation. To comply with the system considered in those papers, the taper parameter (α) and gradation parameters (β) are equated to zero. Also, foundation spring stiffness (k_f) is also set to zero to neglect the effect of the elastic foundation. The comparison of linear dimensionless natural frequencies for first six modes is tabulated in Table 6.3 and it is evident that there is a good match between the different sets of results.

As the focus of the present paper is on the backbone curves of the system, the same is also validated through comparisons with published results. Figure 6.7 presents the comparison of first four backbone curves for CCCC, CCCF and CCFF boundary conditions, respectively. It is to be pointed out that in Figure 6.7(a), i.e., in case of backbone curves for CCCC plate, 2nd and 3rd modes are overlapping each other and hence it apparently looks like only 3 curves are present. The figures show that there is satisfactory matching of the results to establish the validity of the present method, although for system with reduced complexity.

6.4.3.2 Natural frequencies:

Results for linear dimensionless natural frequency parameters for first four modes corresponding to different boundary conditions and foundation stiffness are presented in Table 6.4. These results are generated for no load condition, i.e., the intensity of transverse uniformly distributed load is set to 0. As a result, these results are equivalent to linear vibration frequencies. It is observed that for all the cases with the increase in stiffness of the foundation the natural frequency increases. This increment of frequency is due to the fact that stiffer foundation increases the overall stiffness of the system. It is also observed that the rigidity of the plate edges and consequently the boundary conditions significantly affect the free vibration response. That's why the natural frequency in CCCF plate is highest and in CCFF plate is lowest for a fixed value of foundation stiffness.

Table 6.4: Linear dimensionless Frequencies $\left(\Omega a^2/\sqrt{\rho_0 t_0/D}\right)$ for different Boundary Conditions

Boundary Condition	Stiffness of Foundation	Linear dimensionless Frequencies			
		ω_1	ω_2	ω_3	ω_4
CCCF	0	15.82	30.46	39.16	58.47
	10	16.72	30.84	39.55	58.66
	100	23.17	34.08	42.91	60.34
	1000	50.51	60.51	66.23	75.96
	10000	130.05	141.62	153.80	164.41
CCFF	0	6.50	17.86	21.57	35.38
	10	8.40	18.63	22.12	35.71
	100	17.74	24.46	26.69	38.65
	1000	46.34	51.95	57.46	62.74
	10000	127.59	131.54	144.11	151.28
CCSF	0	12.33	27.89	32.84	51.87
	10	13.45	28.30	33.30	52.08
	100	20.82	31.87	37.13	53.99
	1000	48.92	59.54	61.67	71.53
	10000	129.27	138.29	153.22	160.34
SCSF	0	9.73	26.04	27.13	46.31
	10	11.10	26.49	27.68	46.55
	100	19.30	30.30	32.10	48.69
	1000	47.93	57.84	58.89	68.13
	10000	128.74	135.71	152.79	154.13

6.4.3.3 Backbone curves:

Large amplitude vibration behaviour of the system is represented through backbone curves in a non-dimensional plane, where the abscissa and ordinate are normalised frequency and normalised deflection, respectively. Nonlinear frequency (ω_{nl}) is normalised with respect to the fundamental frequency (ω_1) of the system, whereas, the normalised deflection is the ration of maximum deflection (w_{max}) to the root thickness of the plate (t_0). Although the results in the present paper are in a non-dimensional plane, the dimensional values can be obtained with the help of data provided in Table 6.4 and the system (geometric, stiffness and material) parameter values.

6.4.3.3.1 Effect of boundary condition:

The effect of the boundary conditions of the plate on the backbone curves are shown in Figure 6.8, where two separate plots are furnished to demonstrate the first four backbone curves at $K_f = 0$. From the figures, it is observed that for a particular value of foundation

stiffness, the backbone curves obtained in case of SCSF end condition have lesser slope and in the case of CCCF it is higher. This type of occurrence happens due to the reason that the rigidity of the plate edges and consequently the boundary conditions significantly affect the free vibration response.in general, all the backbone curves lean towards the right, which implies that with increase in deflection, the vibration frequencies increase and it is referred to as hardening type nonlinearity. However, from these figures it is not clear whether any of the backbone curves corresponding to a particular boundary condition have intersection with another. In order to study this feature in detail backbone curves for different boundary conditions need to be plotted separately. It should also be mentioned that the backbone curves for the systems represented in the present paper have not been reported previously.

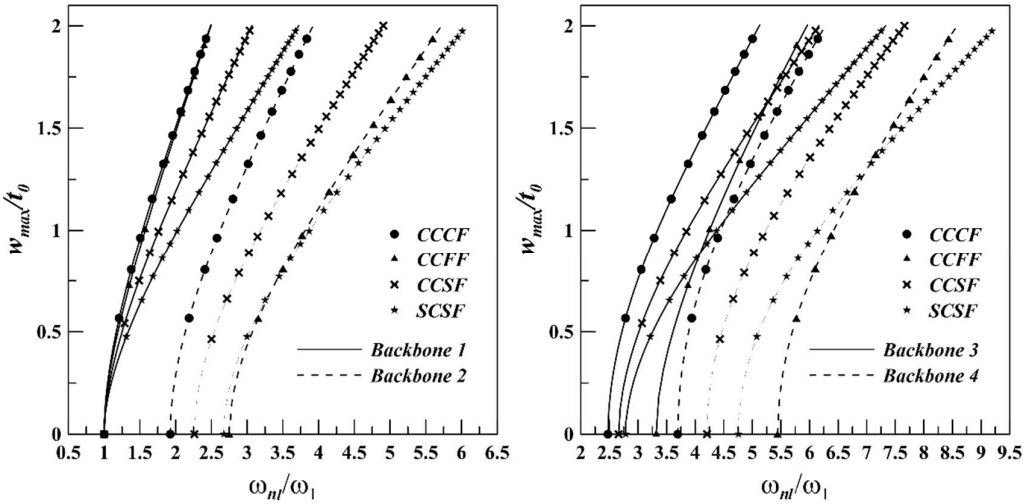

Figure 6.8: Effect of boundary conditions on backbone curves at $K_f = 0$ and $\alpha, \beta = 0.5$

6.4.3.3.2 Mode switching phenomenon:

To detect the mode switching phenomenon, first four backbone curves are plotted in normalised frequency-amplitude plane for each boundary condition corresponding to four foundation stiffness parameter values [K_f = 10, 100, 1000 and 10000]. Figures 6.9-6.12 provides these results for CCCF, CCFF, CCSF and SCSF boundary condition, respectively. In each of these figures there are four plots for the four foundation parameter values and in each plot there are four backbone curves. In all these cases the gradation parameter values are kept fixed at 0.5, i.e., $\alpha = \beta = 0.5$. From Figure 6.9 it is clear that switching does not take place for low stiffness values, but at $K_f = 10000$ mode switching takes place between backbone curves 2 and 3. It is also clearly visible that the fourth

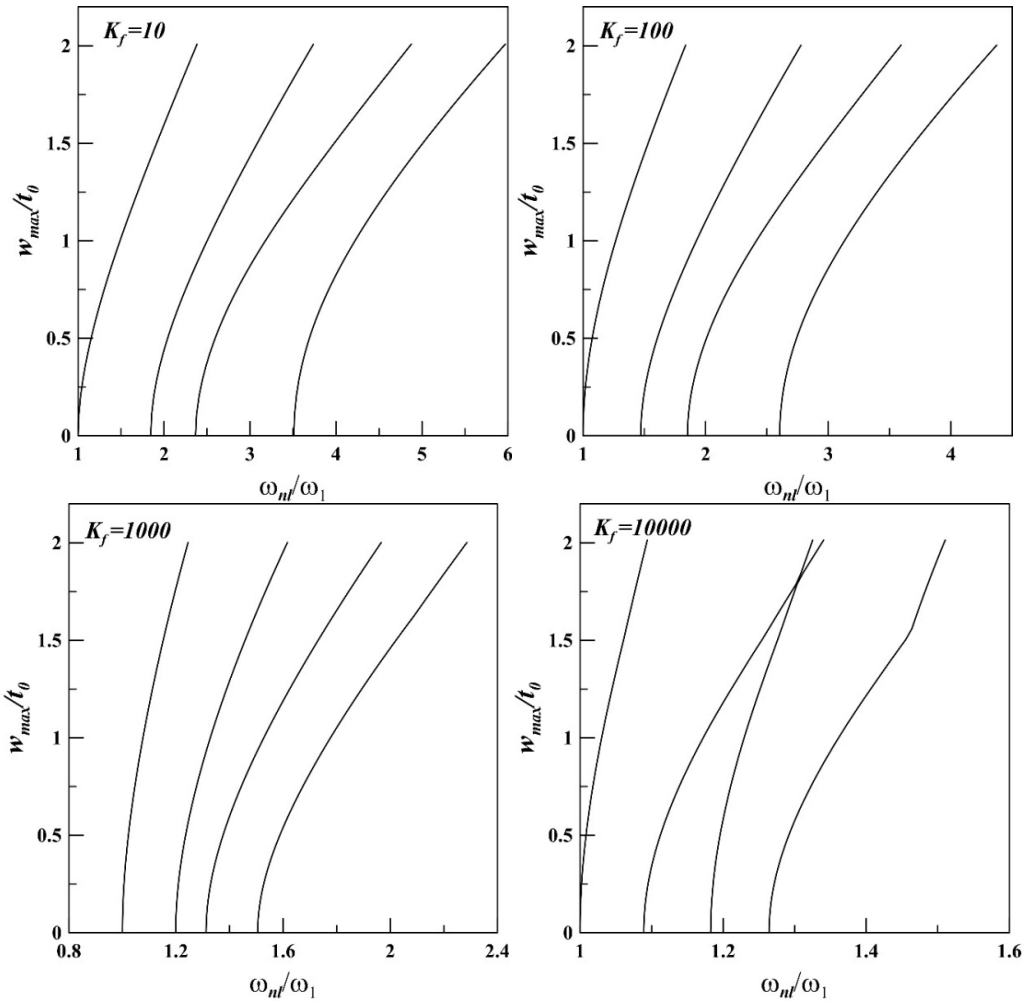

Figure 6.9: Backbone curves of CCCF plate for various foundation stiffness at α, β = 0.5

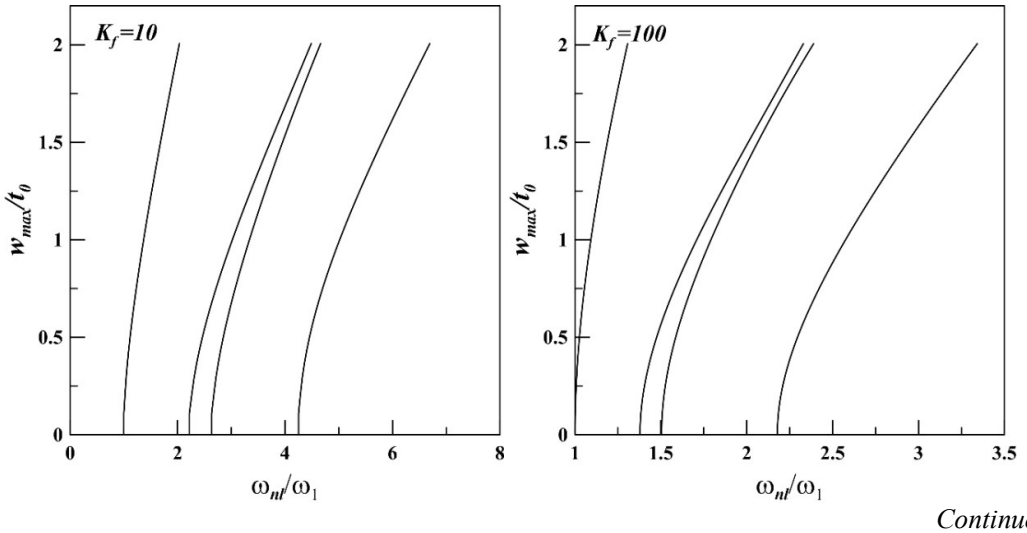

Continued

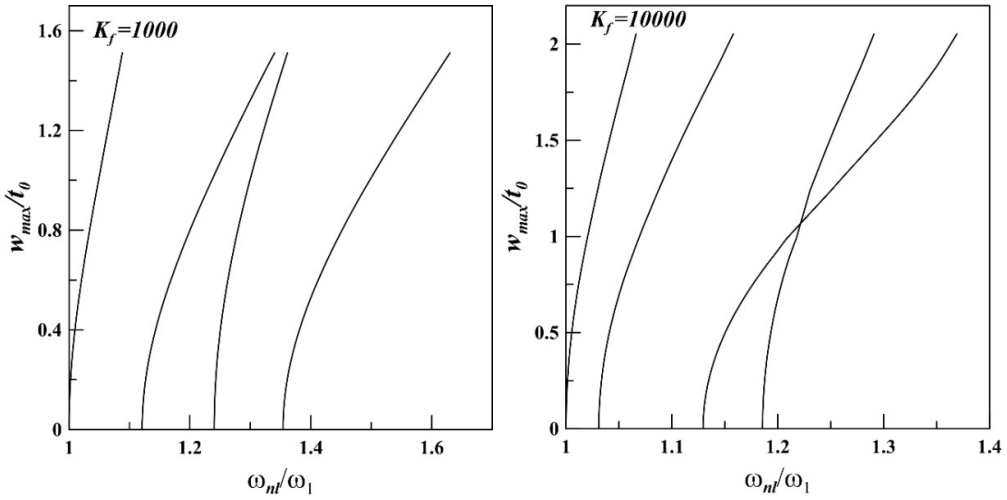

Figure 6.10: Backbone curves of CCFF plate for various foundation stiffness at α, β = 0.5

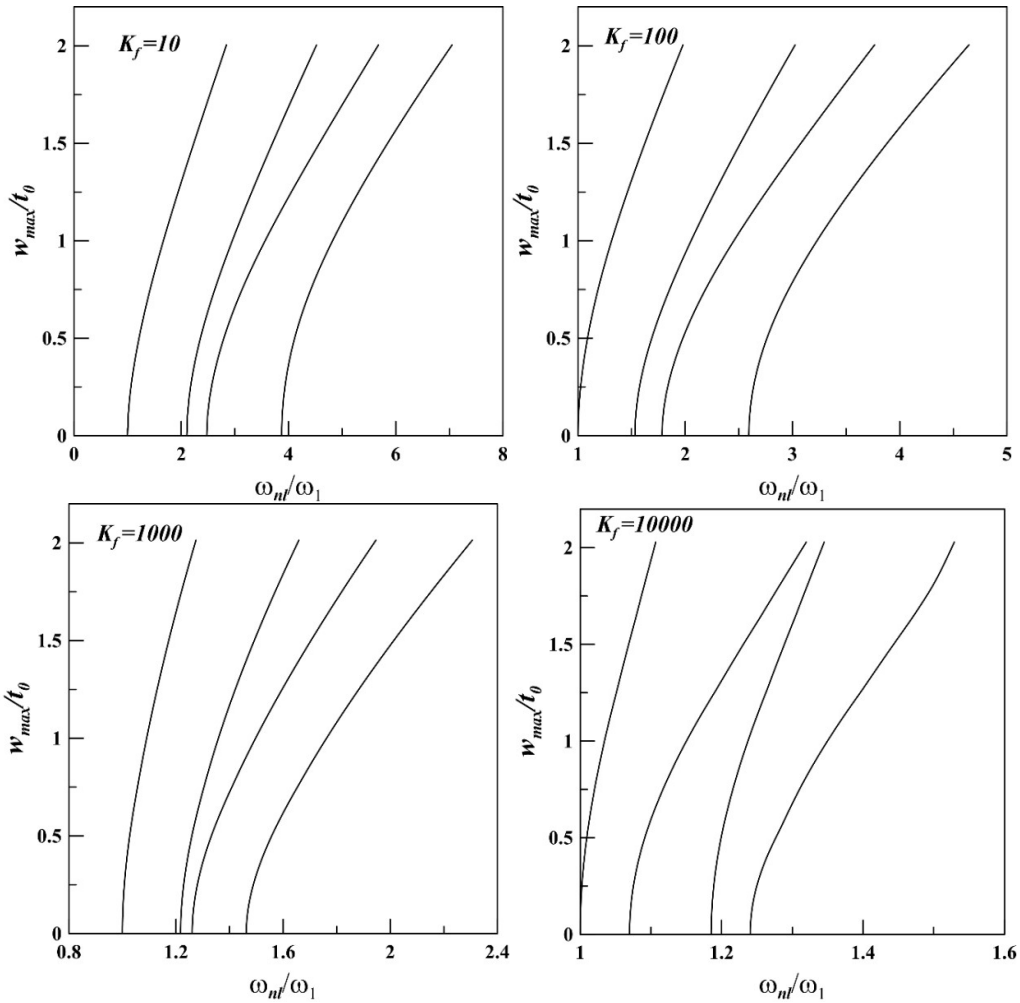

Figure 6.11: Backbone curves of CCSF plate for various foundation stiffness at α, β = 0.5

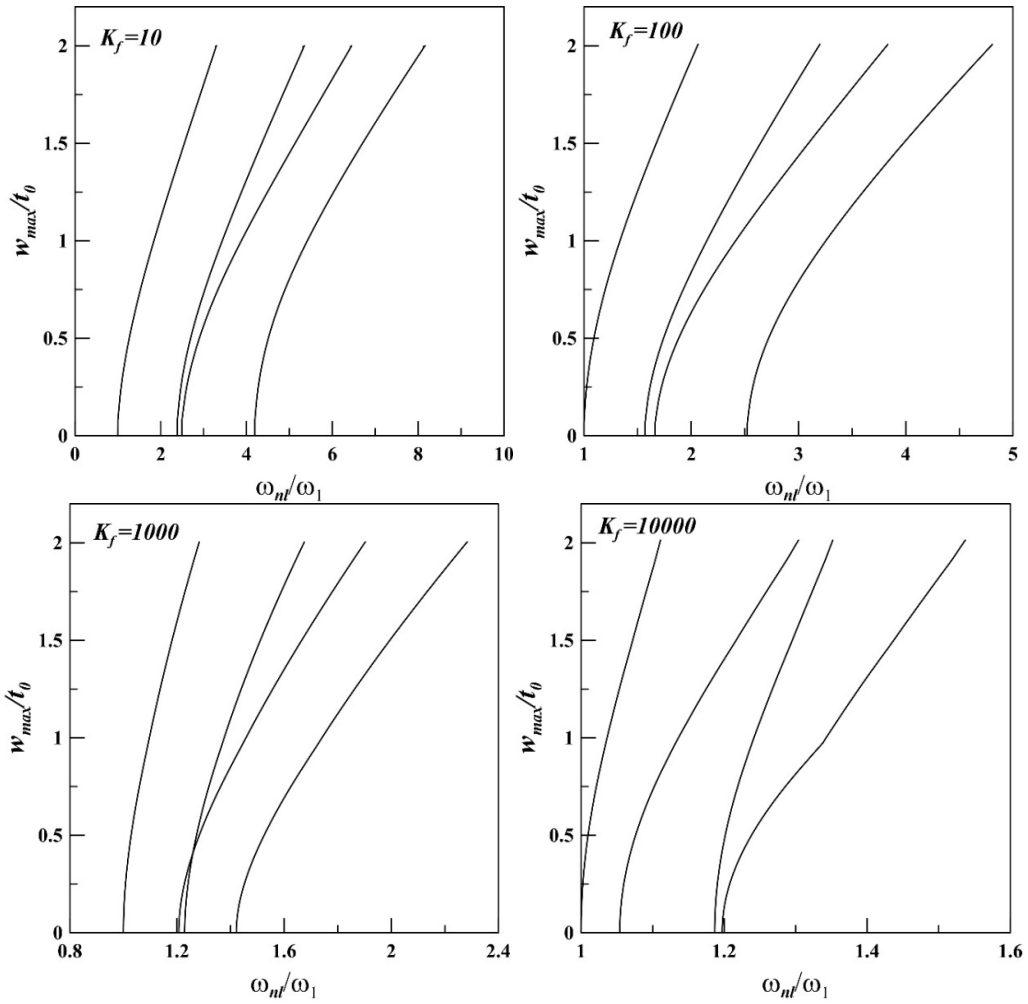

Figure 6.12: Backbone curves of SCSF plate for various foundation stiffness at $\alpha, \beta = 0.5$

backbone curve has a broken and discontinuous appearance, which indicates that switching takes place between 4th and 5th mode as well. Similarly, for CCFF plate, switching phenomenon is observed between backbone 3 and 4 at $K_f = 10000$ as shown in Figure 6.10. However, in Figure 6.11, for CCSF boundary none of the situations considered clearly exhibit mode switching. But, the fourth backbone curve of the plate on foundation with $K_f = 10000$ does show slight bend near the maximum normalised deflection of 2.0. This may be indicative of intersection between backbone 4 and 5 and requires further investigation. Finally, from Figure 6.12 it is observed that switching occurs between mode 2 and 3 at quite low normalized deflection for $K_f = 1000$. At the highest value of stiffness parameter ($K_f = 10000$) the fourth backbone curve has a sharp bend indicating switching between 4th and 5th backbone curves.

Mode shape	**Linear Mode shape ($w_{max}/t_0 = 0$)**	**Non Linear Mode Shape ($w_{max}/t_0 = 2$)**
Mode shape 1	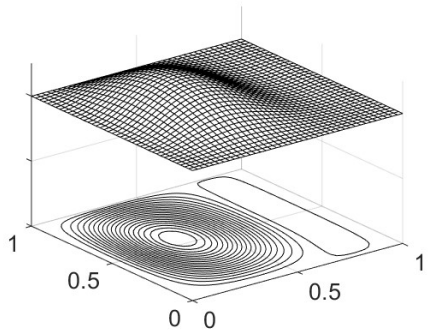	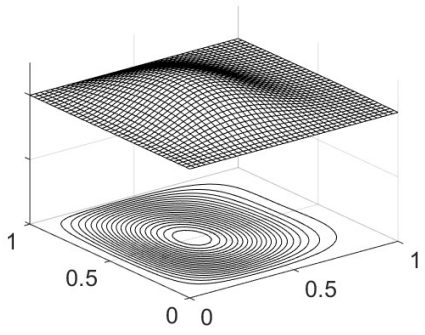
Mode shape 2	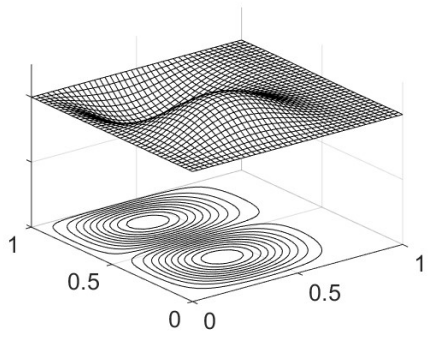	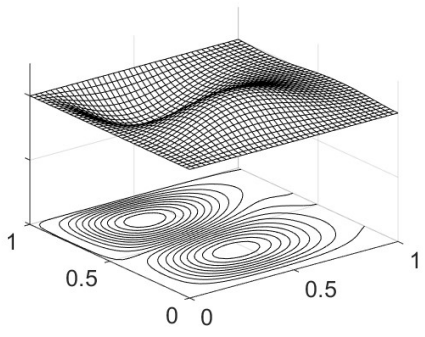
Mode shape 3	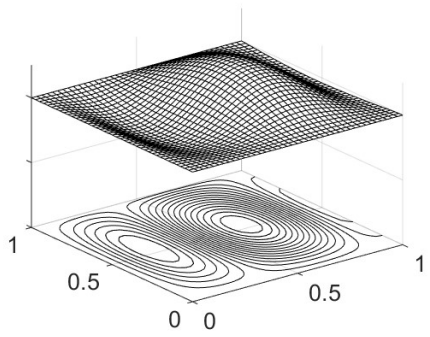	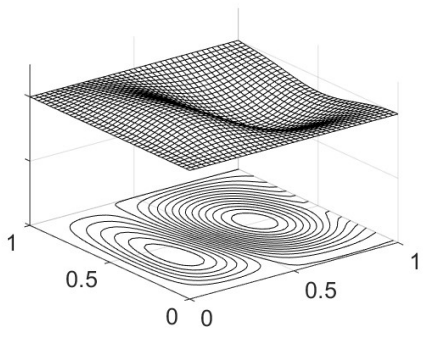
Mode shape 4	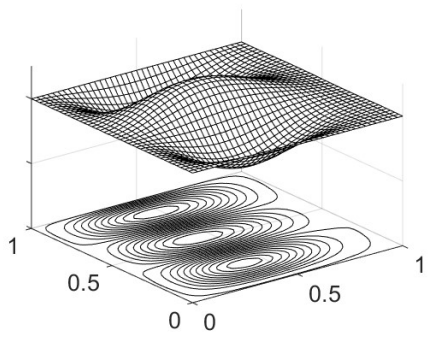	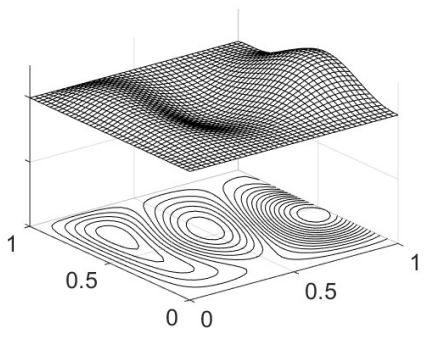

Figure 6.13: Linear and non-linear mode shape plots for CCSF plate at K_f = 10000 and α, β = 0.5

Mode shape	**Linear Mode shape ($w_{max}/t_0 = 0$)**	**Non Linear Mode Shape ($w_{max}/t_0 = 2$)**
Mode shape 1	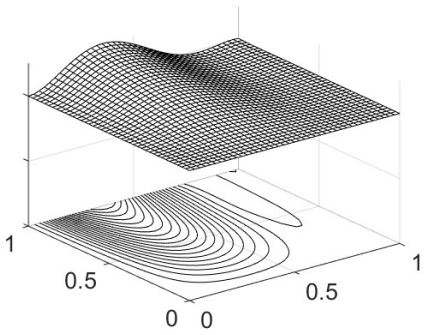	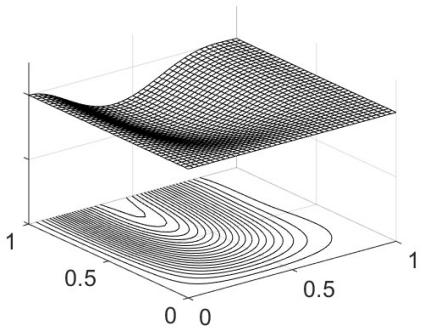
Mode shape 2	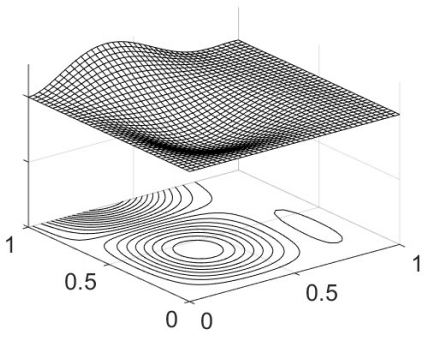	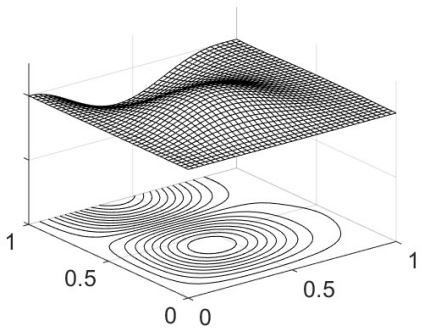
Mode shape 3	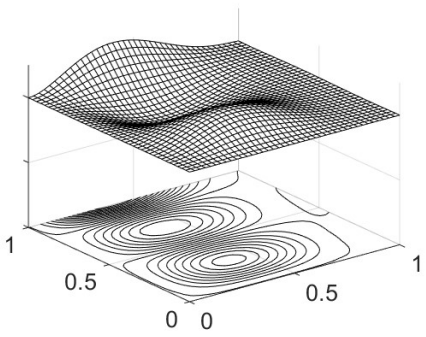	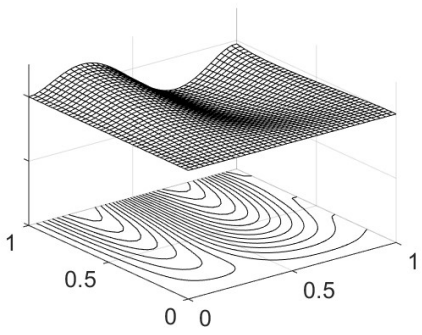
Mode shape 4	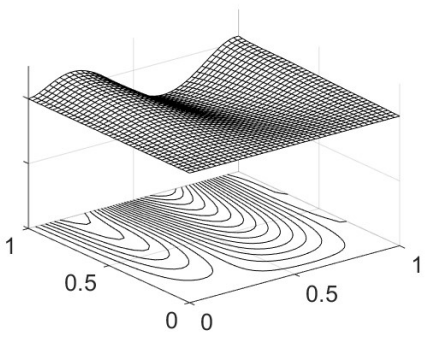	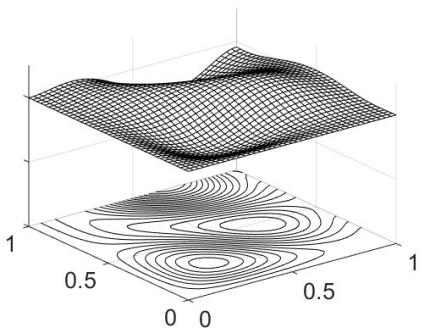

Figure 6.14: Linear and non-linear mode shape plots for CCFF plate at K_f = 10000 and α, β = 0.5

Mode shape	Linear Mode shape ($w_{max}/t_0 = 0$)	Non Linear Mode Shape ($w_{max}/t_0 = 2$)
Mode shape 1	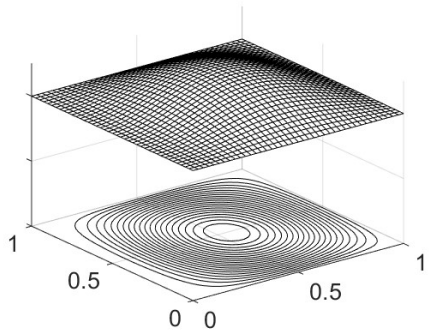	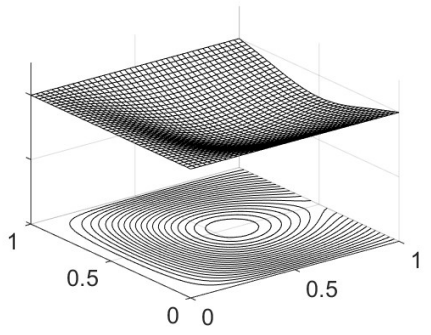
Mode shape 2	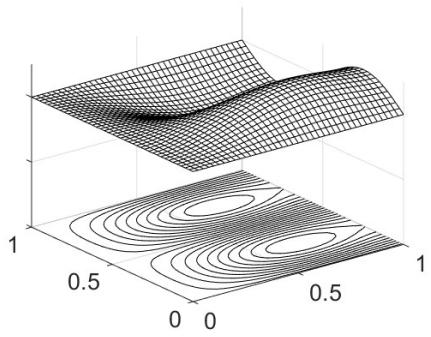	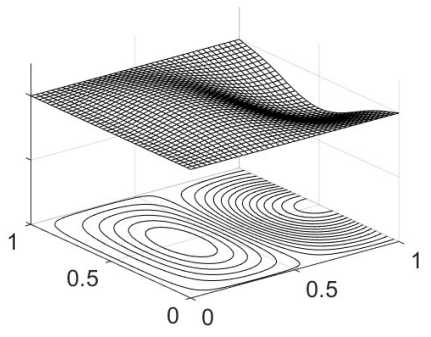
Mode shape 3	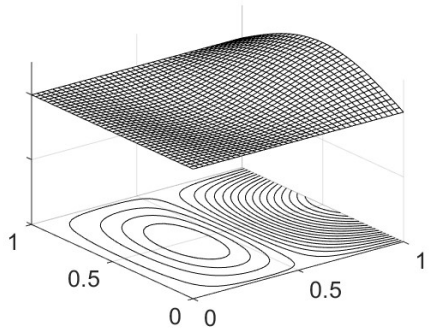	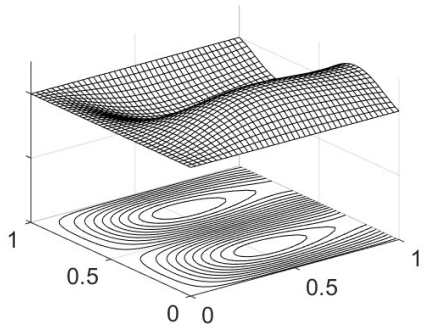
Mode shape 4	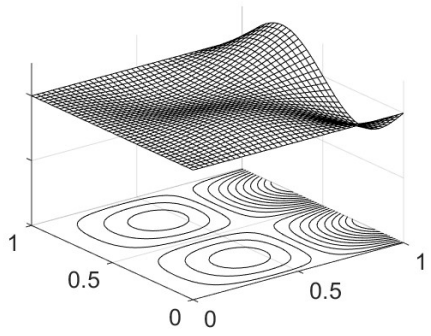	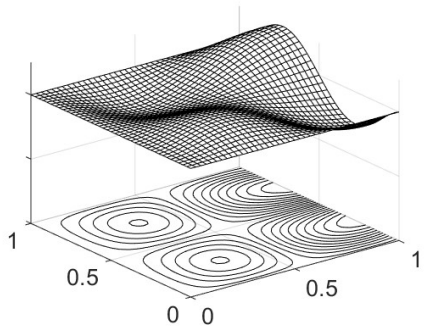

Figure 6.15: Linear and non-linear mode shape plots for SCSF plate at K_f = 1000 and α, β = 0.5

Mode shape	**Linear Mode shape ($w_{max}/t_0 = 0$)**	**Non Linear Mode Shape ($w_{max}/t_0 = 2$)**
Mode shape 1	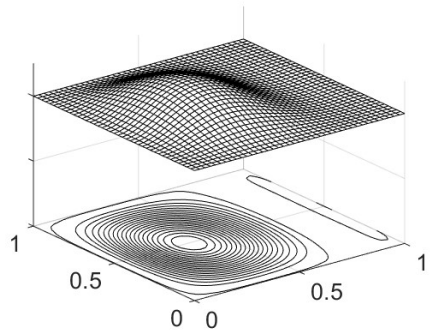	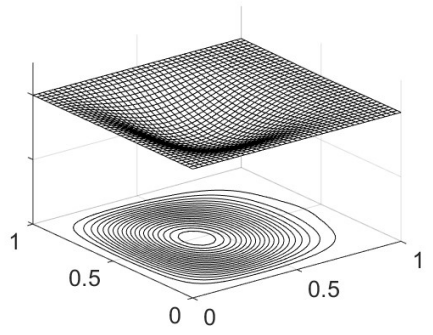
Mode shape 2	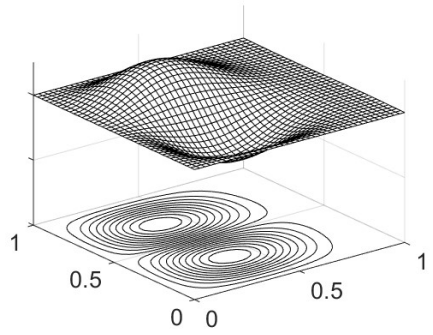	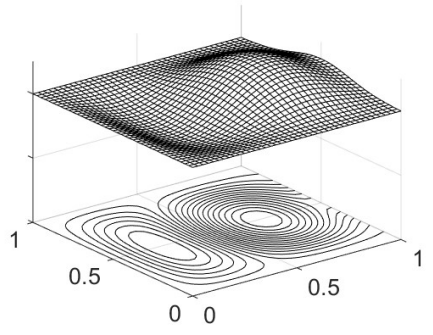
Mode shape 3	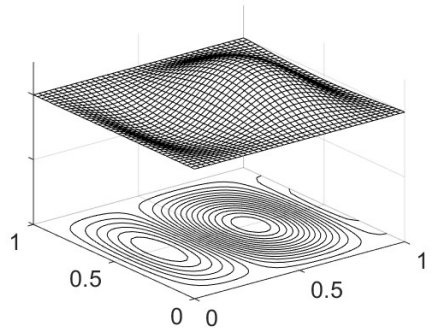	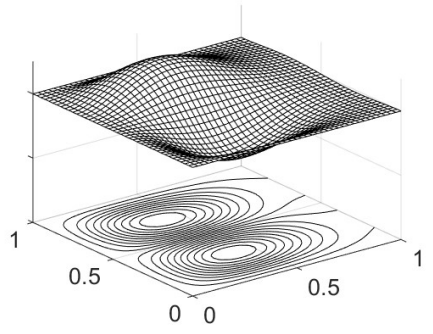
Mode shape 4	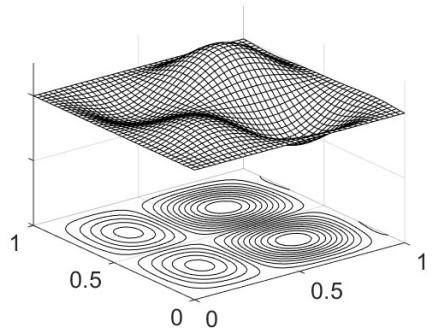	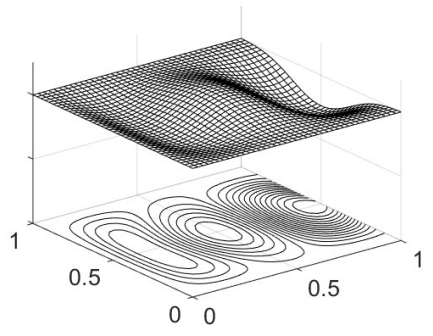

Figure 6.16: Linear and non-linear mode shape plots for CCCF plate at K_f = 10000 and α, β = 0.5

Whether mode switching takes place, the modes between which it occurs and the normalised amplitude at which switching happens is dependent on the system parameters, such as boundary conditions, stiffness parameter, gradation parameters etc. It can be definitely concluded from the furnished results that there is a higher chance of occurrence of mode switching phenomenon at higher stiffness parameter values. However, influence of the boundary conditions also needs to be acknowledged as it is observed that even for high foundation stiffness value (all other parameter values remaining same) there is apparently no switching for CCSF plate. Further detailed studies are necessary to find out how certain other parameters, such as taper and gradation parameters, effect the occurrence of this phenomenon.

6.4.3.4 Mode shape:

Mode shape plots can be used to reinforce the idea of mode switching between different modes. In the following figures (Figures. 6.13 – 6.16) mode shape plots for four vibration modes are presented for the plates with four different boundary conditions and a specific foundation stiffness parameter value. Mode shape plots for all the combinations of boundary condition and stiffness parameter are not presented in order to maintain the brevity of the paper. Instead, only significant situations of interest with respect to switching phenomenon are considered for mode shape results. For each mode of vibration, mode shapes, in terms of surface plots along with corresponding contour plots, are provided at linear ($w_{max}/t_0 = 0$) and nonlinear ($w_{max}/t_0 \neq 0$) frequencies.

As pointed out in previous paragraph, there is need for further investigation to ascertain whether switching takes place for CCSF plate with $K_f = 10000$ (Figure 6.11). So, this case is taken as an example and the mode shape plots are provided in Figure 6.13. It is clear from the figures that linear and nonlinear mode shapes corresponding to a backbone curve without switching are similar. But slight variations in the shapes are apparent from the contour plots. This underlines the effect of vibration amplitude on the free vibration behaviour of the system. Interestingly, linear mode shape of the 4th mode is drastically different from the nonlinear one. It indicates that there is indeed switching between the 4th and 5th backbone curves for CCSF plate. Figure 6.14 represents the linear and non-linear mode shape plots for CCFF plate at $K_f = 1000$ and $\alpha, \beta = 0.5$. As observed from Figure 6.10 there is clear indication of intersection between mode 3 and 4 and the fact is confirmed by

interchanging of the linear and nonlinear mode shapes. It is observed that the linear mode shape for mode 3 is similar to the nonlinear one of mode 4, whereas, the linear mode shape of mode 4 corresponds to nonlinear mode shape of mode 3. Figure 6.15 provides the relevant mode shape plots for in-plane inhomogeneous tapered plate with SCSF boundary condition having K_f = 1000 and α, β = 0.5. These mode shape results also support the occurrence of mode switching between 2nd and 3rd backbone curves as indicated by Figure 6.12. Similar results corresponding to CCCF plate is also presented in Figure 6.16. From the results it can be concluded that mode switching phenomenon for tapered plates with in-plane gradation is likely to occur at high values of foundation stiffness that render the entire system stiff.

6.5 Closure:

The present chapter studies the effect of geometric nonlinearity on static deflection and free vibration behaviour of a non-uniform axially graded plate on elastic foundation. The main objective of the static analysis is to represent the load-deflection characteristics and deflected shape of the plate under static loading, whereas, free vibration analysis is devoted to investigate the mode switching phenomenon for backbone curves with emphasis on variation of foundation stiffness and flexural boundary conditions. Different boundary conditions involving clamped, simply supported and free end has been considered. As part of the formulation, the elastic foundation is idealized as a set of parallel linear spring of constant stiffness. Mathematical formulation is based on energy principle and the problem is set up in two parts. First, a static large deflection problem is set up under uniformly distributed loading. Minimum total potential energy is employed to obtain the governing equations while substitution method with relaxation scheme is utilized to solve for the displacement field. The effect of the foundation is found out through load vs amplitude plot and deflected shape plot for five foundation stiffness values. Subsequently, the free vibration analysis is set up on the basis of deformed static field, thereby incorporating the large deformation effect. Hamilton's principle is used to obtain the standard eigenvalue problem. The methodology of the mathematical formulation is general in nature. It has enough flexibility to cope with other different type of elastic foundation, gradation pattern, taper pattern and boundary conditions as well. Results generated through present methodology are compared with previously published results and it is observed that the

current results match satisfactorily with the established ones. The effect of elastic foundation and end conditions on free vibration behaviour is shown through natural frequencies and backbone curves. Mode switching has been observed for different combinations of boundary conditions and foundation stiffness. However, it is observed that switching occurs at high values of the stiffness parameter for all the boundaries considered. Mode shape surface plots with contours are also provided to confirm the occurrence of the above mentioned phenomenon. Moreover, the results documented in the present paper is capable of serving as benchmark results for axially graded plates on elastic foundation.

Chapter 7

CLOSURE

7.1 Conclusions:

The endeavour of the present thesis work is to analyse static and dynamic behaviour of axially functionally graded structural elements on elastic foundation with different boundary conditions. The structural elements which include both beams and plates, are considered to be resting on elastic foundation with different classical boundary conditions. The foundation has been mathematically incorporated into the analysis as a set of linear springs attached uniformly at the bottom surface of the structure. For beam analyses, both Euler-Bernoulli and Timoshenko beam model are separately considered to study free vibration and forced vibration characteristics. Free vibration study of the system is performed at loaded and unloaded condition. In the present thesis, forced vibration study is performed as an equivalent static one assuming force equilibrium condition at maximum amplitude of excitation. For beams separate results for static analysis are not furnished, although it is in-built with the loaded free vibration study. For plates both static and free vibration analysis are performed, whereas, forced vibration study has not been included within the scope of the present thesis. For all the studies presented in the thesis, geometric nonlinearity induced in the system through large displacement has been taken into consideration. To account for the nonlinearity, Von Karman's nonlinear strain-displacement relations are employed to obtain the equations of motion. All the studies are restricted within the elastic limit as consideration of material nonlinearity is kept out of the scope of the thesis. Various classical boundary conditions including free edges along with the elastic foundation are taken into account.

Non-uniform geometry has also been taken into account in the present analysis considering variation in thickness along the axial direction. Three different taper patterns, i.e., linear, parabolic and exponential, are chosen for the variations of thickness as a

function of axial coordinates, whereas other dimensions (i.e. length and width) of the structures are taken as constant.

The material of the structures is considered to be functionally graded continuously along spatial directions. To incorporate this material gradation in the analysis, three different material models are selected depending on the gradation of elastic modulus and density in the axial direction. For forced vibration analysis of Timoshenko beams a separate material model is considered, which exhibits continuous gradation of material properties from pure form of metal to pure ceramic. Poisson's ratio throughout the whole thesis is kept as constant.

Mathematical formulation, solution methodologies and techniques used in the entire thesis are general in nature and flexible enough to incorporate other type of material gradation, taper pattern and loading type. A displacement based semi-analytical method associated with the whole physical domain of the system is utilized for formulation of the problems throughout the thesis. In other words, the formulation for all the simulation studies is based on the displacement fields, which are again dependent on the entire domain. Although, the physical domain is not discretized, a grid of reference points is generated in order to transform the physical domain of interest into suitable computational domain for the two dimensional problem. According to whether the problem under consideration is static or dynamic in nature, suitable energy methods are adopted to derive the governing equations of the system. For static problem, governing equations are obtained by applying the principle of minimum total potential energy. On the other hand, Hamilton's principle is employed to formulate the free and forced vibration problems.

The displacement fields associated with the problem can be approximated as finite linear combination of admissible orthogonal coordinate functions and a set of unknown coefficients, which are to be evaluated. The start functions for the above mentioned set of orthogonal functions are suitably selected so as to satisfy the flexural and membrane boundary conditions. The higher order orthogonal functions are generated numerically by using Gram Schmidt scheme from the selected start functions. Due to consideration of geometric nonlinearity, the set of governing equations are found to be nonlinear in nature. The set of nonlinear equations, describing the static system behaviour under transverse external load, are solved using direct substitution technique with suitable successive

relaxation scheme throughout the present thesis. The converged solution at the end of the static analysis provides the stiffness matrix for the deformed configuration and it is used as input to the formulation of free vibration problem. The governing equations for large amplitude free vibration analysis are in the form of a classical eigenvalue problem and solutions are achieved by utilising in-built Matlab functions. In case of forced vibration analysis (system governing equations here are again non-linear due to consideration of large displacement), a multi-dimensional secant method, known as Broyden method, is utilized for solution in the vicinity of natural frequency (fundamental mode) of the system. In case of all the studies, the results generated from the present formulation and solution technique has been validated with established data, albeit for systems with less complexity.

The main concern of the static analysis is to represent the load versus deflection plot and deflected shape plot under the application of steady state loading considering the effect of various parameters viz. material model, material gradient, system geometry and elastic foundation. As already mentioned, static analysis results are specifically furnished in case of axially graded plates on elastic foundation. It is observed that with the increase of the foundation stiffness the load-deflection curve gradually shifts towards the right side of the non-dimensional plane. It is also observed that for the same load application the deflection of the SSSS plate is more than the CCCC plate. From the deflected shape plot of plate, it is seen that deflection is maximum near the middle of the plate. It is also observed that at zero value of stiffness the deflection is maximum and it is minimum when stiffness is maximum. Further, it is also clear from the plots that SSSS plate deflect more than the CCCC plate under same load application. These are reasonably expected outcomes that can be thought of as universally true. But the novelty of such results is in the fact that these can be considered as benchmark for the system under consideration.

The main focus of the free vibration analysis is to represent backbone curves and corresponding mode shapes. In order to generate these, it is necessary to find out the natural frequencies of the system under undeformed and deformed conditions. The free vibration problem is solved in two steps where the objective of the first part is to compute the stiffness matrix in deflected configuration through a static analysis. This equivalent stiffness matrix is directly used in dynamic analysis (second part) for obtaining eigenvalues and eigenvectors which provide the natural frequencies and mode shape of the system,

respectively. For all the structural elements under consideration (thin as well as thick beams and plates, on elastic foundation) in the current thesis, the free vibrational frequencies are tabulated for different taper profiles, taper parameters and foundation stiffness. The dynamic behaviour of the system is presented in the form of backbone curves in dimensionless frequency-amplitude plane. The linear and nonlinear mode shapes are also furnished to support the presence of nonlinearity in the system. It must be reiterated that such detailed results for backbone curves for axially graded structural elements on foundation are furnished for the first time and hence worthy of serving as benchmark. For AFG plates on elastic foundation, mode switching is detected in certain specific situations. To support the presence of switching phenomenon backbone curves along with the linear and nonlinear mode shapes are also furnished.

Forced vibration analysis is conducted with an objective to find out the response of the system, in terms of displacement amplitude, under externally applied time varying excitations. In the present work, only steady-state response is presented and frequency of response of the undamped system is assumed to be equal to that of the external excitation. An indirect approach is adopted for solving the problem, where it is reduced to a static scenario by assuming that under maximum amplitude of excitation, i.e., when the system suffers maximum deformation, the dynamic system fulfils force equilibrium conditions. This supposition converts the problem of solving for the dynamic system into an equivalent static situation, where the excitation frequency and amplitude of the harmonic excitation are the parameters that control system response. Frequency vs. amplitude curve corresponding to different combinations of system parameters are presented and are capable of serving as benchmark results. The effects of excitation frequency on the operational deflected shape (ODS) is also presented.

7.2 Future Scope of Work:

This study invokes few other possibilities which may be treated as scope for future research activities in this area.

1. Large amplitude forced vibration study of in-plane inhomogeneous plates on elastic foundation has not been included in the present thesis. Incorporation of Broyden

solution technique to solve for the nonlinear governing equations of the system is a valid an interresting extension of the present study.

2. The damping effect has not been included in the present thesis but may provide an interesting avunue of study involving damped graded structures in nonlinear dynamics.

3. There is always scope for improving the simulation model by incorporating complications hitherto neglected. Analysis of AFG thick plates on elastic foundation is also very important topic in this regard and can be explored in near future. For better representation of the practical situation, there is always scope to extend the present study considering other type of elastic foundations (Pasternak foundation, Kerr foundation etc.) and introducing elastic restrains at the boundaries.

4. FGMs with macroscopic properties varying in two or three directions to withstand a more general temperature field can be considered as a natural extension of the present analysis. There is a scope to investigate bi-directional or tri-directional functionally graded structural elements that are supported on elastic foundation.

6. In the present work geometric nonlinearity is incorporated in the methodology using Von Karman's strain-displacement relations, which neglects the effect of large rotations. Hence in the near future similar studies including the effect of large rotation may be performed, based on Green Lagrange strain-displacement relations.

7. In structural analysis another form of nonlinearity is encountered very often and it is material nonlinearity, which is manifested by nonlinear stress-strain relationship. There is a scope for extending the studies carried out in the present thesis work to post-elastic domain.

8. Generalized problem which includes both geometric and material nonlinearity can also be considered in near future. Incremental nonlinear analysis incorporating Updated Lagrangian (UL) formulation to capture appreciable change in geometry is a potential domain to explore.

9. Investigation of free vibration and frequency response of other two dimensional structural elements with regular (circular plates, disks, skew plates etc.) and irregular

geometry (plates with cut outs of various shapes, cracked beam etc.) may be considered as future scope of the present thesis work.

10. Further experimental investigations are required to understand various nonlinear phenomena associated with the dynamic characteristics of structures. Especially, experimental studies of axially graded structures are quite limited. Experimental studies on free/forced vibration problems considering AFG beams and plates can be performed in future.

Appendix

A1: Axially Functionally Graded Thin Beams on Elastic Foundation

The form of stiffness matrix is given by,

$$[K_s]=\begin{bmatrix} K_{11} & K_{12} \\ K_{21} & K_{22} \end{bmatrix},$$

The elements of the stiffness matrix are,

$$[K_{11}]=\frac{1}{L^3}\sum_{j=1}^{nw}\sum_{i=1}^{nw}\int_0^1 \frac{d^2\phi_i}{d\xi^2}\frac{d^2\phi_j}{d\xi^2}E(\xi)I(\xi)d\xi+\frac{1}{2L^3}\sum_{j=1}^{nw}\sum_{i=1}^{nw}\int_0^1\left(\sum_{i=1}^{nw}c_i\frac{d\phi_i}{d\xi}\right)^2\frac{d\phi_i}{d\xi}\frac{d\phi_j}{d\xi}E(\xi)A(\xi)d\xi$$
$$+\frac{1}{L}\sum_{j=1}^{nw}\sum_{i=1}^{nw}\int_0^1\left(\sum_{i=1+nw}^{nw+nu}c_i\frac{d\psi_{i-nw}}{d\xi}\right)^2\frac{d\phi_i}{d\xi}\frac{d\phi_j}{d\xi}E(\xi)A(\xi)d\xi+KL\sum_{j=1}^{nw}\sum_{i=1}^{nw}\int_0^1 p(\xi)\phi_i\phi_j d\xi$$

$$[K_{12}]=0$$

$$[K_{21}]=\frac{1}{2L^2}\sum_{j=nw+1}^{nw+nu}\sum_{i=1}^{nw}\int_0^1\left(\sum_{i=1}^{nw}c_i\frac{d\phi_i}{d\xi}\right)^2\frac{d\phi_i}{d\xi}\frac{d\psi_{i-nw}}{d\xi}E(\xi)A(\xi)d\xi$$

$$[K_{22}]=\frac{1}{L}\sum_{j=nw+1}^{nw+nu}\sum_{i=nw+1}^{nw+nu}\int_0^1\frac{d\psi_{i-nw}}{d\xi}\frac{d\psi_{i-nw}}{d\xi}E(\xi)A(\xi)d\xi$$

The form of load vector is given by,

$$\{f\}=\{f_{11}\quad f_{12}\}^T$$

The elements of the load vector are,

$$\{f_{11}\}=L\sum_{j=1}^{nw}\int_0^1 p(\xi)\phi_j d\xi$$

$$\{f_{12}\}=0$$

The form of mass matrix is given by,

$$[M]=\begin{bmatrix} M_{11} & M_{12} \\ M_{21} & M_{22} \end{bmatrix}$$

The elements of the mass matrix are,

$$[M_{11}]=L\sum_{j=1}^{nw}\sum_{i=1}^{nw}\int_0^1 \phi_i\phi_j\rho(\xi)\,A(\xi)\,d\xi$$

$$[M_{12}]=0\,,\ [M_{21}]=0$$

$$[M_{22}]=L\sum_{j=nw+1}^{nw+nu}\sum_{i=nw+1}^{nw+nu}\int_0^1 \psi_{i-nw}\psi_{j-nw}\rho(\xi)\,A(\xi)\,d\xi$$

A2: Axially Functionally Graded Timoshenko Beam on Elastic Foundation

The elements of the stiffness matrix *[K_{ij}]* are:

$$\left[K_{ij}\right]_{j=1,nw}^{i=1,nw}=\frac{1}{2L^3}\int_0^1\left(\sum_{k=1}^{nw}d_k\frac{d\phi_k}{d\xi}\right)^2\frac{d\phi_i}{d\xi}\frac{d\phi_j}{d\xi}A(\xi)E(\xi)d\xi+$$
$$\frac{1}{2L^2}\int_0^1\left(\sum_{k=nw+1}^{nw+nu}d_k\frac{d\phi_{k-nw}}{d\xi}\right)\frac{d\phi_i}{d\xi}\frac{d\phi_j}{d\xi}A(\xi)E(\xi)d\xi$$
$$+\frac{k_{scf}}{L}\int_0^1\frac{d\phi_i}{d\xi}\frac{d\phi_j}{d\xi}A(\xi)G(\xi)d\xi+K_fL\sum_{j=1}^{nw}\sum_{i=1}^{nw}\int_0^1 q(\xi)\phi_i\phi_j d\xi$$

$$\left[K_{ij}\right]_{j=nw+1,nw+nu}^{i=nw+1}=0$$

$$\left[K_{ij}\right]_{j=nw+1,nw+nu}^{i=1,nw}=-k_{scf}\int_0^1\frac{d\phi_i}{d\xi}B_{j-nw-nu}A(\xi)G(\xi)d\xi$$

$$\left[K_{ij}\right]_{j=1,nw}^{i=nw+1,nw+nu}=\frac{1}{2L^2}\int_0^1\left(\sum_{k=1}^{nw}d_k\frac{d\phi_k}{d\xi}\right)\frac{d\alpha_{i-nw}}{d\xi}\frac{d\phi_i}{d\xi}A(\xi)E(\xi)d\xi$$

$$\left[K_{ij}\right]_{j=nw+1,nw+nu}^{i=nw+1}=\frac{1}{L}\int_0^1\frac{d\alpha_{i-nw}}{d\xi}\frac{d\phi_{j-nw}}{d\xi}A(\xi)E(\xi)d\xi$$

$$\left[K_{ij}\right]_{j=nw+nu+1,nw+nu+nsi}^{i=nw+1,nw+nu}=0$$

$$\left[K_{ij}\right]_{j=1,nw}^{i=nw+nu+1,nw+nu+nsi} = -k_{scf}\int_0^1 \beta_{i-nw-nu}\frac{d\phi_j}{d\xi}A(\xi)G(\xi)d\xi$$

$$\left[K_{ij}\right]_{j=nw+1,nw+nu}^{i=nw+nu+1,nw+nu+nsi} = 0$$

$$\left[K_{ij}\right]_{j=nw+nu+1,nw+nu+nsi}^{i=nw+nu+1,nw+nu+nsi} = \frac{1}{L}\int_0^1 \frac{d\beta_{i-nw-nu}}{d\xi}\frac{d\beta_{j-nw-nu}}{d\xi}I(\xi)E(\xi)d\xi +$$

$$+k_{scf}L\int_0^1 \beta_{i-nw-nu}\beta_{j-nw-nu}A(\xi)G(\xi)d\xi$$

The elements of the load vector $\{f_i\}$ are,

$$\{f_i\}_{i=1,nw} = qL\int_0^1 \phi_i d\xi$$

$$\{f_i\}_{i=nw+1,nw+nu} = 0$$

$$\{f_i\}_{i=nw+nu+1,nw+nu+nsi} = 0$$

The elements of the mass matrix $[M_{ij}]$ are,

$$\left[M_{ij}\right]_{\substack{i=1,nw\\j=1,nw}} = L\int_0^L \phi_i\phi_j A(\xi)\rho(\xi)d\xi$$

$$\left[M_{ij}\right]_{\substack{i=nw+1,nw+nu\\j=nw+1,nw+nu}} = L\int_0^L \alpha_{i-nw}\alpha_{j-nw}A(\xi)\rho(\xi)d\xi$$

$$\left[M_{ij}\right]_{\substack{i=nw+nu+1,nw+nu+nsi\\j=nw+nu+1,nw+nu+nsi}} = L\int_0^L \beta_{i-nw-nu}\beta_{j-nw-nu}I(\xi)\rho(\xi)d\xi$$

Rest all other elements of the mass matrix $[M_{ij}]$ are zero.

A3: Axially Functionally Graded Thin Plates on Elastic Foundation

The of the stiffness matrix due to bending $[K^b]$, stretching $[K^m]$ and elastic foundation $[K^f]$ are as follow:

Appendix

$$\left[K^b\right]=\begin{bmatrix} k_{11}^b & k_{12}^b & k_{13}^b \\ k_{21}^b & k_{22}^b & k_{23}^b \\ k_{31}^b & k_{32}^b & k_{33}^b \end{bmatrix}$$

$$\left[K^m\right]=\begin{bmatrix} k_{11}^m & k_{12}^m & k_{13}^m \\ k_{21}^m & k_{22}^m & k_{23}^m \\ k_{31}^m & k_{32}^m & k_{33}^m \end{bmatrix}$$

$$\left[K^f\right]=\begin{bmatrix} k_{11}^f & k_{12}^f & k_{13}^f \\ k_{21}^f & k_{22}^f & k_{23}^f \\ k_{31}^f & k_{32}^f & k_{33}^f \end{bmatrix}$$

The individual elements of stiffness matrices and load vector are presented as follows:

$$k_{11}^b=\frac{a}{2\left(1-\mu^2\right)}\sum_{j=1}^{nfw}\sum_{i=1}^{nfw}\int_0^1\int_0^1\left[\begin{Bmatrix} \frac{1}{a^4}\left(\frac{\partial^2\phi_i}{\partial\xi^2}\right)\left(\frac{\partial^2\phi_j}{\partial\xi^2}\right)+\frac{1}{b^4}\left(\frac{\partial^2\phi_i}{\partial\eta^2}\right)\left(\frac{\partial^2\phi_j}{\partial\eta^2}\right) \\ +\frac{1}{a^2b^2}\left(\frac{\partial^2\phi_i}{\partial\xi^2}\right)\left(\frac{\partial^2\phi_j}{\partial\xi^2}\right)+\frac{1}{a^2b^2}\left(\frac{\partial^2\phi_i}{\partial\eta^2}\right)\left(\frac{\partial^2\phi_j}{\partial\eta^2}\right) \end{Bmatrix} -\frac{1-\mu}{a^2b^2}\left\{\left(\frac{\partial^2\phi_i}{\partial\xi^2}\right)\left(\frac{\partial^2\phi_j}{\partial\eta^2}\right)+\left(\frac{\partial^2\phi_i}{\partial\eta^2}\right)\left(\frac{\partial^2\phi_j}{\partial\xi^2}\right)-2\left(\frac{\partial^2\phi_i}{\partial\xi\partial\eta}\right)\left(\frac{\partial^2\phi_j}{\partial\xi\partial\eta}\right)\right\}\right]E(\xi,\eta)I(\xi)d\xi d\eta$$

$$k_{12}^b=k_{13}^b=k_{21}^b=k_{22}^b=k_{23}^b=k_{13}^b=k_{23}^b=k_{33}^b=0$$

$$k_{21}^m=\frac{a}{2\left(1-\mu^2\right)}\sum_{j=nfw+1}^{nfw+nfu}\sum_{i=1}^{nfw}\int_0^1\int_0^1\left[\begin{Bmatrix} \frac{1}{a^3}\left(\sum_{i=1}^{nfw}d_i\frac{\partial\phi_i}{\partial\xi}\right)\left(\frac{\partial\phi_i}{\partial\xi}\right)\left(\frac{\partial\alpha_{j-nfw}}{\partial\xi}\right) \\ +\frac{\mu}{ab^2}\left(\sum_{i=1}^{nfw}d_i\frac{\partial\phi_i}{\partial\eta}\right)\left(\frac{\partial\phi_i}{\partial\eta}\right)\left(\frac{\partial\alpha_{j-nfw}}{\partial\xi}\right) \\ +\frac{1-\mu}{ab^2}\left(\sum_{i=1}^{nfw}d_i\frac{\partial\phi_i}{\partial\xi}\right)\left(\frac{\partial\phi_i}{\partial\eta}\right)\left(\frac{\partial\alpha_{j-nfw}}{\partial\eta}\right) \end{Bmatrix}\right]E(\xi,\eta)A(\xi)d\xi d\eta$$

$$k_{22}^m=\frac{a}{2\left(1-\mu^2\right)}\sum_{j=nfw+1}^{nfw+nfu}\sum_{i=nfw+1}^{nfw+nfu}\int_0^1\int_0^1\left[\begin{Bmatrix} \frac{2}{a^2}\left(\frac{\partial\alpha_{i-nfw}}{\partial\xi}\right)\left(\frac{\partial\alpha_{j-nfw}}{\partial\xi}\right) \\ +\frac{1-\mu}{b^2}\left(\frac{\partial\alpha_{i-nfw}}{\partial\eta}\right)\left(\frac{\partial\alpha_{j-nfw}}{\partial\eta}\right) \end{Bmatrix}\right]E(\xi,\eta)A(\xi)d\xi d\eta$$

$$k_{23}^{m}=\frac{a}{2\left(1-\mu^{2}\right)}\sum_{j=nfw+1}^{nfw+nfu}\sum_{i=nfw+nfu+1}^{nfw+nfu+nfv}\int_{0}^{1}\int_{0}^{1}\left[\left\{\begin{array}{l}2\mu\left(\dfrac{\partial\beta_{i-nfw-nfu}}{\partial\eta}\right)\left(\dfrac{\partial\alpha_{j-nfw}}{\partial\xi}\right)\\+\left(1-\mu\right)\left(\dfrac{\partial\beta_{i-nfw-nfu}}{\partial\xi}\right)\left(\dfrac{\partial\alpha_{j-nfw}}{\partial\eta}\right)\end{array}\right\}\right]E\left(\xi,\eta\right)A\left(\xi\right)d\xi d\eta$$

$$k_{31}^{m}=\frac{a}{2\left(1-\mu^{2}\right)}\sum_{j=nfw+nfu+1}^{nfw+nfu+nfv}\sum_{i=1}^{nfw}\int_{0}^{1}\int_{0}^{1}\left[\left\{\begin{array}{l}\dfrac{1}{b^{3}}\left(\displaystyle\sum_{i=1}^{nfw}d_{i}\frac{\partial\phi_{i}}{\partial\eta}\right)\left(\dfrac{\partial\phi_{i}}{\partial\xi}\right)\left(\dfrac{\partial\beta_{j-nfw-nfu}}{\partial\eta}\right)\\+\dfrac{\mu}{a^{2}b}\left(\displaystyle\sum_{i=1}^{nfw}d_{i}\frac{\partial\phi_{i}}{\partial\xi}\right)\left(\dfrac{\partial\phi_{i}}{\partial\xi}\right)\left(\dfrac{\partial\alpha_{j-nfw-nfu}}{\partial\eta}\right)\\+\dfrac{1-\mu}{a^{2}b}\left(\displaystyle\sum_{i=1}^{nfw}d_{i}\frac{\partial\phi_{i}}{\partial\xi}\right)\left(\dfrac{\partial\phi_{i}}{\partial\eta}\right)\left(\dfrac{\partial\beta_{j-nfw-nfu}}{\partial\xi}\right)\end{array}\right\}\right]E\left(\xi,\eta\right)A\left(\xi\right)d\xi d\eta$$

$$k_{32}^{m}=\frac{a}{2\left(1-\mu^{2}\right)}\sum_{j=nfw+nfu+1}^{nfw+nfu+nfv}\sum_{i=nfw+1}^{nfw+nfu}\int_{0}^{1}\int_{0}^{1}\left[\left\{\begin{array}{l}2\mu\left(\dfrac{\partial\alpha_{i-nfw}}{\partial\xi}\right)\left(\dfrac{\partial\beta_{j-nfw-nfu}}{\partial\eta}\right)\\+\left(1-\mu\right)\left(\dfrac{\partial\alpha_{i-nfw}}{\partial\eta}\right)\left(\dfrac{\partial\beta_{j-nfw-nfu}}{\partial\xi}\right)\end{array}\right\}\right]E\left(\xi,\eta\right)A\left(\xi\right)d\xi d\eta$$

$$k_{33}^{m}=\frac{a}{2\left(1-\mu^{2}\right)}\sum_{j=nfw+nfu+1}^{nfw+nfu+nfv}\sum_{i=nfw+nfu+1}^{nfw+nfu+nfv}\int_{0}^{1}\int_{0}^{1}\left[\left\{\begin{array}{l}\dfrac{2}{b^{2}}\left(\dfrac{\partial\beta_{i-nfw-nfu}}{\partial\eta}\right)\left(\dfrac{\partial\beta_{j-nfw-nfu}}{\partial\eta}\right)\\+\dfrac{\left(1-\mu\right)}{a^{2}}\left(\dfrac{\partial\beta_{i-nfw-nfu}}{\partial\xi}\right)\left(\dfrac{\partial\beta_{j-nfw-nfu}}{\partial\xi}\right)\end{array}\right\}\right]E\left(\xi,\eta\right)A\left(\xi\right)d\xi d\eta$$

$$k_{11}^{f}=\left(ab\right)K_{f}\sum_{j=1}^{nfw}\sum_{i=1}^{nfw}\int_{0}^{1}\int_{0}^{1}\phi_{i}\phi_{j}d\xi d\eta$$

$$k_{12}^{f}=k_{13}^{f}=k_{21}^{f}=k_{22}^{f}=k_{23}^{f}=k_{13}^{f}=k_{23}^{f}=k_{33}^{f}=0$$

The form of load vector *{f}* is presented as:

$$\left\{f\right\}=\left\{f_{11}\quad f_{12}\quad f_{3}\right\}^{T}$$

The individual elements of load vector are presented as follows:

$$f_{11}=\left(ab\right)\sum_{j=1}^{nfw}\int_{0}^{1}\int_{0}^{1}\phi_{j}d\xi d\eta$$

$$f_{12} = f_{13} = 0$$

The mass matrix $[M]$ is expressed as:

$$[M] = \begin{bmatrix} M_{11} & 0 & 0 \\ 0 & M_{22} & 0 \\ 0 & 0 & M_{33} \end{bmatrix}$$

The individual elements of mass matrix are presented as follows:

$$M_{11} = a \sum_{j=1}^{nfw} \sum_{i=1}^{nfw} \int_0^1 \int_0^1 \phi_i \phi_j \rho(\xi,\eta) A(\xi) d\xi d\eta$$

$$M_{22} = a \sum_{j=1+nfw}^{nfw+nfu} \sum_{i=1+nfw}^{nfw+nfu} \int_0^1 \int_0^1 \alpha_{i-nfw} \alpha_{j-nfw} \rho(\xi,\eta) A(\xi) d\xi d\eta$$

$$M_{33} = a \sum_{j=1+nfw+nfu}^{nfw+nfu+nfv} \sum_{i=1+nfw+nfu}^{nfw+nfu+nfv} \int_0^1 \int_0^1 \beta_{i-nfw-nfu} \beta_{i-nfw-nfu} \rho(\xi,\eta) A(\xi) d\xi d\eta$$

Bibliography

A

Abrate, S., 2008, Functionally Graded Plates Behave Like Homogeneous Plates, Composites: Part B. 39, 151–158.

Adineh, M. and Kadkhodayan, M., 2017, Three-Dimensional Thermo-Elastic Analysis and Dynamic Response of a Multi-Directional Functionally Graded Skew Plate on Elastic Foundation. Composites Part B, 125, 227-240.

Akavci, S.S., 2016, Mechanical Behavior of Functionally Graded Sandwich Plates on Elastic Foundation. Composites Part B, 96, 136-152.

Akbarzadeh, A.H., Hosseini zad, S.K., Eslami, M.R.and Sadighi, M., 2011, Mechanical Behaviour of Functionally Graded Plates under Static and Dynamic Loading. Proceedings of the Institution of Mechanical Engineers Part C Journal of Mechanical Engineering Science, 203-210, 1989-1996.

Akgöz, B. and Civalek, Ö., 2013, Free Vibration Analysis of Axially Functionally Graded Tapered Bernoulli–Euler Microbeams Based on the Modified Couple Stress Theory. Composite Structures, 98, 314-322.

Akgöz, B. and Civalek, Ö., 2015, Bending Analysis of FG Microbeams Resting on Winkler Elastic Foundation Via Strain Gradient Elasticity. Composite Structures, 134, 294-301.

Akgöz, B. and Civalek, Ö., 2016, Bending Analysis of Embedded Carbon Nanotubes Resting on an Elastic Foundation Using Strain Gradient Theory. Acta Astronautica, 119, 1-12.

Alshorbagy, A.E., Eltaher, M.A. and Mahmoud, F.F., 2011, Free Vibration Characteristics of a Functionally Graded Beam by Finite Element Method. Applied Mathematical Modelling, 35, 412–425.

Ansari, R., Gholami, R. and Sahmani, S., 2011, Free Vibration Analysis of Size-Dependent Functionally Graded Microbeams Based on the Strain Gradient Timoshenko Beam Theory. Composite Structures, 94, 221–228.

Ansari, R., Gholami, R., Shojaei, M.F., Mohammadi, V. and Sahmani S., 2013, Size-Dependent Bending, Buckling and Free Vibration of Functionally Graded Timoshenko Microbeams Based on the Most General Strain Gradient Theory. Composite Structures, 100, 385–397.

Arefi, M. and Zenkour, A.M., 2017, Analysis of Wave Propagation in a Functionally Graded Nanobeam Resting on Visco-Pasternak's Foundation. Theoretical & Applied Mechanics Letters, 7, 145–151.

Arefi, M. and Zenkour, A.M., 2017, Wave Propagation Analysis of a Functionally Graded Magneto-Electro-Elastic Nanobeam Rest on Visco-Pasternak Foundation. Mechanics Research Communications, 79, 51–62.

Asghari, M., Rahaeifard, M., Kahrobaiyan, M.H. and Ahmadian M.T., 2011, The Modified Couple Stress Functionally Graded Timoshenko Beam Formulation. Materials and Design, 32, 1435–1443.

B

Barati, M.R., Sadr, M.H. and Zenkour, A.M., 2016, Buckling Analysis of Higher Order Graded Smart Piezoelectric Plates with Porosities Resting on Elastic Foundation. International Journal of Mechanical Sciences, 117, 309–320.

Benferhat, R., Daouadji, T.H. and Mansour, M.S., 2016, Free Vibration Analysis of FG Plates Resting on an Elastic Foundation and Based on the Neutral Surface Concept Using Higher-Order Shear Deformation Theory. C. R. Mecanique, 344, 631–641.

Bernardo, G.M.S., Damásio, F.R., Silva, T.A.N. and Loja, M.A.R., 2016, A Study on the Structural Behaviour of FGM Plates Static and Free Vibrations Analyses. Composite Structures, 136, 124–138.

Birman, V. and Byrd, L.W., 2007, Modeling and Analysis of Functionally Graded Materials and Structures. Applied Mechanics Reviews, 60, 195-216.

C

Calim, F.F., 2016, Free and Forced Vibration Analysis of Axially Functionally Graded Timoshenko Beams on Two-Parameter Viscoelastic Foundation. Composites Part B, 103, 98-112.

Calim, F.F., 2016, Transient Analysis of Axially Functionally Graded Timoshenko Beams with Variable Cross-Section. Composites Part B, 98, 472-483.

Chen, D.Q., Sun, D.L., and Li, X.F., 2017, Surface Effects on Resonance Frequencies of Axially Functionally Graded Timoshenko Nanocantilevers with Attached Nanoparticle. Composite Structures, 173, 116–126.

Chi, S.H. and Chung, Y.L., 2006, Mechanical Behavior of Functionally Graded Material Plates under Transverse Load—Part I: Analysis. International Journal of Solids and Structures, 43, 3657–3674.

Chu, F., He, J., Wang, L. and Zhong, Z., 2016, Buckling Analysis of Functionally Graded Thin Plate with In-Plane Material Inhomogeneity. Engineering Analysis with Boundary Elements, 65, 112–125.

Chu, F., Wang, L., Zhong, Z. and He, J., 2014, Hermite Radial Basis Collocation Method for Vibration of Functionally Graded Plates with In-Plane Material Inhomogeneity. Computers and Structures, 142, 79–89.

D

Deng, H., Chen, K.D., Cheng, W. and Zhao, S.G., 2017, Vibration and Buckling Analysis of Double-Functionally Graded Timoshenko Beam System on Winkler-Pasternak Elastic Foundation. Composite Structures, 160,152–168.

Do, T.V., Nguyen, D.K., Duc, N.D., Doan, D.H. and Bui, T.Q., 2017, Analysis of Bi-Directional Functionally Graded Plates by FEM and a New Third-Order Shear Deformation Plate Theory. Thin-Walled Structures, 119, 687–699.

E

Ebrahimi, F., Ghasemi, F. and Salari, E., 2016, Investigating thermal effects on vibration behaviour of temperature-dependent compositionally graded Euler beams with porosities. Meccanica, 51, 223–249.

Ebrahimi, F., Jafari, A. and Barati, M.R., 2017, Vibration Analysis of Magneto-Electro-Elastic Heterogeneous Porous Material Plates Resting on Elastic Foundations. Thin-Walled Structures, 119, 33–46.

El-Ashmawy, A.M., Kamel, M.A. and Elshafei, M.A., 2016, Thermo-Mechanical Analysis of Axially and Transversally Function Graded Beam. Composites Part B, 102, 134-149.

Eltaher, M.A., Alshorbagy, A.E. and Mahmoud, F.F., 2013, Determination of Neutral Axis Position and Its Effect on Natural Frequencies of Functionally Graded Macro/Nanobeams. Composite Structures, 99, 193–201.

Eltaher, M.A., Emam, S.A. and Mahmoud, F.F., 2012, Free Vibration Analysis of Functionally Graded Size-Dependent Nanobeams. Applied Mathematics and Computation, 218, 7406–7420.

Eltaher, M.A., Emam, S.A. and Mahmoud, F.F., 2013, Static and Stability Analysis of Nonlocal Functionally Graded Nanobeams. Composite Structures, 96, 82–88.

Esfahani, S.E., Kiani, Y. and Eslami, M.R., 2013, Non-Linear Thermal Stability Analysis of Temperature Dependent FGM Beams Supported on Non-Linear Hardening Elastic Foundations. International Journal of Mechanical Sciences, 69, 10–20.

Eshraghi, I., Dag, S. and Soltani, N., 2016, Bending and Free Vibrations of Functionally Graded Annular and Circular Micro-Plates under Thermal Loading. Composite Structures, 137, 196–207.

F

Feldman, E. and Aboudi, J., 1997, Buckling Analysis of Functionally Graded Plates Subjected to Uniaxial Loading. Composite Structures, 38, 29-36.

Filonenko-Borodich, 1940, Some Approximate Theories of Elastic Foundation. Uchenyie Zapiski Moskovskogo Gosudarstvennogo Universiteta, Mekhanica 46, 3–18 [in Russian].

G

Gao, K., Gao, W., Wu, D. and Song, C., 2017, Nonlinear Dynamic Characteristics and Stability of Composite Orthotropic Plate on Elastic Foundation under Thermal Environment. Composite Structures, 168, 619–632.

Ghayesh, M.H., 2018, Nonlinear Vibrations of Axially Functionally Graded Timoshenko Tapered Beams. Journal of Computational and Nonlinear Dynamics, 13 041002-1-10.

Gupta, A., Talha, M. and Chaudhari, V.K., 2016, Natural Frequency of Functionally Graded Plates Resting on Elastic Foundation Using Finite Element Method. Procedia Technology, 23, 163 – 170.

Gupta, R.K., Babu, G.J., Janardhan, G.R. and Rao G.V., 2009, Relatively Simple Finite Element Formulation for the Large Amplitude Free Vibrations of Uniform Beams. Finite Elements in Analysis and Design, 45, 624-631.

H

Hao, D. and Wei, C., 2016, Dynamic Characteristics Analysis of Bi-Directional Functionally Graded Timoshenko Beams. Composite Structures, 141, 253–263.

Hetenyi, M., 1946, Beams on Elastic Foundation. Scientific Series, vol. XVI. Ann Arbor: The University of Michigan Press, University of Michigan Studies.

Horvath, J.S., 1983, Modulus of Subgrade Reaction: New Perspective. Journal of Geotechnical Engineering 109 (12), 1591–1596.

Horvath, J.S., 1983, New Subgrade Model Applied to Mat Foundations. Journal of Geotechnical Engineering 109 (12), 1567–1587.

Horvath, J.S., 1993, Beam-Column-Analogy Model for Soil—Structure Interaction Analysis. Journal of Geotechnical Engineering 119 (2), 358–364.

Huang, Y. and Luo, Q.Z., 2011, A Simple Method to Determine the Critical Buckling Loads for Axially Inhomogeneous Beams with Elastic Restraint. Computers and Mathematics with Applications, 61, 2510–2517.

Huang, Y., Wang, T., Zhao, Y. and Wang, P., 2018, Effect of Axially Functionally Graded Material on Whirling Frequencies and Critical Speeds of a Spinning Timoshenko Beam. Composite Structures, 192, 355–367.

Huang, Y., Yang, L.E. and Luo Q.Z., 2013, Free Vibration of Axially Functionally Graded Timoshenko Beams with Non-Uniform Cross-Section. Composites: Part B, 45, 1493–1498.

Huang, Y., Zhang, M. and Rong, H., 2016, Buckling Analysis of Axially Functionally Graded and Non-Uniform Beams Based on Timoshenko Theory. Acta Mechanica Solida Sinica, 29 (2), 200-207.

Hussein, O.S. and Mulani, S.B., 2018, Optimization of In-Plane Functionally Graded Panels for Buckling Strength: Unstiffened, Stiffened Panels, and Panels with Cutouts. Thin-Walled Structures, 122, 173–181.

J

Jha, D.K., Kant, T. and Singh, R.K., 2013, A Critical Review of Recent Research on Functionally Graded Plates. Composite Structures, 96, 833–849.

K

Kägo, E. and Lellep, J., 2013, Free Vibrations of Plates on Elastic Foundation. Procedia Engineering, 57, 489 – 496.

Kahrobaiyan, M.H., Rahaeifardn M., Tajalli, S.A. and Ahmadian, M.T., 2012, A Strain Gradient Functionally Graded Euler–Bernoulli Beam Formulation. International Journal of Engineering Science, 52, 65–76.

Kanani, A.S., Niknam, H., Ohadi A.R. and Aghdam M.M., 2014, Effect of Nonlinear Elastic Foundation on Large Amplitude Free and Forced Vibration of Functionally Graded Beam. Composite Structures, 115, 60-68.

Ke L.L., Yang, J., Kitipornchai S., 2010, An Analytical Study on the Nonlinear Vibration of Functionally Graded Beams. Meccanica, 45, 743–752.

Ke, L.L., Wang, Y.S., Yang, J., Kitipornchai, S., 2012, Nonlinear Free Vibration of Size-Dependent Functionally Graded Microbeams. International Journal of Engineering Science, 50, 256–267.

Ke, L.L., Yang, J. and Kitipornchai, S., 2009, Postbuckling Analysis of Edge Cracked Functionally Graded Timoshenko Beams under End Shortening. Composite Structures, 90, 152–160.

Ke, L.L., Yang, J. and Kitipornchai, S., 2010, Nonlinear Free Vibration of Functionally Graded Carbon Nanotube-Reinforced Composite Beams. Composite Structures, 92, 676–683.

Ke, L.L., Yang, J., Kitipornchai, S. and Xiang, Y., 2009, Flexural Vibration and Elastic Buckling of a Cracked Timoshenko Beam Made of Functionally Graded Materials. Mechanics of Advanced Materials and Structures, 16, 488–502.

Kennedy, D., Cheng, R.K.H., Wei, S. and Alcazar Arevalo, F.J., 2016, Equivalent Layered Models for Functionally Graded Plates. Computers and Structures, 174, 113–121.

Kermani, I.D., Ghayour, M. and Mirdamadi, H.R., 2012, Free Vibration Analysis of Multi-Directional Functionally Graded Circular and Annular Plates. Journal of Mechanical Science and Technology, 26 (11), 3399-3410.

Kerr, A.D., 1965, A study of a new foundation model. Acta Mechanica 1/2, 135–147.

Kerr, A.D., 1985. On the Determination of Foundation Model Parameters. Journal of Geotechnical Engineering 111 (11), 1334–1340.

Khalili, S.M.R., Jafari, A.A. and Eftekhari, S.A., 2010, A Mixed Ritz-DQ Method for Forced Vibration of Functionally Graded Beams Carrying Moving Loads. Composite Structures, 92, 2497–2511.

Kiani, K., 2016, Thermo-Elasto-Dynamic Analysis of Axially Functionally Graded Non-Uniform Nanobeams with Surface Energy. International Journal of Engineering Science, 106, 57–76.

Kiani, Y., Akbarzadeh, A.H., Chen, Z.T. and Eslami, M.R., 2012, Static and Dynamic Analysis of an FGM Doubly Curved Panel Resting on the Pasternak-Type Elastic Foundation. Composite Structures, 94, 2474–2484.

Kien, N., 2013, Large Displacement Response of Tapered Cantilever Beams Made of Axially Functionally Graded Material. Composites: Part B, 55, 298–305.

Kitipornchai, S., Ke, L.L., Yang, J. and Xiang, Y., 2009, Nonlinear Vibration of Edge Cracked Functionally Graded Timoshenko Beams. Journal of Sound and Vibration, 324, 962–982.

Komijani, M., Esfahani, S.E., Reddy, J.N., Liu, Y.P. and Eslami, M.R., 2014, Nonlinear Thermal Stability and Vibration of Pre/Post-Buckled Temperature and Microstructure-Dependent Functionally Graded Beams Resting on Elastic Foundation. Composite Structures, 112, 292–307.

Kumar, S., Mitra A. and Roy H., 2015, Geometrically Nonlinear Free Vibration Analysis of Axially Functionally Graded Taper Beams. Engineering Science and Technology, an International Journal, 18, 579-593.

Kumar, S., Mitra, A. and Roy, H., 2014, Large Amplitude Free Vibration Analysis of Axially Functionally Graded Plates. Proc. Of ASME 2014 Gas Turbine India Conference - GTINDIA2014, New Delhi, India, 1-8.

Kumar, S., Mitra, A. and Roy, H., 2015, Forced Vibration Analysis of Functionally Graded Plates with Geometric Nonlinearity. Proc. Of ASME 2015 Gas Turbine India Conference - GTINDIA2015, Hyderabad, India, 1-8.

Kumar, S., Mitra, A. and Roy, H., 2016, Large Amplitude Free Vibration Study of Non-Uniform Plates with In-Plane Material Inhomogeneity. Proceedings of IMechE, Part L, Journal of Materials: Design and Applications. DOI: 10.1177/1464420715627477.

Kumar, S., Mitra, A. and Roy, H., 2017, Forced Vibration Response of Axially Functionally Graded Non-Uniform Plates Considering Geometric Nonlinearity. International Journal of Mechanical Sciences, 128-129, 194-205.

Kutlu, A., U_gurlu, B. and Omurtag, M.H., 2017, A Combined Boundary-Finite Element Procedure for Dynamic Analysis of Plates with Fluid and Foundation Interaction Considering Free Surface Effect. Ocean Engineering, 145, 34–43.

L

Leissa, A.W., 1973, The Free Vibration of Rectangular Plates. Journal of Sound and Vibration, 31, 257–293.

Lezgy-Nazargah, M., 2015, Fully Coupled Thermo-Mechanical Analysis of Bi-Directional FGM Beams using NURBS Isogeometric Finite Element Approach. Aerospace Science and Technology, 45, 154–164.

Li, R., Zhong, Y. and Li, M., 2013, Analytic Bending Solutions of Free Rectangular Thin Plates Resting on Elastic Foundations by a New Symplectic Superposition Method. Proceeding of Royal Society A, 469: 20120681.http: //dx.doi.org/10.1098/ rspa.2012.0681.

Li, S., Zhang, J. and Zhao, Y., 2006, Thermal Post-Buckling of Functionally Graded Material Timoshenko Beams. Applied Mathematics and Mechanics, 27(6), 803–810.

Li, S.R. and Batra, R.C., 2013, Relations between Buckling Loads of Functionally Graded Timoshenko and Homogeneous Euler–Bernoulli Beams. Composite Structures, 95, 5–9.

Li, X.-F., 2008, A Unified Approach for Analyzing Static and Dynamic Behaviors of Functionally Graded Timoshenko and Euler–Bernoulli Beams. Journal of Sound and Vibration, 318, 1210–1229.

Li, X.F., Kang, Y.A. and Wu, J.X., 2013, Exact Frequency Equations of Free Vibration of Exponentially Functionally Graded Beams. Applied Acoustics, 74, 413-420.

Liew, K.M., Zhao, X. and Ferreira, A.J., 2011, A Review of Meshless Methods for Laminated and Functionally Graded Plates and Shells. Composite Structures, 93(8), 2031-2041.

Liu, D.Y., Wang, C.Y. and Chen, W.Q., 2010, Free Vibration of FGM Plates with In-Plane Material Inhomogeneity. Composite Structures, 92, 1047–1051.

Liu, S., Yu, T., Bui, T.Q., Yin, S., Thai, D.K. and Tanaka, S., 2017, Analysis of Functionally Graded Plates by a Simple Locking-Free Quasi-3D Hyperbolic Plate Isogeometric Method. Composites Part B, 120, 182-196.

Lü, C.F., Chen, W.Q., Xu, R.Q. and Lim, C.W., 2008, Semi-Analytical Elasticity Solutions for Bi-Directional Functionally Graded Beams. International Journal of Solids and Structures, 45(1), 258-275.

Lu, C.F., Lim, C.W. and Chen, W.Q., 2009, Semi-Analytical Analysis for Multi-Directional Functionally Graded Plates: 3-D Elasticity Solutions. International Journal for Numerical Methods in Engineering, **79**, 25–44.

M

Mantari, J.L. and Monge, J.C., 2016, Buckling, Free Vibration and Bending Analysis of Functionally Graded Sandwich Plates Based on an Optimized Hyperbolic Unified Formulation. International Journal of Mechanical Sciences, 119, 170–186.

Markworth, A.J., Ramesh, K.S. and Parks, W.P., 1995, Modelling Studies Applied to Functionally Graded Materials. Journal of Materials Science, 30(9), 2183-2193.

Mohammadzadeh, B. and Noh, H.C., 2017, Analytical Method to Investigate Nonlinear Dynamic Responses of Sandwich Plates with FGM Faces Resting on Elastic Foundation Considering Blast Loads, Composite Structures, 174, 142–157.

Mohammadzadeh-Keleshteri, M., Asadi, H. and Aghdam, M.M., 2017, Geometrical Nonlinear Free Vibration Responses of FG-CNT Reinforced Composite Annular Sector Plates Integrated with Piezoelectric Layers. Composite Structures, 171, 100–112.

Mohanty, S.C., Dash, R.R. and Rout, T., 2011, Parametric Instability of a Functionally Graded Timoshenko Beam on Winkler's Elastic Foundation. Nuclear Engineering and Design, 241, 2698– 2715.

Mukherjee, B. and Dillard, D.A., 2017, On Buckling of a Thin Plate on an Elastomeric Foundation. International Journal of Mechanical Sciences, 000, 1–7.

Murin, J., Aminbaghai, M., Kutis, V. and Hrabovsky J., 2013, Modal Analysis of the FGM Beams with Effect of Axial Force under Longitudinal Variable Elastic Winkler Foundation. Engineering Structures, 49, 234-247.

N

Najafi, F., Shojaeefard, M.H. and Saeidi Googarchin, H., 2016, Nonlinear Low-Velocity Impact Response of Functionally Graded Plate with Nonlinear Three-Parameter Elastic Foundation in Thermal Field. Composites Part B, 107, 123-140.

Nejad, M.Z. and Hadi, A., 2016, Eringen's Non-Local Elasticity Theory for Bending Analysis of Bi-Directional Functionally Graded Euler–Bernoulli Nano-Beams. International Journal of Engineering Science, 106, 1–9.

Nejad, M.Z. and Hadi, A., 2016, Non-Local Analysis of Free Vibration of Bi-Directional Functionally Graded Euler–Bernoulli Nano-Beams. International Journal of Engineering Science, 105, 1–11.

Nejad, M.Z., Hadi, A. and Rastgoo, A. 2016, Buckling Analysis of Arbitrary Two-Directional Functionally Graded Euler–Bernoulli Nano-Beams Based on Nonlocal Elasticity Theory. International Journal of Engineering Science, 103, 1–10.

Nemat-Alla, M., 2003, Reduction of Thermal Stresses by Developing Two-Dimensional Functionally Graded Materials. International Journal of Solids and Structures, 40, 7339–7356.

Nemat-Alla, M., 2009, Reduction of Thermal Stresses by Cmposition Optimization of Two-Dimensional Functionally Graded Materials. Acta Mech, 208, 147–161.

Nemat-Alla, M., Ahmed, K.I.E. and Hassab-Allah, I., 2009, Elastic–Plastic Analysis of Two Dimensional Functionally Graded Materials under Thermal Loading. International Journal of Solids and Structures, 46, 2774–2786.

Nguyen, D.K., Nguyen, Q.H., Tran, T.T. and Bui, V.T., 2017, Vibration of Bi-Dimensional Functionally Graded Timoshenko Beams Excited by a Moving Load. Acta Mech, 228, 141–155.

Nguyen-Xuan, H., Tran, L.V., Nguyen-Thoi, T. and Vu-Do, H.C., 2011, Analysis of Functionally Graded Plates Using an Edge-Based Smoothed Finite Element Method. Composite Structures, 93, 3019–3039.

Nie, G. and Zhong, Z., 2010, Dynamic Analysis of Multi-Directional Functionally Graded Annular Plates, Applied Mathematical Modelling, 34, 608–616.

Niknam, H. and Aghdam, M.M., 2015, A Semi Analytical Approach for Large Amplitude Free Vibration and Buckling of Nonlocal FG Beams Resting on Elastic Foundation. Composite Structures, 119, 452-462.

P

Panyatong, M., Chinnaboon, B. and Chucheepsakul, S., 2016, Free Vibration Analysis of FG Nanoplates Embedded in Elastic Medium Based on Second-Order Shear Deformation Plate Theory and Nonlocal Elasticity. Composite Structures, 153, 428–441.

Pasternak, P.L., 1954, On a New Method of Analysis of an Elastic Foundation by Means of Two-Constants. Moscow, USSR: Gosudarstvennoe Izdatelstvo Literaturi po Stroitelstvu I Arkhitekture [in Russian].

Pradhan, K.K. and Chakraverty, S., 2013, Free Vibration of Euler and Timoshenko Functionally Graded Beams by Rayleigh–Ritz Method. Composites: Part B, 51, 175–184.

Press, W.H., Teukolsky, S.A., Vetterling, W.T. and Flannery, B.P., 2005, Numerical Recipes in Fortran 77. 2nd Edition, Cambridge, USA: Press Syndicate.

Pydah, A. and Batra, R.C., 2017, Shear Deformation Theory using Logarithmic Function for Thick Circular Beams and Analytical Solution for Bi-Directional Functionally Graded Circular Beams. Composite Structures, 172, 45–60.

Pydah, A. and Sabale, A., 2017, Static Analysis of Bi-Directional Functionally Graded Curved Beams. Composite Structures, 160, 867–876.

R

Rahmani, O. and Pedram, O., 2014, Analysis and Modeling the Size Effect on Vibration of Functionally Graded Nanobeams Based on Nonlocal Timoshenko Beam Theory. International Journal of Engineering Science, 77, 55–70.

Rajasekaran, S., 2013, Free Vibration of Centrifugally Stiffened Axially Functionally Graded Tapered Timoshenko Beams using Differential Transformation and Quadrature Methods. Applied Mathematical Modelling, 37, 4440–4463.

Ramu, I. and Mohanty, S.C., 2014, Buckling Analysis of Rectangular Functionally Graded Material Plates under Uniaxial and Biaxial Compression Load. Procedia Engineering, 86, 748 – 757.

Reddy, J. N., 2000, Analysis of Functionally Graded Plates, International Journal for Numerical Methods in Engineering. 47, 663-684.

Reissner, E., 1967, Note on the Formulation of the Problem of the Plate on an Elastic Foundation. Acta Mechanica 4, 88–91.

Ribeiro, P., 2004, Non-Linear Forced Vibrations of Thin/Thick Beams and Plates by the Finite Element and Shooting Methods. Computers and Structures, 82, 1413–1423.

S

Saha, K.N., Misra, D., Pohit, G. and Ghosal S., 2004, Large Amplitude Free Vibration Study of Square Plates under Different Boundary Conditions through a Static Analysis. Journal of Sound and Vibration, 10, 1009-1028.

Sari, M., Shaat, M. and Abdelkefi, A., 2017, Frequency and Mode Veering Phenomena of Axially Functionally Graded Non-Uniform Beams with Nonlocal Residuals. Composite Structures, 163, 280–292.

Sarkar, K. and Ganguli, R., 2014, Closed-Form Solutions for Axially Functionally Graded Timoshenko Beams having Uniform Cross-Section and Fixed–Fixed Boundary Condition. Composites: Part B, 58, 361–370.

Selvadurai, A.P.S., 1979, Elastic Analysis of Soil–foundation Interaction. Elsevier, Amsterdam.

Shafiei, N., Kazemi, M. and Ghadiri, M., 2016, Comparison of Modelling of the Rotating Tapered Axially Functionally Graded Timoshenko and Euler–Bernoulli Microbeams. Physica E: Low-dimensional Systems and Nanostructures, 83, 74–87.

Shafiei, N., Mirjavadi, S.S., Afshari, B.M., Rabby, S. and Kazemi, M., 2017, Vibration of Two-Dimensional Imperfect Functionally Graded (2D-FG) Porous Nano-/Micro-Beams. Computer Methods in Applied Mechanics and Engineering, 322, 615−632.

Shahba, A., Attarnejad, R., Marvi, M.T. and Hajilar, S., 2011, Free Vibration and Stability Analysis of Axially Functionally Graded Tapered Timoshenko Beams with Classical and Non-Classical Boundary Conditions. Composites: Part B, 42, 801–808.

Shahba, A. and Rajasekaran S., 2012, Free Vibration and Stability of Tapered Euler–Bernoulli Beams Made of Axially Functionally Graded Materials. Applied Mathematical Modelling, 36, 3094-3111.

Shahsavari, D., Shahsavari, M., Li, L. and Karami, B., 2018, A Novel Quasi-3D Hyperbolic Theory for Free Vibration of FG Plates with Porosities Resting on Winkler/Pasternak/Kerr Foundation. Aerospace Science and Technology, 72, 134–149.

Shames, I.H. and Dym, C.L., 2009, Energy and Finite Element Methods in Structural Mechanics. New Age International Publishers, Delhi.

Shariyat, M. and Alipour, M.M., 2013, A Power Series Solution for Vibration and Complex Modal Stress Analyses of Variable Thickness Viscoelastic Two-Directional FGM Circular Plates on Elastic Foundations. Applied Mathematical Modelling, 37, 3063–3076.

Shariyat, M. and Jafari, R., 2013, Nonlinear Low-Velocity Impact Response Analysis of a Radially Preloaded Two-Directional-Functionally Graded Circular Plate: A Refined Contact Stiffness Approach. Composites: Part B, 45, 981–994.

Sharma, P. and Parashar, S.K., 2016, Free Vibration Analysis of Shear-Induced Flexural Vibration of FGPM Annular Plate Using Generalized Differential Quadrature Method. Composite Structures, 155, 213–222.

Simsek, M. and Cansız S., 2012, Dynamics of Elastically Connected Double-Functionally Graded Beam Systems with Different Boundary Conditions under Action of a Moving Harmonic Load. Composite Structures, 94, 2861-2878.

Simsek, M. and Kocatürk, T., 2009, Free and Forced Vibration of a Functionally Graded Beam Subjected to a Concentrated Moving Harmonic Load. Composite Structures, 90, 465–473.

Simsek, M. and Yurtcu, H.H., 2013, Analytical Solutions for Bending and Buckling of Functionally Graded Nanobeams Based on the Nonlocal Timoshenko Beam Theory. Composite Structures, 97, 378–386.

Simsek, M., 2010, Non-Linear Vibration Analysis of a Functionally Graded Timoshenko Beam under Action of a Moving Harmonic Load. Composite Structures, 92, 2532–2546.

Simsek, M., 2010, Vibration Analysis of a Functionally Graded Beam under a Moving Mass by Using Different Beam Theories. Composite Structures, 92, 904–917.

Simsek, M., 2015, Bi-Directional Functionally Graded Materials (BDFGMs) for Free and Forced Vibration of Timoshenko Beams with Various Boundary Conditions. Composite Structures, 133, 968–978.

Simsek, M., 2016, Buckling of Timoshenko Beams Composed of Two-Dimensional Functionally Graded Material (2D-FGM) having Different Boundary Conditions. Composite Structures, 149, 304–314.

Simsek, M., Kocatürk, T. and Akbas, S.D., 2013, Static Bending of a Functionally Graded Microscale Timoshenko Beam Based on the Modified Couple Stress Theory. Composite Structures, 95, 740–747.

Singha, M.K., Prakash, T. and Ganapathi, M., 2011, Finite Element Analysis of Functionally Graded Plates under Transverse Load. Finite Elements in Analysis and Design, 47, 453–460.

Steinberg, M.A., 1986, Materials for Aerospace. Scientific American, 255 (4), 59–64.

Suresh, S., Mortensen, A., 1998, Fundamentals of Functionally Graded Materials. The Institute of Materials, London.

T

Taczała, M., Buczkowski, R. and Kleiber, M., 2015, Postbuckling Analysis of Functionally Graded Plates on an Elastic Foundation. Composite Structures, 132, 842–847.

Tahouneh V. and Naei, M.H., 2014, A Novel 2-D Six-Parameter Power-Law Distribution for Three-Dimensional Dynamic Analysis of Thick Multi-Directional Functionally Graded Rectangular Plates Resting on a Two-Parameter Elastic Foundation. Meccanica, 49, 91–109.

Thai, H.T. and Kim, S.E., 2015, A Review of Theories for the Modeling and Analysis of Functionally Graded Plates and Shells. Composite Structures, 128, 70-86.

Timoshenko, S. and Woinowsky-Krieger, S., 1964, Theory of Plates and Shells. 2nd Edition, New York: McGraw-Hill Classic Textbook Reissue Series, New York, USA.

Tornabene, F. and Viola, E., 2009, Free Vibration Analysis of Functionally Graded Panels and Shells of Revolution. Meccanica, 44, 255–281.

Tossapanon, P. and Wattanasakulpong, N., 2016, Stability and Free Vibration of Functionally Graded Sandwich Beams Resting on Two-Parameter Elastic Foundation. Composite Structures, 142, 215–225.

U

Uymaz, B., Aydogdu, M. and Filiz, S., 2012, Vibration Analyses of FGM Plates with In-Plane Material Inhomogeneity by Ritz Method. Composite Structures, 94, 1398–1405.

V

Vlasov, V.Z. and Leontiev, U.N., 1966, Beams, Plates, and Shells on Elastic Foundation. Jerusalem: Israel Program for Scientific Translations [translated from Russian].

Vu, T.V., Nguyen, N.H., Khosravifard, A., Hematiyan, M.R. and Tanaka, S., 2017, A Simple FSDT-Based Meshfree Method for Analysis of Functionally Graded Plates. Engineering Analysis with Boundary Elements, 79, 1–12.

W

Wang, Y. and Wu, D., 2016, Thermal Effect on the Dynamic Response of Axially Functionally Graded Beam Subjected to a Moving Harmonic Load. Acta Astronautica, 127, 171–181.

Wattanasakulpong, N. and Chaikittiratana, A., 2015, Exact Solutions for Static and Dynamic Analyses of Carbon Nanotube-Reinforced Composite Plates with Pasternak Elastic Foundation. Applied Mathematical Modelling, 39, 5459–5472.

Winkler, E., 1867, Die Lehre Von Der Elastizitat Und Festigkeit. Dominicus, Prague.

X

Xiang, T., Natarajan, S., Man, H., Song, C. and Gao, W., 2014, Free Vibration and Mechanical Buckling of Plates with In-Plane Material Inhomogeneity – A Three Dimensional Consistent Approach. Composite Structures, 118, 634–642.

Y

Yan, T., Kitipornchai, S., Yang, J. and He, X.Q., 2011, Dynamic Behaviour of Edge-Cracked Shear Deformable Functionally Graded Beams on an Elastic Foundation under a Moving Load. Composite Structures, 93, 2992–3001.

Yang, Z., Yuan-Yuan, G. and Fangin, B.B., 2012, Solution for a Rectangular Plate on Elastic Foundation with Free Edges using Reciprocal Theorem Method. Mathematica Aeterna, 2, 335 – 343.

Yas, M.H. and Aragh, B.S., 2010, Free Vibration Analysis of Continuous Grading Fiber Reinforced Plates on Elastic Foundation. International Journal of Engineering Science, 48, 1881–1895.

Yas, M.H. and Moloudi, N., 2015, Three-Dimensional Free Vibration Analysis of Multi-Directional Functionally Graded Piezoelectric Annular Plates on Elastic Foundations via State Space Based Differential Quadrature Method. Applied Mathematics and Mechanics, 36(4), 439–464.

Yas, M.H. and Samadi, N., 2012, Free Vibrations and Buckling Analysis of Carbon Nanotube-Reinforced Composite Timoshenko Beams on Elastic Foundation. International Journal of Pressure Vessels and Piping, 98, 119-128.

Yin, S., Yu, T., Bui, T.Q., Zheng, X. and Tanaka, S., 2016, In-Plane Material Inhomogeneity of Functionally Graded Plates: A Higher-Order Shear Deformation Plate Isogeometric Analysis. Composites Part B, 106, 273-284.

Yin, S., Yu, T., Bui, T.Q., Zheng, X. and Yi, G., 2017, Rotation-Free Isogeometric Analysis of Functionally Graded Thin Plates, Considering In-Plane Material Inhomogeneity. Thin-Walled Structures, 119, 385–395.

Z

Zamani, H.A., Aghdam, M.M. and Sadighi, M., 2017, Free Vibration Analysis of Thick Viscoelastic Composite Plates on Visco-Pasternak Foundation Using Higher-Order Theory. Composite Structures, 182, 25–35.

Zeighampour, H. and Beni, Y.T., 2015, Free Vibration Analysis of Axially Functionally Graded Nanobeam with Radius Varies along the Length Based on Strain Gradient Theory. Applied Mathematical Modelling, 39, 5354-5369.

Zhao, L., Chen, W.Q., Lü, C.F., 2012, Symplectic Elasticity for Bi-Directional Functionally Graded Materials. Mechanics of Materials, 54, 32–42.

Zhao, L., Zhu, J. and Wen, X.D., 2016, Exact Analysis of Bi-Directional Functionally Graded Beams with Arbitrary Boundary Conditions via the Symplectic Approach. Structural Engineering and Mechanics, 59 (1), 101-122.

Zhao, Y., Huang, Y. and Guo, M., 2017, A Novel Approach for Free Vibration of Axially Functionally Graded Beams with Non-Uniform Cross-Section Based on Chebyshev Polynomials Theory. Composite Structures, 168, 277–284.